MATHEMATICAL MODELING OF HIV-1 THERAPEUTIC INITIATIVES: SHOCK AND KILL STRATEGY IN THE BRAIN AND THE NATURAL CONTROL OF THE VIRUS IN THE PLASMA

by

Weston Christopher Roda

A thesis submitted in partial fulfillment of the requirements for the degree of

Doctor of Philosophy

in

Applied Mathematics

Department of Mathematical and Statistical Sciences
University of Alberta

© Weston Christopher Roda, 2024

Abstract

This thesis is based on four main studies. The first two studies present a detailed methodology for completing dynamical system parameter estimation using Bayesian inference. The next two studies are about using this methodology to investigate critical human immunodeficiency virus-1 therapeutic initiatives: "Shock and Kill" strategy in the brain and the natural control of the virus in the plasma.

The first study in this thesis is based on the 2020 paper "Bayesian inference for dynamical systems" in the journal *Infectious Disease Modelling*. This paper described a comprehensive methodology for dynamical system parameter estimation using Bayesian inference and it covered the topics of utilizing different distributions, Markov Chain Monte Carlo (MCMC) sampling, obtaining credible intervals for parameters, and prediction intervals for solutions. It also included a logistic growth example to illustrate the methodology. This study is described in Chapter 2.

The next study in this thesis is about the first MATLAB implementation of the Diffusive Nested Sampling (DNS) algorithm called "MatlabDiffNestAlg", which is available to the community on the MATLAB Central File Exchange and uploaded into the CERN supported repository Zenodo. DNS is a Bayesian inference method that is capable of reliably estimating parameters in a high dimensional space. The DNS algorithm is also able to effectively sample from multimodal distributions and it provides samples that are estimates of the actual posterior density. Chapter 3 describes the DNS algorithm, and the MATLAB implementation of the DNS algorithm is explained in Section 3.C.

The third study in this thesis is based on the 2021 paper "Modeling the effects of latency reversing drugs during HIV-1 and SIV brain infection with implications for the "Shock and Kill" strategy" in the *Bulletin of Mathematical Biology*. This was the first mathematical model to qualitatively analyze the dynamics of latently and productively infected cells in the brain during human immunodeficiency virus-1 (HIV-1) and simian immunodeficiency virus (SIV) infection and to quantify the size of the latent reservoir in the brain for SIV animal studies. After this latent SIV reservoir was estimated, the effect of latency reversing agents in the brain was evaluated and the mathematical model indicated that there exists a biologically realistic parameter regime where the "Shock and Kill" therapy strategy is safe and effective in the brain. This study is described in Chapter 4 and Chapter 5.

The fourth study in this thesis is about estimating and predicting HIV-1 infection in the plasma for HIV-1 Elite Controllers and a comparison group of HIV-1 patients from the Northern Alberta HIV Program. This was the first mathematical modeling study to directly estimate the differences between a group of HIV-1 Elite Controllers with a comparison group of HIV-1 patients using empiric data and it is also the first HIV-1 mathematical model to consider both effector cytotoxic CD4 T lymphocytes' and effector cytotoxic CD8 T lymphocytes' impact on HIV-1 disease and other diseases present in each patient. The response function used for the HIV-1 specific effector cytotoxic T lymphocytes has a biological interpretation based on the phases of antiviral cytotoxic T lymphocyte response and it was found that this response function was important for explaining the observed viral load behavior for the HIV-1 patients in this study. The Elite Controller group was found to have a stronger antiviral immune response than the comparison group. In contrast, the com-

parison group was found to have more chronic immune activation but a less effective immune response. The Elite Controller immune response estimates given in this study quantifies a biologically realistic optimal immune response goal for HIV-1 therapeutic initiatives. This study is presented in Chapter 6 and Chapter 7.

Preface

While studying towards my Doctor of Philosophy degree in Applied Mathematics at the University of Alberta, we published eight disease analyses papers [1, 2, 3, 4, 5, 6, 7, 8]. I was the first author on four of these papers discussed below. Also, I was the lead developer of a Bayesian inference software program [9].

I have worked on mathematical and statistical disease models for lentiviral infections, immunodeficiency-associated lentiviruses include human immunodeficiency virus-1 (HIV-1) and simian immunodeficiency virus (SIV). I have also worked on modeling related to influenza, coronavirus disease (COVID-19), and multiple sclerosis (MS). My PhD research has been mainly centred on mathematical modeling of lentiviral infections, more specifically modeling with the objective of aiding HIV-1 therapeutic initiatives, and this is the primary focus of my PhD thesis. I refer to other diseases in this thesis in relation to mathematical and statistical tools that I have helped to develop, and where applicable these tools are applied to mathematical modeling of lentiviral infections.

We published the paper "Modeling brain lentiviral infections during antiretroviral therapy in AIDS" in the *Journal of NeuroVirology* in 2017 [1]. This was the first mathematical model to quantify HIV-1 and SIV infection dynamics in the brain. This was also the first mathematical model of an infectious disease in the brain. Our study indicated that HIV-1 and SIV pro-virus burdens in brain increase slowly over time [1]. Assuming cART suppressed HIV-1 outside the brain, our model showed that an effective cART could sup-

press HIV-1 infection in the brain, although over a decade for patients without neurological complications and over two decades for those with HAND [1]. The research collaboration included the following coauthors: Dr. Michael Y. Li and Dr. Michael S. Akinwumi at the Department of Mathematical and Statistical Sciences and Dr. Eugene L. Asahchop and Dr. Christopher Power at the Division of Neurology, Department of Medicine, at University of Alberta; Dr. Benjamin B. Gelman at the Texas NeuroAIDS Research Center and Department of Pathology at University of Texas Medical Branch; and Dr. Kenneth W. Witwer at the Department of Molecular and Comparative Pathobiology at John Hopkins University School of Medicine. This paper covers topics from my MSc thesis [10].

In 2020, I published the paper "Bayesian inference for dynamical systems" in the journal *Infectious Disease Modelling* [2]. This paper presented a comprehensive methodology for dynamical system parameter estimation using Bayesian inference and it covered the topics of utilizing different distributions, Markov Chain Monte Carlo (MCMC) sampling, obtaining credible intervals for parameters, and prediction intervals for solutions. It also included a logistic growth example to illustrate the methodology. Chapter 2 is primarily based on this paper.

When the COVID-19 outbreak began in Wuhan, China, Michael Li's lab at University of Alberta was fast to respond with COVID-19 mathematical models of disease transmission, prediction of the COVID-19 waves, and techniques to accurately estimate epidemics using mathematical models. We published the paper "Why is it difficult to accurately predict the COVID-19 epidemic" in the journal *Infectious Disease Modelling* in 2020 [3]. Thus far, this paper remains among the top 4 most cited papers in the journal *Infectious Disease*

Modelling. Our study demonstrated that nonidentifiability in model calibrations using the confirmed-case data is the main reason for such wide variations in COVID-19 modeling studies. This study exemplified the ability of Bayesian inference, when an efficient algorithm is used, to determine the extent of nonidentifiability in a mathematical model. This study also illustrated that, even in the presence of nonidentifiability, Bayesian inference can produce workable credible intervals that significantly reduce the wide parameter ranges found in the specified prior distribution. Using the Akaike Information Criterion (AIC) for model selection, we showed that an SIR model performs much better than an SEIR model in representing the information contained in the confirmed-case data. This indicated that predictions using more complex models may not be more reliable compared to using a simpler model. The research collaboration included the following coauthors: Dr. Michael Y. Li and Ms. Donglin Han at the Department of Mathematical and Statistical Sciences and Dr. Marie B. Varughese at the Analytics and Performance Reporting Branch, Government of Alberta Ministry of Health. The Bayesian inference tools used in this COVID-19 paper are covered in Chapter 2.

I have collaborated with the Analytics and Performance Reporting Branch, Government of Alberta Ministry of Health, in Michael Li's lab at University of Alberta since 2016. During the COVID-19 pandemic, we needed to fit large mathematical models to multiple datasets simultaneously in order to meet the prediction requests of the Alberta Ministry of Health. These mathematical models were often age group compartmental models. At times, these age group compartmental models included separate vaccinated and unvaccinated compartments within each age group. This resulted in a mathematical model with more than one hundred parameters that needed to be estimated by data

fitting. As the COVID-19 mathematical models grew in size, it was necessary to use a data fitting method that could reliably estimate parameters in a high dimensional parameter space. Diffusive Nested Sampling (DNS) is a Bayesian inference method that is capable of reliably estimating parameters in a high dimensional space [11, 12]. The DNS algorithm is also able to effectively sample from multimodal distributions and it provides samples that are estimates of the actual posterior density [11, 12]. Since our mathematical modeling code is written in MATLAB, myself and Ms. Donglin Han at the Department of Mathematical and Statistical Sciences programmed the first MATLAB implementation of the DNS algorithm called "MatlabDiffNestAlg" in 2021 and we have continued updating the software features since its debut [9]. The "MatlabDiffNestAlg" Bayesian inference software program is available to the community on the MATLAB Central File Exchange and uploaded into the CERN supported repository Zenodo, which is capable of DOI versioning to make academic software programs easily citable. The "MatlabDiffNestAlg" program was successfully used to fit the large COVID-19 mathematical models to multiple datasets in order to predict the Alberta COVID-19 waves. Chapter 3 describes the DNS algorithm, and the MATLAB implementation of the DNS algorithm is explained in Section 3.C. The "MatlabDiffNestAlg" program is used to effectively fit the HIV-1 plasma infection model with natural immune responses to empirical patient data and this is presented in Chapters 6 and 7.

We published the paper "Modeling the effects of latency reversing drugs during HIV-1 and SIV brain infection with implications for the "Shock and Kill" strategy" in the *Bulletin of Mathematical Biology* in 2021 [4]. In this study, a mathematical model was used to analyze the dynamics of latently and productively infected brain macrophages during viral infection and this math-

ematical model enabled prediction of the effects of latency reversing agents applied to the "Shock and Kill" strategy in the brain. The model was calibrated using reported data from simian immunodeficiency virus (SIV) studies. Our model produces the overarching observation that effective cART can suppress productively infected brain macrophages but leaves a residual latent viral reservoir in brain macrophages. In addition, our model demonstrates that there exists a parameter regime wherein the "Shock and Kill" strategy can be safe and effective for SIV infection in the brain. The results indicate that the "Shock and Kill" strategy can restrict brain viral RNA burden associated with severe neuroinflammation and can lead to the eradication of the latent reservoir of brain macrophages. The research collaboration included the following coauthors: Dr. Michael Y. Li at the Department of Mathematical and Statistical Sciences and Dr. Christopher Power at the Division of Neurology, Department of Medicine, at University of Alberta; Dr. Suli Liu at the School of Mathematics, Jilin University. Chapters 4 and 5 are based on this paper.

In the study "Modeling the natural control of HIV-1 in the plasma: comparative analyses of patients from the Northern Alberta HIV Program", a mathematical model was used to estimate and predict HIV-1 infection in the plasma for HIV-1 Elite Controllers and a comparison group of HIV-1 patients from the Northern Alberta HIV Program. The response function used for the HIV-1 specific effector cytotoxic T lymphocytes in the mathematical model has a biological interpretation based on the phases of antiviral cytotoxic T lymphocyte response and it was found that this response function was important for explaining the observed viral load behavior for the HIV-1 patients in this study. The Elite Controller group was found to have a stronger antiviral immune response than the comparison group. In contrast, the comparison group

was found to have more chronic immune activation but a less effective immune response. The Elite Controller immune response estimates given in this study quantifies a biologically realistic optimal immune response goal for HIV-1 therapeutic initiatives. The research collaboration included Dr. Michael Y. Li at the Department of Mathematical and Statistical Sciences, and Dr. Christopher Power and Dr. Shannon Turvey at the Department of Medicine, at University of Alberta. Chapters 6 and 7 are based on this study.

Acknowledgements

I would like to thank the members of the committee Dr. Brendan Pass, Dr. Michael Li, Dr. Christopher Power, Dr. Hao Wang, Dr. Yingfei Yi, Dr. Bei Jiang, and Dr. Junling Ma for their time and help in the completion of this thesis. I also would like to express my gratitude for many insightful discussions and for the help in completing this thesis to Dr. James Muldowney posthumously.

I would like to thank my family and friends for their support over these years while completing my PhD degree. I would like to convey my gratefulness to my supervisor, Dr. Michael Li, for helping, supporting, and inspiring my research endeavors over the course of my program and providing me with this excellent opportunity. I would additionally like to thank all of the members of the Dr. Michael Li Lab. Special thanks to Dr. Marie B. Varughese for the fascinating infectious disease modeling collaborations over the years and Ms. Donglin Han for the wonderful MATLAB, Bayesian inference and modeling collaborations.

I am really appreciative for all of the thoughtful discussions, motivation, and opportunities that my co-supervisor, Dr. Christopher Power, has provided during my PhD program. I would like to thank the entire Power Lab. Special thanks for the great collaboration on the brain lentiviral infection projects and the multiple sclerosis project to Ms. Nazanin Mohammadzadeh and Dr. Majed Alluqmani, respectively.

I thank Dr. Suli Liu for her fantastic dynamical systems collaboration and perceptive comments regarding the dynamical systems research.

Thanks to Dr. Shannon Turvey and the Northern Alberta HIV Program for their collaboration on HIV-1 research.

I thank Dr. Margaret L. Russell for her encouragement during my PhD program, and I thank Dr. Larry Svenson for the significant infectious disease collaboration at the Government of Alberta Ministry of Health posthumously.

I thank the Collaborative Mathematical Biology Group at University of Alberta for the great opportunities to network, discuss, and present mathematical biology research with special thanks to Dr. Thomas Hillen, Dr. Mark Lewis, and Dr. Gerda de Vries.

I should like to thank the Department of Mathematical and Statistical Sciences at University of Alberta for their generous financial support and encouragement during my PhD program.

Table of Contents

List of Tables

List of Figures

Chapter 1

Introduction

In 2021, an estimated 38.4 (33.9 - 43.8) million people were living with HIV-1 globally with 1.5 (1.1 - 2.0) million people becoming newly infected [13]. Even with the success of combination antiretroviral therapy (cART), HIV-1 remains a global health issue [14, 15]. The virus persists in many different cells and tissues, and tissues that have minimal cART penetration and limited host immune responses make ideal locations for viral reservoirs [16, 17, 14]. These viral reservoirs contain latently infected long-lived cells [18, 14]. Latency is defined as the state where individual infected cells do not produce infectious virus but can become reactivated to produce infectious virus [19, 20]. The "Shock and Kill" therapy aims to reactivate latently infected cells by latency reversing agents (LRAs) and eliminate these reactivated cells by strategies involving the host immune system [18, 21]. Other therapeutic initiatives include developing an HIV-1 vaccine, both therapeutic and prophylactic vaccines, and increase antiviral immune protection to establish post cART control for patients [18, 14, 22]. The goal of these therapeutic initiatives either being a complete sterilizing cure where the virus is eradicated or a functional cure

where the virus is permanently suppressed in the absence of cART [14, 15].

The brain is a natural anatomical reservoir for HIV-1 infection [23, 24]. The brain is devoid of in situ adaptive immune responses and the blood-brain barrier (BBB) restricts antiretroviral agents from entering the brain [24]. Evidence shows HIV-1 can enter the brain through trafficking infected macrophages [25, 26, 27]. Brain macrophages, including microglia and perivascular macrophages, display productive HIV-1 infections [23]. Brain macrophages are long-lived cells [28]. Infected brain macrophages can cause neurological damage by direct and indirect mechanisms [26]. Despite effective cART in the plasma, HIV-1 infection can lead to neurological disorders including HIV-associated neurocognitive disorders (HAND) [29]. The extent of cART's impact on the brain viral reservoir is still under investigation. Certain experimental and clinical studies have suggested that cART is capable of reducing viral replication, viral RNA, in brain but exerts little impact on HIV-1 and SIV viral DNA levels in the brain [30, 31], and we have published experimental and clinical evidence that cART has had diminutive impact on both viral RNA and DNA levels in the brain [7].

In a recent simian immunodeficiency virus (SIV) study using the "Shock and Kill" therapy, LRA treatment reactivated latent virus that could be detected in the brain [32]. The authors of the SIV study caution that certain LRA treatment may cause harmful inflammatory responses in the brain even in the presence of cART [32]. This study emphasizes the key medical problem of determining the dynamics of LRA treatment in the brain viral reservoir.

In the plasma, cytotoxic T lymphocytes (CTL), both cytotoxic CD8 T lymphocytes (CD8 CTL) and cytotoxic CD4 T lymphocytes (CD4 CTL), are the main adaptive branch of the immune system that eliminate virus-infected

cells [33, 34, 35, 36, 37]. Precursor CD8 CTLs and precursor CD4 CTLs are cells that terminally differentiate into effector CD8 CTLs and effector CD4 CTLs, respectively [37, 38, 39]. Effector CD8 CTLs and effector CD4 CTLs have the capability to recognize and kill infected cells that produce viral antigens on MHC class I and MHC class II molecules, respectively [35, 36]. HIV-1 experiments have shown that the combined activity of HIV-1 specific effector CD4 CTLs and HIV-1 specific effector CD8 CTLs, through the killing of virus-infected cells, maintain viral clearance [40, 41].

Therapeutic initiatives for patients may be advanced by vital information from HIV-1 Elite Controllers [18, 42, 14]. HIV-1 Elite Controllers are HIV-1 infected patients that can naturally suppress viral replication to undetectable levels for extended periods of time without cART impeding the development of acquired immunodeficiency syndrome (AIDS) [18, 42]. There is evidence that the maintenance of HIV-1 specific effector CD4 CTLs in HIV-1 Elite Controllers along with HIV-1 specific effector CD8 CTLs contribute to their control of HIV-1 infection [41]. A crucial medical problem is determining the differences in the natural immune response of HIV-1 Elite Controllers in comparison to the natural immune response of typical HIV-1 patients.

Since the beginning of HIV-1 in 1981, mathematical models have been a core tool used to guide the effectiveness of drug therapy. Mathematical models can investigate the benefit of particular therapeutic strategies and they supply essential information for the design of future experiments and clinical trials [43].

1.A Review of previous mathematical models

1.A.1 Modeling HIV-1 brain infection

Prior mathematical models have aimed to measure the dynamics of HIV-1 infection by modeling the compartments of peripheral blood, lymph nodes, and the central nervous system (CNS) together [44, 45, 46]. One study modeled the migration of monocytes from the peripheral blood to the CNS but the progression of the disease within the CNS was not modeled [44]. Another study created a model including the dynamics of uninfected monocytes, infected monocytes, uninfected macrophages, and infected macrophages in the CNS but the formulation of the model in the CNS was unclear and the CNS dynamics were not fit to CNS data [45]. A third study created a model that connected the same ODE model to each compartment of peripheral blood, lymph nodes, and the brain together but this model did not consider that the same ODE model located in each compartment was not biologically appropriate and their model displays incorrect solutions in the brain based off of current knowledge about brain derived tissue data [46].

We published the first mathematical model to quantify HIV-1 and SIV infection dynamics in the brain based off of the current biology and brain derived tissue data [1]. In our model, the brain macrophage population was divided into two compartments: susceptible brain macrophages, x, and infected brain macrophages, y. Given the limited data at the time, the infected brain macrophage population, y, included productively and latently infected brain macrophages. HIV-1 and SIV infections of brain macrophages were assumed to spread principally through direct cell-to-cell interaction [26, 47]. Although the brain macrophage population differs in morphology and perhaps

cell density depending on the anatomic region, for this study, it was assumed to be uniform throughout the brain. We followed an established method of modeling direct transmission between two populations by using the rate βxy as the number of new infections per unit time, where β is the transmission coefficient [48, 49]. Without the presence of infection in the model, the number of susceptible brain macrophages was regulated at the equilibrium value $\frac{\lambda}{d}$, where λ was the source of new susceptible brain macrophages and k was the natural death rate for brain macrophages. Susceptible and infected brain macrophages were presumed to have the same death rate k because our group's earlier studies did not observe increased cellular death in HIV-infected versus uninfected brain macrophages [50]. We considered the percentage of cART effectiveness $\epsilon \times 100\%$, where $0 \leq \epsilon \leq 1$. The parameter ϵ was set to zero when there was no treatment, and $\beta_\epsilon = (1-\epsilon)\beta$ was the effective transmission coefficient under cART with effectiveness ϵ. The model was described by the following set of ODEs:

$$\begin{aligned} \frac{dx}{dt} &= \lambda - kx - (1-\epsilon)\beta xy = \lambda - kx - \beta_\epsilon xy \\ \frac{dy}{dt} &= (1-\epsilon)\beta xy - ky = \beta_\epsilon xy - ky \end{aligned} \tag{1.1}$$

Our model estimation indicated that HIV-1 and SIV proviral burdens in the brain increase much slower over time in comparison to the proviral burden among T cells in the peripheral blood.

With the availability of both brain viral DNA and brain viral RNA data, we further published another mathematical model that was used to analyze the dynamics of latently and productively infected brain macrophages during viral infection, and this mathematical model enabled prediction of the effects

of LRAs applied to the "Shock and Kill" strategy in the brain [4]. Chapters 4 and 5 present this study.

In between the publication of our first [1] and second [4] HIV-1 and SIV brain infection modeling studies, another study modeled HIV-1 brain infection with an ODE model connecting plasma, cerebrospinal fluid (CSF), and BBB together to infer the brain macrophage population dynamics [51]. The model in their study was fit to plasma viral load and CSF viral load data coming from three rhesus macaques infected with a mixture of simian-human immunodeficiency virus (SHIV) and SIV, but it was not fit to brain derived tissue data. The idea of including uninfected and infected trafficking macrophages back and forth through the BBB in the mathematical model is intriguing in this study and it is an important modeling endeavor to explore. However, the distinction between infection in brain tissue and infection in CSF is not clear in this study and the CSF data is used to mainly infer what is occurring inside the brain as a whole rather than using CSF data and brain derived tissue data to more accurately describe the infection dynamics in the brain.

1.A.2 Modeling HIV-1 Elite Controllers

The earliest mathematical model of HIV-1 infection in the plasma that attempted to explain the phenomenon of Elite Controllers was developed by Dominik Wodarz and Martin Nowak [52]. It is an ODE model with the following four compartments: susceptible CD4 T cells, x; HIV-1 infected CD4 T cells, y; precursor CTLs, w_p; and effector CTLs, w. It is assumed that the CD4 T cells are produced at a constant rate λ and become infected by free virus at a rate βxy, though no viral compartment is included. Infected CD4 T

cells are killed by CTL effectors at the rate γyw. Proliferation of the precursor CTL population is based on the help of CD4 T cells and the size of the HIV-1 infected CD4 T cell population, $cxyw_p$, and effector CTLs are stimulated based on the size of the HIV-1 infected cell and precursor CTL populations, $cqyw_p$. The μ variables are the death rates of the respective populations. The ODE model is the following:

$$\begin{aligned}
\frac{dx}{dt} &= \lambda - \mu_x x - \beta xy \\
\frac{dy}{dt} &= \beta xy - \mu_y y - \gamma yw \\
\frac{dw_p}{dt} &= cxyw_p - cqyw_p - \mu_{w_p} w_p \\
\frac{dw}{dt} &= cqyw_p - \mu_w w.
\end{aligned} \tag{1.2}$$

The authors mention that the equilibrium with sustained precursor and effector CTL populations and viral load at a low level may be attributed to HIV-1 Elite Controllers.

The first author on this study published a further expansion of this model that included two types of CTL responses: a helper-independent response and a helper-dependent response [53]. The helper-independent effector CTLs, w_1, are stimulated based on the size of the HIV-1 infected cell and helper-independent effector CTL populations, $c_1 y w_1$ whereas the helper-dependent effector CTLs, w_2, are stimulated based on the size of the HIV-1 infected cell and precursor CTL populations, $c_2 qyw_p$. It is assumed in the model that the helper-independent effector CTLs are short lived in comparison to the precursor CTL population with $\frac{1}{\mu_{w_p}} > \frac{1}{\mu_{w_1}}$. The ODE model is the following:

$$
\begin{aligned}
\frac{dx}{dt} &= \lambda - \mu_x x - \beta xy \\
\frac{dy}{dt} &= \beta xy - \mu_y y - \gamma_1 y w_1 - \gamma_2 y w_2 \\
\frac{dw_1}{dt} &= c_1 y w_1 - \mu_{w_1} w_1 \\
\frac{dw_p}{dt} &= c_2 x y w_p - c_2 q y w_p - \mu_{w_p} w_p \\
\frac{dw_2}{dt} &= c_2 q y w_p - \mu_w w_2.
\end{aligned}
\tag{1.3}
$$

A couple other theoretical mathematical models used ODE system 1.2 or 1.3 to justify their next step in modeling HIV-1 Elite Controllers [54, 55]. System 1.2, 1.3, and other theoretical ODE models based off of this system [54, 55] have not been fit to empiric data for a HIV-1 Elite Controller.

A later mathematical model that was fit to empiric data for a untreated HIV-1 Elite Controller transplant patient was an ODE model with the following six compartments: susceptible CD4 T cells, x; HIV-1 infected CD4 T cells, y_1; productively HIV-1 infected CD4 T cells, y_2; long-lived HIV-1 infected cells, M^*; HIV-1 specific effector CD8 CTLs, z_E; and virus, v. [56] The ODE model is the following:

$$
\begin{aligned}
\frac{dx}{dt} &= rx\left(1 - \frac{x + y_1 + y_2}{x_{max}}\right) - \beta_1 vx - \mu_x x H(t_1 - t) \\
\frac{dy_1}{dt} &= \beta_1 vx - \gamma_1 z_E y_1 - \alpha y_1 \\
\frac{dy_2}{dt} &= \alpha y_1 - \gamma_2 z_E y_2 - \mu_{y_2} y_2 \\
\frac{dM^*}{dt} &= \beta_2 vM - \gamma_3 z_E M^* - \mu_{M^*} M^* \\
\frac{dz_E}{dt} &= q\frac{(I_1 + I_2 + M^*) z_E}{k + z_E} \\
\frac{dv}{dt} &= p_1 y_2 + p_2 M^* - \mu_v v.
\end{aligned}
\tag{1.4}
$$

Since the authors were interested in early infection dynamics after the transplant, the population of susceptible long-lived cells M was set to a constant value. This model includes a logistic growth term for the growth of susceptible CD4 T cells, a Heaviside function

$$
H(t_1 - t) = \begin{cases} 1 & 0 \leq t < t_1 \\ 0 & t \geq t_1 \end{cases}
$$

multiplied to the death of susceptible CD4 T cells to model the drop of CD4 T cells during the first six days after the transplant, $t_1 = 6$, and a Monod function for modeling the saturation effect of the HIV-1 specific effector CD8 CTLs. CD4 T cells and long-lived cells become infected by virus-to-cell infections with the transmission rates β_1 and β_2, respectively. The μ variables are the death rates of the respective populations. Productively infected CD4 T cells and infected long-lived cells produce new virus at the rates p_1 and p_2, respectively. HIV-1 specific effector CD8 CTLs kill HIV-1 infected CD4 T cells, productively HIV-1 infected infected CD4 T cells, and HIV-1 infected long-lived cells at the

rates γ_1, γ_2, and γ_3 respectively.

The initial transplant for the untreated HIV-1 Elite Controller caused their viral load to increase and afterward their immune system was capable of suppressing the virus. There was about a year of empiric data on the HIV-1 Elite Controller patient presented in the study. System 1.4 fit to the empiric data revealed that the untreated HIV-1 Elite Controller suppressed the virus at rates equivalent to an untreated patient starting cART.

1.B Themes and objectives

1.B.1 Modeling HIV-1 and SIV brain infection

There are very few studies that quantify data for HIV-1 and SIV infection in the brain. The difficulty of separating the population of latently and productively infected brain macrophages using a mathematical model is dependent on the available data. Since there is minimal knowledge regarding the duration of infection for each HIV-1 patient, it was tougher to separate the population of latently and productively infected brain macrophages for HIV-1 patients than for SIV animal models where the duration of infection and start of treatment is known.

The main objectives of this topic were to develop a mathematical model of latently and productively infected cells in the brain for HIV-1 patients and SIV animal models and to simulate the "Shock and Kill" therapy in the brain using the developed mathematical model.

This was the first mathematical model to qualitatively analyze the dynamics of latently and productively infected cells in the brain during HIV-1 and

SIV infection and to quantify the size of the latent reservoir in the brain for SIV animal studies. Furthermore, after this latent reservoir was estimated, the effect of LRA in the brain was evaluated and the mathematical model indicated that there exists a biologically realistic parameter regime where the "Shock and Kill" therapy strategy is safe and effective in the brain.

1.B.2 Modeling the natural control of HIV-1 in the plasma

The biological theory for how HIV-1 Elite Controllers suppress the virus naturally with their own immune system is still under development and there is evidence that the maintenance of HIV-1 specific effector CD4 CTLs in HIV-1 Elite Controllers along with HIV-1 specific effector CD8 CTLs contribute to their control of HIV-1 infection [41]. Unique attempts to explain mathematically how HIV-1 Elite Controllers suppress the virus naturally are sparse [52, 53, 54, 55, 56]. It was challenging to create a mathematical model to describe the important attributes of the immune system to effectively compare HIV-1 Elite Controllers with other HIV-1 patients.

The main objectives of this topic were to formulate a mathematical model for HIV-1 infection dynamics in the plasma with natural immune responses, fit this mathematical model to historical data for HIV-1 Elite Controllers and a comparison group of HIV-1 patients, and discern the difference in dynamics and natural immune responses between patients.

This was the first mathematical modeling study to directly estimate the differences between a group of HIV-1 Elite Controllers with a comparison group of HIV-1 patients using empiric data and it is also the first HIV-1

mathematical model to consider both effector CD4 CTLs' and effector CD8 CTLs' impact on HIV-1 disease and other diseases present in each patient. The Elite Controller group was found to have a stronger antiviral immune response than the comparison group. In contrast, the comparison group was found to have more chronic immune activation but a less effective immune response. The Elite Controller immune response estimates given in this study quantifies a biologically realistic optimal immune response goal for HIV-1 therapeutic initiatives.

1.C Methods

1.C.1 Modeling HIV-1 and SIV brain infection

Data was collected from research literature, which measured SIV viral RNA and SIV viral DNA in monkey brains at different time points. The monkeys were either untreated or treated at the time of collection. This data was used for fitting the mathematical models.

Mathematical models were developed that include three cell populations: uninfected brain macrophages, productively infected, and latently infected brain macrophages. These models incorporated the effect of cART and these models qualitatively analyzed the dynamics of latently and productively infected cells in the brain during HIV-1 and SIV infection. The models were used to quantify the size of the latent reservoir in the brain for SIV infected animals. Furthermore, the "Shock and Kill" therapy on the brain macrophage population was simulated using the model.

Bayesian inference and Markov Chain Monte Carlo (MCMC) sampling

methods were used to fit the mathematical model to the data and obtain best-fit values and 95% credible intervals for the model parameters and prediction intervals for the model solutions. Mathematical models were calibrated and simulated using the software MATLAB. Model outcomes were used to estimate the progression of latently and productively infected brain macrophages, the size of the reservoir given cART effectiveness, and reactivation rate and additional kill rate needed to eliminate the burden of infected brain macrophages using the "Shock and Kill" therapy.

1.C.2 Modeling the natural control of HIV-1 in the plasma

Data was provided by the Northern Alberta HIV Program, which measured viral load, total CD4 T cells, and total CD8 T cells for HIV-1 infection in the plasma for HIV-1 Elite Controllers and a comparison group of HIV-1 patients at different time points. The ART-naïve (no previous ART had been taken) time period in the data for each patient was used for fitting the mathematical model.

A mathematical model was formulated that incorporated the viral dynamics and the natural immune response of CD4 and CD8 T cells. This model was used to estimate the differences in immune response and dynamics between HIV-1 Elite Controllers and a comparison group of HIV-1 patients.

Similarly, Bayesian inference and diffusive nested sampling methods were used to fit the mathematical model to the data and mathematical models were calibrated and simulated using the software MATLAB. Model outcomes were used to estimate the dynamics of the host immune responses for HIV-1

Elite Controllers and a comparison group of HIV-1 patients and fitted model parameters were used to discern the important differences in how the immune system behaved.

1.D Chapter overview

Chapters 2 and 3 of this thesis describes the Bayesian inference tools that were used to fit the brain macrophage infection model with cART (4.1) and the plasma infection model with natural immune responses (6.1) to data. Chapter 2 is based on the "Bayesian inference for dynamical systems" paper published in the journal *Infectious Disease Modelling* in 2020 [2]. Section 3.C contains a Bayesian inference Diffusive Nested Sampling example that uses the MATLAB implementation of the DNS algorithm called "MatlabDiffNestAlg" [9].

Chapter 4 is about modeling the progression of the latent HIV-1 and SIV brain viral reservoir and simulating the "Shock and Kill" therapy. Chapter 5 contains further details about the HIV-1 brain macrophage infection model with cART (4.1) and the HIV-1 brain macrophage infection model with cART and "Shock and Kill" therapy (4.5). Chapter 6 is about estimating and predicting HIV-1 infection in the plasma for HIV-1 Elite Controllers and a comparison group of HIV-1 patients from the Northern Alberta HIV Program. Chapter 7 contains supplementary material about the HIV-1 plasma infection model with natural immune responses (6.1). Chapter 8 is the conclusion of the thesis.

Chapter 2

Bayesian inference for dynamical systems

2.A Introduction

A common method for performing parameter estimation for dynamical systems is to use Bayesian inference [57, 58, 59, 60, 61]. Despite the popularity of using Bayesian inference for performing parameter estimation for dynamical systems and useful computational manuals, there is a need for a formalized and comprehensive methodology.

The methods described in this paper assume that the behaviors of the dynamical system of interest have been mathematically analyzed and that the solutions of the dynamical system are well-behaved. Additionally, it is assumed that if a numerical scheme is being used to solve the dynamical system that the numerical scheme is stable. The methodology is presented from a mathematical biology perspective and it will focus on systems of ordinary differential equations (ODEs); however, the Bayesian inference methodology

presented can be applied to other areas of applied mathematics and other differential equations systems such as partial differential equations (PDEs). This paper will provide a formalized methodology for dynamical system parameter estimation using Bayesian inference and it will cover utilizing different distributions, Markov Chain Monte Carlo (MCMC) sampling, obtaining credible intervals for parameters, and prediction intervals for solutions. The methodology is illustrated by using a logistic growth example.

2.B Dynamical system

Assume that the dynamical system of interest can be described by the following autonomous ODE system (2.1) written as a vector differential equation:

$$\mathbf{x}' = \mathbf{f}(\mathbf{x}), \tag{2.1}$$

where $\mathbf{x} = \langle x_1, \ldots, x_k \rangle$ and $\mathbf{f} = \langle f_1(\mathbf{x}), \ldots, f_k(\mathbf{x}) \rangle$, with the vector of initial conditions $\mathbf{x}_0 = \langle x_1^0, \ldots, x_k^0 \rangle$.

It is assumed that the that the unique solution vector, $\mathbf{x}(t)$, of system (2.1) exists and can be obtained either explicitly or using numerical approximation. If a numerical approximation method is used, it is assumed that the numerical approximation scheme is stable.

All the parameters in system (2.1) will be denoted by the vector $\boldsymbol{\beta}$. If the initial conditions $x_1^0, \ldots, x_k^0$ will also be estimated, then let the initial conditions $x_1^0, \ldots, x_k^0$ be contained in vector $\boldsymbol{\beta}$ as well.

The dependence of the unique solution vector $\mathbf{x}$ on both time, t, and the vector of parameters, $\boldsymbol{\beta}$, will be emphasized and the unique solution vector

will be denoted as $\mathbf{x}(\boldsymbol{\beta}, t)$.

2.C Data

Suppose there are m data sets. It is important to ensure that the correct ODE model solution or combination of ODE model solutions is fit to the j^{th} data set ($j = 1, \ldots, m$).

Sometimes a data set is scaled differently than the model solutions or the data set can be described by a summation of the ODE model solutions. In order to include these situations, we can use a linear combination of the ODE model solutions, $a_1^j x_1(\boldsymbol{\beta}, t) + \cdots + a_k^j x_k(\boldsymbol{\beta}, t)$, to fit to the j^{th} data set. (The simpler case where only the i^{th} specific ODE model solution $x_i(\boldsymbol{\beta}, t)$ is to be fit to the j^{th} data set, is included in the linear combination where $a_i^j = 1$ and the other constants are zero.) If the nonzero vector of constants, $\mathbf{a}^j$, will be estimated, then let the nonzero vector of constants, $\mathbf{a}^j$, for $j = 1, \ldots m$, be contained in vector

$$\boldsymbol{\nu} = \begin{bmatrix} \boldsymbol{\beta} \\ \mathbf{a}^1 \\ \vdots \\ \mathbf{a}^m \end{bmatrix}.$$

Also, if the j^{th} data set can be described by a nonlinear combination of the ODE model solutions, then, similarly, let any estimated nonzero vector of constants, $\mathbf{a}^j$, be contained in vector

$$\boldsymbol{\nu} = \begin{bmatrix} \boldsymbol{\beta} \\ \mathbf{a}^1 \\ \vdots \\ \mathbf{a}^m \end{bmatrix}.$$

So, in general, we fit the function, $F(x_1(\boldsymbol{\beta}, t_i^j), ..., x_k(\boldsymbol{\beta}, t_i^j), \mathbf{a}^1, ..., \mathbf{a}^m)$, to the j^{th} data set.

2.D Distribution of data over time

The distribution of the observations over time for each j^{th} data set must be chosen before fitting system (2.1) to the data. The following sections will describe the Gaussian, Poisson, Negative Binomial, and other distribution options.

2.D.1 Gaussian distribution

Let Y be a random variable from the Gaussian distribution with parameters μ and $\sigma^2 = \frac{1}{\tau} > 0$, $Y \sim \mathrm{N}(\mu, \theta^2)$. The formulation of the Gaussian distribution is given by the following continuous probability density function (pdf), $f(y)$ [62]:

$$f(y) = \frac{1}{\sqrt{2\pi\sigma^2}} \exp(-\frac{1}{2\sigma^2}(y-\mu)^2) = \sqrt{\frac{\tau}{2\pi}} \exp(-\frac{1}{2}\tau(y-\mu)^2) \tag{2.2}$$

The mean, $\mathrm{E}[Y]$, of the Gaussian distribution is given by μ and the variance, $\mathrm{Var}[Y]$, of this distribution is given by $\sigma^2 = \frac{1}{\tau}$.

Assume that the j^{th} data set is given by observations $D_j = \{d_1^j, \ldots, d_{n_j}^j\}$

with corresponding times $T_j = \{t_1^j, \ldots, t_{n_j}^j\}$ and that the probability of observing d_i^j is given by the Gaussian distribution:

$$f(d_i^j) = \sqrt{\frac{\tau^j}{2\pi}} \exp(-\frac{1}{2}\tau^j (d_i^j - \mu_i^j)^2) \tag{2.3}$$

where the mean μ_i^j changes depending on the time, t_i^j and the variance $\frac{1}{\tau^j}$ is specific to the j^{th} data set.

Given our assumption of fitting the function of the ODE model solutions and any necessary constants, $F(x_1(\boldsymbol{\beta}, t_i^j), ..., x_k(\boldsymbol{\beta}, t_i^j), \mathbf{a}^1, ..., \mathbf{a}^m)$, to the j^{th} data set, we set

$$E[D_i^j] = \mu_i^j = F(x_1(\boldsymbol{\beta}, t_i^j), ..., x_k(\boldsymbol{\beta}, t_i^j), \mathbf{a}^1, ..., \mathbf{a}^m). \tag{2.4}$$

Equation (2.4) can be thought of as a type of link function. In statistics, for generalized linear models (GLMs), a link function is defined as the function that transforms the mean of a distribution to a linear regression model [63]. Equation (2.4) equates the mean of the Gaussian distribution to the ODE model solutions.

2.D.2 Gaussian distribution with non-constant variance over time

Assume that the j^{th} data set is given by observations $D_j = \{d_1^j, \ldots, d_{n_j}^j\}$ with corresponding times $T_j = \{t_1^j, \ldots, t_{n_j}^j\}$ and that the probability of observing d_i^j is given by the Gaussian distribution with non-constant variance:

$$f(d_i^j) = \sqrt{\frac{\tau_i^j}{2\pi}} \exp(-\frac{1}{2}\tau_i^j (d_i^j - \mu_i^j)^2) \tag{2.5}$$

with the mean μ_i^j, the variance $\frac{1}{\tau_i^j}$ is given by $\frac{1}{\tau_i^j} = v^j g(\mu_i^r)$, $v^j > 0$ is a constant, and $g(\mu_i^r)$ is a positive function of the mean μ_i^r from the r^{th} data set, for some $r \in \{1, \ldots, m\}$. Here both the mean μ_i^j and the variance $\frac{1}{\tau_i^j} = v^j g(\mu_i^r)$ change depending on the time t_i and r is chosen from among the m data sets.

Given our assumption of fitting the function of the ODE model solutions and any necessary constants, $F(x_1(\boldsymbol{\beta}, t_i^j), ..., x_k(\boldsymbol{\beta}, t_i^j), \mathbf{a}^1, ..., \mathbf{a}^m)$, to the j^{th} data set, we set

We will use equation (2.4) to equate the mean, $E[D_i^j] = \mu_i^j$, to the ODE model solutions. Equation (2.4) equates the mean of the Gaussian distribution with non-constant variance to the ODE model solution(s).

2.D.3 Poisson distribution

Let Y be a random variable from the Poisson distribution with parameter $\mu > 0$, $Y \sim \text{POI}(\mu)$. The formulation of the Poisson distribution is given by the following discrete pdf, $f(y)$ [62]:

$$f(y) = \frac{\exp(-\mu)\mu^y}{y!} \tag{2.6}$$

where $y = 0, 1, \ldots$.

The mean, E[Y], of the Poisson distribution is given by μ. For the Poisson distribution, the variance is equal to the mean, Var[Y] = E[Y] = μ.

Assume that the j^{th} data set is given by observations $D_j = \{d_1^j, \ldots, d_{n_j}^j\}$ with corresponding times $T_j = \{t_1^j, \ldots, t_{n_j}^j\}$ and that the probability of observing d_i^j is given by the Poisson distribution:

$$f(d_i^j) = \frac{\exp(-\mu_i^j)\mu_i^{j(d_i^j)}}{d_i^j!} \tag{2.7}$$

where the mean $E[D_i^j] = \mu_i^j$ changes depending on the time, t_i^j. Hence, the variance, $\mathrm{Var}[D_i^j] = \mathrm{E}[D_i^j] = \mu_i^j$, also changes over time.

Again, we will use equation (2.4) to equate the mean, $E[D_i^j] = \mu_i^j$, to the ODE model solutions.

The Poisson distribution is used for count data of rare events. The fact that the variance is dependent on the mean is particularly useful since in practice when observing count data over time the count data generally expresses more variability at higher values than at lower values [64]. The restriction that the variance is strictly equal to the mean is commonly violated for many types of count data. Count data where the variance is larger than the mean is called overdispersed. The negative binomial distribution can be used for count data with overdispersion.

2.D.4 Negative binomial distribution

Let Y be a random variable from the negative binomial distribution with parameters $0 < p < 1$ and $r \geq 0$, $Y \sim \mathrm{NB}(r, p)$. The formulation of the negative binomial distribution is given by the following discrete pdf, $f(y)$ [65]:

$$f(y) = \frac{\Gamma(y+r)}{y!\,\Gamma(r)} p^r (1-p)^y \tag{2.8}$$

where $y = 0, 1, 2 \ldots$.

The interpretation of this formulation of the negative binomial distribution is that y are the number of failures before the r^{th} success and p is the probability of success per trial [65].

The mean, $\mathrm{E}[Y]$, of the negative binomial distribution is given by $\mu = \frac{r(1-p)}{p}$ and the variance, $\mathrm{Var}[Y]$, of this distribution is given by

$\sigma^2 = \frac{r(1-p)}{p^2} = \frac{\mu}{p}$.

For count data, the negative binomial distribution can be interpreted as the mean number of counts $\mathrm{E}[Y] = \mu$ with the variance $\mathrm{Var}[Y] = \frac{\mu}{p}$ overdispersed, since $0 < p < 1$, $\mathrm{Var}[Y] > \mathrm{E}[Y]$ [64].

Assume that the j^{th} data set is given by observations $D_j = \{d_1^j, \ldots, d_{n_j}^j\}$ with corresponding times $T_j = \{t_1^j, \ldots, t_{n_j}^j\}$ and that the probability of observing d_i^j is given by the negative binomial distribution:

$$f(d_i^j) = \frac{\Gamma(d_i^j + r_i^j)}{d_i^j!\,\Gamma(r_i^j)}(p^j)^{(r_i^j)}(1-p^j)^{d_i^j} \tag{2.9}$$

where $r_i^j = \frac{(p^j)(\mu_i^j)}{1-(p^j)} \iff \mu_i^j = \frac{(r_i^j)(1-p^j)}{p^j}$ changes depending on the time, t_i^j and p^j is specific to the j^{th} data set. Hence, the variance, $\mathrm{Var}[D_i^j] = \frac{\mu_i^j}{p^j}$, also changes over time.

As before, we will use equation (2.4) to equate the mean, $E[D_i^j] = \mu_i^j$, to the ODE model solutions.

2.D.5 Other distributions

It is seen from Sections 2.D.1, 2.D.3, and 2.D.4 that in general if the j^{th} data set is given by observations $D_j = \{d_1^j, \ldots, d_{n_j}^j\}$ with corresponding times $T_j = \{t_1^j, \ldots, t_{n_j}^j\}$ and the probability of observing d_i^j is given by the distribution with pdf $f(d_i^j)$ with mean $E[D_i^j] = \mu_i^j$, then equation (2.4) is used to equate the mean, $E[D_i^j] = \mu_i^j$, to the ODE model solutions.

2.E Likelihood function

In a dynamical system, the dependency of solutions $x_1, \ldots, x_k$ on each other is built into the mathematical model itself. Assuming that the mathematical model correctly describes the data sets of interest, the data sets can be considered independent from each other. With m independent data sets, there will be m likelihood functions associated with each of the independent data sets and the combined likelihood function is given by

$$L(\boldsymbol{\theta}) = CL_1(\boldsymbol{\theta}) \cdot \ldots \cdot L_m(\boldsymbol{\theta}) \tag{2.10}$$

where θ is the vector of parameters to estimate, and C is any positive constant not depending on θ used to simplify the likelihood function [66].

2.E.1 Gaussian probability model for m data sets and combined likelihood function

Assume, for $j = 1, \ldots, m$, that the j^{th} data set is given by observations $D_j = \{d_1^j, \ldots, d_{n_j}^j\}$ with corresponding times $T_j = \{t_1^j, \ldots, t_{n_j}^j\}$ and that the probability of observing d_i^j is given by the Gaussian distribution in equation (2.3) where the mean μ_i^j changes depending on the time, t_i^j and the variance $\frac{1}{\tau^j} > 0$ is specific to the j^{th} data set. Then the probability of the observed counts $D = \{D_1, \ldots, D_m\}$ is given by

$$P(D|\boldsymbol{\theta}) = \prod_{j=1}^{m}\prod_{i=1}^{n_j}\sqrt{\frac{\tau^j}{2\pi}}\exp(-\frac{1}{2}\tau^j(d_i^j-\mu_i^j)^2)$$
$$= (\frac{1}{2\pi})^{(\sum_{j=1}^{m}\frac{n_j}{2})}(\tau^1)^{\frac{n_1}{2}}\cdot\ldots\cdot(\tau^m)^{\frac{n_m}{2}}\exp(-\frac{1}{2}\sum_{j=1}^{m}\tau^j\sum_{i=1}^{n_j}(d_i^j-\mu_i^j)^2) \tag{2.11}$$

where equation (2.4) is used to equate the mean, μ_i^j, to the ODE model solutions and

$$\boldsymbol{\theta} = \begin{bmatrix} \boldsymbol{\nu} \\ \tau^1 \\ \vdots \\ \tau^m \end{bmatrix}.$$

The Gaussian probability model is very beneficial for fitting since even poor initial guesses of the vector of parameters, $\boldsymbol{\theta}$, will still produce a nonzero probability.

The combined likelihood function is given by

$$L(\boldsymbol{\theta}) = C(\frac{1}{2\pi})^{(\sum_{j=1}^{m}\frac{n_j}{2})}(\tau^1)^{\frac{n_1}{2}}\cdot\ldots\cdot(\tau^m)^{\frac{n_m}{2}}\exp(-\frac{1}{2}\sum_{j=1}^{m}\tau^j\sum_{i=1}^{n_j}(d_i^j-\mu_i^j)^2)$$
$$= (\tau^1)^{\frac{n_1}{2}}\cdot\ldots\cdot(\tau^m)^{\frac{n_m}{2}}\exp(-\frac{1}{2}\sum_{j=1}^{m}\tau^j\sum_{i=1}^{n_j}(d_i^j-\mu_i^j)^2) \tag{2.12}$$

where C = $(\frac{1}{2\pi})^{(-\sum_{j=1}^{m}\frac{n_j}{2})}$ simplifies the likelihood function. The value of $\boldsymbol{\theta}$ that maximizes $P(D|\boldsymbol{\theta})$ will also maximize $L(\boldsymbol{\theta})$ [66].

The combined log likelihood function is given by

$$\log(L(\boldsymbol{\theta})) = \frac{n_1}{2}\log(\tau^1) + \ldots + \frac{n_m}{2}\log(\tau^m) - \frac{1}{2}\sum_{j=1}^{m}\tau^j\sum_{i=1}^{n_j}(d_i^j - \mu_i^j)^2) \qquad (2.13)$$

the value of $\boldsymbol{\theta}$ that maximizes $\log(L(\boldsymbol{\theta}))$ will also maximize $L(\boldsymbol{\theta})$ [66].

2.E.2 Gaussian probability model with non-constant variance over time for m data sets and combined likelihood function

Assume, for $j = 1, \ldots, m$, that the j^{th} data set is given by observations $D_j = \{d_1^j, \ldots, d_{n_j}^j\}$ with corresponding times $T_j = \{t_1^j, \ldots, t_{n_j}^j\}$ and that the probability of observing d_i^j is given by the Gaussian distribution with non-constant variance in equation (2.3) where the mean μ_i^j and variance $\frac{1}{\tau_i^j}$ changes depending on the time, t_i^j, and the variance $\frac{1}{\tau_i^j} = v^j g(\mu_i^r)$ is specific to the j^{th} data set and the positive function g depends on the mean μ_i^r from the r^{th} data set, for some $r \in \{1, \ldots, m\}$. For clarity, we will assume that the same $g(\mu_i^r)$ function is assumed for each j^{th} data set, though the function and value of r could vary for each j^{th} data set, $g_j(\mu_i^{r_j})$. Then the probability of the observed counts $D = \{D_1, \ldots, D_m\}$ is given by

$$
\begin{aligned}
P(D|\boldsymbol{\theta}) &= \prod_{j=1}^{m}\prod_{i=1}^{n_j}\sqrt{\frac{\tau_i^j}{2\pi}}\exp\left(-\frac{1}{2}\tau_i^j(d_i^j-\mu_i^j)^2\right) \\
&= \left(\frac{1}{2\pi}\right)^{(\sum_{j=1}^{m}\frac{n_j}{2})}\left(\prod_{j=1}^{m}\prod_{i=1}^{n_j}\tau_i^j\right)^{1/2}\exp\left(-\frac{1}{2}\sum_{j=1}^{m}\sum_{i=1}^{n_j}\tau_i^j(d_i^j-\mu_i^j)^2\right) \\
&= \left(\frac{1}{2\pi}\right)^{(\sum_{j=1}^{m}\frac{n_j}{2})}\left(\prod_{j=1}^{m}\prod_{i=1}^{n_j}v^j g(\mu_i^r)\right)^{-1/2}\exp\left(-\frac{1}{2}\sum_{j=1}^{m}\sum_{i=1}^{n_j}(v^j g(\mu_i^r))^{-1}(d_i^j-\mu_i^j)^2\right)
\end{aligned}
\tag{2.14}
$$

where equation (2.4) is used to equate the mean, μ_i^j, to the ODE model solutions and

$$
\boldsymbol{\theta} = \begin{bmatrix} \boldsymbol{\nu} \\ v^1 \\ \vdots \\ v^m \end{bmatrix}.
$$

The combined likelihood function is given by

$$
\begin{aligned}
L(\boldsymbol{\theta}) &= C\left(\frac{1}{2\pi}\right)^{(\sum_{j=1}^{m}\frac{n_j}{2})}\left(\prod_{j=1}^{m}\prod_{i=1}^{n_j}v^j g(\mu_i^r)\right)^{-1/2}\exp\left(-\frac{1}{2}\sum_{j=1}^{m}\sum_{i=1}^{n_j}(v^j g(\mu_i^r))^{-1}(d_i^j-\mu_i^j)^2\right) \\
&= \left(\prod_{j=1}^{m}\prod_{i=1}^{n_j}v^j g(\mu_i^r)\right)^{-1/2}\exp\left(-\frac{1}{2}\sum_{j=1}^{m}\sum_{i=1}^{n_j}(v^j g(\mu_i^r))^{-1}(d_i^j-\mu_i^j)^2\right)
\end{aligned}
\tag{2.15}
$$

where $\mathrm{C} = \left(\frac{1}{2\pi}\right)^{-(\sum_{j=1}^{m}\frac{n_j}{2})}$ simplifies the likelihood function. The value of $\boldsymbol{\theta}$ that maximizes $P(D|\boldsymbol{\theta})$ will also maximize $L(\boldsymbol{\theta})$ [66].

The combined log likelihood function is given by

$$\log(L(\boldsymbol{\theta})) = -\frac{1}{2}\sum_{j=1}^{m}\sum_{i=1}^{n_j}\log(v^j g(\mu_i^r)) - \frac{1}{2}\sum_{j=1}^{m}(v^j)^{-1}\sum_{i=1}^{n_j}(g(\mu_i^r))^{-1}(d_i^j - \mu_i^j)^2 \tag{2.16}$$

the value of $\boldsymbol{\theta}$ that maximizes $\log(L(\boldsymbol{\theta}))$ will also maximize $L(\boldsymbol{\theta})$ [66].

If the m data sets have the same number of observations $n = n_1, \ldots, n_m$, then the combined likelihood function can be written in the following way

$$\begin{aligned} L(\boldsymbol{\theta}) &= \left(\prod_{j=1}^{m}\prod_{i=1}^{n} v_j g(\mu_i^r)\right)^{-1/2} \exp\left(-\frac{1}{2}\sum_{j=1}^{m}\sum_{i=1}^{n}(v_j g(\mu_i^r))^{-1}(d_i^j - \mu_i^j)^2\right) \\ &= \left(\prod_{j=1}^{m}\det(\mathrm{diag}(\boldsymbol{\tau}^j))\right)^{1/2} \exp\left(-\frac{1}{2}\mathrm{tr}\,(EA)\right) \end{aligned} \tag{2.17}$$

where

$$\boldsymbol{\tau}^j = \begin{bmatrix} (v^j g(\mu_1^r))^{-1} \\ \vdots \\ (v^j g(\mu_n^r))^{-1} \end{bmatrix},$$

$$\boldsymbol{\epsilon}^j = \begin{bmatrix} d_1^j - \mu_1^j \\ \vdots \\ d_n^j - \mu_n^j \end{bmatrix},$$

$$E = \begin{bmatrix} d_1^1 - \mu_1^1 & \ldots & d_n^1 - \mu_n^1 \\ \vdots & & \vdots \\ d_1^m - \mu_1^m & \ldots & d_n^m - \mu_n^m \end{bmatrix} = \begin{bmatrix} \boldsymbol{\epsilon}^{1'} \\ \vdots \\ \boldsymbol{\epsilon}^{m'} \end{bmatrix}, \text{ and}$$

$$A = \begin{bmatrix} (v^1 g(\mu_1^r))^{-1} & \ldots & (v^n g(\mu_1^r))^{-1} \\ \vdots & & \vdots \\ (v^1 g(\mu_n^r))^{-1} & \ldots & (v^n g(\mu_n^r))^{-1} \end{bmatrix} = \begin{bmatrix} \boldsymbol{\tau}^1 \ldots \boldsymbol{\tau}^m \end{bmatrix}$$

The equation (2.17) can be a helpful way to compute the likelihood computationally in terms of vectors and matrices.

2.E.3 Poisson probability model for m data sets and combined likelihood function

Assume, for $j = 1, \ldots, m$, that the j^{th} data set is given by observations $D_j = \{d_1^j, \ldots, d_{n_j}^j\}$ with corresponding times $T_j = \{t_1^j, \ldots, t_{n_j}^j\}$ and that the probability of observing d_i^j is given by the Poisson distribution in equation (2.7) where the mean μ_i^j (and hence the variance, μ_i^j) changes depending on the time, t_i^j. Then the probability of the observed counts $D = \{D_1, \ldots, D_m\}$ is given by

$$\begin{aligned} P(D|\boldsymbol{\theta}) &= \prod_{j=1}^{m}\prod_{i=1}^{n_j} \frac{\exp(-\mu_i^j){\mu_i^j}^{(d_i^j)}}{d_i^j!} \\ &= \frac{1}{d_1^1! \cdot \ldots \cdot d_{n_1}^1!} \cdot \ldots \cdot \frac{1}{d_1^m! \cdot \ldots \cdot d_{n_m}^m!} \exp(-\sum_{j=1}^{m}\sum_{i=1}^{n_j}\mu_i^j) \prod_{j=1}^{m}((\mu_1^j)^{d_1^j} \cdot \ldots \cdot (\mu_{n_j}^j)^{d_{n_j}^j}) \end{aligned} \tag{2.18}$$

where equation (2.4) is used to equate the mean, μ_i^j, to the ODE model solutions and $\boldsymbol{\theta} = \boldsymbol{\nu}$.

The combined likelihood function is given by

$$\begin{aligned} L(\boldsymbol{\theta}) &= C\frac{1}{d_1^1! \cdot \ldots \cdot d_{n_1}^1!} \cdot \ldots \cdot \frac{1}{d_1^m! \cdot \ldots \cdot d_{n_m}^m!} \exp(-\sum_{j=1}^{m}\sum_{i=1}^{n_j}\mu_i^j) \prod_{j=1}^{m}((\mu_1^j)^{d_1^j} \cdot \ldots \cdot (\mu_{n_j}^j)^{d_{n_j}^j}) \\ &= \exp(-\sum_{j=1}^{m}\sum_{i=1}^{n_j}\mu_i^j) \prod_{j=1}^{m}((\mu_1^j)^{d_1^j} \cdot \ldots \cdot (\mu_{n_j}^j)^{d_{n_j}^j}) \end{aligned} \tag{2.19}$$

where $\mathrm{C} = (d_1^1! \cdot \ldots \cdot d_{n_1}^1!) \cdot \ldots \cdot (d_1^m! \cdot \ldots \cdot d_{n_m}^m!)$ simplifies the likelihood function.

The combined log likelihood function is given by

$$\log(L(\boldsymbol{\theta})) = \sum_{j=1}^{m} \sum_{i=1}^{n_j} \log((\mu_i^j)^{d_i^j}) - \mu_i^j. \tag{2.20}$$

2.E.4 Negative binomial probability model for m data sets and combined likelihood function

Assume, for $j = 1, \ldots, m$, that the j^{th} data set is given by observations $D_j = \{d_1^j, \ldots, d_{n_j}^j\}$ with corresponding times $T_j = \{t_1^j, \ldots, t_{n_j}^j\}$ and that the probability of observing d_i^j is given by the negative binomial distribution in equation (2.9) where the mean μ_i^j (and hence the variance $\mathrm{Var}[D_i^j] = \frac{\mu_i^j}{p^j}$) changes depending on the time, t_i^j. Then the probability of the observed counts $D = \{D_1, \ldots, D_m\}$ is given by

$$\begin{aligned}
P(D|\boldsymbol{\theta}) &= \prod_{j=1}^{m} \prod_{i=1}^{n_j} \frac{\Gamma(d_i^j + r_i^j)}{d_i^j! \, \Gamma(r_i^j)} (p^j)^{(r_i^j)} (1-p^j)^{d_i^j} \\
&= \left(\frac{1}{d_1^1! \cdot \ldots \cdot d_{n_1}^1!} \cdot \ldots \cdot \frac{1}{d_1^m! \cdot \ldots \cdot d_{n_m}^m!} \right) \\
&\left(\frac{\Gamma(d_1^1 + r_1^1) \cdot \ldots \cdot \Gamma(d_{n_1}^1 + r_{n_1}^1)}{\Gamma(r_1^1) \cdot \ldots \cdot \Gamma(r_{n_1}^1)} \cdot \ldots \cdot \frac{\Gamma(d_1^m + r_1^m) \cdot \ldots \cdot \Gamma(d_{n_m}^m + r_{n_m}^m)}{\Gamma(r_1^m) \cdot \ldots \cdot \Gamma(r_{n_m}^m)} \right) \\
&\left((p^1)^{\sum_{i=1}^{n_1} r_i^j} \cdot \ldots \cdot (p^m)^{\sum_{i=1}^{n_m} r_i^j} \right) \left((1-p^1)^{\sum_{i=1}^{n_1} d_i^j} \cdot \ldots \cdot (1-p^m)^{\sum_{i=1}^{n_m} d_i^j} \right)
\end{aligned} \tag{2.21}$$

where $r_i^j = \frac{(p^j)(\mu_i^j)}{1-(p^j)} \iff \mu_i^j = \frac{(r_i^j)(1-p^j)}{p^j}$, the equation (2.4) is used to equate the mean, μ_i^j, to the ODE model solutions and

$$\boldsymbol{\theta} = \begin{bmatrix} \boldsymbol{\nu} \\ p^1 \\ \vdots \\ p^m \end{bmatrix}.$$

The combined likelihood function is given by

$$\begin{aligned} L(\boldsymbol{\theta}) = C &\left(\frac{1}{d_1^1! \cdot \ldots \cdot d_{n_1}^1!} \cdot \ldots \cdot \frac{1}{d_1^m! \cdot \ldots \cdot d_{n_m}^m!} \right) \\ &\left(\frac{\Gamma(d_1^1 + r_1^1) \cdot \ldots \cdot \Gamma(d_{n_1}^1 + r_{n_1}^1)}{\Gamma(r_1^1) \cdot \ldots \cdot \Gamma(r_{n_1}^1)} \cdot \ldots \cdot \frac{\Gamma(d_1^m + r_1^m) \cdot \ldots \cdot \Gamma(d_{n_m}^m + r_{n_m}^m)}{\Gamma(r_1^m) \cdot \ldots \cdot \Gamma(r_{n_m}^m)} \right) \\ &\left((p^1)^{\sum_{i=1}^{n_1} r_i^1} \cdot \ldots \cdot (p^m)^{\sum_{i=1}^{n_m} r_i^m} \right) \left((1-p^1)^{\sum_{i=1}^{n_1} d_i^1} \cdot \ldots \cdot (1-p^m)^{\sum_{i=1}^{n_m} d_i^m} \right) \\ = &\left(\frac{\Gamma(d_1^1 + r_1^1) \cdot \ldots \cdot \Gamma(d_{n_1}^1 + r_{n_1}^1)}{\Gamma(r_1^1) \cdot \ldots \cdot \Gamma(r_{n_1}^1)} \cdot \ldots \cdot \frac{\Gamma(d_1^m + r_1^m) \cdot \ldots \cdot \Gamma(d_{n_m}^m + r_{n_m}^m)}{\Gamma(r_1^m) \cdot \ldots \cdot \Gamma(r_{n_m}^m)} \right) \\ &\left((p^1)^{\sum_{i=1}^{n_1} r_i^1} \cdot \ldots \cdot (p^m)^{\sum_{i=1}^{n_m} r_i^m} \right) \left((1-p^1)^{\sum_{i=1}^{n_1} d_i^1} \cdot \ldots \cdot (1-p^m)^{\sum_{i=1}^{n_m} d_i^m} \right) \end{aligned} \tag{2.22}$$

where C = $(d_1^1! \cdot \ldots \cdot d_{n_1}^1!) \cdot \ldots \cdot (d_1^m! \cdot \ldots \cdot d_{n_m}^m!)$ simplifies the likelihood function.

The combined log likelihood function is given by

$$\log(L(\boldsymbol{\theta})) = \sum_{j=1}^{m} \sum_{i=1}^{n_j} \log(\Gamma(d_i^j + r_i^j)) - \log(\Gamma(r_i^j)) + r_i^j \log(p^j) + d_i^j \log(1-p^j). \tag{2.23}$$

2.F Bayesian framework

The Bayesian framework is set up by first assuming a probability model for the observed data D given a $p \times 1$ vector of unknown parameters $\boldsymbol{\theta}$, which is $P(D|\boldsymbol{\theta})$. Then it is assumed that $\boldsymbol{\theta}$ is randomly distributed from the prior

distribution $P(\boldsymbol{\theta})$. Statistical inference for $\boldsymbol{\theta}$ is based on the posterior distribution, $P(\boldsymbol{\theta}|D)$. Using Bayes' theorem we have

$$\begin{aligned} P(\boldsymbol{\theta}|D) &= \frac{P(D|\boldsymbol{\theta})P(\boldsymbol{\theta})}{P(D)} \\ &= \frac{P(D|\boldsymbol{\theta})P(\boldsymbol{\theta})}{\int_\Omega P(D|\boldsymbol{\theta})P(\boldsymbol{\theta})d\boldsymbol{\theta}} \\ &\propto L(\boldsymbol{\theta})P(\boldsymbol{\theta}) = \pi(\boldsymbol{\theta}|D) \end{aligned} \tag{2.24}$$

where Ω is the parameter space of $\boldsymbol{\theta}$ and $L(\boldsymbol{\theta})$ is the likelihood function. $P(D) = \int_\Omega P(D|\boldsymbol{\theta})P(\boldsymbol{\theta})d\boldsymbol{\theta}$ is called the prior predictive distribution and it is the normalizing constant of the posterior distribution $P(\boldsymbol{\theta}|D)$ [67]. The unnormalized posterior distribution is given by $\pi(\boldsymbol{\theta}|D) = L(\boldsymbol{\theta})P(\boldsymbol{\theta})$.

The Bayesian framework is very useful to use for statistical inference that occurs in mathematical biology since there is generally prior information about the unknown parameters in the literature.

2.F.1 Prior distribution

In biological applications there may exist literature regarding an appropriate prior distribution for a parameter of interest. However, in many cases, only a general range is known from the literature about a parameter of interest and the uniform distribution is usually chosen as the prior distribution for the parameter of interest.

For parameters that take positive values and that have an uncertainty that spans several orders of magnitude, it is useful to use the loguniform distribution as the prior distribution [68]. The loguniform distribution views the logarithm range as uniform. Using the loguniform distribution as a prior distribution for a parameter can help Bayesian inference to more easily explore a parameter's

uncertainty. It is usual to view the orders of magnitude in terms of base 10 and then the loguniform distribution with base 10 would be chosen as the prior.

If there are independent prior distributions, Ψ_l, chosen for each of the parameters, then the combined prior distribution is given by

$$P(\boldsymbol{\theta}) = \prod_{l=1}^{p} \Psi_l(\theta_p). \tag{2.25}$$

2.G Markov Chain Monte Carlo algorithms

Markov Chain Monte Carlo (MCMC) algorithms are designed to sample and to fully explore the parameter space where the unnormalized posterior distribution is positive [69]. The MCMC algorithms involve a process where a new vector of parameter values is sampled from the posterior distribution, $\boldsymbol{\theta}^{(t)}$, based off of the previous vector of parameter values, $\boldsymbol{\theta}^{(t-1)}$. A successful MCMC algorithm results in a **sample path** (also called a **chain** or **walker**) that has arrived at a stationary process and covers the domain of the target unnormalized posterior distribution.

2.G.1 Metropolis-Hastings algorithm

The Metropolis-Hastings algorithm is one of the classic MCMC algorithms [67]:

A starting point $\boldsymbol{\theta}^{(0)}$ is selected.

For every iteration $t = 1, 2, ..., T$:

randomly select a proposal for $\boldsymbol{\theta}^{(t)}$, $\boldsymbol{\gamma}$, from the proposal distribution

$f(\boldsymbol{\theta}^{(t)}|\boldsymbol{\theta}^{(t-1)})$

proposal for $\boldsymbol{\theta}^{(t)}$ is accepted with probability $\alpha = \min\{1, \frac{\pi(\boldsymbol{\gamma}|D)}{\pi(\boldsymbol{\theta}^{(t-1)}|D)} \frac{f(\boldsymbol{\theta}^{(t-1)}|\boldsymbol{\gamma})}{f(\boldsymbol{\gamma}|\boldsymbol{\theta}^{(t-1)})}\}$

random sample u from $U(0,1)$

if $u < \alpha$, the proposal is accepted and $\boldsymbol{\theta}^{(t)} = \boldsymbol{\gamma}$.

If not, $\boldsymbol{\theta}^{(t)} = \boldsymbol{\theta}^{(t-1)}$

where $\pi(\boldsymbol{\theta}|D)$ is the unnormalized posterior distribution.

2.G.2 Random-walk Metropolis-Hastings algorithm

If a symmetric proposal distribution is chosen in the Metropolis-Hastings Algorithm, then the proposal distribution randomly perturbs the current position of the vector of unknown parameters, $\boldsymbol{\theta}^{(t-1)}$, and these algorithms are called Random-Walk Metropolis-Hastings algorithms [69].

A symmetric proposal distribution has the property that $f(\gamma|\boldsymbol{\theta}^{(t-1)}) = f(\boldsymbol{\theta}^{(t-1)}|\gamma)$ and this simplifies the acceptance probability to $\alpha = \min\{1, \frac{\pi(\boldsymbol{\gamma}|D)}{\pi(\boldsymbol{\theta}^{(t-1)}|D)}\}$.

2.G.3 Affine invariant ensemble Markov Chain Monte Carlo algorithm

The affine invariant ensemble MCMC algorithm is shown to perform better than the Metropolis-Hastings algorithm and other MCMC algorithms [70]. Affine invariance here means that the performance of the algorithm is independent of the aspect ratio in anisotropic (directional density) posterior distributions [70]. The algorithm uses K walkers and the positions of the walkers are updated based on the present positions of the K walkers [71]. The following is the affine invariant ensemble MCMC algorithm:

A starting point $\boldsymbol{\theta}_i^{(0)}$ is selected for each of the walkers, $i = 1, 2, ..., K$.

For every iteration $t = 1, 2, ..., T$:

For $i = 1, 2, ..., K$:

randomly select a walker j from the K walkers such that $j \neq i$

randomly choose z from the distribution $f(z) = \frac{1}{\sqrt{az}}$, $\frac{1}{a} \leq z \leq a$

proposal for $\boldsymbol{\theta}_i^{(t)}$ is $\boldsymbol{\gamma} = \boldsymbol{\theta}_j^{(t-1)} + z(\boldsymbol{\theta}_i^{(t-1)} - \boldsymbol{\theta}_j^{(t-1)})$ (Stretch Move)

proposal for $\boldsymbol{\theta}_i^{(t)}$ is accepted with probability $\alpha = \min\{1, z^{p-1}\frac{\pi(\boldsymbol{\gamma}|D)}{\pi(\boldsymbol{\theta}_i^{(t-1)}|D)}\}$

If the proposal is accepted, $\boldsymbol{\theta}_i^{(t)} = \boldsymbol{\gamma}$. If not, $\boldsymbol{\theta}_i^{(t)} = \boldsymbol{\theta}_i^{(t-1)}$

where $\pi(\boldsymbol{\theta}|D)$ is the unnormalized posterior distribution, $a > 1$ is adjusted to improve performance, and $f(z)$ satisfies the symmetry condition $f(\frac{1}{z}) = zf(z)$.

The equation $\boldsymbol{\theta}_j^{(t-1)} + z(\boldsymbol{\theta}_i^{(t-1)} - \boldsymbol{\theta}_j^{(t-1)})$ is the equation of a line parallel to the vector $(\boldsymbol{\theta}_i^{(t-1)} - \boldsymbol{\theta}_j^{(t-1)})$. By randomly choosing z, the stretch move in the algorithm moves to a vector position, $\boldsymbol{\gamma}$, a certain distance up or down the line. Then the vector proposal, $\boldsymbol{\gamma}$, is either accepted or rejected based on the acceptance probability, α.

The set of samples from each of the K walkers will converge to the unnormalized posterior distribution, $\pi(\boldsymbol{\theta}|D)$. After running the method, the set of samples from each of the K walkers can be pooled together to form a larger sample from the unnormalized posterior distribution, KT samples. Since the samples from the first iterations are generally far away from the highest density of the unnormalized posterior distribution, the first iterations are usually deleted from each of the K walkers; the deletion of the first iterations is called *burn-in*. Let H be the number of pooled samples after the burn-in is completed.

2.H Diagnostics

The samples from the MCMC provide a sample path. It is important to diagnose if this sample path produces a sample from the target unnormalized posterior distribution, $\pi(\boldsymbol{\theta}|D)$. In other words, the sample path converges to the target unnormalized posterior distribution, $\pi(\boldsymbol{\theta}|D)$. From the plot of the sample path, it is vital to find that the sample path has arrived at a stationary process and the sample path covers the domain of the target unnormalized posterior distribution, $\pi(\boldsymbol{\theta}|D)$.

The sample path for each parameter θ_i should be plotted. It is ideal to find that the sample path for each parameter θ_i is oscillating very fast and displays no apparent trend; this indicates that the sample path has arrived at a stationary process. Provided that the sample path for θ_i has converged, the samples for θ_i is a random sample from the marginal posterior distribution for θ_i. The samples for each parameter θ_i can be viewed on separate histograms and the frequencies on the histogram approximates the marginal posterior distribution for θ_i. A robust way to view the posterior distribution is from the parameter θ_i perspective and this is accomplished by plotting the sample unnormalized posterior density values by the θ_i sample values.

A formalized test of the convergence of the MCMC sampling to the estimated unnormalized posterior distribution for each parameter θ_i is found by using a general univariate comparison method [72]. The general univariate comparison method uses the distance between the upper and lower values of the $100(1-\alpha)\%$ interval for the pooled samples, S, and divides this distance by the average of the distances between the upper and lower values of the $100(1-\alpha)\%$ interval for each of the K walkers, s_i, to receive the potential

scale reduction factor, η [72]:

$$\eta = \frac{S}{\sum_{i=1}^{K} \frac{s_i}{K}} \tag{2.26}$$

When the potential scale reduction factor, η, is close to 1 for all the estimated parameters, this indicates that the MCMC sampling converged to the estimated posterior distribution for each parameter.

2.I Point estimate for parameters

The point estimate is a single vector of the parameters used to summarize the posterior distribution. The point estimate is generally given by one of the following [68]: the posterior mean, which is the mean of each marginal posterior distribution $\pi(\theta_i|D)$ and it is computed by taking the mean of the θ_i samples; the posterior median, which is the median of each marginal posterior distribution $\pi(\theta_i|D)$, and it is computed by taking the median of the θ_i samples; and the maximum posterior, which is the $\boldsymbol{\theta}$ that corresponds to the maximum of the posterior distribution.

2.J Credible Intervals for parameters

For a marginal posterior distribution, $\pi(\theta_i|D)$, for θ_i, the most common 95% credible interval for θ_i is given by the 2.5 and 97.5 percentiles of the marginal posterior distribution $\pi(\theta_i|D)$ and it is computed by taking the 2.5 and 97.5 percentiles of the θ_i samples [67, 68]. It is sometimes called the centred 95% credible interval since there is the same amount of probability lying outside of the interval on both sides.

2.J.1 Non-uniqueness

Non-uniqueness occurs when there is more than one solution vector $\boldsymbol{\theta}$ that explains the data, D, equally as well.

When there is non-uniqueness, the marginal posterior distribution, $\pi(\theta_i|D)$, for θ_i is constant over an interval and the credible interval for θ_i is given by the upper and lower limits of the interval [67].

The credible intervals resulting from non-uniqueness can still be very beneficial since they are often more specific than the initial prior distributions specified for the parameters.

2.K Posterior predictive distribution

Let $\tilde{D} = \{\tilde{D}_1, \ldots, \tilde{D}_m\}$ be future responses of interest (replicated data) for the m datasets. The posterior predictive distribution of $\tilde{D}$ is given by

$$P(\tilde{D}|D) = \int_{\Omega} P(\tilde{D}|\boldsymbol{\theta}) P(\boldsymbol{\theta}|D) d\boldsymbol{\theta} \tag{2.27}$$

where $P(\boldsymbol{\theta}|D)$ is the posterior distribution and $P(\tilde{D}|\boldsymbol{\theta})$ is the same probability model for the data specified in the Bayesian framework (2.24).

To generate the posterior predictive distribution

For each pooled sample $t = 1, 2, ..., H$:
randomly sample $\tilde{D}$ from the probability distribution specified for the data $P(D|\boldsymbol{\theta}^{(t)})$ at $\boldsymbol{\theta}^{(t)}$

where H is the number of samples from the unnormalized posterior distribu-

tion.

The 95% prediction intervals for each data set D_j is found by determining the 2.5 and 97.5 percentiles of the posterior predictive distribution at each t_i^j.

The posterior predictive mean is found by taking the mean of the replicated data at each t_i^j.

2.L Bayesian Goodness of Fit

The Bayesian p-value (posterior predictive p-value) is used for testing the goodness of fit of a model to the data [73, 74]. The Bayesian p-value quantifies the discrepancies between the data and the model and it gauges whether these discrepancies could have happened by chance.

In order to carry out the Bayesian p-value test, a discrepancy measure needs to be chosen. The χ^2 discrepancy is a commonly used discrepancy measure. The χ^2 discrepancy is the sum of squares of standardized residuals of the data with respect to their true unknown expectations and it is a function of the data, $D = \{D_1, \ldots, D_m\}$, as well as the unknown parameters, $\boldsymbol{\theta}$:

$$\chi^2(D, \boldsymbol{\theta}) = \sum_{j=1}^{m} \sum_{i=1}^{n_j} \frac{(d_i^j - \mathrm{E}[d_i^j, \boldsymbol{\theta}])^2}{\mathrm{Var}[d_i^j, \boldsymbol{\theta}]}. \tag{2.28}$$

The Bayesian p-value, p_B, is defined as the probability that the replicated data could be more extreme than the observed data:

$$p_B = P(\chi^2(\tilde{D}, \boldsymbol{\theta}) \geq \chi^2(D, \boldsymbol{\theta})|D) \tag{2.29}$$

where the probability is evaluated over the posterior distribution of $\boldsymbol{\theta}$ and the posterior predictive distribution of $\tilde{D}$.

To calculate the Bayesian p-value, p_B

For each pooled sample $t = 1, 2, ..., H$:

randomly sample $\tilde{D}$ from the probability distribution specified for the data $P(D|\boldsymbol{\theta}^{(t)})$ at $\boldsymbol{\theta}^{(t)}$
(This is how the replicated data from the posterior predictive distribution was generated.)

calculate $\chi^2(\tilde{D}, \boldsymbol{\theta}^{(t)})$ and $\chi^2(D, \boldsymbol{\theta}^{(t)})$

record if $\chi^2(\tilde{D}, \boldsymbol{\theta}^{(t)})$ exceeds $\chi^2(D, \boldsymbol{\theta}^{(t)})$

where H is the number of samples from the unnormalized posterior distribution.
The estimated Bayesian p-value, p_B, is the proportion of times that $\chi^2(\tilde{D}, \boldsymbol{\theta}^{(t)})$ exceeds $\chi^2(D, \boldsymbol{\theta}^{(t)})$.

If the model predictions fit the data, ideally p_B will be close to 0.5. If p_B is between 0.05 and 0.95, then the p-value is considered to be in a reasonable range and there is no evidence against the null hypothesis that the model predictions fit the data.

If p_B is close to 0 or 1, then there is evidence against the null hypothesis that the model predictions fit the data. Extreme tail-area probabilities, less than 0.01 or more than 0.99, indicate a major failure of the model predictions to fit the data.

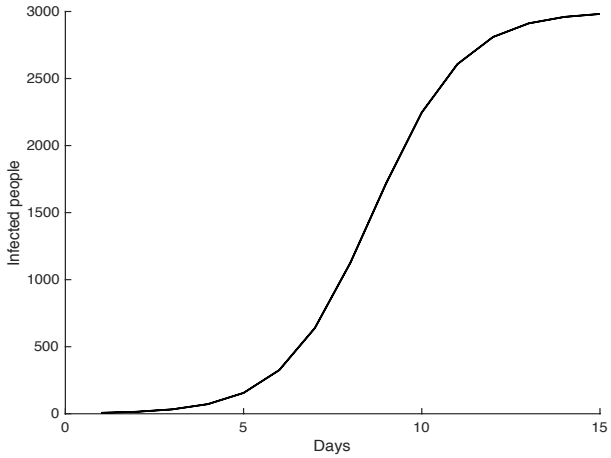

Figure 2.1: The true logistic growth model for the spread of viral infection in the small town with $x_0 = 3$, $r = 0.8$ and $N = 3000$

2.M Logistic growth example

Assume there are three people infected with a virus in an isolated town of 3000 people. Furthermore, assume that the true model for the first 15 days of the virus across the population is plotted in Figure 2.1 and given by the following differential equation

$$\frac{dx}{dt} = x(r - \frac{r}{N}x) \tag{2.30}$$

where $x_0 = 3$, $r = 0.8$ and $N = 3000$.

Now, this differential equation (2.30) can be solved analytically and we receive the logistic equation

$$x(\boldsymbol{\beta}, t_i) = \frac{rx_0}{\frac{r}{N}x_0 + (r - \frac{r}{N}x_0)e^{-rt_i}} \tag{2.31}$$

where

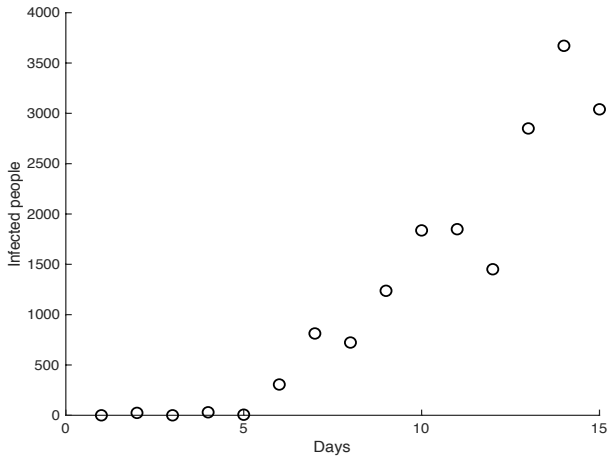

Figure 2.2: The generated data for the spread of a viral infection in the small town

$$\boldsymbol{\beta} = \begin{bmatrix} x_0 \\ r \\ N \end{bmatrix}.$$

Now, assume that the town collects count data for the number of people infected with the virus. We will generate this observed data by randomly sampling from the Negative Binomial distribution with mean given by (2.31) with $x_0 = 3$, $r = 0.8$ and $N = 3000$, and variance given by the mean divided by p, where p is chosen as 0.005. The generated observed data for the first 15 days of the virus across the population is plotted in Figure 2.2.

Now, we will use Bayesian inference to determine the following unknown vector of parameters

$$\boldsymbol{\theta} = \begin{bmatrix} \boldsymbol{\beta} \\ p \end{bmatrix}$$

$$= \begin{bmatrix} x_0 \\ r \\ N \\ p \end{bmatrix}.$$

In this scenario, equation (2.4) is $E[D_i] = \mu_i = x(\boldsymbol{\beta}, t_i)$ and the negative binomial distribution (2.9) is chosen to describe the observed data.

The following uniform prior distributions are chosen for the parameters:

x_0 with distribution $U(1, 50)$

r with distribution $U(0.1, 2)$

N with distribution $U(100, 6000)$

p with distribution $U(1 \times 10^{-5}, 1 \times 10^{-1})$.

The affine invariant ensemble MCMC algorithm is used with $T = 100000$ iterations and $K = 8$ walkers. The potential scale reduction factor, η, for each parameter:

$\eta = 0.9941$ for x_0

$\eta = 0.9977$ for r

$\eta = 0.9963$ for N

$\eta = 0.9987$ for p.

All potential scale reduction factors are close to 1 and this indicates that the algorithm converged to the posterior distribution.

The Bayesian p-value, p_B, was

$p_B = 0.4058$

which indicates that there is no evidence against the null hypothesis that the model predictions fit the data.

The histogram of each parameter is plotted in Figure 2.3. The unnormalized posterior distribution from each parameter's perspective is plotted in Figure 2.4. The point estimate for the parameters is the maximum posterior. The point estimate with the 95% credible interval for each parameter are the following:

x_0 is estimated to be 4.13 (1.68, 19.58),
r is estimated to be 0.690 (0.474, 0.834),
N is estimated to be 2.99×10^3 (2.46×10^3, 4.47×10^3), and
p is estimated to be 0.0070 (0.0032, 0.0111).

The true parameter values for x_0, r, N, and p all lie within the 95% credible intervals.

Samples from the posterior predictive distribution and the posterior predictive mean are displayed in Figure 2.5. The true model, best fit model (model with the highest unnormalized posterior probability), and posterior predictive mean are compared in Figure 2.6. It is seen that the best fit model (red curve) lies very close to the posterior predictive mean (black curve) and is near the true model (blue curve). It is observed that the true model (blue curve) and all of the generated data (red circles) lie within the 95% prediction intervals (dashed black curves).

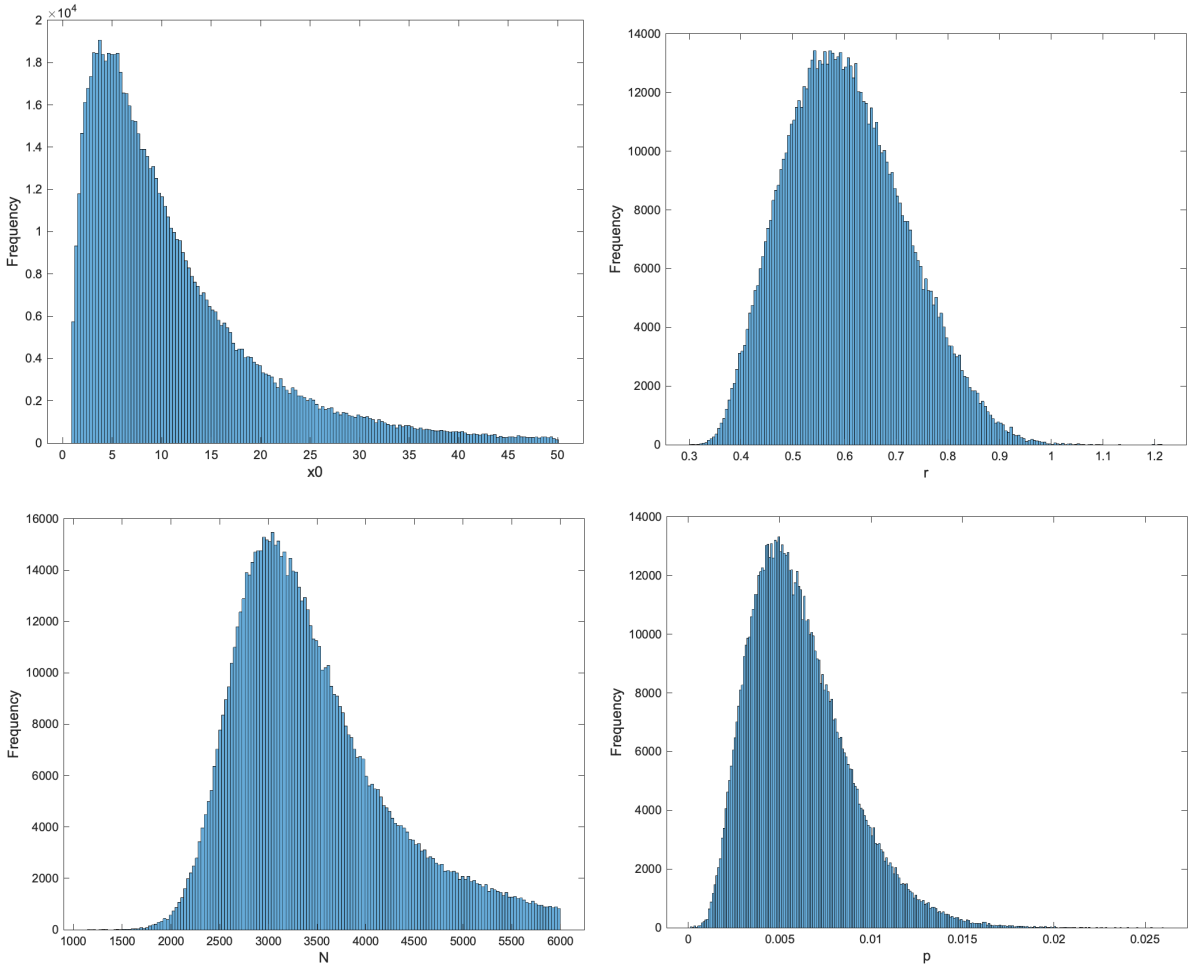

Figure 2.3: Histogram of **(a)** x_0, **(b)** r, **(c)** N, and **(d)** p

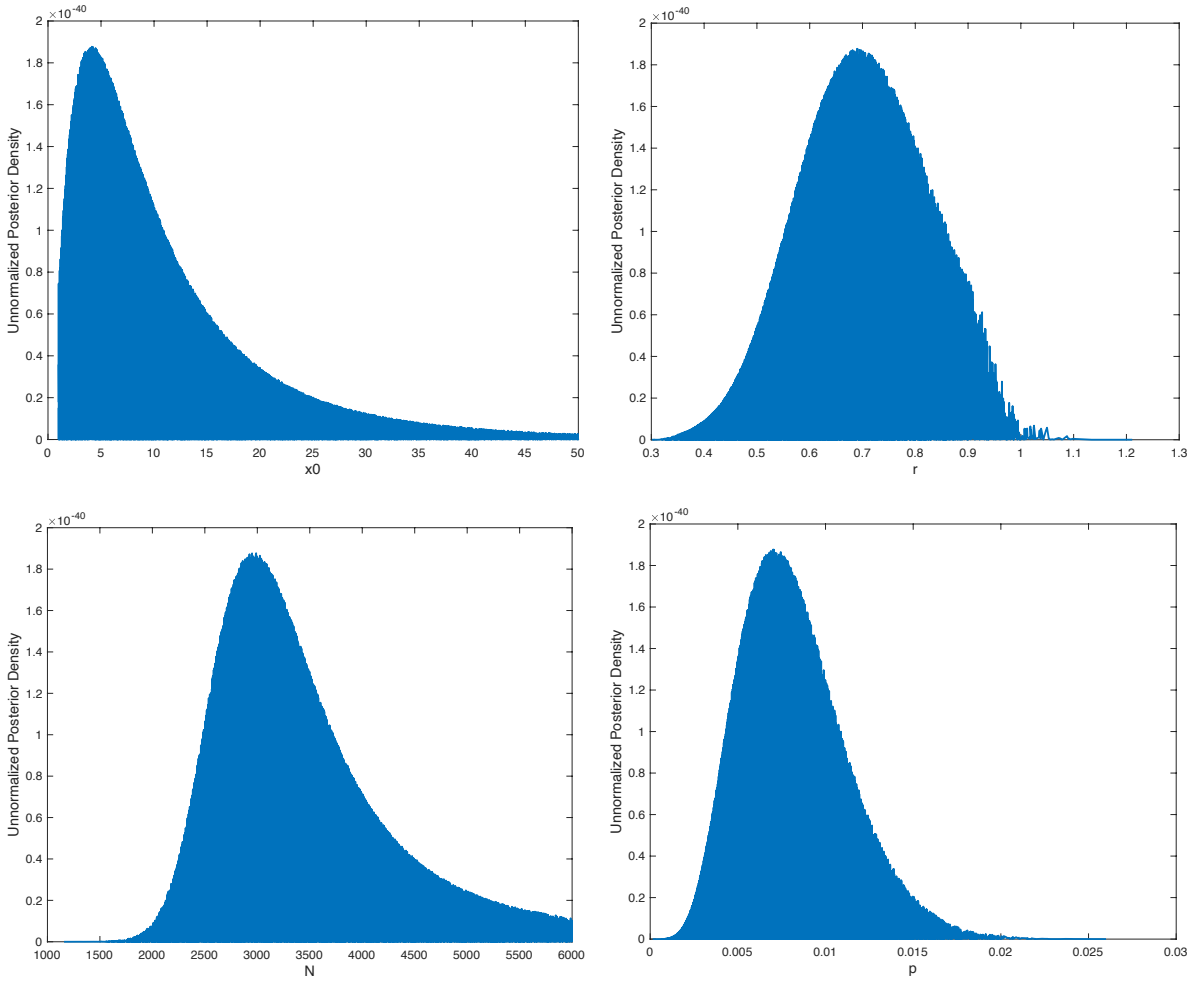

Figure 2.4: Unnormalized posterior distribution from parameter's perspective: **(a)** x_0, **(b)** r, **(c)** N, and **(d)** p

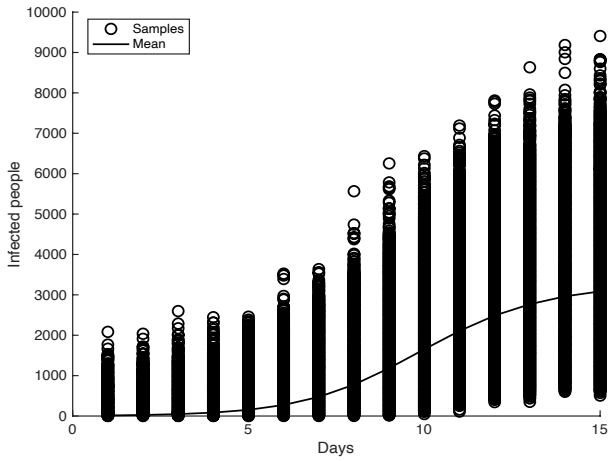

Figure 2.5: Posterior predictive distribution with the posterior predictive mean

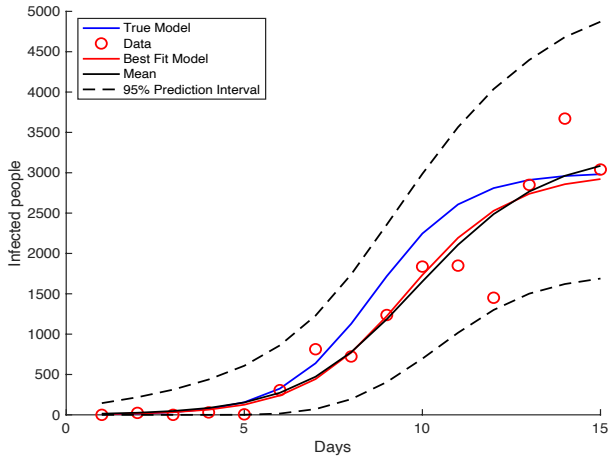

Figure 2.6: Best fit and true model for the spread of a viral infection in the small town with 95% prediction interval

Chapter 3

Bayesian inference using diffusive nested sampling

3.A Nested sampling

Nested sampling estimates the normalizing constant (called the prior predictive distribution, marginal likelihood, or evidence),

$$Z = P(D) = \int_{\Omega} P(D|\boldsymbol{\theta})P(\boldsymbol{\theta})d\boldsymbol{\theta}, \tag{3.1}$$

of the posterior distribution $P(\boldsymbol{\theta}|D)$, by relating the likelihood function, L, to the prior mass, X [75]. As a result of estimating the normalizing constant, Z, with nested sampling, the posterior samples become available as a consequence of this sampling, which provides another way of performing Bayesian inference. Since the normalizing constant, Z, is being estimated, nested sampling provides an estimate of the true posterior density,

$$
\begin{aligned}
P(\boldsymbol{\theta}|D) &= \frac{P(D|\boldsymbol{\theta})P(\boldsymbol{\theta})}{P(D)} \\
&= \frac{P(D|\boldsymbol{\theta})P(\boldsymbol{\theta})}{Z}.
\end{aligned}
\tag{3.2}
$$

Nested sampling also provides a way to carry out model selection within the Bayesian framework since normalizing constants are estimated. Consider two models, M_1 and M_2, proposed to explain the data D. Suppose that the two normalizing constants, Z_1 and Z_2, are estimated for each model, respectively. Also, it is assumed that the prior distribution attributed to each model is equal, $P(M_1) = P(M_2)$, which means that there is no prior belief that one model is better than the other. Then model selection is performed by comparing the evidence Z_1 to the evidence Z_2 with the following ratio called the Bayes' factor [76]:

$$
B = \frac{Z_1}{Z_2}. \tag{3.3}
$$

The value of the Bayes factor, B, is interpreted in the following way [77]:

- if $10^2 < B$, then there is decisive evidence against M_2
- if $10^{3/2} < B < 10^2$, then there is very strong evidence against M_2
- if $10 < B < 10^{3/2}$, then there is strong evidence against M_2
- if $10^{1/2} < B < 10$, then there is substantial evidence against M_2
- if $1 < B < 10^{1/2}$, then there is minimal evidence against M_2
- if $10^{-1/2} < B < 1$, then there is minimal evidence against M_1
- if $10^{-1} < B < 10^{-1/2}$, then there is substantial evidence against M_1

- if $10^{-3/2} < B < 10^{-1}$, then there is strong evidence against M_1
- if $10^{-2} < B < 10^{-3/2}$, then there is very strong evidence against M_1
- if $B < 10^{-2}$, then there is decisive evidence against M_1

From the Bayes factor, B, interpretation, a model can be selected.

Nested sampling is accomplished by first defining the quantity

$$X(L^*) = \int_{L(\boldsymbol{\theta})>L^*} P(\boldsymbol{\theta}) d\boldsymbol{\theta}, \tag{3.4}$$

which is the cumulant prior mass covering all likelihood values greater than L^*. It is assumed that the prior distribution is normalized to unit total. Hence, $0 \leq X(L^*) \leq 1$ and as L^* increases, the enclosed prior mass X decreases from 1 to 0.

Nested sampling estimates $L(X)$, which is the likelihood, L, as a function of prior mass, X. The evidence, Z, is estimated by the approximate integration of

$$\int_0^1 L(X) dX. \tag{3.5}$$

By estimating the normalizing constant, Z with the integral 3.5, nested sampling turns a multidimensional sampling problem into a one dimensional sampling problem.

Let $L_i = L(X_i)$ be a right-to-left sequence of m points. Denote $L_{max} = L_{m+1}$ as the maximum likelihood. In practice, the true maximum likelihood is not determined by nested sampling or any other type of sampling; so, the highest value of the likelihood found during the sampling is used, which is

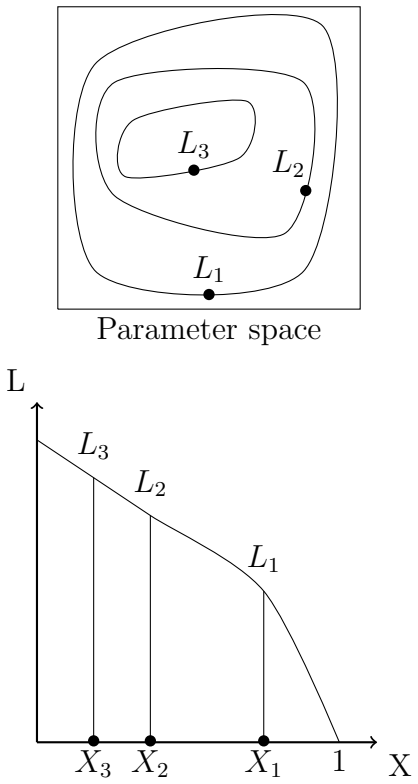

Figure 3.1: The nested likelihood, L_i, contours are sorted by enclosed prior mass, X_i with $m = 3$.

denoted as $\tilde{L}_{max}$). The corresponding sequence of X_i values decrease in value as m increases

$$X_{m+1} = 0 < X_m < \cdots < X_2 < X_1 < 1 = X_0.$$

Figure 3.1 displays an example of nested likelihood, L_i, contours sorted by enclosed prior mass, X_i with $m = 3$. The Trapezoidal Rule is used as the approximate integration method for estimating Z, equation (3.5):

$$Z = \int_0^1 L(X)dX \approx \sum_{i=0}^{m-1}(X_i - X_{i+1})\frac{L_i + L_{i+1}}{2} + X_m\tilde{L}_{max}. \tag{3.6}$$

Up to this point, it has been assumed that the corresponding constrained prior mass X_i value is known for each likelihood, L_i. However, in practice,

the corresponding constrained prior mass X_i values are unknown. Thus, the corresponding constrained prior mass X_i value for each L_i needs to be estimated. An estimate for the constrained prior mass X_i value can be found by using knowledge about the distribution of order statistics and knowledge about solutions to linear difference equations.

Consider a random sample $U_1, U_2, ..., U_n$ from the standard uniform distribution, $U(0,1)$. The pdf of the k^{th} order statistic, $U_{(k)}$, is given by

$$f_{U_{(k)}}(u) = \frac{n!}{(k-1)!\,(n-k)!} u^{k-1}(1-u)^{n-k} \tag{3.7}$$

which is the pdf of a beta distribution with parameters $a = k$ and $b = n-k+1$ [78]. Therefore, the pdf of the n^{th} order statistic (which is the same as the maximum), $U_{(n)}$, is given by

$$f_{U_{(n)}}(u) = n(u)^{n-1} \tag{3.8}$$

which is the pdf of a beta distribution with parameters $a = n$ and $b = 1$, BETA$(n, 1)$.

Nested sampling begins by randomly sampling n points $\boldsymbol{\theta}_1, \boldsymbol{\theta}_2, ..., \boldsymbol{\theta}_n$ from the prior distribution with corresponding likelihood values $L(\boldsymbol{\theta}_1), L(\boldsymbol{\theta}_2), ..., L(\boldsymbol{\theta}_n)$. Then the lowest likelihood value is selected (which will enclose the maximum prior mass among this sample) and this lowest likelihood value is denoted as L_1. Without loss of generality, it is assumed that this lowest likelihood value, L_1, corresponds to the point $\boldsymbol{\theta}_k$ among the n points. Hence, $L_1 = L(\boldsymbol{\theta}_k)$. Given that $X_0 = 1$ and since the lowest likelihood value was selected, then the random variable for the amount of prior mass enclosed by L_1 is

$$X_1 = \psi_1 X_0,$$

where $0 < \psi_1 < 1$ and $\psi_1 \sim \text{BETA}(n, 1)$.
Let L_1 be the current likelihood cut off value denoted by L^*.

Since $\boldsymbol{\theta}_k$ is on the boundary of the new cut off $L^* = L_1$ and the other $n - 1$ points are already inside of the new cut off value $L^* = L_1$, we randomly draw a new point $\boldsymbol{\theta}^*$ within the prior with the constraint $L > L^* = L_1$, save the original point $\boldsymbol{\theta}_k$ for analysis later, and replace the point $\boldsymbol{\theta}_k$ with $\boldsymbol{\theta}^*$. This results in a new random sample of size n that is all within the prior with constraint $L > L^* = L_1$.

As this process is continued, each next L_i will further enclose the prior mass and we can represent the sequence of enclosed prior mass as the following:

$$X_0 = 1, X_1 = \psi_1 X_0, ..., X_m = \psi_m X_{m-1}$$

where each $\psi_i \sim BETA(n, 1)$.

This leads to needing to solve the following nonhomogeneous linear difference equation iteratively:

$$X_0 = 1$$

$$X_i = \psi_i X_{i-1}$$

$i = 0, 1, 2, ...$.

By substituting, we receive the expression

$$X_i = \psi_i X_{i-1} = \psi_i(\psi_{i-1} X_{i-2}) = \psi_i(\psi_{i-1}(\psi_{i-2} X_{i-3})) = \psi_i(\psi_{i-1}(\psi_{i-2}(...(\psi_0 X_0)))).$$

Hence,

$$X_i = \prod_{j=0}^{i} \psi_j \tag{3.9}$$

is the solution of the nonhomogeneous linear difference equation.

After m iterations of nested sampling, from equation 3.9, the enclosed prior mass above $L^* = L_m$ is

$$X_m = \prod_{j=0}^{m} \psi_j. \tag{3.10}$$

Then

$$\log(X_m) = \sum_{j=0}^{m} \log(\psi_j). \tag{3.11}$$

Since each ψ_j are random variables, $\psi_j \sim BETA(n, 1)$, we need to find the $E[\log(\psi_j)]$ in order to determine how the enclosed prior mass is expected to reduce each iteration.

As the domain of $g(\psi) = \log(\psi)$ includes the possible values of ψ, by the definition of the expected value and the pdf of $BETA(n, 1)$, we receive

$$E[\log(\psi)] = \int_0^1 \log(\psi) n\psi^{n-1} d\psi = n \int_0^1 \psi^{n-1} \log(\psi) d\psi. \tag{3.12}$$

Now, integrating by parts, we receive

$$n \int \psi^{n-1} \log(\psi) d\psi = n\left(\frac{1}{n}\psi^n \log(\psi) - \int \frac{1}{n}\psi^n \frac{1}{\psi} d\psi\right) = \psi^n \log(\psi) - \int \psi^{n-1} d\psi. \tag{3.13}$$

By using equation 3.13 into equation 3.12, we have

$$E[\log(\psi)] = \lim_{a \to 0^+} n \int_a^1 \psi^{n-1} \log(\psi) d\psi = \lim_{a \to 0^+} -a^n \log(a) - \frac{1}{n} + \frac{1}{n} a^n. \tag{3.14}$$

Using L'Hospital's rule, we have

$$\lim_{a \to 0^+} -a^n \log(a) = 0. \tag{3.15}$$

Using equation 3.15 and evaluating the limit in equation 3.14, we have

$$E[\log(\psi)] = -\frac{1}{n}. \tag{3.16}$$

Therefore, after m iterations of nested sampling, from equation 3.11 and 3.16, we have

$$E[\log(X_m)] = E\left[\sum_{j=0}^{m} \log(\psi_j)\right] = \sum_{j=0}^{m} -\frac{1}{n} = -\frac{m}{n}. \tag{3.17}$$

Hence, deterministically, after m iterations, $X_m = \exp(-\frac{m}{n})$. After one iteration, the enclosed prior mass is expected to reduce by $\exp(-\frac{1}{n})$.

The following is the nested sampling algorithm:

Sample n points $\boldsymbol{\theta}_1, \boldsymbol{\theta}_2, ..., \boldsymbol{\theta}_n$ from the prior $P(\boldsymbol{\theta})$

Initialize $Z = 0$ and $X_0 = 1$

For every iteration $i = 1, 2, ..., T$:
Find the point $\boldsymbol{\theta}_k$ that corresponds to the lowest of the current likelihood values and record this value as L_i
From equation 3.17, deterministically X_i is expected to be $\exp(-\frac{i}{n})$, and we use the estimate $X_i = \exp(-\frac{i}{n})$
Z is incremented by $(X_{i-1} - X_i)\frac{L_{i-1}+L_i}{2}$
Replace the point $\boldsymbol{\theta}_k$ with a new point randomly drawn from the prior with constraint $L > L_i$

After the T iterations, increment Z by $X_T L^*_{max}$, where L^*_{max} is the highest value of the likelihood found during the nested sampling algorithm.

3.A.1 Challenges and limitations of nested sampling

In the nested sampling algorithm, it is difficult to draw a **random** point from the prior with constraint $L > L_i$. It is suggested to use MCMC methods to generate this new point from the prior with constraint $L > L_i$ [75]. The

idea with using MCMC to draw this new point is that if the MCMC chain is run long enough within the constrained prior, then the final position should be independent of the initial position and this final position would effectively be the **random** point. In practice, MCMC methods are very efficient at finding the maximum posterior and as a result, the MCMC chain ends up being inaccurate in terms of drawing a **random** point from the constrained prior. When this new point is inaccurate, the Z value becomes inaccurate.

The major drawback of the nested sampling algorithm is the inability of the algorithm to effectively explore multimodal distributions. This is because during the algorithm the nested sampling set of n points can get stuck in a local maximum area of the posterior surface and this set n points will be unable to escape due to the constraint $L > L_i$. The user of the algorithm would not be aware that the set of n points has been trapped in a local maximum area of the posterior surface. This leads to the need of revising the nested sampling algorithm to allow for escaping from local maximum areas of the posterior surface.

3.B Diffusive nested sampling

Diffusive nested sampling (DNS) improves the nested sampling algorithm by incorporating a multi-level exploration of the likelihood cut off regions into the algorithm [11, 12]. The DNS algorithm achieves this by having a particle explore mixtures of constrained distributions determined by the likelihood cut offs and by introducing a weighting scheme that decides how far a particle can move between constrained distributions. The target distribution in the Diffusive Nested Sampling algorithm is not the posterior distribution but a

joint distribution made up of these constrained distributions, which is related to the posterior distribution. After the algorithm is run, the DNS samples obtained from the algorithm are used to determine the representative posterior distribution.

The Bayesian MCMC methods of Gibbs sampling, Hamiltonian MCMC, and affine invariant ensemble MCMC have difficulty sampling multimodal posterior distributions [12]. The advantage of the DNS algorithm is that it samples from the mixture of constrained prior distributions, which is generally easier than sampling from the posterior distribution, and this allows the DNS algorithm to more easily mix between different modes and more effectively sample from a multimodal posterior distribution [11, 12].

3.B.1 Multi-level exploration process

Let the constrained distributions be defined as the following:

$$p_{L_j}(\boldsymbol{\theta}) = \frac{P(\boldsymbol{\theta})}{X_j}\mathbf{1}_j(\boldsymbol{\theta}) \tag{3.18}$$

where $\mathbf{1}_j(\boldsymbol{\theta}) = \begin{cases} 1, L(\boldsymbol{\theta}) > L_j \\ 0, \text{otherwise} \end{cases}$,

$P(\boldsymbol{\theta})$ is the prior distribution, and X_j is the enclosed prior mass above L_j.

The DNS algorithm begins by using MCMC to evolve a particle to obtain Q number of samples over the entire prior parameter space. Here $p_{L_0}(\boldsymbol{\theta}) = \frac{P(\boldsymbol{\theta})}{X_0}\mathbf{1}_0(\boldsymbol{\theta}) = P(\boldsymbol{\theta})$ and this is considered level 0. The parameter vector values and the corresponding likelihood values are saved. When Q number of samples

are found, the likelihood cut off value L_1 is set equal to the $(1 - e^{-1})$ quantile of the likelihood values in this first sample. The constrained distribution p_{L_1} is considered level 1.

Next, MCMC is used to evolve the particle to sample the mixture of constrained distributions, p_{L_0} and p_{L_1}. By sampling from the mixture of distributions, the particle can have a chance to escape to a lower constrained distribution and the particle can explore more freely. MCMC sampling from the mixture of constrained distributions, p_{L_0} and p_{L_1}, is continued until Q number of samples are obtained from p_{L_1}. The likelihood cut off value L_2 is equal to the $(1 - e^{-1})$ quantile of the likelihood samples values found in p_{L_1}. The constrained distribution p_{L_2} is considered level 2.

Then the particle explores a mixture of p_{L_0}, p_{L_1}, and p_{L_2}, and so on. By continuing to take the $(1 - e^{-1})$ quantile of the likelihood values in the highest level constrained distribution, the enclosed prior mass above the highest level likelihood cut off value decreases exponentially.

In order to have the particle explore the mixture of distributions, the current particle vector of parameters $\boldsymbol{\theta}^*$ and current level j^*, $(\boldsymbol{\theta}^*, j^*)$, need to be updated according to a joint distribution, $p(\boldsymbol{\theta}, j)$. Using Bayes' theorem and equation (3.18),

$$\begin{aligned} p(\boldsymbol{\theta}, j) &= p(j)p(\boldsymbol{\theta}|j) = p(j)p_{L_j}(\boldsymbol{\theta}) = w_j p_{L_j}(\boldsymbol{\theta}) \\ &= w_j \frac{P(\boldsymbol{\theta})}{X_j} \mathbf{1}_j(\boldsymbol{\theta}) \\ &= \frac{w_j}{X_j} P(\boldsymbol{\theta}) \mathbf{1}_j(\boldsymbol{\theta}), \end{aligned} \tag{3.19}$$

where $p(j) = w_j$ is a chosen weighting scheme influencing how a particle can move between constrained distributions.

During the first phase of the DNS algorithm, which is the level creation phase, the exponentially-decaying weights are chosen for the weighting scheme:

$$w_j \propto \exp\left(\frac{j-J}{\Lambda}\right), \tag{3.20}$$

where $j \in 0, 1, 2, 3, ..., J$ is the level, J is the current highest created level, and Λ is the diffusive parameter describing how far the particle can backtrack to a lower distribution.

The exponentially-decaying weights help the particle to continue climbing to higher likelihood regions and spend more iterations on higher likelihood regions rather than on lower likelihood regions. If the diffusive parameter Λ is smaller, then the first phase of the DNS algorithm will more aggressively spend time at higher likelihood regions. If the diffusive parameter Λ is larger, then the first phase of the DNS algorithm allows the particle to more easily escape higher likelihood regions and explore other regions. A larger diffusive parameter Λ is considered more fail-safe as it allows the particle to escape local maximums, but the DNS algorithm will also run slower.

The current particle location $(\boldsymbol{\theta}^*, j^*)$ is updated in two actions. The order of these two actions is random, but they must take place one after the other. With the assumption that the level is fixed at j^*, the action of updating the current parameter vector $\boldsymbol{\theta}^*$ is done by proposing a new parameter vector $\boldsymbol{\theta}'$ and then accepting with the following Metropolis acceptance probability:

$$\begin{aligned}\alpha &= \min\left[1, \frac{p(\boldsymbol{\theta}', j^*)}{p(\boldsymbol{\theta}^*, j^*)}\right] \\ &= \min\left[1, \frac{w_{j^*}}{X_{j^*}} P(\boldsymbol{\theta}') \mathbf{1}_{j^*}(\boldsymbol{\theta}') \frac{X_{j^*}}{w_{j^*}} \frac{1}{P(\boldsymbol{\theta}^*)\mathbf{1}_{j^*}(\boldsymbol{\theta}^*)}\right] \\ &= \min\left[1, \frac{P(\boldsymbol{\theta}')}{P(\boldsymbol{\theta}^*)} \mathbf{1}_{j^*}(\boldsymbol{\theta}')\right],\end{aligned} \tag{3.21}$$

where $\mathbf{1}_{j^*}(\boldsymbol{\theta}^*) = 1$ since $\boldsymbol{\theta}^*$ was already accepted in level j^*.

With the assumption that the parameter vector is fixed at $\boldsymbol{\theta}^*$, the action of updating the current level j^* is done by proposing a new level j' and then accepting with the following Metropolis acceptance probability:

$$\begin{aligned}\alpha &= \min\left[1, \frac{p(\boldsymbol{\theta}^*, j')}{p(\boldsymbol{\theta}^*, j^*)}\right] \\ &= \min\left[1, \frac{w_{j'}}{X_{j'}} P(\boldsymbol{\theta}^*) \mathbf{1}_{j'}(\boldsymbol{\theta}^*) \frac{X_{j^*}}{w_{j^*}} \frac{1}{P(\boldsymbol{\theta}^*)\mathbf{1}_{j^*}(\boldsymbol{\theta}^*)}\right] \\ &= \min\left[1, \frac{w_{j'}}{X_{j'}} \frac{X_{j^*}}{w_{j^*}} \mathbf{1}_{j'}(\boldsymbol{\theta}^*)\right],\end{aligned} \tag{3.22}$$

where $\mathbf{1}_{j^*}(\boldsymbol{\theta}^*) = 1$ since $\boldsymbol{\theta}^*$ was already accepted in level j^*.

As the sampling progresses and more levels are added in the first phase, the actual X_j values can become different than the theoretical expectation of $X_{j+1} = e^{-1} X_j \iff \frac{X_{j+1}}{X_j} = e^{-1}$, which would be realized if our sampling were perfect. This causes difficulty for MCMC to explore the mixture of constrained distributions. The likelihood values within the level j should exceed L_{j+1} a fraction of the time, with the fraction given by $\frac{X_{j+1}}{X_j}$. Counting the number of times that the likelihood values within a particular level j exceed L_{j+1} provides a way to estimate the actual fractions $\frac{X_{j+1}}{X_j}$.

Let $n(L > L_{j+1}|j)$ denote the number of times that the particle likelihood values within a particular level j exceed L_{j+1} and let $n(j)$ denote the number of times that the particle has visited level j. Hence, the actual fraction $\frac{X_{j+1}}{X_j}$ can be estimated by

$$\frac{n(L > L_{j+1}|j) + Ce^{-1}}{n(j) + C}, \tag{3.23}$$

where the inclusion of the constant C is used here to stabilize the estimate when the number of visits to level j is low, $n(j)$, and C represents the amount of confidence in the theoretical expectation $X_{j+1} = e^{-1}X_j$.

These fractions are continually refined as the DNS algorithm runs.

The first phase of the DNS algorithm is completed when the desired number of levels are created. The desired maximum number of created levels can be set by the user or a level creation stopping criteria can be made based on a tolerance. During the first phase, the number of times that the particle has been proposed to a particular level j (this does not mean it necessarily went to this level j) is also tracked, and this number will be denoted by $\xi(j)$.

During the second phase of the DNS algorithm, the weights are generally chosen to be uniform, though non-uniform weights can also be used, to allow the particle to freely mix through the constrained distributions. This is done to further refine the estimates of the actual fractions $\frac{X_{j+1}}{X_j}$. The number $\xi(j)$ is continued to be tracked during the second phase and the number $\xi(j)$ is used to modify the acceptance probability of the jump proposal (3.22) during the second phase of the DNS algorithm:

$$\begin{aligned}\alpha &= \min\left[1, \frac{p(\boldsymbol{\theta}^*, j')}{p(\boldsymbol{\theta}^*, j^*)}\right] \\ &= \min\left[1, \left(\frac{C+\xi(j')}{C+\xi(j^*)}\right)^{\beta} \frac{X_{j^*}}{X_{j'}} \mathbf{1}_{j'}(\boldsymbol{\theta}^*)\right],\end{aligned} \tag{3.24}$$

where uniform weights have been chosen $\left(\frac{w_{j'}}{w_{j^*}} = 1\right)$, C is the same constant used in equation (3.23), and β controls the strength of the effect $\left(\frac{C+\xi(j')}{C+\xi(j^*)}\right)$. The purpose of $\left(\frac{C+\xi(j')}{C+\xi(j^*)}\right)$ is to more surely visit those locations that have not been proposed to as often.

3.B.2 Proposal options

Recall that in the DNS algorithm the current particle location $(\boldsymbol{\theta}^*, j^*)$ is updated in two actions. There needs to be a proposal for moving to a new parameter vector $\boldsymbol{\theta}'$ and there needs to be a proposal for going to a new level j'.

For proposing a new parameter vector $\boldsymbol{\theta}'$, first a certain number of parameters, $r \leq p$, are chosen to be moved within the current parameter vector, $\boldsymbol{\theta}^*$, where p is the total number of parameters. Let the certain number of parameters to be moved r be a random variable with the following pdf, $f(r)$:

$$f(r) = \frac{1}{r}, \tag{3.25}$$

where $1 < r < p$. The cumulative distribution function (cdf) is given by $F(r) = \ln(r)$, where $1 < r < p$.

The pdf, $f(r)$, emphasizes a smaller number of parameters chosen r, while still allowing for the possibility of a larger number of parameters to be chosen.

This helps to speed up the movement of θ within a level in the DNS algorithm.

After r is chosen from the pdf, $f(r)$, a random sample of r parameters without replacement is chosen to be moved within the current parameter vector, $\boldsymbol{\theta}^* = \langle \theta_1^*, \theta_2^*, ..., \theta_p^* \rangle$. For each of the r chosen parameters within $\boldsymbol{\theta}^*$, θ_i^* is moved with either of two recommended options [68, 12, 79]:

$$\theta_i' = \theta_i^* + \left(q_i^2 - q_i^1\right)\left(10^{1.5-3*|t|}\right)h, \tag{3.26}$$

where $h \sim N(0,1)$, $t = \frac{a}{\sqrt{-\ln(b)}}$ with $a \sim N(0,1)$ and $b \sim U(0,1)$ (here t has a Student's t distribution with 2 degrees of freedom, $t \sim t(2)$), and assuming that θ_i has the uniform prior distribution $U(q_i^1, q_i^2)$,

or

$$\theta_i' = \theta_i^* + (q_i^2 - q_i^1)\left(10^{(1-|c|)}\right)h, \tag{3.27}$$

where $h \sim N(0,1)$, $c = \tan(\pi(b-0.5))$ with $b \sim U(0,1)$ (here c has a standard Cauchy distribution, $c \sim CAU(1,0)$), and assuming that θ_i has the uniform prior distribution $U(q_i^1, q_i^2)$.

Since the standard Cauchy distribution has heavier tails than the Student's t distribution with 2 degrees of freedom, this second proposal option will propose more extreme guesses than the first proposal option.

The main idea of these proposal options is that each time a symmetric proposal is made the width of the proposal distribution randomly changes and is drawn from a range [68]. The largest possible width should be roughly the order of magnitude of the width of the prior as the posterior is generally

narrower than the prior [68, 12]. Other proposal options for θ are possible. The type of options mentioned here are recommended [68, 12, 79].

3.B.3 Representative posterior samples

The samples returned from the DNS algorithm are posterior samples in the sense that the parameter vector samples are from the posterior distribution. However, since the target distribution in the DNS algorithm is a joint distribution made up of constrained distributions rather than the posterior distribution directly, the frequency of the parameter vector samples returned are generally imbalanced. For instance, there may be many parameter vector samples taken at the top levels when the algorithm is reaching convergence and this would lead to an over representation of samples near the maximum posterior. In order to adjust for this, a post-processing phase is completed after the DNS algorithm is run.

The first step of this post-processing phase is to order the parameter vector samples returned from the DNS algorithm by increasing likelihood values. Let the ordered parameter vector samples be denoted as $\theta^{(i)}$ with corresponding likelihood value $L^{(i)}$. Next, the samples are assigned a level j based off of the sample's likelihood value. Then there are n_j number of samples in increasing order of likelihood values within each level. Let $n = \sum_{j=0}^{J} n_j$ be the total number of samples returned from the DNS algorithm, where J is the highest level created. The DNS algorithm provides estimates for the enclosed prior mass values X_j. Thus, it is known that each of the n_j samples has a prior mass value in between X_{j+1} and X_j, but a specific prior mass value is not known for each sample. Since it is known that the MCMC sampling taking place within

each level in the DNS algorithm, should effectively be a random sample. Thus, in each level j, a uniform random sample of size n_j between X_{j+1} and X_j can be taken, and then these random samples can be ordered. Let these ordered prior mass samples be denoted by $X^{(i)}$. These ordered prior mass samples, $X^{(i)}$, are then assigned to each $\theta^{(i)}$ with corresponding likelihood value $L^{(i)}$. Figure 3.2 illustrates this ordering process.

The fraction of posterior density attributed to each i^{th} ordered DNS sample can be approximated by

$$\omega_i = \frac{L^{(i)}(X^{(i)} - X^{(i-1)})}{\tilde{Z}}, \tag{3.28}$$

where $\tilde{Z}$ is given by

$$\tilde{Z} = \sum_{i=1}^{n} L^{(i)}(X^{(i)} - X^{(i-1)}) \approx Z = \int_0^1 L(X)dX. \tag{3.29}$$

The values ω_i in equation (3.28) are called posterior weights.

From equation (3.28),

$$\sum_{i=1}^{n} \omega_i = 1. \tag{3.30}$$

The cumulative posterior weight is given by

$$\Omega_l = \sum_{i=1}^{l} \omega_i. \tag{3.31}$$

Each cumulative posterior weight, Ω_l, corresponds to an ordered parameter vector sample $\theta^{(l)}$ in the sense that $\theta^{(l)}$ is the specific parameter vector where the posterior weight cumulates to the value Ω_l.

To obtain a representative posterior sample of size H, a uniform random sample of size H is taken between 0 and 1. Let these uniform random sample values be given by $u_1, u_2, ..., u_H$. Then the closest cumulative posterior weight value is found for each $u_1, u_2, ..., u_H$. Let these closest cumulative posterior weight values be given by $\Omega^1, \Omega^2, ..., \Omega^H$. Each of these cumulative posterior weight values $\Omega^1, \Omega^2, ..., \Omega^H$ corresponds to a specific ordered parameter vector sample and this set of specific ordered parameter vector samples will be denoted as $\theta^1, \theta^2, ..., \theta^H$. This set of H parameter vector samples, $\theta^1, \theta^2, ..., \theta^H$, is a representative posterior sample of size H.

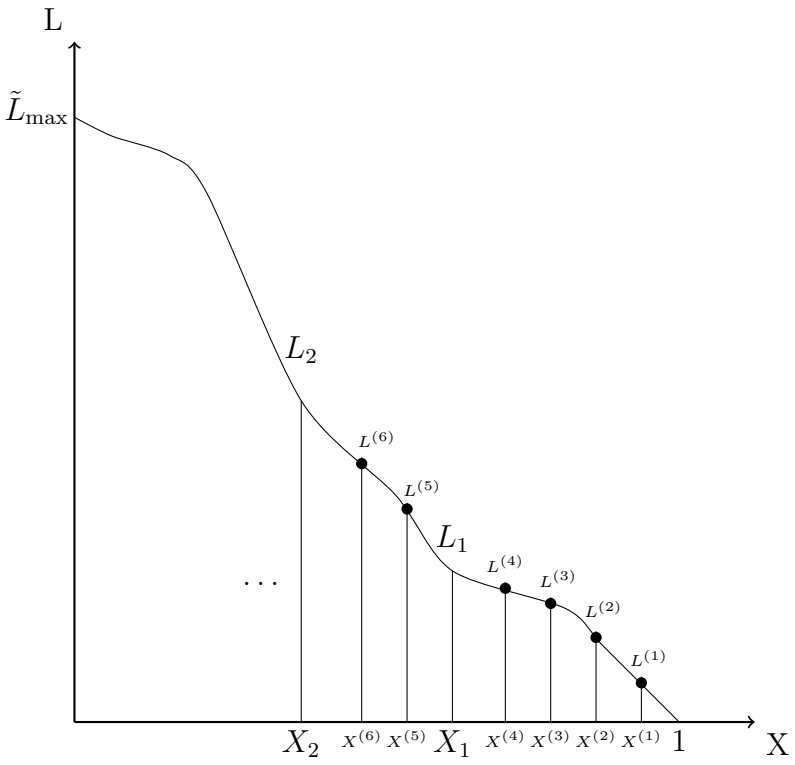

Figure 3.2: The parameter vector samples from DNS algorithm are ordered by increasing likelihood values, $L^{(i)}$. The likelihood level cut offs, L_j, determine which level each sample is assigned. Within each level j, the enclosed prior mass is between X_{j+1} and X_j. It is unknown what the enclosed prior mass value is for each DNS sample within a level. Within a level j, a uniform sample equal to the number of DNS samples within each level is taken between X_{j+1} and X_j. These randomly sampled enclosed prior mass values within each level are ordered $X^{(i)}$ and then assigned to the ordered likelihood values, $L^{(i)}$.

3.C MATLAB implementation of diffusive nested sampling

3.C.1 Overview of "MatlabDiffNestAlg"

We programmed the first MATLAB implementation of the DNS algorithm called "MatlabDiffNestAlg" in 2021 and we have continued updating the software features since its debut [9]. This program is a derived work based off of elements of "DNest5" (©2020 Brendon J. Brewer) [79] and the following papers: "Diffusive Nested Sampling", "DNest4: Diffusive Nested Sampling in C++ and Python", and "Nested Sampling for General Bayesian Computation" [11, 12, 75].

The "Diff_Nest_Alg" .m file is the main function that runs the DNS algorithm. The "Diff_Nest_Alg" .m file explains the input and output functions of this software. The target distribution in the DNS algorithm is not the posterior distribution but a joint distribution related to the posterior distribution. The "find_level_assign", "find_log_post_weights", "find_log_post" .m files are used after the DNS algorithm is completed to determine the representative posterior distribution.

This DNS MATLAB implementation is designed to use uniform prior distributions for each parameter. (Theoretical Example 3 in the "MatlabDiffNestAlg" code demonstrates how to use a uniform prior when a parameter is assumed to have a loguniform distribution.) The width of the uniform prior distributions specified for each parameter are used inside of the algorithm to generate proposals for that parameter during the particle's "move" phase. This DNS MATLAB implementation also assumes that the integration

of the prior over the parameter space equals 1. Since the prior distribution used in "TheoreticalExample1", "TheoreticalExample2", and "TheoreticalExample3" is a product of uniform distributions, the resulting joint distribution does integrate to one.

The "Diff_Nest_Alg_key_detect" .m file is the function that runs the DNS algorithm with the option of being able to use the keyboard to select between different proposal options and to manually exit the level creation step early if the maximum number of levels specified has not been reached or the tolerance has not been reached. (The convenience of being able to use the keyboard while the algorithm is running does impact the speed of the algorithm.)

The "Examples" folder contains three different example subfolders. The first subfolder is "TheoreticalExample1", which is a theoretical example for fitting a multimodal posterior distribution using "MatlabDiffNestAlg" shown in Section 3.C.2 of this thesis, and this example problem setup is from Section 5 of the paper "Diffusive Nested Sampling" [11]. In the next subfolder is "TheoreticalExample2", which is the same logistic growth theoretical example as presented in Section 2.M of this thesis except the DNS algorithm is used instead of the affine invariant ensemble MCMC algorithm. The results of the logistic growth theoretical example using the DNS algorithm are similar to the affine invariant ensemble MCMC algorithm. In the last subfolder is "TheoreticalExample3", which is a theoretical example motivated by the lentiviral brain macrophage infection model with cART, system 4.1, and this example illustrates how to fit a mathematical model to multiple datasets and how to use a loguniform distribution as the prior for a positive parameter whose uncertainty spans multiple magnitudes.

3.C.2 Multimodal posterior example

This example problem setup is from Section 5 of the paper "Diffusive Nested Sampling" [11]. Consider a 20×1 vector of unknown parameters

$$\boldsymbol{\theta} = \begin{bmatrix} x_1 \\ \vdots \\ x_{20} \end{bmatrix},$$

where each x_l parameter has an independent and identically distributed uniform prior $U(-0.5, 0.5)$. Also, assume that the likelihood function is given by the sum of two Gaussian probability models, one centred at the origin with standard deviation $v = 0.1$ and the other centred at $(0.031, 0.031, ..., 0.031)$ with 100 times more density and smaller standard deviation of $u = 0.01$,

$$L(\boldsymbol{\theta}) = \prod_{l=1}^{20} \frac{\exp(-\frac{1}{2}(x_l/v)^2)}{v\sqrt{2\pi}} + 100 \prod_{l=1}^{20} \frac{\exp(-\frac{1}{2}((x_l - 0.031)/u)^2)}{u\sqrt{2\pi}}. \tag{3.32}$$

This likelihood is purposefully structured to create a difficult multimodal posterior for typical Bayesian inference algorithms to sample, as the smaller but more dense part of the posterior distribution is harder to locate.

The MATLAB implementation of the DNS algorithm, "MatlabDiffNestAlg", was used with the following settings: five particles; the number of samples needed above the current likelihood cut off to create another level was 1000 with at least 1500 samples per level overall; the diffusivity term $\lambda = 30$; the number of samples used during the second phase of the sampler was 5×10^6; the tolerance used to stop level creation was 1×10^{-4}; $C = 100$, which is

the number providing the amount of confidence in the theoretical expectation $X_{j+1} = \exp(-1)X_j$; only every 100^{th} sample was saved; $\beta = 100$, which is the parameter that controls the strength of the effect to correct the mass X values in the second phase of the DNS algorithm; and the combined proposal distribution discussed in Section 3.B.2 was used for the parameter proposals.

The progress of the DNS algorithm can be seen in Figure 3.3. This plot shows the particles moving with log likelihood level creation during the first phase of the algorithm (level values in blue) and then the particles move about the posterior surface refining the estimated compression of $\log(X)$ between each level in the second phase of the algorithm (level values in black). It can be seen, in both the first and second phases of the DNS algorithm, that the particles diffuse through the log likelihood cut off levels when sampling the posterior surface.

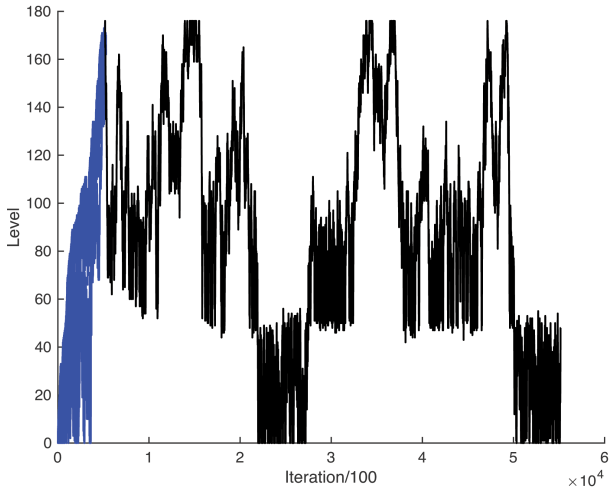

Figure 3.3: Progress of the DNS algorithm, where the level values in blue show the particles moving with log likelihood level creation during the first phase of the algorithm and the level values in black show the particles moving around the posterior surface refining the estimated compression of $\log(X)$ between each level in the second phase of the algorithm.

Figure 3.4 displays the posterior weights over the $\log(X)$ values. There is a clear peak of the posterior weights and the samples to the left of the peak have small posterior weights in comparison to the peak weight values, and and this indicates that the algorithm converged to the posterior distribution.

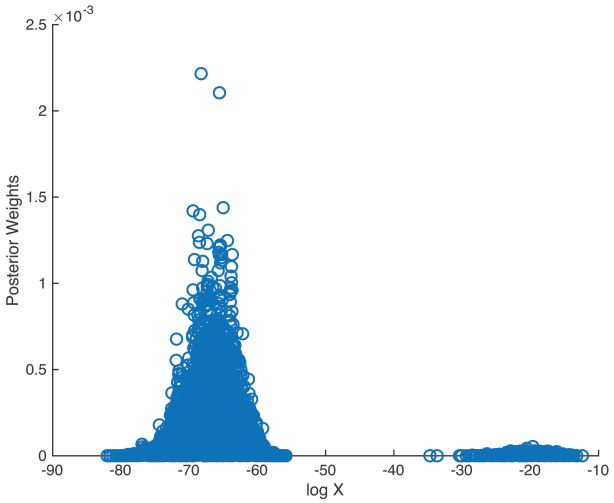

Figure 3.4: Posterior weights over the $\log(X)$ values for multimodal posterior example

The true value of Z for this distribution is approximately 101. Consequently, the true value of $\log(Z)$ is approximately 4.6151. The converged $\log(Z)$ estimates from this DNS algorithm had the median value of 4.3783.

The posterior distribution from parameter x_1's perspective is plotted in Figure 3.5 and it can be seen that the smaller but denser part of the posterior distribution is clearly sampled by the DNS algorithm with the posterior distribution peak centred at $(0.031, 0.031, ..., 0.031)$. The plots of the posterior distribution from the other parameter perspectives look similar.

The point estimate for the parameters is the maximum posterior. The point estimate with the 95% credible interval for each parameter are located in Table 3.1.

Table 3.1: Fitted parameter estimates and 95% credible intervals for multimodal posterior example

Symbol	Estimate (95% credible interval)
x_1	$0.0298\ (0.0099, 0.0496)$
x_2	$0.0359\ (0.0093, 0.0511)$
x_3	$0.0300\ (0.0107, 0.0505)$
x_4	$0.0325\ (0.0113, 0.0512)$
x_5	$0.0318\ (0.0117, 0.0528)$
x_6	$0.0368\ (0.0113, 0.0528)$
x_7	$0.0343\ (0.0116, 0.0527)$
x_8	$0.0278\ (0.0119, 0.0515)$
x_9	$0.0290\ (0.0095, 0.0504)$
x_{10}	$0.0295\ (0.0113, 0.0508)$
x_{11}	$0.0317\ (0.0089, 0.0498)$
x_{12}	$0.0374\ (0.0120, 0.0509)$
x_{13}	$0.0242\ (0.0101, 0.0513)$
x_{14}	$0.0404\ (0.0105, 0.0505)$
x_{15}	$0.0347\ (0.0081, 0.0505)$
x_{16}	$0.0287\ (0.0105, 0.0505)$
x_{17}	$0.0271\ (0.0103, 0.0521)$
x_{18}	$0.0293\ (0.0106, 0.0500)$
x_{19}	$0.0400\ (0.0092, 0.0509)$
x_{20}	$0.0255\ (0.0120, 0.0508)$

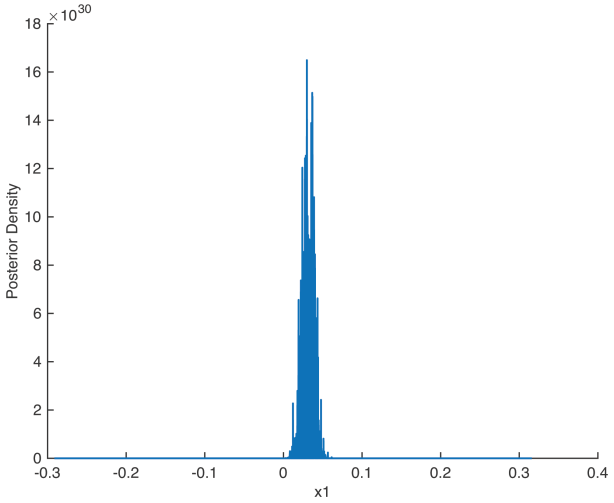

Figure 3.5: Posterior distribution from the x_1 perspective for multimodal posterior example

Figure 3.6 displays the cut off values of the log likelihood over the $\log(X)$ values. It shows that as the log likelihood cut offs increase the $\log(X)$ values decrease. This is because the amount of log prior mass contained above the log likelihood cut off decreases as the log likelihood cut offs increase. It is also seen that near where $\log(X) = -50$ the cut off values of the log likelihood suddenly continues to increase again until the completion of the algorithm. This occurs because the DNS algorithm found the smaller but denser part of this posterior distribution.

Figure 3.7 shows the estimated compression of $\log(X)$ between each level. If the sampling was perfect, then the $\log(X)$ difference would be at -1. The visits matrix helps to correct the imperfect sampling and provides a better estimate of the actual compression of $\log(X)$ between levels and this is displayed in Figure 3.7.

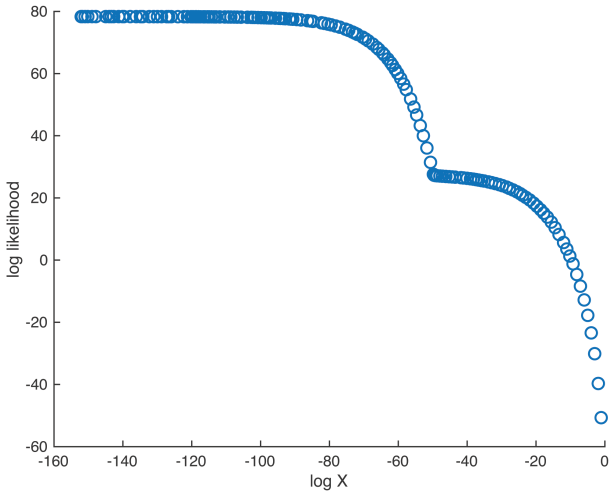

Figure 3.6: The cut off values of the log likelihood over the $\log(X)$ values for the multimodal posterior example

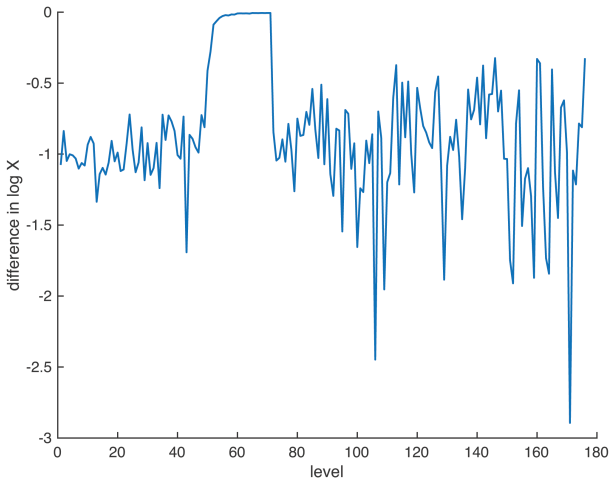

Figure 3.7: The estimated compression of $\log(X)$ between each level

Chapter 4

Modeling the effects of latency reversing drugs during HIV-1 and SIV brain infection with implications for the "Shock and Kill" strategy

4.A Introduction

Combination antiretroviral therapy (cART) has greatly reduced the overall morbidity and mortality among human immunodeficiency virus-1 (HIV-1) infected patients [23, 80]. cART has suppressed the virus in the plasma, improved the immune system, and significantly increased life expectancy for HIV-1 infected patients worldwide [23, 81]. Even with the success of cART, the virus persists in many different cells and tissues, and in tissues that dis-

play minimal cART penetration and limited host immune responses, creating ideal locations for viral reservoirs [16, 17]. Commonly known viral reservoirs include latently infected resting memory $CD4^+$ T cells and several anatomical compartments that harbour HIV-infected cells [18, 82]. Latency is defined as the state in which individual infected cells do not produce infectious viruses although they can become reactivated to produce infectious virus by specific stimuli [19, 20]. Viral reservoirs are a major obstacle for the eradication of HIV-1 infection. The "Shock and Kill" therapeutic strategy aims to reactivate latently infected cells by latency reversing agents (LRAs) and kill these reactivated cells by engaging a restored host immune system and using specific antiretroviral medications [18, 21].

The brain is an established and compelling anatomical reservoir for HIV-1 infection [23, 24, 83]. Indeed, the brain is devoid of in situ adaptive immune responses and the blood-brain barrier (BBB) restricts many established antiretroviral medications from entering the brain [24]. Evidence shows HIV-1 can enter the brain using trafficking infected macrophages as vehicles [25, 26, 27]. Brain macrophages, including microglia and perivascular macrophages, display productive HIV-1 infection [23]. Brain macrophages are long-lived cells [28]. Infected brain macrophages can cause neurological damage by direct and indirect mechanisms [26]. Despite cART's effective control of virus in blood, HIV-1 infection can lead to neurological disorders including HIV-associated neurocognitive disorders (HAND) [29], indicating an ineffective cART suppression of infection in the brain. A recent meta-analysis study [84] has shown that the global prevalence of HAND among HIV patients was 42.6% (95% confidence interval 39.7-45.5). These studies also show the importance of studying the brain reservoir for achieving viral clearance and a cure for HIV-1. Even

when HIV-1 is cleared from the rest of the body, reactivated latent infections in the brain can re-seed the infection outside the brain by means of infected trafficking macrophages.

Experimental and clinical studies suggest that cART is capable of reducing HIV-1 RNA production and ensuing replication in brain but exerts little impact on viral DNA levels in the brain [30, 31, 85, 86]. This suggests that productive infection in the brain is reduced by cART but there remains persistent latent virus located in brain cells. In a recent study of simian immunodeficiency virus (SIV) infection, the premier HIV-1 animal model, using the "Shock and Kill" therapeutic strategy, LRA treatment reactivated latent virus that could be detected in the brain [32]. One of the two animals (macaques) that received cART and LRA treatment had neurological signs after LRA therapy, implying that viral reactivation resulted in brain damage. The authors of this SIV study caution that certain LRA treatments may cause harmful inflammatory responses in the brain even in the presence of cART [32]. The study in [32] emphasizes the key medical challenge of determining the dynamics of LRA treatment in the brain viral reservoir. Mathematical modeling can be an effective tool for understanding both qualitatively and quantitatively the dynamics of latent infections and LRA treatment in the brain.

To realistically study the effectiveness of an experimental strategy such as "Shock and Kill" using mathematical models, it is imperative that the dynamics of the model be investigated in a parameter region that is informed by clinical or experimental data. The majority of modeling research on the "Shock and Kill" strategy have focused on the latently infected resting memory CD4 T cells. Modeling results on the "Shock and Kill" strategy in the literature include the estimated magnitude of the reservoir reduction needed

to prevent viral rebound for one year after stoppage of cART [87]. These estimates crucially depend on model parameters that were informed by clinical data from CD4 T cells. For mathematical modeling of the "Shock and Kill" strategy, we refer the reader to a recent review [87] and references therein. Resident macrophages are the primary target and main reservoir for HIV-1 and SIV infection in the brain. They have distinct biological properties from those of T cells in peripheral blood or tissues. This is one of the challenges in modeling brain infections, since the parameter values from modeling research on T cells in the literature are not applicable to the modeling of brain macrophages. Another challenge of modeling HIV-1 infection in the brain is the scarcity of data. Much of the data is from studies on SIV infections in animal models. For these reasons, establishing parameter regions informed by clinical and experimental data is a significant first step for modeling HIV-1 and SIV infection in the brain.

In an earlier modeling study, we were able to use a mathematical model to quantify the progression rate of HIV-1 and SIV infection in the brain [1] by fitting the model to clinical and experimental brain viral DNA data. Our model estimation in [1] indicated that HIV-1 and SIV proviral burdens in brain increase much slower over time in comparison to the proviral burden among T cells in the peripheral blood. Assuming cART suppressed HIV-1 outside the brain, the study showed that a marginal increase in the efficacy of the current cART treatment could suppress HIV-1 infection in the brain, over a decade for patients without neurological complications and over two decades for those with HAND [1].

Our previous mathematical model in [1] did not distinguish between latently and productively infected cells and these cell populations were regarded

as a single infected cell population. With the availability of both viral DNA and RNA data, we were able to expand the model in [1] by separating the infected cell population into productively and latently infected cells. Our current study aimed to qualitatively and quantitatively analyze the dynamics of latently and productively infected cells in the brain during HIV-1 and SIV infection. Our mathematical analysis showed that the expanded model provided a mechanism for the establishment of a latent viral reservoir among the brain macrophages under cART. We also calibrated the model at baseline without LRA treatment using data for SIV infected macaques and estimated model parameter values with their 95% credible intervals using Bayesian inference. This establishes a baseline parameter region for the model that is informed by SIV data. The "Shock and Kill" therapeutic strategy is then incorporated into the baseline model by including both a reactivation rate of the latent reservoir and an additional kill rate of productively infected brain macrophages into the model, and numerical studies were carried out in the data-informed parameter region to investigate the effectiveness and safety of the "Shock and Kill" therapeutic strategy. Results of our numerical investigation indicates that there exists a biologically plausible parameter region wherein the "Shock and Kill" can be safe and effective.

4.B Mathematical model and analysis

4.B.1 HIV-1 brain macrophage infection model with cART

Brain macrophages are the primary target for productive HIV-1 infections in the brain [23]. HIV-1 infection of a target cell by cell-free virion have been extensively studied in the literature. Evidence from recent research suggest that intracellular viral transfer through direct cell-to-cell contacts may be the predominant mode of HIV-1 transmission among cells, because of its high efficiency in the transfer of viral materials and of its ability to evade immune responses and cART drugs [26, 47, 83, 88, 89, 90]. Based on the research evidence, we made the assumption that HIV-1 and SIV infections in the brain spread principally through direct cell-to-cell contact [83]. Brain macrophages are long-lived cells and recent data indicate that brain macrophages may die over months to years [91]. Studies have not observed increased cellular death in HIV-infected versus susceptible brain macrophages [50] and thus, it is assumed that the death rates of susceptible, and productively or latently infected brain macrophages are similar.

To derive our model, we divide the resident brain macrophage population into three compartments: susceptible brain macrophages, x; productively infected brain macrophages y; and latently infected brain macrophages, l. The transfer diagram for the model is shown in Figure 4.1. The model structure and our mathematical results about the global dynamics can be applied to HIV-1 infection of macrophages in other tissues. We caution that our application of the model to the understanding of the effectiveness of the "Shock and

Kill" strategy was carried out numerically using parameter values informed by data on SIV infection in the brain, and the resulting conclusions may not be applicable to the infection of macrophages in other tissues because of the distinct biology.

Without the presence of infection in the model, the number of susceptible brain macrophages is regulated at the equilibrium value $\frac{\lambda}{k}$, where λ is the source of new susceptible brain macrophages and k is the death rate of brain macrophages. With the presence of infection, it is possible for HIV-1 infected macrophages from the cerebrospinal fluid (CSF) or blood to enter and exit the brain [92]. Under cART, the movement of trafficking infected macrophages is minimal [93]. Even without cART, resident microglia are much more permissive to HIV-1 infection and spread than trafficking macrophages [94]. Our earlier study demonstrates that the persistence of HIV-1 infection in the brain can be explained by a model that does not rely on an influx of trafficking infected macrophages [1]. For these reasons, after initial brain infection, it is assumed there is no influx of trafficking infected macrophages. The interaction between susceptible versus productively or latently infected brain macrophages is modeled by the mass action terms $\beta_1 xy$ and $\beta_2 xl$ respectively. It is assumed that the majority of newly infected cells will enter the latently infected population, only a proportion p of the cells newly infected by productively infected cells will enter the productively infected population. It is assumed that cART exerts its effects solely on productively infected cells since latently infected cells remain largely unaffected by cART [95]. We considered the percentage of cART effectiveness $\epsilon \times 100\%$, where $0 \leq \epsilon \leq 1$. The cART effectiveness parameter ϵ describes the efficacy of cART and the concentration of cART drugs able to penetrate through the BBB and affect brain macrophages. There is

always a random baseline exchange, both activation and deactivation, between latently and productively infected brain macrophages. In the model, it is assumed that the natural net effect of this exchange is negligible. The reduction of virus in the brain by cART is plausibly related to decreased levels of activated brain macrophages [96], and in the model it is assumed that in the presence of cART there is a strong effect above the baseline exchange that favours the direction of deactivation. Since cART drugs show variable concentrations and efficacies in brain macrophages and tissues [93], it is assumed that the higher the drug effectiveness the greater the effect on the deactivation rate of productively infected brain macrophages, $\epsilon\gamma$. The parameter ϵ is set to zero when there is no cART. The total number of infected macrophages are called stably infected macrophages given by $s(t) = y(t) + l(t)$. The variable $s(t)$ is fit to the integrated viral DNA copies in the data. Viral RNA copies is given by $v(t) = Ny(t)$, where N is a constant, and $v(t)$ is fit to the viral RNA copies in the data. In brain HIV-1 and SIV infection, the majority of the viral RNAs reside inside the productively infected macrophages. Using the transfer diagram, our model is described by the set of ordinary differential equations (ODEs):

$$\begin{aligned}
\frac{dx}{dt} &= \lambda - kx - (1-\epsilon)\beta_1 xy - \beta_2 xl \\
\frac{dy}{dt} &= p(1-\epsilon)\beta_1 xy - ky - \epsilon\gamma y \\
\frac{dl}{dt} &= (1-p)(1-\epsilon)\beta_1 xy + \beta_2 xl - kl + \epsilon\gamma y.
\end{aligned} \tag{4.1}$$

By adding all the equations of system (4.1), we have that

$(x + y + l)' = \lambda - k(x + y + l)$. Therefore,

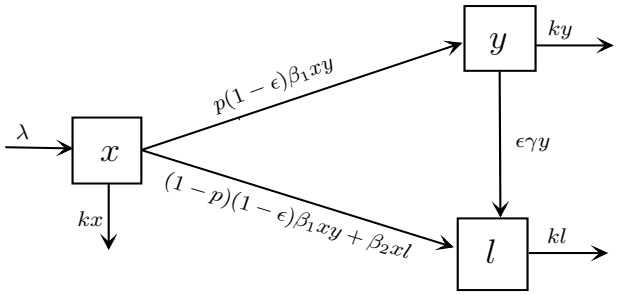

Figure 4.1: Transfer diagram for model (4.1) that considered both latently and productively infected cells in the brain with cART.

$$x(t) + y(t) + l(t) = \tfrac{\lambda}{k} + Ce^{-kt},$$

where C is a constant. When $t \to \infty$, the total number of brain macrophages approaches the constant $\frac{\lambda}{k}$. Therefore, the asymptotic behavior of solutions to system (4.1) can be restricted to the following region:

$$\Gamma = \{(x, y, l) \in \mathbb{R}^3_+ : x + y + l = \frac{\lambda}{k}\}, \tag{4.2}$$

Let $\mathring{\Gamma}$ denote the interior of Γ with respect to the hyperplane $x + y + l = \frac{\lambda}{k}$.

System (4.1) has three possible equilibria:

$P_0 = (\frac{\lambda}{k}, 0, 0)$, disease-free equilibrium

$P_1 = (x_1, y_1, l_1)$, productive equilibrium

$P_2 = (x_2, 0, l_2)$, latent equilibrium,

where $x_1 = \frac{k+\epsilon\gamma}{p(1-\epsilon)\beta_1}$,

$y_1 = \frac{(\lambda p(1-\epsilon)\beta_1 - k(k+\epsilon\gamma))(p(1-\epsilon)\beta_1 k - \beta_2(k+\epsilon\gamma))}{p(1-\epsilon)\beta_1 k(k+\epsilon\gamma)((1-\epsilon)\beta_1 - \beta_2)}$,

$l_1 = \frac{((1-p)k+\epsilon\gamma)(\lambda p(1-\epsilon)\beta_1 - k(k+\epsilon\gamma))}{pk(k+\epsilon\gamma)((1-\epsilon)\beta_1 - \beta_2)}$,

$x_2 = \frac{k}{\beta_2}$,

and $l_2 = \frac{\lambda}{k} - \frac{k}{\beta_2}$.

At equilibrium P_0 all the brain macrophages are healthy. At equilibrium P_1 the viral infection is chronic with both productively and latently infected brain macrophages present. At the equilibrium P_2, due to cART, the viral infection is in the latent state wherein productively infected brain macrophages are suppressed and only latently infected brain macrophages are present.

Let

$$F_1 = \begin{bmatrix} \frac{p(1-\epsilon)\beta_1\lambda}{k} & 0 \\ \frac{(1-p)(1-\epsilon)\beta_1\lambda}{k} & \frac{\beta_2\lambda}{k} \end{bmatrix} \text{ and } V_1 = \begin{bmatrix} k+\epsilon\gamma & 0 \\ -\epsilon\gamma & k \end{bmatrix}.$$

Then

$$F_1V_1^{-1} = \begin{bmatrix} \frac{p(1-\epsilon)\beta_1\lambda}{k(k+\epsilon\gamma)} & 0 \\ \frac{(1-p)(1-\epsilon)\beta_1\lambda}{k(k+\epsilon\gamma)} + \frac{\beta_2\lambda\epsilon\gamma}{k^2(k+\epsilon\gamma)} & \frac{\beta_2\lambda}{k^2} \end{bmatrix}. \tag{4.3}$$

Using the next generation matrix method in [97, 98], the control reproduction number is given by the spectral radius of the matrix $F_1V_1^{-1}$:

$$R_c = \rho(F_1V_1^{-1}) = \max\{R_{c1}, R_{c2}\}, \tag{4.4}$$

where $R_{c1} = \frac{p(1-\epsilon)\beta_1\lambda}{(k+\epsilon\gamma)k}$ and $R_{c2} = \frac{\beta_2\lambda}{k^2}$. The final outcomes of system (4.1) are determined by the value of these two threshold parameters, R_{c1} and R_{c2}. The global dynamics of system (4.1) is summarized in Table 4.1 and depicted in Figure 4.2. The detailed stability analysis is given in Chapter 5.

In the clinical context, the distinction between productively and latently infected cells is that latently infected cells have no detectable viral production. Below the limit of viral detection, there can be a very low level of viral production among latently infected cells [19]. It is assumed that the infec-

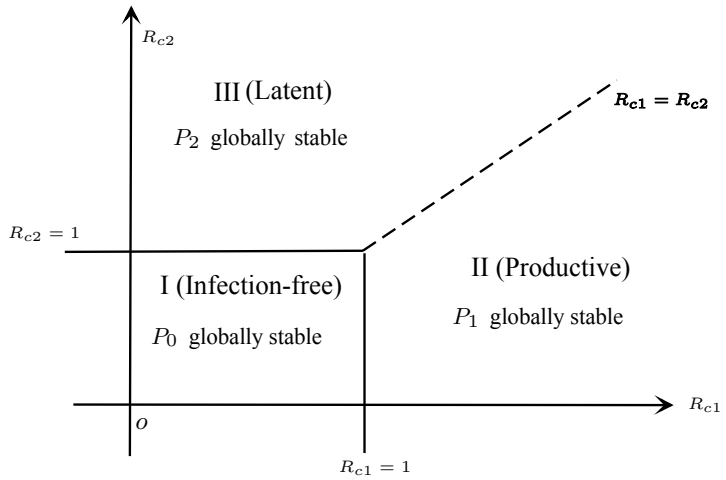

Figure 4.2: Parameter regions of distinct model outcomes based on the stability analysis of the equilibria of model (4.1). Almost all HIV-1 infected patients cannot clear the virus, and the infection-free region I is not biological. If no cART is applied, the model outcomes are that productively infected cells persist (region II). With increasingly more efficacious cART, the model outcomes gradually shift from the productive region II to the latent region III, in which the virus persists within latently infected cells.

tivity of latently infected brain macrophages is much lower than that of the productively infected brain macrophages, namely, $\beta_2 < p\beta_1$. Without cART, the system stays in the productive region (Region II in Figure 4.2). Applying effective cART will cause $R_{c1} < R_{c2}$, and the system switches from the productive region to the latent region (Region III in Figure 4.2). The model outcomes realistically capture the clinical and experimental outcomes of the current cART treatment in the brain [30, 31, 85, 86, 83].

4.B.2 HIV-1 brain macrophage infection model with cART and "Shock and Kill" therapy

A reactivation rate, α, is added to system (4.1) to incorporate the effect of latency reversing agents (LRAs) during therapy in the brain. In the presence

Table 4.1: Global dynamics of system (4.1)

Threshold value	P_0	P_1	P_2	Region
$0 < R_c < 1$	GAS	DNE	DNE	I
$1 < R_c, R_{c2} < R_{c1}$	Unstable	GAS	DNE or Unstable*	II
$1 < R_c, R_{c1} < R_{c2}$	Unstable	DNE	GAS	III

GAS: Globally Asymptotically Stable, DNE: Does not exist
* If $1 < R_{c1}$, $0 < R_{c2} < 1$, then P_2 DNE. If $1 < R_{c2} < R_{c1}$, then P_2 is unstable.

of LRA treatment latently infected brain macrophages are reactivated at the rate α. An additional rate, ω, is put into system (4.1) to include the effect of killing reactivated cells during the "Shock and Kill" strategy. The parameter α is set to zero when there is no LRA treatment and the parameter ω is set to zero if there is no kill treatment strategy. The transfer diagram for the model including the effect of LRAs and kill treatment strategy is displayed in Figure 4.3. This model is described by the set of ODEs:

$$\begin{aligned}
\frac{dx}{dt} &= \lambda - kx - (1-\epsilon)\beta_1 xy - \beta_2 xl \\
\frac{dy}{dt} &= p(1-\epsilon)\beta_1 xy - ky - \epsilon\gamma y + \alpha l - \omega y \\
\frac{dl}{dt} &= (1-p)(1-\epsilon)\beta_1 xy + \beta_2 xl - kl + \epsilon\gamma y - \alpha l.
\end{aligned} \tag{4.5}$$

As in model (4.1), the variable $s(t)$ is fit to the integrated viral DNA copies in the data and $v(t)$ is fit to the viral RNA copies in the data.

Let

$$F_2 = \begin{bmatrix} \frac{\lambda p(1-\epsilon)\beta_1}{k} & 0 \\ \frac{\lambda(1-p)(1-\epsilon)\beta_1}{k} & \frac{\lambda\beta_2}{k} \end{bmatrix} \text{ and } V_2 = \begin{bmatrix} k+\epsilon\gamma+\omega & -\alpha \\ -\epsilon\gamma & k+\alpha \end{bmatrix}.$$

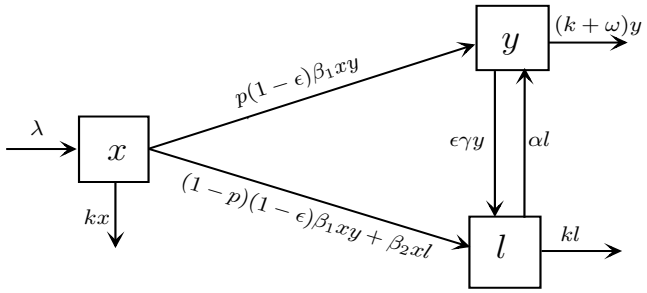

Figure 4.3: Transfer diagram for the model given by equations (4.5) that considered both latently and productively infected cells in the brain with cART and "Shock and Kill" therapy. The αl term represents the reactivation of latently infected macrophages by LRA (the "Shock"), and the ωy term represent the additional death of productively infected cells due to the "Kill" strategy.

Then

$$F_2 V_2^{-1} = \begin{bmatrix} \frac{\lambda p(1-\epsilon)\beta_1(k+\alpha)}{k((k+\epsilon\gamma+\omega)(k+\alpha)-\alpha\epsilon\gamma)} & \frac{\lambda p(1-\epsilon)\beta_1\alpha}{k((k+\epsilon\gamma+\omega)(k+\alpha)-\alpha\epsilon\gamma)} \\ \frac{\lambda(1-p)(1-\epsilon)\beta_1(k+\alpha)+\lambda\beta_2\epsilon\gamma}{k((k+\epsilon\gamma+\omega)(k+\alpha)-\alpha\epsilon\gamma)} & \frac{\lambda(1-p)(1-\epsilon)\beta_1\alpha+\lambda\beta_2(k+\epsilon\gamma+\omega)}{k((k+\epsilon\gamma+\omega)(k+\alpha)-\alpha\epsilon\gamma)} \end{bmatrix}. \tag{4.6}$$

By using the next generation matrix method in [97, 98], we can take the spectral radius of the matrix $F_2 V_2^{-1}$ and derive the control reproduction number

$$\begin{aligned} \overline{R}_c &= \rho(F_2 V_2^{-1}) \\ &= \left[\frac{\lambda}{2k(k(k+\alpha+\epsilon\gamma+\omega)+\omega\alpha)}\right] \\ &[((1-\epsilon)\beta_1(qk+\alpha)+\beta_2(k+\epsilon\gamma+\omega)) \\ &+ \sqrt{((1-\epsilon)\beta_1(qk+\alpha)+\beta_2(k+\epsilon\gamma+\omega))^2 - 4k(1-\epsilon)\beta_1\beta_2(k(k+\epsilon\gamma+\alpha+\omega)+\omega\alpha)}]. \end{aligned} \tag{4.7}$$

4.C Numerical investigation using brain viral data from SIV infection

4.C.1 Data and parameter estimates

A summery of the published SIV brain viral data used in this study is listed in Table 4.2. The SIV studies measuring viral DNA and RNA in brain tissues used different units for measuring viral DNA and RNA. The conversion of SIV DNA to the estimated number of stably infected brain macrophages per gram of brain tissue, and SIV RNA to the estimated SIV RNA copies per gram of brain tissue are given in Section 5.B. A detailed list of the data is located in Table 5.1 in Section 5.B.

Uniform prior distributions were specified for β_1, β_2, k, x_0, y_0, N, ϵ, and γ in system (4.1) since there is a general range for these parameters given in the literature. The uniform prior distributions are based on model estimates in our earlier study [1]. The prior distributions are listed in Table 5.2 in Section 5.C.

The parameters β_1, β_2, k, x_0, y_0, N, ϵ, and γ were estimated by fitting system (4.1) simultaneously to the SIV brain viral data for untreated and cART-exposed animals (data in the first eight rows of Table 4.2). For count data, the negative binomial distribution can be interpreted as the mean number of counts $\mathrm{E}[Y] = \mu$ with the variance $\mathrm{Var}[Y] = \frac{\mu}{p}$ overdispersed, since $0 < p < 1$, $\mathrm{Var}[Y] > \mathrm{E}[Y]$ [64]. Since each of the observed SIV brain viral datasets are overdispersed count data (variance of the data is larger than the mean of the data), a negative binomial distribution is chosen to describe each of the datasets except for the untreated SIV brain viral RNA dataset.

The untreated SIV brain viral RNA dataset is also overdispersed count data; however, many of the counts in this dataset are very large positive numbers. For this reason, a normal distribution is used to describe the $\log_{10}$ of the untreated SIV brain viral RNA dataset. The probability models describing these datasets is given in equations (5.13) and (5.14) and the likelihood function is given by equation (5.15). The estimated parameter values for system (4.1) are displayed in Table 4.3 and the fit of system (4.1) to the data is visualized in Figure 4.4. The method of Bayesian inference was used for fitting system (4.1) simultaneously to the eight datasets and this method is described in Section 5.D. The estimated parameters were used to predict the effects of LRA drugs in an SIV experiment (study in the last row of Table 4.2) by using system (4.5) with $\omega = 0$ and varying the reactivation rate, α, from 0.01 to 100. The mean prediction of the LRA drugs SIV experiment is shown in Figure 4.5. The estimated parameters were also used to predict the "Shock and Kill" strategy by varying the reactivation rate, α, and additional kill rate, ω, from 0 to 40. From the prediction of the "Shock and Kill" strategy, a parameter region is found wherein the strategy is safe and effective. This parameter region is displayed in Figure 4.6 and the mean of the predicted model solutions within this region are shown in Figure 4.7. Further details about the completion of these predictions are presented in Section 5.D.

The estimated parameter values in Table 4.3 are consistent with those estimated in our earlier modeling work on HIV-1 and SIV infection in the brain [1]. The use of additional viral RNA data in the fitting allowed narrower credible intervals for the estimated parameter values than obtain in [1]. Comparisons between the estimated parameter values in Table 4.3 and those estimated for HIV-1 infection of $CD4^+$ T cells in the peripheral blood reveal the distinct

biology and viral dynamics in the brain. More specifically, the transmission coefficients β_1 and β_2 for SIV infection in the brain are at least $3\log_{10}$ fold smaller than the transmission rate for the HIV-1 infection of $CD4^+$ T cells in the peripheral blood after the units are converted from per year to per day [99]. Our earlier estimates in [1] on HIV-1 and SIV-1 infection in the brain showed that SIV infection in the brain of macaques from this animal model can be 10 times faster than HIV-1 infection in human brains. These estimates together show that the HIV-1 infection rate in the brain is much slower than the infection rate among T cells in peripheral blood.

Table 4.2: SIV brain viral DNA and RNA data

Type of SIV brain viral data	Number of animals	Treatment*	Source and Reference
DNA	30	untreated	[100, 31, 85]
RNA	116	untreated	[101, 102, 103, 100, 85, 104, 105, 106, 107, 108, 31]
DNA	6	cART 4 days p.i.	[85]
RNA	6	cART 4 days p.i.	[85]
DNA	5	cART 12 days p.i.	[31]
RNA	5	cART 12 days p.i.	[31]
DNA	2	cART 42 days p.i.	[86]
RNA	2	cART 42 days p.i.	[86]
RNA	2	cART 12 days p.i., LRA 530-594 days p.i.	[32]

* p.i. denotes post-innoculation.

Table 4.3: Fitted parameter estimates with the maximum posterior as the point estimate and 95% credible intervals

Symbol	Parameter	Estimate (95% credible interval)	Unit
β_1	Transmission rate between susceptible and productively infected brain macrophages	1.17×10^{-5} $(5.75 \times 10^{-6}, 1.52 \times 10^{-5})$	g per year
β_2	Transmission rate between susceptible and latently infected brain macrophages	2.23×10^{-6} $(2.92 \times 10^{-7}, 4.18 \times 10^{-6})$	g per year
k	Natural death rate of brain macrophages	4.45 $(0.627, 9.84)$	per year
x_0	Initial value for x	2.13×10^{6} $(2.09 \times 10^{6}, 3.85 \times 10^{6})$	per g
y_0	Initial value for y	11.0 $(9.06, 11.1)$	per g
N	viral RNA copies produced by a productively infected brain macrophage	1.35×10^{3} $(773, 1.85 \times 10^{3})$	per g
ϵ	cART effectiveness $\epsilon \times 100\%$	0.180 $(0.150, 0.654)$	-
γ	$\epsilon\gamma$ is the rate productive brain macrophages deactivate once cART is applied	124 $(27.8, 152)$	per year

Table 4.4: Range of SIV RNA copies per gram of brain tissue corresponding to brain lesion severity for untreated SIV-infected animals in experimental studies.

Brain lesion severity	Range (minimum to maximum) of SIV RNA copies per gram of brain tissue	Brain lesion severity graphical visualization region color**	Brain lesion severity graphical visualization point color	Source and Reference
Unknown*	1.25×10^1 - 1.10×10^8	-	Black	[103, 100, 85, 105, 106, 108]
None	2.5×10^1 - 1.06×10^6	No color	Blue	[101, 102, 104, 106, 107, 31]
Mild	1.97×10^3 - 2.86×10^7	Yellow	Red	[101, 102, 106, 31]
Moderate	1.12×10^5 - 4.35×10^8	Orange	Red	[102, 104, 106, 107, 31]
Severe	2.97×10^7 - 1.18×10^9	Red	Red	[101, 102, 104, 106, 107, 31]

* The brain lesion severity status of some animals is unknown because brain lesions for untreated SIV infection in these experimental studies are historically observed after 42 days post-inoculation (p.i.) [106]. In other cases, the brain lesion severity status of some animals is unknown because the brain lesion severity statuses were not published in the experimental results.

** The minimum of the brain lesion severity ranges is visualized in the yellow (mild), orange (moderate), and red (severe) regions found in Figures 4.4, 4.5, and 4.7.

4.C.2 Establishment of latent reservoir of brain macrophages in model (4.1)

Untreated SIV-infected animals in experimental studies that showed brain lesions had a minimum number of SIV RNA copies per gram of brain tissue of 1.97×10^3 and a maximum number of SIV RNA copies per gram of brain tissue of 1.18×10^9. A summary of the SIV RNA copies per gram of brain tissue ranges corresponding to brain lesion severity for these animals is given in Table 4.4.

The mean model predictions and 95% prediction interval in Figure 4.4 (a - c) shows the progression of untreated SIV infection in the brain. These SIV experimental studies use an animal model that consistently results in encephalitis by 84 days p.i. for untreated SIV infection [31, 85]. SIV encephalitis in these experimental studies is typically characterized by the formation of moderate or severe brain lesions [107]. The mean model prediction in Figure 4.4 (c) at 84 days p.i. shows that the model (4.1) solution for the SIV viral load is approaching the known range for presenting moderate brain lesions.

The mean model predictions and 95% prediction intervals in Figure 4.4 (d - f), (g - i), and (j - l) show that once cART is applied the productively infected brain macrophages are suppressed but there remains persistent and latently infected brain macrophages. Our model demonstrates that initiation of early cART at 4 days p.i. (Figure 4.4 (c - d)) and initiation of cART at 12 days p.i. (Figure 4.4 (e - f)) suppresses the SIV viral load to below the range associated with presenting mild brain lesions. However, when cART is initiated later at 42 days p.i., our model indicates that after 42 days p.i. there is about 70 days of exposure to the SIV viral load range associated with presenting mild brain

lesions before falling below this range. The red points in Figure 4.4 (l) denote the two animals with brain lesions at autopsy 224 and 231 days p.i. and the brain lesion severity for these animals is mild [86, 102]. The observation of both animals having mild brain lesions after cART initiation at 42 days p.i. is consistent with the model showing that after cART initiation at 42 days p.i. there is about 70 days of exposure to the SIV viral load range associated with presenting mild brain lesions Figure 4.4 (l).

Model (4.1) successfully reproduces the effects seen in experimental SIV studies of the brain viral reservoir: without cART, viral infection increases slowly over time, and with effective cART, productive infection in the brain is reduced or suppressed but there remains persistent latent virus in brain cells (Figure 4.4) [31, 85, 86].

4.C.3 Studying the effects of LRA treatment using model (4.5)

The prediction in Figure 4.5 (a - c) and (d - f) initially present similar results as in Figure 4.4 (g - i) where cART is started at 12 days p.i. leading to the suppression of productively infected brain macrophages and the persistence of latently infected brain macrophages. The cART is continued throughout the prediction in Figure 4.5 (a - c) and (d - f). LRA drugs are initiated during the period between 530-594 days p.i. causing the latently infected brain cells to reactivate. The prediction in Figure 4.5 (a - c) reactivates latently infected brain cells at a low reactivation rate ($0.01 \leq \alpha \leq 0.03$) and avoids the SIV viral load range associated with presenting mild brain lesions (Figure 4.5 (b)). The blue point in Figure 4.5 (b) represents the average number of SIV RNA

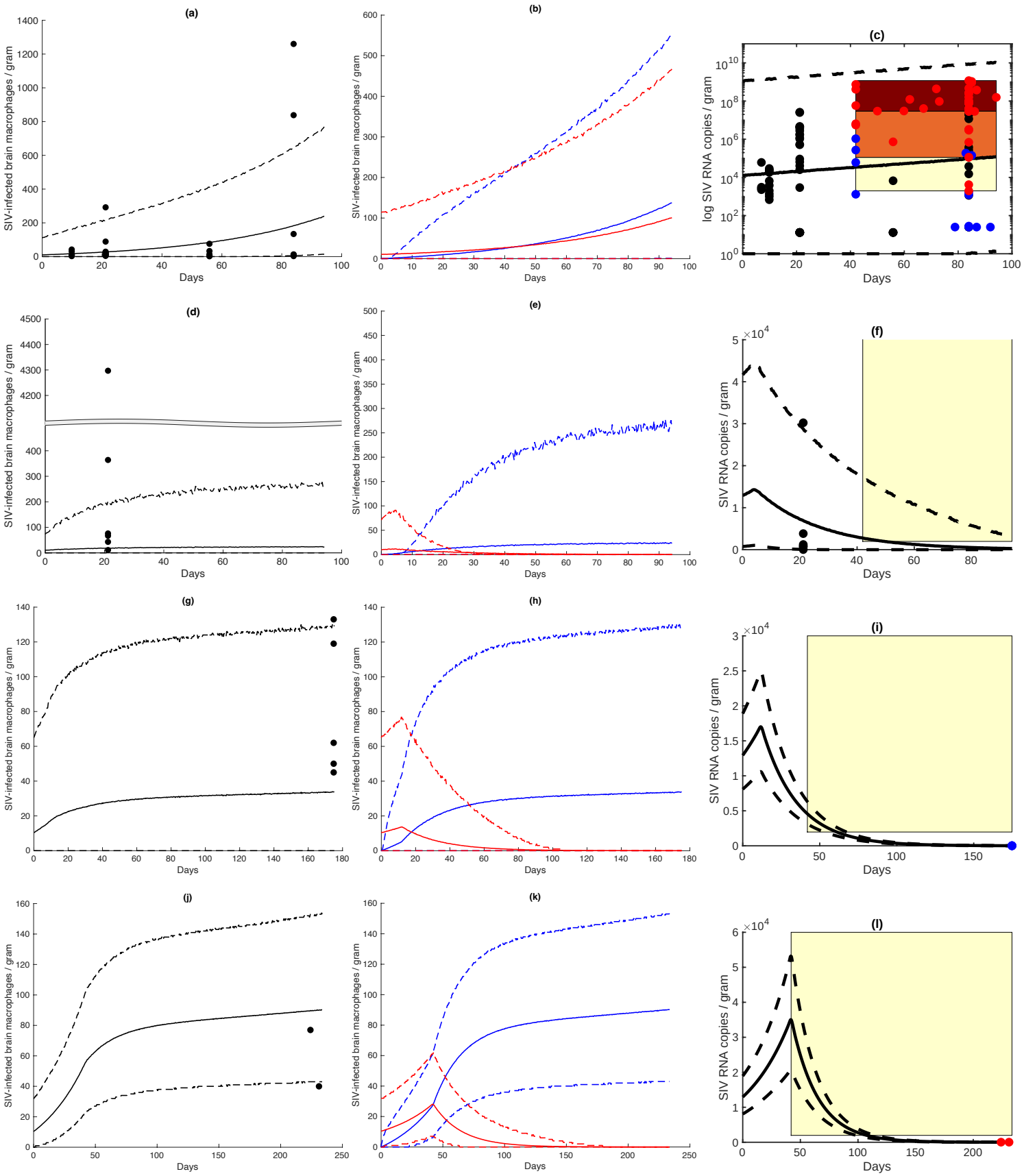

Figure 4.4: Modeling SIV infection of the brain: first row **(a)-(c)** untreated animals; second row **(d)-(f)** cART-exposed animals at 4 days p.i.; third row **(g)-(i)** cART-exposed animals at 12 days post-inoculation (p.i.); fourth row **(j)-(l)** cART-exposed animals at 42 days p.i.; first column **(a)-(j)** stably infected brain macrophages, data (black points), mean model prediction (black curve), 95% prediction interval (dashed black curves); second column **(b)-(k)** productively and latently infected brain macrophages are shown in red and blue respectively, mean model prediction (solid curve), 95% prediction interval (dashed curves); third column **(c)-(l)** viral load, unknown brain lesion status data (black points), without brain lesions data (blue points), and with brain lesions data (red points), mean model prediction (black curve), 95% prediction interval (dashed black curves). Animals that showed mild, moderate, and severe brain lesions had SIV RNA copies per gram of brain tissue ranges 1.97×10^3 to 2.86×10^7, 1.12×10^5 to 4.35×10^8, and 2.97×10^7 to 1.18×10^9, respectively. (The minimum of these brain lesion severity ranges is visualized in the yellow (mild), orange (moderate), and dark red (severe) regions in the third column **(c)-(l)**.

copies per gram of brain tissue of the macaque without brain lesions [32]. The prediction in Figure 4.5 (d - f) reactivates latently infected brain cells and produce SIV RNA copies per gram of brain tissue that reach a dangerous level (spike into the yellow region with $8.88 \leq \alpha \leq 30.9$ and into the orange region $32.7 \leq \alpha \leq 73.0$) associated with the formation of brain lesions and neurological disorders (Figure 4.5 (f)). The red open circle in Figure 4.5 (f) represents the average number of SIV RNA copies per gram of brain tissue and the red point in Figure 4.5 (f) represents the SIV RNA copies per gram of brain tissue in the occipital cortex of the macaque with brain lesions [32]. In all predictions (Figures 4.5 (a - c) and 4.5 (d - f)), after LRA drugs are stopped at 594 days p.i., the number of SIV RNA copies per gram of brain tissue decreases due to the continued use of cART. In Figure 4.5 (d - f), despite the number of SIV RNA copies per gram of brain tissue subsiding after the LRA drugs are stopped, once the number of SIV RNA copies per gram of brain tissue reaches the high threshold associated with the formation of brain lesions, this acts as a trigger for continued neuroinflammation and signal disruption in the brain.

4.C.4 Identifying a parameter region for safe and effective "Shock and Kill" strategy using model (4.5)

The mean control reproduction number for the "Shock and Kill" therapy model, mean $\overline{R}_c$, (4.7) is varied by the reactivation rate, α, and an additional kill rate, ω, to find a suitable balance between the effect of LRA drugs and the kill strategy (Figure 4.6). When $\overline{R}_c < 1$, both productively and latently infected brain macrophages are eradicated. The turquoise region in Figure 4.6 displays the values of α and ω that lead to a safe and effective

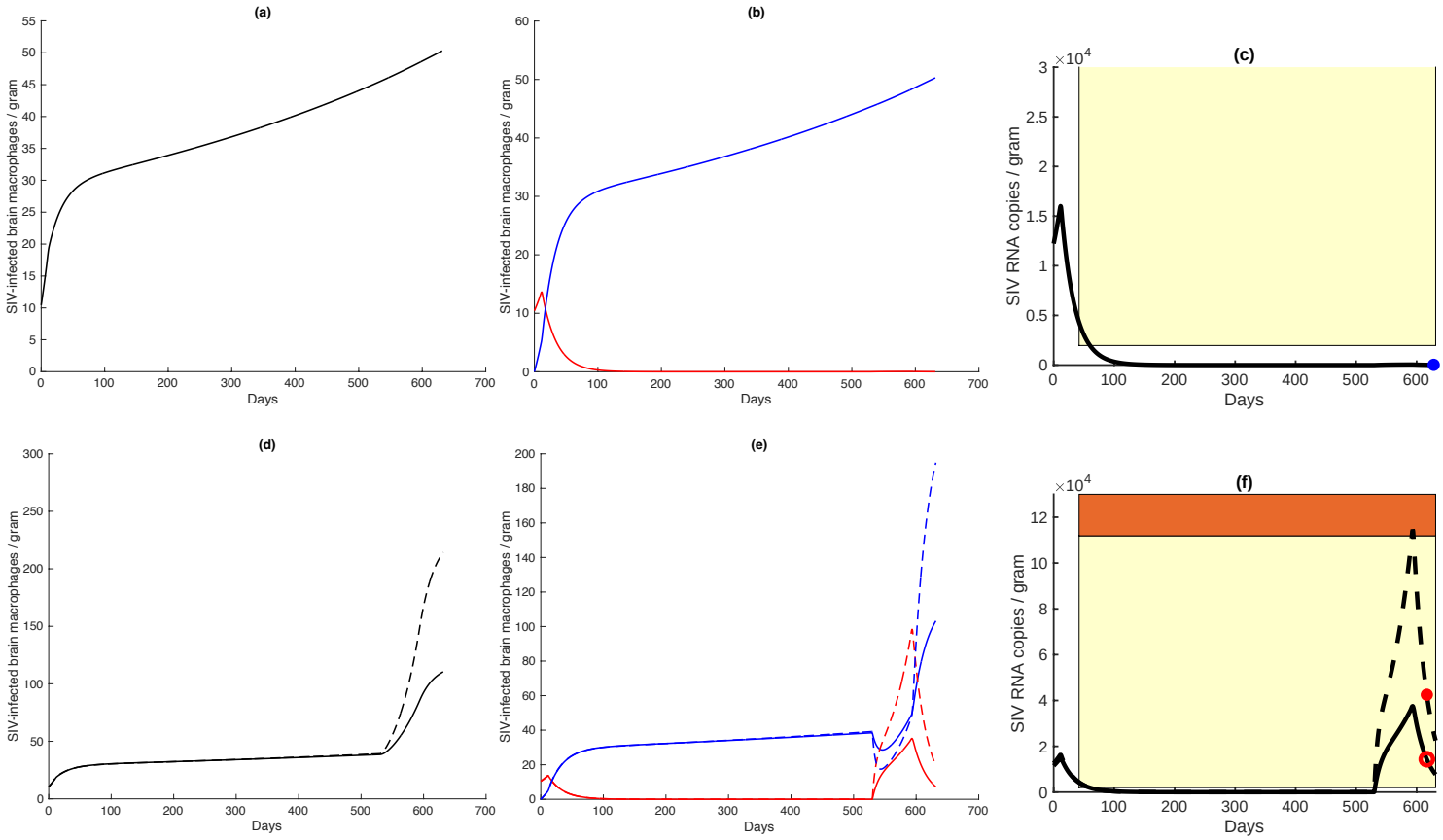

Figure 4.5: Mean predicted solution for SIV **(a)** stably, **(b)** productively and latently infected brain macrophages and **(c)** viral load for cART exposure at 12 days post-inoculation (p.i.) and LRA initiated during the period 530-594 days p.i. for macaque without brain lesions (blue point in **(c)**). Mean predicted solution for SIV **(d)** stably, **(e)** productively and latently infected brain macrophages and **(f)** viral load for cART exposure at 12 days p.i. and LRA initiated during the period 530-594 days p.i. for macaque with brain lesions (red open circle average viral RNA per gram, red point viral RNA per gram in occipital cortex in **(f)**). Productively and latently infected brain macrophages in column two **(b)-(e)** are shown in red and blue respectively. Animals that showed mild and moderate brain lesions had SIV RNA copies per gram of brain tissue ranges 1.97×10^3 to 2.86×10^7 and 1.12×10^5 to 4.35×10^8, respectively. (The minimum of these brain lesion severity ranges is visualized in the yellow (mild) and orange (moderate) regions in the third column **(c)-(f)**.

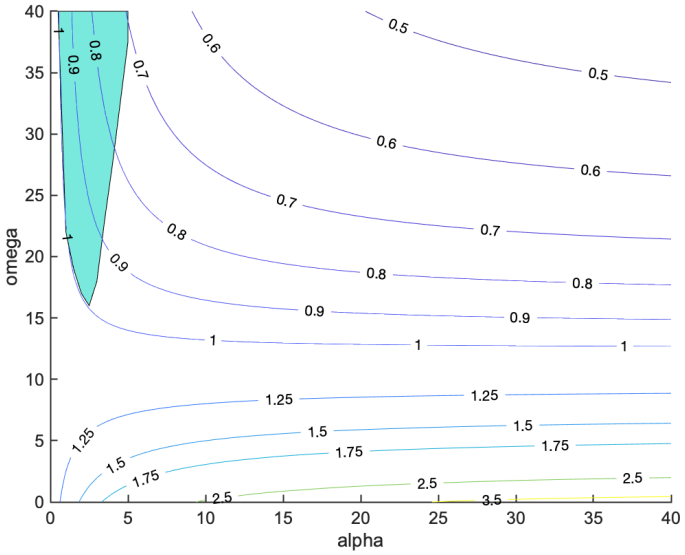

Figure 4.6: Mean control reproduction number for the "Shock and Kill" therapy model given by equations (4.5), mean $\overline{R}_c$, varied by α and ω. The turquoise region displays the values of α and ω that lead to a safe and effective treatment strategy.

treatment strategy, restricting brain viral RNA burden associated with neuroinflammation and eradicating the latent reservoir of brain macrophages. In the prediction displayed in Figure 4.7, cART is started at 12 days p.i. leading to the suppression of productively infected brain macrophages and the persistence of latently infected brain macrophages and the cART is continued throughout the prediction in Figure 4.7. LRA drugs and a kill treatment strategy are initiated at 175 days p.i. causing the productively and latently infected brain macrophages to be eradicated while avoiding the SIV viral load range associated with neuroinflammation (Figure 4.7).

4.D Discussion

Our mathematical model recapitulates the clinical and experimental observations that effective cART can suppress productive infection of brain macrophages

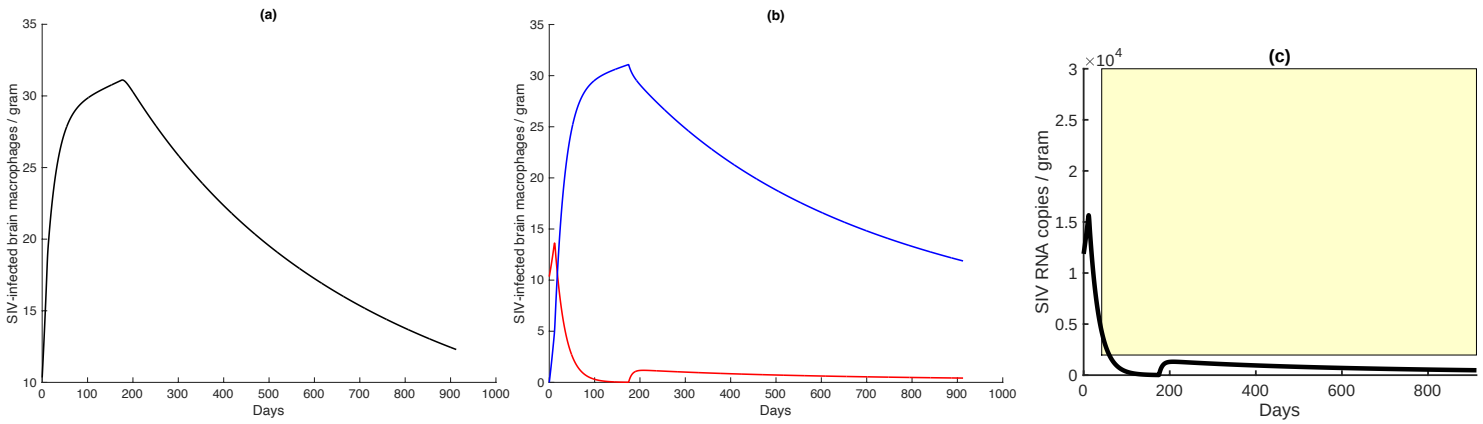

Figure 4.7: Mean predicted solution for SIV **(a)** stably, **(b)** productively and latently infected brain macrophages (shown in red and blue respectively) and **(c)** viral load for cART treated macaques at 12 days post-inoculation (p.i.) and "Shock and Kill" therapy initiated at 175 days p.i. for model solutions within the turquoise region in Figure 4.6. Macaques with mild brain lesions have SIV RNA copies/g between 1.97×10^3 to 2.86×10^7, which is visualized in the yellow region in **(c)**.

but leaves a latent reservoir of brain macrophages. By adding a reactivation rate of the latent reservoir into the model, we can assess the LRA strategy, prompting the model to offer an explanation for the experimental observation of SIV encephalitis and viral RNA copy number per gram of brain tissue from LRA-exposed animals. Furthermore, our mathematical model indicates that there exists a biologically realistic parameter regime where the "Shock and Kill" strategy is safe and effective in the brain.

There is limited data available for HIV-1 brain infection and there is difficulty in obtaining precise estimates for the duration a person might have had HIV-1 infection. In SIV studies the duration of infection and time of treatment are known. SIV studies from the same animal model were used to confirm the behavior of the mathematical models [101, 102, 103, 100, 85, 104, 105, 106, 107, 108, 31, 86]. In a SIV study from 2011, twelve pigtailed macaques were inoculated with the virus and three of these macaques were treated with cART

at 4 days p.i. [85]. It was found that the macaques treated at 4 days p.i. had reduced brain viral RNA at 21 days p.i. but there was not a reduction in viral DNA at 21 days p.i. Similarly, in a SIV study from 2010, eleven pigtailed macaques were inoculated with virus and five of these macaques were treated with cART at 12 days p.i. [31]. It was discovered that the macaques treated at 12 days p.i. had reduced brain viral RNA at 175 days p.i. but there was not a reduction in viral DNA at 175 days p.i. Also, in a SIV study from 2005, four pigtailed macaques were inoculated with virus and two of these macaques were treated with cART at 42 days p.i. [86]. It was determined that the macaques treated at 42 days p.i. had reduced brain viral RNA at 224 and 231 days p.i. but there was not a reduction in viral DNA at 224 and 231 days p.i. The mathematical model given by system (4.1) produces this phenomenon (see Section 4.B.1 and 4.C.2). In a SIV study from 2017, two macaques (Mn1 and Mn2) were treated with cART 12 days p.i., LRA was started 530 days p.i. and LRA therapy was finished 594 days p.i. [32]. Since macaque Mn2 was presenting neurological symptoms after the use of LRA therapy, the two macaques were euthanized at 612 days p.i. It was found that LRA treatment reactivated latent virus that could be detected in the brain of macaque Mn2. The number of viral RNA copies per gram of brain tissue in basal ganglia (75), parietal cortex (475), and occipital cortex (42500) for Mn2 is lower than RNA levels historically observed in their SIV animal model of animals with symptoms associated with SIV encephalitis (in Section 4.C.2 the range 1.12×10^5 to 1.18×10^9 SIV RNA copies per gram of brain tissue was determined to be associated with moderate or severe brain lesions and SIV encephalitis). The mathematical model that includes the effect of LRAs, given by system (4.5), offers an explanation for why macaque Mn2 developed neurological symptoms

despite having a lower number of viral RNA copies per gram of brain tissue than expected at autopsy. The mathematical model prediction indicates that if the experimental conditions of starting cART at 12 days p.i., initiating LRA at 530 days p.i., finishing LRA therapy at 594 days p.i., and measuring the viral load at 612 days p.i., then the viral load in the occipital cortex would have to pass through the region associated with SIV-induced brain disease (encephalitis) in order to have the level of 42500 viral RNA copies per gram of brain tissue in the occipital cortex at autopsy (see Section 4.C.3).

A full mathematical analysis of the "Shock and Kill" model given by equations (4.5) is warranted to further investigate solutions that lead to a safe and effective "Shock and Kill" strategy in the brain. Indeed, developing mathematical models that incorporate a more realistic additional kill term in equations (4.5) to kill reactivated infected brain macrophages by host immune responses is needed to test different treatment strategies. Potential strategies could be to bolster the CD8+ T cell response in the brain to kill reactivated infected brain macrophages or to strengthen the innate mechanisms in the brain that lead to programmed cell death in reactivated infected brain macrophages. Using HIV-1 post-mortem patient data and other SIV animal models such as ones that use Indian rhesus macaques that have a longer duration of infection would assist in further validating the qualitative behaviors of the mathematical models for HIV-1 brain infection.

Chapter 5

Supplementary material for Chapter 4

5.A Mathematical results and proofs

Using the theory of asymptotically autonomous differential equations [109, 110], the asymptotic behaviors of system (4.1) are the same as the following 2-dimensional system of differential equations in the bounded feasible region $D = \{(x, y) \in \mathbb{R}^2_+ : 0 \leq x + y \leq \frac{\lambda}{k}\}$:

$$\begin{aligned} \frac{dx}{dt} &= \lambda - kx - (1-\epsilon)\beta_1 xy - \beta_2 x(\frac{\lambda}{k} - x - y) = g(x, y), \\ \frac{dy}{dt} &= p(1-\epsilon)\beta_1 xy - (k + \epsilon\gamma)y = h(x, y). \end{aligned} \tag{5.1}$$

The Jacobian matrix of system (5.1) is

$$J = \begin{bmatrix} -k - (1-\epsilon)\beta_1 y + \beta_2 x - \beta_2(\frac{\lambda}{k} - x - y) & -(1-\epsilon)\beta_1 x + \beta_2 x \\ p(1-\epsilon)\beta_1 y & p(1-\epsilon)\beta_1 x - k - \epsilon\gamma \end{bmatrix}. \quad (5.2)$$

Theorem 5.1: *1. If the control reproduction number $R_c < 1$, then the disease-free equilibrium P_0 is locally asymptotically stable. If $R_c > 1$, then P_0 is unstable.*

2. If $R_c > 1$ and $R_{c1} > R_{c2}$, then the productive equilibrium P_1 is locally asymptotically stable.

3. If $R_c > 1$ and $R_{c1} < R_{c2}$, then the latent equilibrium P_2 is locally asymptotically stable.

Proof. The Jacobian matrix evaluated at P_0 is

$$J(P_0) = \begin{bmatrix} -k + \beta_2\frac{\lambda}{k} & (\beta_2 - (1-\epsilon\beta_1))\frac{\lambda}{k} \\ 0 & p(1-\epsilon)\beta_1\frac{\lambda}{k} - (k+\epsilon\gamma) \end{bmatrix}. \quad (5.3)$$

Since the matrix (5.3) is upper triangular, the eigenvalues of the matrix $J(P_0)$ are $\mu_1 = -k + \beta_2\frac{\lambda}{k}$ and $\mu_2 = p(1-\epsilon)\beta_1\frac{\lambda}{k} - (k+\epsilon\gamma)$. If $R_c < 1$, then $\mu_1, \mu_2 < 0$ and the disease-free equilibrium P_0 is locally asymptotically stable. If $R_c > 1$, then $\max\{\mu_1, \mu_2\} > 0$ and P_0 is unstable.

The Jacobian matrix evaluated at P_1 is

$$J(P_1) = \begin{bmatrix} -k-(1-\epsilon)\beta_1 y_1 + \beta_2 x_1 - \beta_2(\frac{\lambda}{k} - x_1 - y_1) & -(1-\epsilon)\beta_1 x_1 + \beta_2 x_1 \\ p(1-\epsilon)\beta_1 y_1 & p(1-\epsilon)\beta_1 x_1 - k - \epsilon\gamma \end{bmatrix}$$
$$= \begin{bmatrix} -k-(1-\epsilon)\beta_1 y_1 + \beta_2 x_1 - \beta_2(\frac{\lambda}{k} - x_1 - y_1) & -(1-\epsilon)\beta_1 x_1 + \beta_2 x_1 \\ p(1-\epsilon)\beta_1 y_1 & 0 \end{bmatrix} \tag{5.4}$$

since $p(1-\epsilon)\beta_1 x_1 - k - \epsilon\gamma = \frac{(p(1-\epsilon)\beta_1)(k+\epsilon\gamma)}{p(1-\epsilon)\beta_1} - (k+\epsilon\gamma) = 0$. If $R_c > 1$ and $R_{c1} > R_{c2}$, then $R_{c1} > 1 > \frac{R_{c2}}{R_{c1}}$ and by using the productive equilibrium P_1,

$$\begin{aligned} \mathrm{tr}(\mathrm{J}(P_1)) &= -k - \frac{\lambda}{k}\beta_2 + 2x_1\beta_2 - ((1-\epsilon)\beta_1 - \beta_2)y_1 \\ &= k(\frac{R_{c2}}{R_{c1}} - R_{c1}) \\ &< 0 \end{aligned} \tag{5.5}$$

and

$$\begin{aligned} \det(\mathrm{J}(P_1)) &= ((1-\epsilon)\beta_1 - \beta_2)p(1-\epsilon)\beta_1 x_1 y_1 \\ &= (1 - \frac{1}{R_{c1}})(1 - \frac{R_{c2}}{R_{c1}}) \\ &> 0. \end{aligned} \tag{5.6}$$

By the Routh-Hurwitz condition, P_1 is locally asymptotically stable.

The Jacobian matrix evaluated at P_2 is

$$J(P_2) = \begin{bmatrix} k - \frac{\lambda}{k}\beta_2 & \frac{-(1-\epsilon)\beta_1 k}{\beta_2} + k \\ 0 & p(1-\epsilon)\beta_1\frac{k}{\beta 2} - k - \epsilon\gamma \end{bmatrix}. \tag{5.7}$$

Since the matrix (5.7) is upper triangular, the eigenvalues of the matrix 5.7

are $\mu_1 = k - \frac{\lambda}{k}\beta_2$ and $\mu_2 = p(1-\epsilon)\beta_1\frac{k}{\beta 2} - k - \epsilon\gamma$. If $R_c > 1$ and $R_{c1} < R_{c2}$, then $\mu_1, \mu_2 < 0$ and the latent equilibrium P_2 is locally asymptotically stable.

□

Theorem 5.2: *If the control reproduction number $0 < R_c \leq 1$, then the disease-free equilibrium P_0 is globally asymptotically stable in Γ.*

Proof. When $0 < R_c \leq 1$, P_0 is the only equilibrium.

Consider the Lyapunov function $L = y$. Then

$$\begin{aligned} L' = y' &= p(1-\epsilon)\beta_1 xy - ky - \epsilon\gamma y \leq (k+\epsilon\gamma)y(R_{c1}-1) \\ &\leq (k+\epsilon\gamma)y(R_c - 1) \leq 0. \end{aligned}$$

The maximal invariant set in $\{(x, y, l) \in \Gamma : L' = 0\}$ is the singleton P_0. By LaSalle's Invariance Principle, all limit points of solutions belong to the largest invariant set in $\{(x, y, l) \in \Gamma : L' = 0\}$. Therefore, all solutions in Γ converge to P_0 and P_0 is globally asymptotically stable in Γ.

□

Theorem 5.3: *If $R_c > 1$ and $R_{c1} > R_{c2}$, then the productive equilibrium P_1 is globally asymptotically stable in $\mathring{\Gamma}$. If $R_c > 1$ and $R_{c1} < R_{c2}$, then the latent equilibrium P_2 is globally asymptotically stable in Γ.*

Proof. The asymptotic behaviors of system (4.1) in Γ are the same as the asymptotic behaviors of system (5.1) in D. In system (5.1), let $\mathbf{f}(x, y) = (g(x, y), h(x, y))$.

Consider a scalar-valued function $\alpha(x, y) = \frac{1}{xy(\frac{\lambda}{k} - x - y)}$,
where $(x, y) \in \mathring{D} = \{(x, y) : 0 < x + y < \frac{\lambda}{k}\}$. For all $(x, y) \in \mathring{D}$,

$$
\begin{aligned}
div(\alpha \mathbf{f}) &= \frac{\partial}{\partial x}(\alpha g) + \frac{\partial}{\partial y}(\alpha h) \\
&= \frac{1}{xy(\frac{\lambda}{k} - x - y)}\Big(\frac{-\lambda}{x} + \frac{\lambda - kx}{(\frac{\lambda}{k} - x - y)} - \frac{(1-p)(1-\epsilon)\beta_1 xy}{(\frac{\lambda}{k} - x - y)} - \frac{(k+\epsilon\gamma)y}{\frac{\lambda}{k} - x - y}\Big) \\
&< \frac{1}{xy(\frac{\lambda}{k} - x - y)}\Big(\frac{-\lambda}{x} + k - \frac{(1-p)(1-\epsilon)\beta_1 xy}{(\frac{\lambda}{k} - x - y)} - \frac{(k+\epsilon\gamma)y}{\frac{\lambda}{k} - x - y}\Big) \\
&< \frac{1}{xy(\frac{\lambda}{k} - x - y)}\Big(\frac{-\lambda}{x} + k\Big) \\
&= \frac{k}{x^2 y(\frac{\lambda}{k} - x - y)}(x - \frac{\lambda}{k}) \\
&< 0.
\end{aligned}
$$

Therefore, by Dulac's criteria, system (5.1) has no closed orbit lying entirely in $\mathring{D}$. So, no periodic solutions can exist.

By the Poincare-Bendixson Theorem, if $R_c > 1$ and $R_{c1} > R_{c2}$, all solutions with initial condition in $\mathring{D}$ must have P_1 as an ω-limit point. Since P_1 is locally asymptotically stable, solutions that get close to P_1 must converge to P_1 and all ω-limit sets in $\mathring{D}$ are equal to the singleton $\{P_1\}$. Therefore, P_1 is globally stable in $\mathring{D}$ when $R_c > 1$ and $R_{c1} > R_{c2}$.

Similarly, by using the Poincare-Bendixson Theorem, if $R_c > 1$ and $R_{c1} < R_{c2}$, then P_2 is globally stable in $\mathring{D}$.

□

5.B Data conversion

SIV brain viral DNA was measured in three different units [100, 31, 85, 86]: $\log_{10}$ SIV DNA copy equivalents per 2 micrograms of total DNA, $\log_{10}$ SIV

DNA copy equivalents per 10,000 cells, and SIV DNA copy equivalents per microgram of total DNA.

The first and second SIV brain viral DNA units were converted to integrated SIV DNA per gram of brain tissue in the same fashion as described in the supplementary material of our previous modeling study [1]. Since each SIV-infected brain macrophage is assumed to contain a single copy of integrated viral DNA, the integrated SIV DNA per gram of brain tissue is equal to the number of stably infected brain macrophages per gram of brain tissue.

For the third SIV brain viral DNA unit, this data was converted to integrated SIV DNA per gram of brain tissue in a similar way to the first SIV brain viral DNA unit. The SIV DNA copy equivalents per microgram of total DNA was converted to SIV DNA copy equivalents per gram of brain tissue by using the conversion that each gram of brain tissue contains 4 micrograms of total host genomic DNA. By using the ratio of integrated proviral DNA to total viral DNA (1:86) [111] and our assumption that each SIV-infected brain macrophage is assumed to contain a single copy of integrated viral DNA, we obtain the number of stably infected brain macrophages per gram of brain tissue.

SIV brain viral RNA was measured in five different units [101, 102, 103, 100, 85, 104, 105, 106, 107, 108, 31]: SIV RNA copy equivalents per microgram of total RNA, $\log_{10}$ SIV RNA copy equivalents per microgram of total RNA, SIV RNA copy equivalents per 2 micrograms of total RNA, $\log_{10}$ SIV RNA copy equivalents per 2 micrograms of total RNA, and 10^6 SIV RNA copy equivalents per microgram of total RNA. When the SIV brain viral RNA unit is not already in the form of SIV RNA copy equivalents per microgram of total RNA, they are converted to SIV RNA copy equivalents per microgram of total RNA by

exponentiation. The SIV RNA copy equivalents per microgram of total RNA was converted to SIV RNA copy equivalents per gram of brain tissue by using the conversion that each gram of brain tissue contains 25 micrograms of total host genomic RNA.

Some SIV studies measured SIV brain viral DNA and RNA in multiple regions of the brain [101, 100, 85, 104, 106, 107, 86]. For these SIV studies, the average SIV brain viral DNA and RNA across the brain regions was used. This was done so that the fitted system (4.1) and prediction using system (4.5) would be projecting the average viral dynamics per gram of brain tissue.

After these conversions are completed, the data for SIV RNA copies per gram of brain tissue and the estimated number of stably infected brain macrophages per gram of brain tissue are located in Table 5.1.

Table 5.1: SIV RNA copies per gram of brain tissue and estimated number of stably infected brain macrophages per gram of brain tissue at different times post-inoculation (p.i.).

Brain lesion severity	cART treatment start time (days p.i.)	Time of collection (days p.i.)	Viral RNA copies/g	Estimated stably infected brain macrophages/g*	Reference
Severe	Untreated	62	1.22×10^8	NA	[101]
Severe	Untreated	60	3.01×10^7	NA	[101]
Severe	Untreated	50	2.97×10^7	NA	[101]
Severe	Untreated	84	8.19×10^7	NA	[101]
Mild	Untreated	86	2.86×10^7	NA	[101]
Severe	Untreated	84	1.18×10^9	NA	[102]
Severe	Untreated	84	4.64×10^8	NA	[102]

Severe	Untreated	84	2.62×10^8	NA	[102]
Moderate	Untreated	84	2.51×10^8	NA	[102]
Moderate	Untreated	84	1.58×10^8	NA	[102]
Moderate	Untreated	84	7.72×10^7	NA	[102]
Moderate	Untreated	84	4.36×10^7	NA	[102]
Mild	Untreated	84	3.30×10^6	NA	[102]
Mild	Untreated	84	4.16×10^3	NA	[102]
Brain lesions present	Untreated	56	7.31×10^5	76	[100]
Severe	Untreated	67	4.06×10^7	NA	[104]
Severe	Untreated	73	9.55×10^7	NA	[104]
Moderate	Untreated	84	1.04×10^8	NA	[104]
Moderate	Untreated	84	3.12×10^6	NA	[104]
Moderate	Untreated	84	1.12×10^5	NA	[104]
Severe	Untreated	42	4.12×10^8	NA	[106]
Severe	Untreated	42	7.42×10^8	NA	[106]
Moderate	Untreated	42	5.80×10^7	NA	[106]
Mild	Untreated	42	5.53×10^6	NA	[106]
Mild	Untreated	42	6.46×10^6	NA	[106]
Severe	Untreated	85	1.06×10^9	NA	[107]
Severe	Untreated	94	1.56×10^8	NA	[107]
Severe	Untreated	85	9.13×10^8	NA	[107]
Moderate	Untreated	87	3.77×10^8	NA	[107]
Moderate	Untreated	72	4.35×10^8	NA	[107]
Moderate/ severe	Untreated	84	1.15×10^5	NA	[108]
Moderate/ severe	Untreated	84	2.96×10^6	NA	[108]

Moderate/ severe	Untreated	84	3.62×10^7	NA	[108]
Moderate/ severe	Untreated	84	7.40×10^7	NA	[108]
Moderate/ severe	Untreated	84	1.02×10^8	NA	[108]
Severe	Untreated	84	8.16×10^7	838	[31]
Severe	Untreated	84	2.66×10^8	1.26×10^3	[31]
Moderate	Untreated	84	2.83×10^7	134	[31]
Mild	Untreated	84	1.97×10^3	12	[31]
Mild	Untreated	84	6.94×10^5	13	[31]
None	Untreated	85	1.42×10^5	NA	[101]
None	Untreated	83	1.88×10^5	NA	[101]
None	Untreated	79	25	NA	[101]
None	Untreated	87	25	NA	[101]
None	Untreated	84	25	NA	[101]
None	Untreated	84	28	NA	[102]
None	Untreated	84	1.23×10^3	NA	[104]
None	Untreated	42	1.31×10^3	NA	[106]
None	Untreated	42	6.10×10^4	NA	[106]
None	Untreated	42	2.70×10^5	NA	[106]
None	Untreated	42	1.06×10^6	NA	[106]
None	Untreated	92	25	NA	[107]
None	Untreated	84	1.66×10^3	3	[31]
Unknown	Untreated	7	3.06×10^3	NA	[103]
Unknown	Untreated	7	2.28×10^3	NA	[103]
Unknown	Untreated	7	6.08×10^4	NA	[103]
Unknown	Untreated	7	2.62×10^3	NA	[103]
Unknown	Untreated	10	6.52×10^3	NA	[103]

Unknown	Untreated	10	1.83×10^4	NA	[103]
Unknown	Untreated	10	1.01×10^3	NA	[103]
Unknown	Untreated	10	1.38×10^3	NA	[103]
Unknown	Untreated	21	12	NA	[103]
Unknown	Untreated	21	12	NA	[103]
Unknown	Untreated	21	12	NA	[103]
Unknown	Untreated	21	12	NA	[103]
Unknown	Untreated	10	2.01×10^3	3	[100]
Unknown	Untreated	10	3.81×10^3	9	[100]
Unknown	Untreated	10	2.92×10^4	42	[100]
Unknown	Untreated	10	679	5	[100]
Unknown	Untreated	10	2.34×10^4	30	[100]
Unknown	Untreated	10	2.48×10^4	12	[100]
Unknown	Untreated	21	12	22	[100]
Unknown	Untreated	21	12	5	[100]
Unknown	Untreated	21	12	11	[100]
Unknown	Untreated	21	12	12	[100]
Unknown	Untreated	21	12	27	[100]
Unknown	Untreated	21	12	13	[100]
Unknown	Untreated	56	6.68×10^3	4	[100]
Unknown	Untreated	56	12	2	[100]
Unknown	Untreated	56	12	13	[100]
Unknown	Untreated	56	12	6	[100]
Unknown	Untreated	56	12	32	[100]
Unknown	Untreated	21	5.28×10^5	5	[85]
Unknown	Untreated	21	1.18×10^6	13	[85]

Unknown	Untreated	21	1.76×10^6	19	[85]
Unknown	Untreated	21	4.32×10^6	29	[85]
Unknown	Untreated	21	4.68×10^6	89	[85]
Unknown	Untreated	21	2.50×10^7	292	[85]
Unknown	Untreated	84	25	NA	[105]
Unknown	Untreated	84	25	NA	[105]
Unknown	Untreated	84	25	NA	[105]
Unknown	Untreated	84	1.52×10^4	NA	[105]
Unknown	Untreated	84	3.78×10^4	NA	[105]
Unknown	Untreated	84	2.60×10^5	NA	[105]
Unknown	Untreated	84	3.73×10^5	NA	[105]
Unknown	Untreated	84	1.17×10^7	NA	[105]
Unknown	Untreated	84	2.79×10^7	NA	[105]
Unknown	Untreated	84	4.00×10^7	NA	[105]
Unknown	Untreated	84	1.10×10^8	NA	[105]
Unknown	Untreated	84	1.04×10^8	NA	[105]
Unknown	Untreated	84	1.94×10^7	NA	[105]
Unknown	Untreated	84	3.56×10^7	NA	[105]
Unknown	Untreated	84	4.82×10^7	NA	[105]
Unknown	Untreated	21	2.92×10^3	NA	[106]
Unknown	Untreated	21	2.52×10^4	NA	[106]
Unknown	Untreated	21	4.04×10^4	NA	[106]
Unknown	Untreated	21	6.47×10^4	NA	[106]
Unknown	Untreated	21	9.20×10^4	NA	[106]
Unknown	Untreated	21	5.16×10^5	NA	[106]
Unknown	Untreated	21	1.04×10^6	NA	[106]

Unknown	Untreated	21	1.74×10^6	NA	[106]
Unknown	Untreated	21	2.78×10^6	NA	[106]
Unknown	Untreated	21	3.66×10^6	NA	[106]
Unknown	Untreated	21	4.46×10^6	NA	[106]
Unknown	Untreated	21	2.60×10^7	NA	[106]
Unknown	Untreated	84	1.14×10^3	NA	[108]
Brain lesions present	42	231	25	40	[86]
Brain lesions present	42	224	25	77	[86]
None	12	175	12	119	[31]
None	12	175	12	133	[31]
None	12	175	12	45	[31]
None	12	175	12	50	[31]
None	12	175	12	62	[31]
Unknown	4	21	25	11	[85]
Unknown	4	21	866	43	[85]
Unknown	4	21	683	67	[85]
Unknown	4	21	1.23×10^3	76	[85]
Unknown	4	21	3.82×10^3	364	[85]
Unknown	4	21	3.02×10^4	4.30×10^3	[85]
None	12 (LRA from 530-594)	628	25	NA	[32]

Moderate/ severe	12 (LRA from 530-594)	617	1.44×10^4	NA	[32]

* If viral DNA was not measured in a study, then the number of stably infected brain macrophages per gram of brain tissue cannot be estimated and not applicable (NA) is written in the cell.

5.C Prior distributions for Bayesian inference.

Uniform prior distributions were specified for β_1, β_2, k, x_0, y_0, N, ϵ, and γ in system (4.1) since there is a general range for these parameters given in the literature. The prior distributions are listed in Table 5.2. The parameters β_1, β_2, k, and x_0 used the same uniform prior distributions as described in [1] and they are the following:

$\beta_1 \sim U(1 \times 10^{-8}, 1 \times 10^{-4})$, $\beta_2 \sim U(1 \times 10^{-8}, 1 \times 10^{-4})$, $k \sim U(0.5, 10.22)$, and $x_0 \sim U(2.07 \times 10^6, 3.94 \times 10^6)$. The constraint $\beta_2 < p\beta_1$ was used for the assumption that infection due to productively infected brain macrophages, β_2, is sufficiently larger than that due to latently infected brain macrophages, β_1. Since $x_0 = \frac{\lambda}{k}$, λ is determined by x_0 and k. Simple linear regression is used to estimate, $\log_{10}(y_0)$, by fitting the following linear model to the $\log_{10}$ SIV DNA copies per gram data for untreated infection (row 1 in Table 4.2):

$$\log_{10}(y) = \log_{10}(y_0) + m_y t_y, \tag{5.8}$$

where $\log_{10}(y)$ is the $\log_{10}$ SIV DNA copies per gram data for untreated infection, $\log_{10}(y_0)$ is the intercept, m_y is the slope, and t_y is the independent

variable time. The intercept of this regression model, $\log_{10}(y_0)$, is estimated to be 1.045, and consequently, y_0 is estimated to be 11.1 and the chosen prior distribution is $y_0 \sim U(1, 11.1)$. It is assumed that $l_0 = 0$. The initial viral load is given by $v_0 = Ny_0$ and consequently, $N = \frac{v_0}{y_0}$. Simple linear regression is used to estimate, $\log_{10}(v_0)$, by fitting the following linear model to the $\log_{10}$ SIV RNA copies per gram data for untreated infection (row 2 in Table 4.2):

$$\log_{10}(v) = \log_{10}(v_0) + m_v t_v, \tag{5.9}$$

where $\log_{10}(v)$ is the $\log_{10}$ SIV RNA copies per gram data for untreated infection, $\log_{10}(v_0)$ is the intercept, m_v is the slope, and t_v is the independent variable time. The intercept of this regression model, $\log_{10}(v_0)$, is estimated to be 3.676 and hence v_0 is estimated to be 4.74×10^3. Since v_0 is estimated to be 4.74×10^3 and $y_0 \sim U(1, 11.1)$, $N \sim U(427, 4.74 \times 10^3)$. The cART effectiveness, ϵ, varies between 0 and 1 and the prior distribution is $\epsilon \sim U(0.01, 1)$. The rate productively infected brain macrophages are deactivated once cART is applied, $\epsilon\gamma$, is unknown and a broad range is chosen for $\gamma \sim U(0.01, 200)$. The proportion of newly infected susceptible brain macrophages by productively infected brain macrophages that enter the productively infected population is assumed to be $p = 0.5$.

Table 5.2: Uniform prior distributions for parameters

Symbol	Parameter	Prior distribution	Unit	Reference(s)
β_1	Transmission rate between susceptible and productively infected brain macrophages	$U(1 \times 10^{-8}, 1 \times 10^{-4})$	g per year	[48]
β_2	Transmission rate between susceptible and latently infected brain macrophages	$U(1 \times 10^{-8}, 1 \times 10^{-4})$ with the constraint $\beta_2 < p\beta_1$	g per year	[48]
k	Natural death rate of brain macrophages	$U(0.5, 10.22)$	per year	[49]
x_0	Initial value for x	$U(2.07 \times 10^6, 3.94 \times 10^6)$	per g	[112, 113, 114]
y_0	Initial value for y	$U(1, 11.1)$	per g	[100, 31, 85]
N	viral RNA copies produced by a productively infected brain macrophage	$U(427, 4.74 \times 10^3)$	per g	[101, 102, 103, 100, 85, 104, 105, 106, 107, 108, 31]
ϵ	cART effectiveness $\epsilon \times 100\%$	$U(0.01, 1)$	-	-
γ	$\epsilon\gamma$ is the rate productive brain macrophages deactivate once cART is applied	$U(0.01, 200)$	per year	-

5.D Model fitting and prediction using Bayesian inference.

The parameters β_1, β_2, k, x_0, y_0, N, ϵ, and γ were estimated by fitting system (4.1) simultaneously to the SIV brain viral data for untreated and cART-exposed animals (data in the first eight rows of Table 4.2). The estimated parameter values for system (4.1) are displayed in Table 5.3 and the fit of system (4.1) to the data is visualized in Figure 4.4. The method of Bayesian inference was used for fitting system (4.1) simultaneously to the eight datasets and this method is described below. The estimated parameters were used to predict the effects of LRA drugs in an SIV experiment (study in the last row of Table 4.2) by using system (4.5) with $\omega = 0$ and varying the reactivation rate, α, from 0.01 to 100. The mean prediction of the LRA drugs SIV experiment is shown in Figure 4.5. The estimated parameters were also used to predict the "Shock and Kill" strategy by varying the reactivation rate, α, and additional kill rate, ω, from 0 to 40. From the prediction of the "Shock and Kill" strategy, a parameter region is found wherein the strategy is safe and effective. This parameter region is displayed in Figure 4.6 and the mean of the predicted model solutions within this region are shown in Figure 4.7. Further details about the completion of these predictions are described below.

Bayesian inference is used to fit system (4.1) simultaneously to the SIV brain viral data for untreated and cART-exposed animals (data in the first eight rows of Table 4.2). Let $D_j = \{d_1^j, \ldots, d_{n_j}^j\}$ and $T_j = \{t_1^j, \ldots, t_{n_j}^j\}$ be the SIV brain viral data and times corresponding to the j^{th} row of Table 4.2. Let $D = \{D_1, \ldots, D_8\}$ and $T = \{T_1, \ldots, T_8\}$.

System (4.1) was solved numerically by using the MATLAB function *ode45*

with the option setting *odeset('NonNegative', 2)* to ensure that numerically solved solutions have nonnegative values [115]. The function *ode45* is based on an explicit Runge-Kutta (4,5) formula.

There are four different scenarios being considered when system (4.1) is being fit simultaneously to the SIV brain viral data for untreated and cART-exposed animals: untreated SIV infection, SIV infection with cART initiated at 4 days p.i., SIV infection with cART initiated at 12 days p.i., and SIV infection with cART initiated at 42 days p.i. For untreated SIV infection, ϵ is set to zero in system (4.1). For the scenarios when cART is initiated at a certain time p.i., ϵ is time dependent in system (4.1):

$$\epsilon(t) = \begin{cases} 0 & \text{before cART is initiated} \\ \epsilon & \text{when cART is initiated} \end{cases} \tag{5.10}$$

where the constant ϵ and is to be estimated. The parameter vector to be estimated in system (4.1) is $\boldsymbol{\nu} = \langle \beta_1, \beta_2, k, x_0, y_0, N, \epsilon, \gamma \rangle$. For untreated infection, let the model solution vector over time for stably infected brain macrophages per gram of brain tissue and SIV RNA copy equivalents per gram of brain tissue be given by $s_u(\boldsymbol{\nu}, t)$ and $v_u(\boldsymbol{\nu}, t)$ respectively. The dataset D_1 will be described by the model solution vector over time $s_u(\boldsymbol{\nu}, t)$. The dataset D_2 will be described by the model solution vector over time $v_u(\boldsymbol{\nu}, t)$. Similarly, for the scenarios when cART is initiated at a certain time p.i., D_3 and D_4 will be described by $s_g(\boldsymbol{\nu}, t)$ and $v_g(\boldsymbol{\nu}, t)$ respectively, D_5 and D_6 will be described by $s_z(\boldsymbol{\nu}, t)$ and $v_z(\boldsymbol{\nu}, t)$ respectively, and D_7 and D_8 will be described by $s_c(\boldsymbol{\nu}, t)$ and $v_c(\boldsymbol{\nu}, t)$ respectively. The subscript letters g, z, and c are inspired by the last name of the first author on the SIV studies [85, 31, 86] in order to quickly

keep track of the corresponding model solution vector for each of the datasets D_3 through D_8.

Since each of the observed SIV brain viral datasets D_1 and D_3 through D_8 are overdispersed count data (variance of the data is larger than the mean of the data), a negative binomial distribution is chosen to describe each of the datasets D_1 and D_3 through D_8. The observed SIV brain viral RNA dataset for untreated animals D_2 is also overdispersed count data. However, many of the counts in the dataset D_2 are very large positive numbers. For this reason, a normal distribution is used to describe the $\log_{10}$ of the data D_2.

Hence, for $j = 1, 3, \ldots, 8$, the probability of observing d_i^j is given by the negative binomial distribution:

$$f(d_i^j) = \frac{\Gamma(d_i^j + r_i^j)}{d_i^j!\,\Gamma(r_i^j)}(p^j)^{(r_i^j)}(1-p^j)^{d_i^j}, \tag{5.11}$$

where $r_i^j = \frac{(p^j)(\mu_i^j)}{1-(p^j)} \iff \mu_i^j = \frac{(r_i^j)(1-p^j)}{p^j}$ changes depending on the time t_i^j, and $0 < p^j < 1$ is specific to the j^{th} data set D_j and determines the most likely shape of the negative binomial distribution given the data D_j. Hence, the variance, $Var[D_i^j] = \frac{\mu_i^j}{p^j}$, also changes over time. Here $\mu_i^1 = s_u(\boldsymbol{\nu}, t_i^1)$, $\mu_i^3 = s_g(\boldsymbol{\nu}, t_i^1)$, $\mu_i^4 = v_g(\boldsymbol{\nu}, t_i^1)$, $\mu_i^5 = s_z(\boldsymbol{\nu}, t_i^1)$, $\mu_i^6 = v_z(\boldsymbol{\nu}, t_i^1)$, $\mu_i^7 = s_c(\boldsymbol{\nu}, t_i^1)$, and $\mu_i^8 = v_c(\boldsymbol{\nu}, t_i^1)$.

Based on the data sets $D_1, D_3, \ldots, D_8$, the following uniform prior distributions are chosen for $p^1, p^3, \ldots, p^8$:

$p^1 \sim U(1 \times 10^{-3}, 1)$, $p^3 \sim U(1 \times 10^{-4}, 1)$, $p^4 \sim U(1 \times 10^{-4}, 1)$,

$p^5 \sim U(1 \times 10^{-2}, 1)$, $p^6 \sim U(1 \times 10^{-1}, 1)$, $p^7 \sim U(1 \times 10^{-1}, 1)$, and

$p^8 \sim U(1 \times 10^{-1}, 1)$.

For $j = 2$, the probability of observing $\log_{10}(d_i^2)$ is given by the normal

distribution:

$$g(d_i^2) = \sqrt{\frac{\tau}{2\pi}}\exp(-\frac{1}{2}\tau(\log_{10}(d_i^2) - \mu_i^2)^2), \tag{5.12}$$

where the mean μ_i^2 changes depending on the time, t_i^2, and the variance $\frac{1}{\tau}$ is specific to the data set D_2. Here $\mu_i^2 = \log_{10}(v_u(\boldsymbol{\nu}, t_i^2))$.

Based on the data set D_2, the uniform prior distribution for τ is chosen to be $U(1 \times 10^{-2}, 100)$.

Let $\boldsymbol{\phi} = \langle p^1, \tau, p^3, p^4, p^5, p^6, p^7, p^8 \rangle$. Given the extra parameters in vector $\boldsymbol{\phi}$, we want to estimate the vector $\boldsymbol{\theta} = \langle \boldsymbol{\nu}, \boldsymbol{\phi} \rangle$.

The probability model for data sets $D_1, D_3, \ldots, D_8$ is

$$P_1(D|\boldsymbol{\theta}) = \prod_{j=1,3,\ldots,8} \prod_{i=1}^{n_j} f(d_i^j), \tag{5.13}$$

and the probability model for data set D_2 is

$$P_2(D_2|\boldsymbol{\theta}) = \prod_{i=1}^{n_2} g(d_i^2). \tag{5.14}$$

The likelihood function for $\boldsymbol{\theta}$ is given by

$$L(\boldsymbol{\theta}) = CP_1(D|\boldsymbol{\theta})P_2(D_2|\boldsymbol{\theta}), \tag{5.15}$$

where C is any positive constant not depending on $\boldsymbol{\theta}$ used to simplify the likelihood function. For more information about Bayesian inference for dynamical systems and combining probability models, please see Chapter 2.

The prior distribution for $\boldsymbol{\theta}$ is equal to the product of the uniform distributions specified for the parameters in $\boldsymbol{\theta}$.

The fitting was completed using an affine invariant ensemble Markov Chain

Monte Carlo (MCMC) sampling program from the MATLAB Central File Exchange [116]. The MCMC program sampled from the following unnormalized posterior distribution, $\pi(\boldsymbol{\theta}|D)$:

$$\pi(\boldsymbol{\theta}|D) = L(\boldsymbol{\theta})P(\boldsymbol{\theta}), \tag{5.16}$$

where $\boldsymbol{\theta}$ is the vector of unknown parameters, $D = \{D_1, \ldots, D_8\}$ is the observed data, $L(\boldsymbol{\theta})$ is the likelihood function, and $P(\boldsymbol{\theta})$ is the prior distribution.

The parameters to be estimated in system (4.1) are $\boldsymbol{\nu} = \langle \beta_1, \beta_2, k, x_0, y_0, N, \epsilon, \gamma \rangle$.

The affine invariant ensemble MCMC sampler was used with $T = 375,000$ iterations and $K = 32$ walkers making a total of $KT = 12,000,000$ samples. Every 10^{th} sample is thinned from each walker during the MCMC algorithm to decrease autocorrelation. After the iterations of the MCMC sampler are completed, a burn-in of 10,000 is used for each walker and the number of pooled samples after the burn-in is $H = 880,000$. Convergence of the MCMC sampling to the estimated posterior distribution for each parameter in $\boldsymbol{\theta}$ was determined by using a general univariate comparison method [117]. The general univariate comparison method uses the distance between the upper and lower values of the $100(1-\alpha)\%$ interval for the pooled samples, S, and divides this distance by the average of the distances between the upper and lower values of the $100(1-\alpha)\%$ interval for each of the K walkers, s_i, to receive the potential scale reduction factor, r [117]. Here the 95% interval ($\alpha = 0.05$) is used for the general univariate comparison method. Table 5.3 contains the estimated parameters in $\boldsymbol{\theta}$ with the 95% credible intervals and the potential scale reduction factors, r, for each parameter. The potential scale reduction factors, r, are close to 1 and this indicates that the sampler converged to the

posterior distribution.

The 95% prediction intervals for each data set D_j, $j = 1, \ldots, 8$, are determined by the posterior predictive distribution as described in [2].

For the scenario when cART is initiated at a certain time p.i. and LRA drugs are initiated at a later time p.i., ω is set to zero in system (4.5) and ϵ and α are time dependent in system (4.5). The time dependent ϵ is given by (5.10) and $\alpha(t)$ is given by

$$\alpha(t) = \begin{cases} 0 & \text{before LRA drugs are initiated} \\ \alpha & \text{when LRA drugs are initiated} \\ 0 & \text{when LRA drugs are stopped} \end{cases} \tag{5.17}$$

where α is a constant.

For the model prediction of the LRA drug SIV experiment (data D_9), the vector $\boldsymbol{\nu}$ in the pooled samples of $\boldsymbol{\theta} = \langle \boldsymbol{\nu}, \boldsymbol{\phi} \rangle$ in H are used in system (4.5) with $\omega = 0$ and the reactivation rate, α, in (5.17) is varied from 0.01 to 100 to determine which predicted solutions pass near the points in data D_9. The mean of these predicted solutions is displayed in Figure 4.5.

Likewise, for the scenario when cART is initiated at a certain time p.i. and the "Shock and Kill" strategy is initiated at a later time p.i., ϵ, α, and ω are time dependent in system (4.5). The time dependent ϵ is given by (5.10) and $\alpha(t)$ is given by

$$\alpha(t) = \begin{cases} 0 & \text{before LRA drugs are initiated} \\ \alpha & \text{when LRA drugs are initiated,} \end{cases} \tag{5.18}$$

where α is a constant, and

$$\omega(t) = \begin{cases} 0 & \text{before additional kill strategy is initiated} \\ \omega & \text{when additional kill strategy is initiated,} \end{cases} \tag{5.19}$$

where ω is a constant.

Similarly, for the prediction of the "Shock and Kill" strategy, the vector $\boldsymbol{\nu}$ in the pooled samples of $\boldsymbol{\theta} = \langle \boldsymbol{\nu}, \boldsymbol{\phi} \rangle$ in H are used. For each vector $\boldsymbol{\nu}$, system (4.5) is solved and the control reproduction number, $\overline{R}_c$, is calculated as the reactivation rate, α, in (5.18) and additional kill rate, ω, in (5.19) are varied from 0 to 40. The mean control reproduction number, mean $\overline{R}_c$, is shown in Figure 4.6 and the mean of the predicted model solutions within the safe and effective region (turquoise region in Figure 4.6) are shown in Figure 4.7.

Table 5.3: Fitted parameter estimates in $\boldsymbol{\theta}$ with the maximum posterior as the point estimate, 95% credible intervals, and potential scale reduction factors, r

Symbol	Parameter	Estimate (95% credible interval)	Unit	r
β_1	Transmission rate between susceptible and productively infected brain macrophages	1.17×10^{-5} $(5.75 \times 10^{-6}, 1.52 \times 10^{-5})$	g per year	1.1851
β_2	Transmission rate between susceptible and latently infected brain macrophages	2.23×10^{-6} $(2.92 \times 10^{-7}, 4.18 \times 10^{-6})$	g per year	1.1338
k	Natural death rate of brain macrophages	4.45 $(0.627, 9.84)$	per year	1.0842

x_0	Initial value for x	2.13×10^6 $(2.09 \times 10^6, 3.85 \times 10^6)$	per g	1.3665
y_0	Initial value for y	11.0 $(9.06, 11.1)$	per g	1.3636
N	viral RNA copies produced by a productively infected brain macrophage	1.35×10^3 $(773, 1.85 \times 10^3)$	per g	1.0671
ϵ	cART effectiveness $\epsilon \times 100\%$	0.180 $(0.150, 0.654)$	-	1.0483
γ	$\epsilon\gamma$ is the rate productive brain macrophages deactivate once cART is applied	124 $(27.8, 152)$	per year	1.0999
p^1	parameter determining most likely shape of NB distribution given data D_1	0.0064 $(0.0044, 0.0088)$	per year	1.0760
τ	$\tau = \frac{1}{\sigma^2}$, where σ^2 is the variance of the normal distribution for $\log_{10}$ of data D_2	0.1536 $(0.1312, 0.1917)$	per year	1.0308
p^3	parameter determining most likely shape of NB distribution given data D_3	0.0013 $(0.0007, 0.0022)$	per year	1.0559
p^4	parameter determining most likely shape of NB distribution given data D_4	1.0863×10^{-4} $(1.0034 \times 10^{-4}, 1.5796 \times 10^{-4})$	per year	1.0964

p^5	parameter determining most likely shape of NB distribution given data D_5	0.0280 $(0.0131, 0.0587)$	per year	1.0487
p^6	parameter determining most likely shape of NB distribution given data D_6	0.9203 $(0.3952, 0.9968)$	per year	1.0715
p^7	parameter determining most likely shape of NB distribution given data D_7	0.1128 $(0.1008, 0.3246)$	per year	1.2270
p^8	parameter determining most likely shape of NB distribution given data D_8	0.1479 $(0.1031, 0.4357)$	per year	1.2300

Chapter 6

Modeling the natural control of HIV-1 in the plasma: comparative analyses of patients from the Northern Alberta HIV Program

6.A Introduction

In 2021, an estimated 38.4 (33.9 - 43.8) million people were living with HIV-1 globally with 1.5 (1.1 - 2.0) million people becoming newly infected [13]. Even with the success of combination antiretroviral therapy (cART), HIV-1 remains a global health issue and current therapeutic initiatives include developing HIV-1 vaccines, both therapeutic and prophylactic vaccines, and increase antiviral immune protection to establish post cART control for pa-

tients [18, 14, 15, 22]. The goal of these therapeutic initiatives either being a complete sterilizing cure where the virus is eradicated or a functional cure where the virus is permanently suppressed in the absence of cART [14, 15].

Therapeutic initiatives for patients may be advanced by vital information from HIV-1 Elite Controllers [18, 42, 14]. HIV-1 Elite Controllers are HIV-1 infected patients that can naturally suppress viral replication to undetectable levels for extended periods of time without cART impeding the development of acquired immunodeficiency syndrome (AIDS) [18, 42]. A crucial medical problem is determining the differences in the natural immune response of HIV-1 Elite Controllers in comparison to the natural immune response of typical HIV-1 patients.

In the plasma, cytotoxic T lymphocytes (CTL), both cytotoxic CD8 T lymphocytes (CD8 CTL) and cytotoxic CD4 T lymphocytes (CD4 CTL), are the main adaptive branch of the immune system that eliminate virus-infected cells [33, 34, 35, 36, 37]. Precursor CD8 CTLs and precursor CD4 CTLs are any cells that terminally differentiate into effector CD8 CTLs and effector CD4 CTLs, respectively [37, 38, 39]. Effector CD8 CTLs and effector CD4 CTLs have the capability to recognize and kill infected cells that produce viral antigens on MHC class I and MHC class II molecules, respectively [35, 36]. HIV-1 experiments have shown that the combined activity of HIV-1 specific effector CD4 CTLs and HIV-1 specific effector CD8 CTLs, through the killing of virus-infected cells, maintain viral clearance [40, 41].

The biological theory for how HIV-1 Elite Controllers suppress the virus with their own immune system is still under development and there is evidence that the maintenance of HIV-1 specific effector CD4 CTLs in HIV-1 Elite Controllers along with HIV-1 specific effector CD8 CTLs contribute to their

control of HIV-1 infection [41]. Unique attempts to explain mathematically how HIV-1 Elite Controllers suppress the virus naturally are sparse [52, 53, 54, 55, 56]. The earliest mathematical model of HIV-1 infection in the plasma that attempted to explain the phenomenon of Elite Controllers was developed by Dominik Wodarz and Martin Nowak [52]. The ordinary differential equation (ODE) model contained four compartments: susceptible CD4 T cells; HIV-1 infected CD4 T cells; precursor CTLs; and effector CTLs. The authors mention that the equilibrium with sustained precursor and effector CTL populations and viral load at a low level may be attributed to HIV-1 Elite Controllers. The first author on this study published a further expansion of this model that included two types of CTL responses: a helper-independent response and a helper-dependent response [53]. The helper-independent effector CTLs are stimulated based on the size of the HIV-1 infected cell and helper-independent effector CTL populations, whereas the helper-dependent effector CTLs are stimulated based on the size of the HIV-1 infected cell and precursor CTL populations. It is assumed in the model that the helper-independent effector CTLs are short lived in comparison to the precursor CTL population. A couple other theoretical mathematical models used the mathematical model in study [52] or [53] to justify their next step in modeling HIV-1 Elite Controllers [54, 55]. The mathematical model in study [52], [53], and other theoretical ODE models based off of this system [54, 55] have not been fit to empiric data for a HIV-1 Elite Controller. A later mathematical model that was fit to empiric data for a untreated HIV-1 Elite Controller transplant patient was an ODE model with the following six compartments: susceptible CD4 T cells; HIV-1 infected CD4 T cells; productively HIV-1 infected CD4 T cells; long-lived HIV-1 infected cells; HIV-1 specific effector CD8 CTLs; and virus [56]. The initial

transplant for the untreated HIV-1 Elite Controller caused their viral load to increase and afterward their immune system was capable of suppressing the virus. There was about a year of empiric data on the HIV-1 Elite Controller patient presented in the study. Their mathematical model fit to the empiric data revealed that the untreated HIV-1 Elite Controller suppressed the virus at rates equivalent to an untreated patient starting cART.

Our study formulated a mathematical model of the immune system during HIV-1 infection in the plasma and estimated the disease dynamics among a group of HIV-1 Elite Controllers and a comparison group of HIV-1 patients from the Northern Alberta HIV Program (NAP) in Canada. The mathematical model was fit to the ART-naïve (no previous ART had been taken) time period for each patient. These ART-naïve time periods varied from 2.32 to 18.17 years. Since these ART-naïve time periods covered a span of years, it was necessary to consider the effect of the immune system in reducing and preventing other infections in the plasma besides HIV-1 in order to accurately model the plasma dynamics over the years. This is the first mathematical modeling study to directly estimate the differences between a group of HIV-1 Elite Controllers with a comparison group of HIV-1 patients using empiric data and it is also the first HIV-1 mathematical model to consider both effector CD4 CTLs and effector CD8 CTLs affect on HIV-1 disease and other diseases present in each patient.

The modeling results indicated that the Elite Controller group had a stronger antiviral immune response than the comparison group. In contrast, the comparison group was found to have more chronic immune activation but a less effective immune response. The Elite Controller immune response estimates given in this study quantifies a biologically realistic optimal immune response

goal for HIV-1 therapeutic initiatives.

6.B Mathematical model

6.B.1 HIV-1 plasma infection model with natural immune responses

CD4 T cells are the primary target for productive HIV-1 infection in the plasma [118], and the CD4 T cell population was used as the target cell in this HIV-1 modeling study. Although macrophages do play a significant part of HIV-1 infection in tissues and formation of viral reservoirs [119], to reduce model complexity and focus on the effect of CTLs during HIV-1 infection in the plasma, this study does not include macrophages in the mathematical model.

To derive this model, we first divide the total CD4 T cell population into three compartments: CD4 T cells susceptible to HIV-1, x; HIV-1 specific effector CD4 CTLs, x_E; and CD4 T cells productively infected with HIV-1, y. While the majority of CD4 T cells in the x compartment are considered healthy, the model considers that some of the CD4 T cells in the x compartment can get infected with other diseases, which are not HIV-1, naturally over time. There is one compartment in the model for the HIV-1 replication competent viral particles, v. Lastly, the total CD8 T cell population is divided into two compartments: CD8 T cells that are non HIV-1 specific, z, and HIV-1 specific effector CD8 CTLs, z_E. A compartment for CD4 T cells latently infected with HIV-1 was not included in the mathematical model since a latent compartment could not be reliably estimated due to there being no available

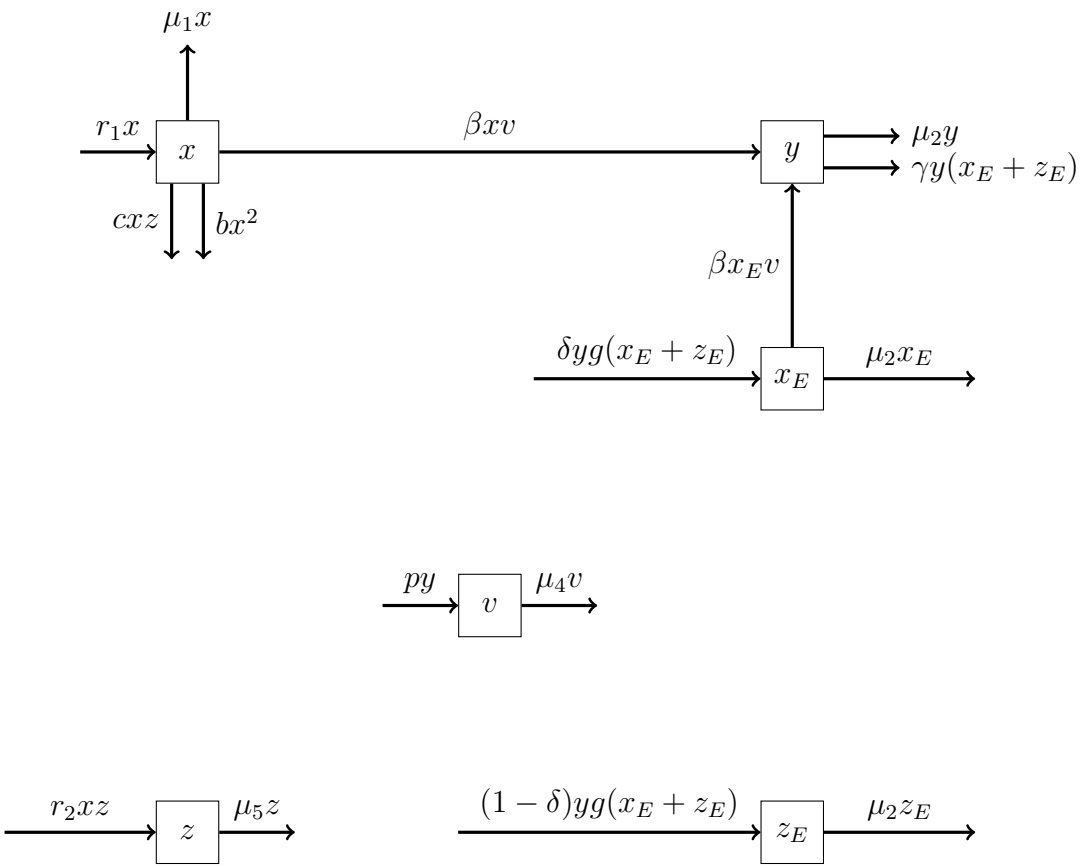

Figure 6.1: Transfer diagram for model (6.1) that considered the CD4 T cell and CD8 T cell natural immune response to HIV-1 infection in the plasma.

viral DNA data for the HIV-1 patients. The transfer diagram for the model is shown in Figure 6.1.

Without the presence of HIV-1 infection in the model ($x_E = 0$, $y = 0$, $v = 0$, $z_E = 0$), the number of CD4 T cells are regulated by the growth rate of new CD4 T cells, r_1, the kill rate from effector CD8 CTLs and CD4 CTLs (due to other infections of CD4 T cells that are not HIV-1) [35, 36], c and b respectively, and the death rate μ_1. The CD8 T cells are regulated by the growth rate, r_2, which is affected by the health of both the CD4 T cell and CD8 T cell populations (CD4 T cells act as helper cells to CD8 T cell generation and function [34]), and the natural death rate μ_5.

With the presence of HIV-1 infection, the interaction between CD4 T cells susceptible to HIV-1 and HIV-1 replication competent viral particles is modeled by the mass action terms βxv and $\beta x_E v$. It is assumed that the newly HIV-1 infected CD4 T cells will enter the productively HIV-1 infected CD4 T cell population, and the death rate of productively HIV-1 infected CD4 T cells is μ_3. The rate replication competent viral particles are produced by HIV-1 infected CD4 T cells is p and the death rate of replication competent viral particles is given by μ_4.

The production of effector CTLs in response to HIV-1 is modeled by $yg(w)$, where $g(w)$ is the HIV-1 specific effector CTL response function and $w = x_E + z_E$ is the total number of HIV-1 specific effector CTLs. Since the time of initial HIV-1 infection for the patients is unknown, the HIV-1 specific effector CTL response function, $g(w)$ is assumed to have already recognized the infiltration of HIV-1 viral particles and the HIV-1 specific effector CTL response function reacts in two phases: induction phase and the activation-induced cell death (AICD) phase [36]. In the induction phase, $g(w) = kw$, the response function scales up the differentiation of T cells into HIV-1 specific effector CTLs. In the AICD phase, effector CTLs are often seen to be at a stable level before transitioning to the silencing phase. We model this stable level in the AICD phase with $g(w) = ka$. The silencing phase, which brings an end to the immune response, is brought about when the number of HIV-1 infected CD4 T cells, y, reduces sufficiently causing production of HIV-1 specific effector CTLs $yg(w)$ to become smaller than the death rate of HIV-1 specific effector CTLs, μ_2. Upon HIV-1 specific effector CTL differentiation, a portion of the HIV-1 specific effector CTLs are HIV-1 specific effector CD4 CTLs, δ, and the other portion are HIV-1 specific effector CD8 CTLs, $(1-\delta)$.

An in vitro study of HIV-1 infection found that HIV-1 specific effector CD4 CTLs displayed comparable killing activity to HIV-1 specific effector CD8 CTLs, working together to kill virally infected cells [40], and, consequently, in this model the rate HIV-1 infected CD4 T cells are killed by HIV-1 specific effector CTLs is given by γ.

The total number of CD4 T cells are given by $x(t) + x_E(t) + y(t)$ and it is fitted to the CD4 absolute cells/mL data. The viral particles are given by $v(t)$ and it is fitted to the viral load copies/mL data. The total number of CD8 T cells are given by $z(t) + z_E(t)$ and it is fitted to the CD8 absolute cells/mL data. Using the transfer diagram, our model is described by the set of ordinary differential equations (ODEs):

$$\begin{aligned}
\frac{dx}{dt} &= r_1 x - \mu_1 x - cxz - bx^2 - \beta xv \\
\frac{dx_E}{dt} &= \delta y g(x_E + z_E) - \mu_2 x_E - \beta x_E v \\
\frac{dy}{dt} &= \beta(x + x_E)v - \mu_3 y - \gamma y(x_E + z_E) \\
\frac{dv}{dt} &= py - \mu_4 v \\
\frac{dz}{dt} &= r_2 xz - \mu_5 z \\
\frac{dz_E}{dt} &= (1-\delta) y g(x_E + z_E) - \mu_2 z_E,
\end{aligned} \tag{6.1}$$

where

$$g(w) = \begin{cases} kw, & w \leq a \\ ka, & w > a \end{cases}$$

and $w = x_E + z_E$.

Let

$$R_1 = \widetilde{R}x_1 = \widetilde{R}\frac{1}{b}(r_1 - \mu_1), \tag{6.2}$$

$$R_2 = \widetilde{R}x_2 = \widetilde{R}\frac{\mu_5}{r_2}, \tag{6.3}$$

$$R_3 = \widetilde{R}\delta\mu_3 - \gamma, \tag{6.4}$$

$$R_4 = \widetilde{R}\mu_3 - \gamma, \tag{6.5}$$

$$R_5 = ka - \mu_3^2, \tag{6.6}$$

$$R_6 = k - \widetilde{R}\mu_3, \tag{6.7}$$

where $\widetilde{R} = \frac{p\beta}{\mu_3\mu_4}$.

The local stability of the disease-free equilibria for system 6.1 and the basic reproduction number of system 6.1 are determined by the values of the threshold parameters R_1 (6.2) and R_2 (6.3). R_3 (6.4)-R_6 (6.7) are suspected thresholds for system 6.1.

System 6.1 has three possible disease-free equilibria:

$P_0 = (0, 0, 0, 0, 0, 0),$

$P_1 = (x_1, 0, 0, 0, 0, 0)$
$= \left(\frac{R_1}{\widetilde{R}}, 0, 0, 0, 0, 0\right),$

$P_2 = (x_2, 0, 0, 0, z_2, 0)$

$= \Big(\frac{R_2}{\widetilde{R}}, 0, 0, 0, \frac{b}{c\widetilde{R}}(R_1 - R_2), 0\Big).$

System 6.1 also has eight possible productive equilibria:

three possible equilibria of the form

$P_3 = (0, x_{E,3}, y_3, v_3, 0, z_{E,3})$

$= (0, x_{E,3}, y_3, v_3, 0, w_3 - x_{E,3}),$

$= \Big(0, x_{E,3}, y_3, v_3, 0, \frac{R_4 w_3 - \mu_3}{\widetilde{R}\mu_3}\Big),$

where $y_3 = \frac{\mu_4}{p} v_3$, $x_{E,3} = \frac{1}{\widetilde{R}}\Big(1 + \frac{\gamma}{\mu_3} w_3\Big)$, $v_3 = \frac{\mu_2}{(1-\delta)\beta}\Big(\frac{R_3 w_3 - \mu_3}{\mu_3 + \gamma w_3}\Big)$,

positive roots of the function

$$h_3(w_3) = \frac{\gamma(R_4)w_3^2 + \mu_3(R_4 - \gamma)w_3 - \mu_3^2}{R_3 w_3 - 1} - g(w_3) = \begin{cases} \frac{(\gamma R_4 - kR_3)w_3^2 + (\mu_3(R_4 - \gamma) + k)w_3 - \mu_3^2}{R_3 w_3 - 1}, & w_4 \leq a \\ \frac{\gamma R_4 w_3^2 + (\mu_3(R_4 - \gamma) - kaR_3)w_3 + R_5}{R_3 w_3 - 1}, & w_4 > a \end{cases};$$

six possible equilibria of the form

$P_4 = (x_4, x_{E,4}, y_4, v_4, 0, z_{E,4})$

$= \Big(\frac{R_1}{\widetilde{R}} - \frac{\beta}{b} v_4, x_{E,4}, y_4, v_4, 0, w_4 - x_{E,4}\Big),$

where $y_4 = \frac{\mu_4}{p} v_4$,

$x_{E,4} = \frac{\beta\mu_3\widetilde{R}v_4 + b\gamma w_4 + b\mu_3(1 - R_1)}{b\mu_3\widetilde{R}},$

$z_{E,4} = \frac{bR_4 w_4 - \beta\mu_3\widetilde{R}v_4 + b\mu_3(R_1 - 1)}{b\mu_3\widetilde{R}},$

solve for w_4 from the following equation

$$-\mu_3\beta^2\widetilde{R}v_4^2+\mu_3 b\beta(R_1-1)v_4+b\beta v_4 g(w_4)-b\gamma\beta v_4 w_4-b\mu_2\mu_3\widetilde{R}w_4=0,$$

and receive

$$w_4=\begin{cases}\frac{\beta\mu_3(\beta\widetilde{R}v_4+b(1-R_1))v_4}{b(\beta(R_4+R_6)v_4-\mu_3\mu_2\widetilde{R})}, & w_4\le a\\ \frac{\beta(-\beta\widetilde{R}\mu_3 v_4+b(\mu_3(R_1-1)+ka))v_4}{b(\gamma\beta v_4+\mu_2\mu_3\widetilde{R})}, & w_4>a\end{cases},$$

$$x_{E,4}=\frac{\beta\mu_3\widetilde{R}v_4+b\gamma w_4+b\mu_3(1-R_1)}{b\mu_3\widetilde{R}}=\begin{cases}\frac{\beta^2\widetilde{R}kv_4^2+\beta(b(1-R_1)k-\mu_3\mu_2\widetilde{R}^2)v_4-b(1-R_1)\mu_3\mu_2\widetilde{R}}{b\widetilde{R}(\beta(R_4+R_6)v_4-\mu_3\mu_2\widetilde{R})}, & w_4\le a\\ \frac{\beta(\mu_2\mu_3^2\widetilde{R}^2+\gamma bka)v_4+b\mu_3^2\mu_2\widetilde{R}(1-R_1)}{b\mu_3\widetilde{R}(\gamma\beta v_4+\mu_2\mu_3\widetilde{R})}, & w_4>a\end{cases},$$

$$z_{E,4}=\frac{bR_4w_4-\beta\mu_3\widetilde{R}v_4+b\mu_3(R_1-1)}{b\mu_3\widetilde{R}}=\begin{cases}\frac{-\beta^2\widetilde{R}R_6v_4^2+\beta(\widetilde{R}^2\mu_3\mu_2-b(1-R_1)R_6)v_4+b(1-R_1)\mu_3\mu_2\widetilde{R}}{b\widetilde{R}(\beta(R_4+R_6)v_4-\mu_3\mu_2\widetilde{R})}, & w_4\le a\\ \frac{-\beta^2\mu_3^2\widetilde{R}^2v_4^2+\beta(\widetilde{R}b\mu_3^2(R_1-1)+R_4bka-\mu_2\mu_3^2\widetilde{R}^2)v_4+\mu_2\mu_3^2\widetilde{R}b(R_1-1)}{b\mu_3\widetilde{R}(\gamma\beta v_4+\mu_2\mu_3\widetilde{R})}, & w_4>a\end{cases},$$

w_4 can be put into the equation

$$(1-\delta)\mu_3\beta^2\widetilde{R}v_4^2+\beta(\mu_3\mu_2\widetilde{R}+b\mu_3(1-\delta)(1-R_1)+b(1-\delta)\gamma w_4)v_4$$
$$+b\mu_2(\mu_3(1-R_1)-R_3w_4)=0,$$

and we receive

$$h_4(v_4)=\begin{cases}(1-\delta)\beta^3\widetilde{R}kv_4^3+\beta^2(\mu_2\widetilde{R}R_6+(1-\delta)(1-R_1)bk)v_4^2 & \\ +\mu_2\beta((1-R_1)bR_6-\mu_2\widetilde{R}^2\mu_3)v_4-\mu_2^2(1-R_1)\mu_3 b\widetilde{R}, & w_4\le a\\ \mu_3(1-\delta)\beta^3\widetilde{R}\gamma(b-1)v_4^3+\beta^2(\mu_2\mu_3^2\widetilde{R}^2(b(1-\delta)+\delta)+(1-\delta)\gamma bka)v_4^2 & \\ +\mu_2\beta(\mu_2\mu_3^2\widetilde{R}^2+b(1-R_1)\mu_3^2\widetilde{R}-R_3bka)v_4+b\mu_2^2\mu_3^2(1-R_1)\widetilde{R}, & w_4>a\end{cases}$$

by solving for the positive roots of the function, $h_4(v_4)$, we can find v_4

; and

three possible equilibria of the form

$P_5 = (x_5, x_{E,5}, y_5, v_5, z_5, z_{E,5})$
$= \left(\frac{R_2}{\widetilde{R}}, x_{E,5}, y_5, v_5, \frac{b}{c\widetilde{R}}(R_1 - R_2 - \frac{\widetilde{R}\beta}{b}v_5), w_5 - x_{E,5}\right),$
$= \left(\frac{R_2}{\widetilde{R}}, x_{E,5}, y_5, v_5, \frac{b}{c\widetilde{R}}(R_1 - R_2 - \frac{\widetilde{R}\beta}{b}v_5), \frac{R_4 w_5 - \mu_3(1-R_2)}{\widetilde{R}\mu_3}\right),$
$= \left(\frac{R_2}{\widetilde{R}}, x_{E,5}, y_5, v_5, \frac{((R_1-R_2)b(1-\delta)\gamma - \widetilde{R}\mu_2 R_3)w_5 + \mu_3(1-R_2)((R_1-R_2)b(1-\delta)+\widetilde{R}\mu_2)}{c\widetilde{R}(1-\delta)(\mu_3(1-R_2)+\gamma w_5)}, \frac{R_4 w_5 - \mu_3(1-R_2)}{\widetilde{R}\mu_3}\right),$

where $y_5 = \frac{\mu_4}{p}v_5$, $x_{E,5} = \frac{\mu_3(1-R_2)+\gamma w_5}{\widetilde{R}\mu_3}$, $v_5 = \frac{\mu_2}{(1-\delta)\beta}\left(\frac{R_3 w_5 - \mu_3(1-R_2)}{\mu_3(1-R_2)+\gamma w_5}\right)$,

positive roots of the function
$h_5(w_5) = \frac{\gamma R_4 w_5^2 + \mu_3(1-R_2)(R_4-\gamma)w_5 - \mu_3^2(1-R_2)^2}{R_3 w_5 - \mu_3(1-R_2)} - g(w_5).$

Theorem 6.1: *1. The disease-free equilibrium P_0 always exists in $\mathbb{R}^6_+$.*

2. *In order for the disease-free equilibrium P_1 to exist in $\mathbb{R}^6_+$ it is necessary and sufficient that $R_1 > 0$.*

3. *In order for the disease-free equilibrium P_2 to exist in $\mathbb{R}^6_+$ it is necessary and sufficient that $R_2 > 0$ and $R_1 > R_2$.*

4. *In order for productive equilibria of the form P_3 to exist in $\mathbb{R}^6_+$ it is necessary that $R_3 > 0$ and $R_4 > 0$.*

5. *In order for productive equilibria of the form* P_4 *to exist in* $\mathbb{R}^6_+$ *it is necessary that* $R_1 > 1$, *or* $R_4 > 0$ *and* $0 < R_1 < 1$.

6. *In order for productive equilibria of the form* P_5 *to exist in* $\mathbb{R}^6_+$ *it is necessary that*

   $R_1 > R_2$ *and one of the following conditions holds:*

   (a) $R_2 > 1$ *and* $R_3 < 0$

   (b) $R_2 > 1$, $R_3 > 0$, *and* $(R_1 - R_2)b(1-\delta)\gamma - \widetilde{R}\mu_2 R_3 > 0$

   (c) $0 < R_2 < 1$, $R_3 > 0$, *and* $R_4 > 0$.

Proof. P_0 is the origin and always exists in $\mathbb{R}^6_+$.

The coordinates $x_{E,1}, y_1, v_1, z_1, z_{E,1}$ of P_1 are zero. Thus, P_1 exists in $\mathbb{R}^6_+$ if and only if $x_1 > 0 \iff R_1 > 0$.

The coordinates $x_{E,2}, y_2, v_2, z_{E,2}$ of P_2 are zero. Hence, P_2 exists in $\mathbb{R}^6_+$ if and only if $x_2, z_2 > 0 \iff R_2 > 0$ and $R_1 > R_2$.

The coordinates x_3 and z_3 of P_3 are zero. Productive equilibria of the form P_3 exist in $\mathbb{R}^6_+$ if and only if $x_{E,3}, y_3, v_3, z_{E,3} = w_3 - x_{E,3} > 0$.

Suppose $x_{E,3}, y_3, v_3, z_{E,3} = w_3 - x_{E,3} > 0$.

Consequently, $v_3 > 0 \iff R_3 w_3 - \mu_3 > 0$.
Assume $R_3 > 0$. Then $R_3 w_3 > \mu_3 \iff w_3 > \frac{\mu_3}{R_3}$.
Assume $R_3 < 0$. Then $R_3 w_3 > \mu_3 \iff w_3 < \frac{\mu_3}{R_3}$, which is a contradiction

since $w_3 > 0$.

Thus, $R_3 > 0$.

As $y_3 = \frac{\mu_4}{p} v_3$, then $y_3 > 0 \iff R_3 > 0$.

Also, $z_{E,3} > 0 \iff R_4 w_3 - \mu_3 > 0$.

Assume $R_4 > 0$. Then $R_4 w_3 > \mu_3 \iff w_3 > \frac{\mu_3}{R_4}$.

Assume $R_4 < 0$. Then $R_4 w_3 > \mu_3 \iff w_3 < \frac{\mu_3}{R_4}$, which is a contradiction since $w_3 > 0$.

Hence, $R_4 > 0$.

The coordinate $x_{E,3} = \frac{1}{\widetilde{R}}\left(1 + \frac{\gamma}{\mu_3} w_3\right)$ is greater than zero.

From equation $h_3(w_3)$, $w_3 \neq \frac{1}{R_3}$. Since $w_3 > \frac{\mu_3}{R_3}$ from $v_3 > 0$, w_3 will be greater than $\frac{1}{R_3}$.

The coordinate z_4 of P_4 is zero. Productive equilibria of the form P_4 exist in $\mathbb{R}^6_+$ if and only if $x_4, x_{E,4}, y_4, v_4, z_{E,4} = w_4 - x_{E,4} > 0$.

Suppose $x_4, x_{E,4}, y_4, v_4, z_{E,4} = w_4 - x_{E,4} > 0$.

Consequently, $x_4 > 0 \iff \frac{R_1}{\widetilde{R}} > \frac{\beta}{b} v_4 > 0$, which implies that $R_1 > 0$.

Now, $z_{E,4} > 0 \iff b R_4 w_4 + b\mu_3(R_1 - 1) > \beta\mu_3 \widetilde{R} v_4 > 0$, which implies that $b R_4 w_4 + b\mu_3(R_1 - 1) > 0$. The inequality, $b R_4 w_4 + b\mu_3(R_1 - 1) > 0$, has a solution provided that $R_1 > 1$, or $R_4 > 0$ and $R_1 < 1$.

Productive equilibria of the form P_5 exist in $\mathbb{R}^6_+$ if and only if all of the

coordinates in P_5 are greater than zero.

Suppose $x_5, x_{E,5}, y_5, v_5, z_5, z_{E,5} = w_5 - x_{E,5} > 0$.

Consequently, $x_5 > 0 \iff R_2 > 0$.

Now, $z_{E,5} > 0$, $x_{E,5} > 0$, and $v_5 > 0$ if and only if
$R_4 w_5 - \mu_3(1 - R_2) > 0$,
$\mu_3(1 - R_2) + \gamma w_5 > 0$,
and $R_3 w_5 - \mu_3(1 - R_2) > 0$.

Using the three above inequalities, the solution for w_5 using assumptions on R_3, R_4, and R_2 are the following:

1. $R_3 > 0$, $R_4 > 0$, and $R_2 > 1$
   (a) solution is $w_5 > -\frac{\mu_3(1-R_2)}{\gamma} > 0$
2. $R_3 > 0$, $R_4 > 0$, and $R_2 < 1$
   (a) solution is $w_5 > \frac{\mu_3(1-R_2)}{R_3} > 0$
3. $R_3 > 0$, $R_4 < 0$, and $R_2 > 1$
   (a) solution is $0 < -\frac{\mu_3(1-R_2)}{\gamma} < w_5 < \frac{\mu_3(1-R_2)}{R_4}$
4. $R_3 > 0$, $R_4 < 0$, and $R_2 < 1$
   (a) $w_5 < \frac{\mu_3(1-R_2)}{R_4} < 0$ is a contradiction since $w_5 > 0$

5. $R_3 < 0$, $R_4 > 0$, and $R_2 > 1$

   (a) solution is $0 < -\frac{\mu_3(1-R_2)}{\gamma} < w_5 < \frac{\mu_3(1-R_2)}{R_3}$

6. $R_3 < 0$, $R_4 > 0$, and $R_2 < 1$

   (a) $w_5 < \frac{\mu_3(1-R_2)}{R_3} < 0$ is a contradiction since $w_5 > 0$

7. $R_3 < 0$, $R_4 < 0$, and $R_2 > 1$

   (a) solution is $0 < -\frac{\mu_3(1-R_2)}{\gamma} < w_5 < \frac{\mu_3(1-R_2)}{R_3}$

8. $R_3 < 0$, $R_4 < 0$, and $R_2 < 1$

   (a) $w_5 < \frac{\mu_3(1-R_2)}{R_4} < \frac{\mu_3(1-R_2)}{R_3} < 0$ is a contradiction since $w_5 > 0$

The three inequalities are satisfied provided that

$R_2 > 1$ or

$R_3 > 0$, $R_4 > 0$, and $R_2 < 1$.

Therefore, $z_{E,5} > 0$, $x_{E,5} > 0$, and $v_5 > 0$ if and only if

$R_2 > 1$ or

$R_3 > 0$, $R_4 > 0$, and $R_2 < 1$.

Since $v_5 > 0$, then $y_5 = \frac{\mu_4}{p} v_5 > 0$.

Now, $z_5 = \frac{b}{c\widetilde{R}}(R_1 - R_2 - \frac{\widetilde{R}\beta}{b} v_5) > 0 \iff R_1 - R_2 > \frac{\widetilde{R}\beta}{b} v_5 > 0 \Rightarrow R_1 > R_2$.
Also, $z_5 = \frac{((R_1-R_2)b(1-\delta)\gamma - \widetilde{R}\mu_2 R_3)w_5 + \mu_3(1-R_2)((R_1-R_2)b(1-\delta)+\widetilde{R}\mu_2)}{c\widetilde{R}(1-\delta)(\mu_3(1-R_2)+\gamma w_5)}$.

We know that $\mu_3(1-R_2)+\gamma w_5 > 0$ from $x_{E,5} > 0$, and that $R_1 - R_2 > 0$. Then $z_5 > 0 \iff$
$((R_1-R_2)b(1-\delta)\gamma - \widetilde{R}\mu_2 R_3)w_5 + \mu_3(1-R_2)((R_1-R_2)b(1-\delta)+\widetilde{R}\mu_2) > 0$.
This inequality has a solution, and hence $z_5 > 0$, provided that one of the following conditions holds:

1. $R_2 > 1$, $R_3 > 0$, and $(R_1-R_2)b(1-\delta)\gamma - \widetilde{R}\mu_2 R_3 > 0$
2. $R_2 > 1$, $R_3 < 0$
3. $R_2 < 1$, $R_3 > 0$

From equation $h_5(w_5)$, $w_5 \neq \frac{\mu_3(1-R_2)}{R_3}$. Since $w_5 > \frac{\mu_3(1-R_2)}{R_3}$ from $v_5 > 0$, w_5 will be greater than $\frac{\mu_3(1-R_2)}{R_3}$.

□

Equilibria existence conditions of system 6.1 are summarized in Theorem 6.1. At equilibrium P_0 all the populations are zero. At equilibrium P_1 the viral infection is gone, but the CD8 T cells are depleted to zero. At equilibrium P_2 the CD4 T cells and CD8 T cells are healthy. At equilibria of the form P_3, the viral infection is chronic and both the CD4 T cell and CD8 T cell populations that are non HIV-1 specific have been eliminated. At equilibria of the form P_4, the viral infection is chronic with the CD8 T cells that are non HIV-1 specific having been eliminated. At equilibria of the form P_5, the viral infection is chronic and all populations are nonzero. Equilibrium P_2 and equilibria of the form P_5 correspond to potential survival states for untreated viral infection.

The local stability analysis of the disease-free equilibria of system (6.1) is located in Section 7.A.

Let

$$F = \begin{bmatrix} 0 & \beta x_{\text{DFE}} \\ 0 & 0 \end{bmatrix} \text{ and } V = \begin{bmatrix} \mu_3 & 0 \\ -p & \mu_4 \end{bmatrix},$$

where x_{DFE} is equal to x_0, x_1, or x_2 from the disease-free equilibria P_0, P_1, P_2. Then

$$FV^{-1} = \begin{bmatrix} \frac{p\beta x_{\text{DFE}}}{\mu_3\mu_4} & \frac{\beta x_{\text{DFE}}}{\mu_4} \\ 0 & 0 \end{bmatrix}. \tag{6.8}$$

Using the next generation matrix method in [97, 98], the basic reproduction number is given by the spectral radius of the matrix FV^{-1}:

$$R_0 = \rho(FV^{-1}) = \max\{0, \widetilde{R}x_{\text{DFE}}\} = \max\{0, R_1, R_2\}. \tag{6.9}$$

6.C Numerical investigation using HIV-1 patient data from the Northern Alberta HIV Program

6.C.1 Definition of an Elite Controller

A literature review study from 2014, evaluated the definitions used for an Elite Controller and determined that there were four definitions that best identified this phenotype (all definitions require that the patient is AIDS-free and ART-

naïve) [42]:

(Definition A) HIV-1 positive $\geq$ 6 months, with $\geq$ 2 consecutive HIV-1 RNA $<$ 75 copies/ml

(Definition E) HIV-1 positive $\geq$ 1 year, with $\geq$ 3 consecutive HIV-1 RNA $<$ 75 copies/ml spanning $\geq$ 12 months

(Definition F) HIV-1 positive $\geq$ 1 year, with $\geq$ 3 consecutive HIV-1 RNA $<$ 75 copies/ml spanning $\geq$ 12 months with no previous blips $\geq$ 1000 copies/ml

(Definition J) HIV-1 positive $\geq$ 10 years, with 90% of HIV-1 RNA ($\geq$ 2 HIV-1 RNA ever) $<$ 400 copies/ml.

(Definition F implies definition E and definition E implies definition A).

In this study, a patient is considered an Elite Controller if at least one of the definitions A, E, F, or J applies for that patient's laboratory data. Otherwise, a patient is not considered an Elite Controller and that patient is in the comparison group.

6.C.2 Data and parameter estimates

The historical HIV-1 patient data used in this study came from the Northern Alberta HIV Program (NAP) in Canada. The data extraction request was to identify patients in the NAP who had laboratory tests taken during an ART-

naïve time period. Given this data request, data for thirty HIV-1 patients was received from the NAP. Sixteen of these patients had an ART-naïve time period with usable data for fitting a mathematical model, and these sixteen patients will comprise the group of HIV-1 patients that are the focus of this study. The HIV-1 group data used in this study is listed in Table 6.2. A detailed list of the data is located in Table 7.1 in Section 7.B. There were nine patients that met the criteria for an Elite Controller by at least one of the definitions A, E, F, J from the 2014 literature review study [42]: patient numbers 1 (met definitions A, E, and F), 6 (met definitions A and E), 14 (met definition A), 16 (met definitions A, E, F, and J), 17 (met definitions A, E, and F), 18 (met definitions A, E, and F), 24 (met definitions A and E), 25 (met definitions A, E, and F), and 28 (met definitions A, E, and F). There were seven patients that did not qualify as Elite Controllers based on the definitions from the 2014 literature review study [42] and these patients comprised the comparison group used in this study: patient numbers 2, 7, 10, 11, 12, 21, and 23. There were two extraction dates. The initial data extraction was received on August 30, 2019. The mathematical model (6.1) was fit to this initial extraction data. The second data extraction was received on January 24, 2023 and its purpose was to obtain any other viral load, CD4 absolute, and CD4/CD8 ratio measurements for HIV-1 patients that had still not taken cART. The mathematical model (6.1) fitted to the initially extracted data was projected forward and the second data extraction was used to validate the model.

The units of the viral load were measured in copies/mL. The units of CD4 absolute were measured in cells/mm3. The CD4/CD8 ratio was used to convert the CD4 absolute cells/mm3 measurement to CD8 absolute cells/mm3. The

conversion 1 mL = 1000 mm3 was used to convert the CD4 absolute cells/mm3 and CD8 absolute cells/mm3 measurements to CD4 absolute cells/mL and CD8 absolute cells/mL.

The clinical and demographic features of the HIV-1 group used in this study are listed in Table 6.1. Continuous variables were reported as the mean and standard deviation. The categorical variable was reported with counts and percentages. The Wilcoxon-Mann-Whitney test was used to compare the medians of the two populations for the continuous variables and Fisher's exact test was used to compare the proportions of the two populations for the categorical variable. The female:male ratio was comparable in the HIV-1 Elite Controller patient group (4:5) and the comparison patient group (4:3), as was the duration of recorded HIV-1 from the seropositive date to the last time an ART-naïve laboratory test was collected (12.14 ± 4.24 yr, Elite Controller; 9.91 ± 3.99 yr, comparison group) and the CD4 absolute count ($6.65 \times 10^5 \pm 2.31 \times 10^5$ cells/mL, Elite Controller; $7.07 \times 10^5 \pm 1.81 \times 10^5$ cells/mL, comparison group). The patients in the Elite Controller group were older (53.56 ± 10.04 yr) than the comparison group (41.28 ± 8.64 yr) ($P<0.05$). Also, the patients in the

Table 6.1: Clinical and demographic features for the NAP HIV-1 patients

Variables	HIV-1 Elite Controllers (n=9)	HIV-1 Comparison Group (n=7)	P-value
Age from birth date to last ART-naïve time collected (yr)	53.56 (10.04)	41.28 (8.64)	0.0283
Gender:			NS
Female	4 (44.44%)	4 (57.14%)	
Male	5 (55.56%)	3 (42.86%)	

Duration of recorded HIV-1 from seropositive date to last ART-naïve time collected (yr)	12.14 (4.24)	9.91 (3.99)*	NS
CD4 absolute (cells/mL)	6.65×10^5 (2.31×10^5)	7.07×10^5 (1.81×10^5)	NS
CD8 absolute (cells/mL)	6.42×10^5 (3.10×10^5)	1.05×10^6 (5.06×10^5)	< 0.0001
CD4/CD8 ratio	1.28 (0.691)	0.788 (0.319)	< 0.0001

Data are mean (SD) or number (percentage). Wilcoxon-Mann-Whitney test was used to compare the medians of the two populations for the continuous variables. Fisher's exact test was used to compare the proportions of the two populations for the categorical variable. The α level was 0.05 for the statistical tests.

* The seropositive date was not available for Patient 7. Consequently, the first time collected was used in place of the seropositive date when calculating the duration of recorded HIV-1 for this patient.

Elite Controller group had a higher CD4/CD8 ratio (1.28 ± 0.691) than the comparison group (0.788 ± 0.319) (P<0.05). The patients in the comparison group had a higher CD8 absolute count ($1.05 \times 10^6 \pm 5.06 \times 10^5$ cells/mL) than the Elite Controller group ($6.42 \times 10^5 \pm 3.10 \times 10^5$ cells/mL) (P<0.05). The range of CD4 absolute and CD8 absolute for a healthy individual is 5×10^5 to 1.2×10^6 cells/ml and 1.5×10^5 to 1×10^6 cells/ml, respectively, and a healthy individual generally has a CD4/CD8 ratio greater than 1.0 [120]. The mean CD4 absolute count for both the Elite Controller (6.65×10^5 cells/mL) and comparison group (7.07×10^5 cells/mL) was within the healthy range of 5×10^5 to 1.2×10^6 cells/ml. The mean CD8 absolute count for the Elite Controller group (6.42×10^5 cells/mL) was within the healthy range of 1.5×10^5 to 1×10^6 cells/ml, however the mean CD8 absolute count was slightly outside the healthy range for the comparison group (1.05×10^6 cells/mL). The mean

CD4/CD8 ratio was greater than 1.0 for the Elite Controller group (1.28), but the mean CD4/CD8 ratio was below 1.0 for the comparison group (0.788).

Uniform or loguniform prior distributions were specified for the parameters in model (6.1) since there is a general range for these parameters given in the literature. The prior distributions are listed in Section 7.C.

The model parameters were estimated by fitting system (6.1) simultaneously to the viral load, CD4 absolute, and CD8 absolute initial extraction data for each patient in Table 6.2. Since the HIV-1 patient data as visualized in Sections 7.D.6 and 7.D.7 display a variety of patterns and scatter around the trends, a Gaussian distribution with non-constant variance over time is chosen to describe each of the datasets for every patient. As this HIV-1 patient data can still be considered count data, which is most likely overdispersed (variance of the data is larger than the mean of the data), the non-constant variance over time in the Gaussian distribution is described by a constant multiplied by the mean. The probability model describing these datasets is given by equation (7.4) and the likelihood function is given by equation (7.5). The estimated parameter values for system (6.1) for each patient are listed in Sections 7.D.4 and 7.D.5 and the fit of system (6.1) to each patient is visualized in Sections 7.D.6 and 7.D.7. Figure 6.3 displays the prediction for the HIV-1 Elite Controllers. The method of Bayesian inference was used for fitting system simultaneously to the three datasets for each patient and this method is described in Section 7.D.

A pooled estimate of the parameter values for system (6.1) for the HIV-1 Elite Controller group and HIV-1 comparison group is located in Table 6.3. Table 6.3 also contains the probability that an Elite Controller group parameter is greater than a comparison group parameter, $P\left(\theta_i^{\mathrm{EC}} > \theta_i^{\mathrm{C}}\right)$. These

Table 6.2: NAP HIV-1 patient data

Patient number	Elite Controller status	Viral load (No. obs.)	CD4 absolute (No. obs.)	CD8 absolute (No. obs.)
1	Yes	7	7	7
6	Yes	13	15	9
14	Yes	15 (+ 2)*	16 (+ 2)*	16 (+ 2)*
16	Yes	21 (+ 2)*	21 (+ 5)*	21 (+ 5)*
17	Yes	9 (+ 1)*	8 (+ 1)*	8 (+ 1)*
18	Yes	7	7	7
24	Yes	30	28	28
25	Yes	8 (+ 6)*	8 (+ 6)*	8 (+ 6)*
28	Yes	9 (+ 1)*	9 (+ 1)*	9 (+ 1)*
2	No	11	10	10
7	No	29 (+ 7)*	29 (+ 7)*	28 (+ 7)*
10	No	14	16	16
11	No	30	31	31
12	No	19	18	16
21	No	6	5	5
23	No	31	32	32

* The additional patient observations received from the second data extraction.

probabilities provide the following information about the parameter differences between the Elite Controller group and the comparison group: there is a 71.10% chance that the growth rate of new CD4 T cells, r_1, is greater for the comparison group than for the Elite Controller group; there is a 72.00% chance that the stable level in the HIV-1 specific effector CTL response func-

tion, $g(E) = ka$, is higher for the Elite Controller group than for the comparison group; there is a 63.50% chance that the number of HIV-1 specific effector CTLs, a, at which the response function switches to a maximum rate is larger for the comparison group than for the Elite Controller group; there is a 63.10% chance that the death rate of productively infected CD4 T cells, μ_3, is faster for the Elite Controller group than for the comparison group; there is a 73.80% chance that the rate infected CD4 T cells are killed by effector CTLs, γ, is greater for the Elite Controller group than for the comparison group; and there is a 65.90% chance that the death rate of the general population of CD8 T cells that are non-HIV-1 specific, μ_5, is more rapid for the Elite Controller group than for the comparison group. The probabilities also indicate the following parameter similarities between the Elite Controller group and the comparison group: the death rate of total CD4 T cells, μ_1; kill rate of CD4 T cells by effector CD8 CTLs due to other infections, c; kill rate of CD4 T cells by effector CD4 CTLs due to other infections, b; transmission rate of HIV-1 to CD4 T cells, β; portion of generated HIV-1 specific effector CTLs that are HIV-1 specific effector CD4 CTLs, δ; death rate of effector CTLs, μ_2; rate replication competent viral particles were produced by HIV-1 infected CD4 T cells, p; death rate of HIV-1 replication competent viral particles, μ_4; and growth rate of new CD8 T cells, r_2. Figure 6.2 displays the model parameter estimates with the median as the point estimate and 95% credible intervals for each of the patients along with the pooled parameter estimates and probabilities $P\left(\theta_i^{\mathrm{EC}} > \theta_i^{\mathrm{C}}\right)$. Overall the estimated parameter values in Table 6.3 and those estimated for the HIV-1 Elite Controller transplant patient study are consistent [56]. The HIV-1 Elite Controller transplant patient study does have an estimated rate replication competent viral parti-

cles were produced by HIV-1 infected CD4 T cells (p), 7.3×10^6 per year, that is larger than the pooled estimated p from either the Elite Controller group, 1.51×10^4 $(1.17 \times 10^3, 1.76 \times 10^5)$, or the comparison group, 7.04×10^3 $(1.00 \times 10^3, 1.24 \times 10^6)$. Also, the HIV-1 Elite Controller transplant patient study has an estimated death rate of productively infected CD4 T cells (μ_3), 328.5 per year, that is larger than the pooled estimated μ_3 from either the Elite Controller group, 1.89×10^2 $(4.47 \times 10^1, 3.19 \times 10^2)$, or the comparison group, 1.49×10^2 $(2.81 \times 10^1, 2.87 \times 10^2)$.

Table 6.3: Pooled parameter estimates with the median as the point estimate and 95% credible intervals for the HIV-1 Elite Controller group and the HIV-1 comparison group (the last column displays the probability that the Elite Controller group parameter in that row is greater than the comparison group parameter in that row)

Symbol	Parameter	Elite Controller group estimate (95% credible interval)	Comparison group estimate (95% credible interval)	Unit	$P(\theta_i^{\mathrm{EC}} > \theta_i^{\mathrm{C}})$
r_1	Growth rate of new CD4 T cells	1.38×10^2 $(1.84 \times 10^1, 7.35 \times 10^2)$	5.80×10^2 $(8.26, 1.32 \times 10^3)$	per year	0.289
μ_1	Death rate of total CD4 T cells	1.46×10^1 $(4.09, 5.44 \times 10^1)$	2.32×10^1 $(2.67 \times 10^{-1}, 4.92 \times 10^1)$	per year	0.461

c	Kill rate of CD4 T cells by effector CD8 CTLs due to other infections	1.89×10^{-4} $(4.07 \times 10^{-6}, 7.65 \times 10^{-4})$	3.47×10^{-4} $(6.82 \times 10^{-6}, 9.61 \times 10^{-4})$	mL per year	0.386
b	Kill rate of CD4 T cells by effector CD4 CTLs due to other infections	3.48×10^{-6} $(1.03 \times 10^{-15}, 2.39 \times 10^{-5})$	3.39×10^{-6} $(1.12 \times 10^{-14}, 2.22 \times 10^{-4})$	mL per year	0.421
β	Transmission rate of HIV-1 to CD4 T cells	2.05×10^{-4} $(1.10 \times 10^{-5}, 1.23 \times 10^{-2})$	2.32×10^{-4} $(3.74 \times 10^{-6}, 2.74 \times 10^{-3})$	mL per year	0.583
δ	Portion of generated HIV-1 specific effector CTLs that are HIV-1 specific effector CD4 CTLs	2.37×10^{-1} $(1.31 \times 10^{-2}, 4.85 \times 10^{-1})$	2.74×10^{-1} $(1.48 \times 10^{-2}, 4.77 \times 10^{-1})$	-	0.459

ka	Maximum proliferation rate of the HIV-1 specific effector CTL response	1.52×10^2 $(1.88, 8.53 \times 10^2)$	7.76×10^1 $(4.23, 7.69 \times 10^2)$	per year	0.72
a	Number of HIV-1 specific effector CTLs at which the proliferation switches to a maximum rate	3.04×10^{-1} $(1.01 \times 10^{-4}, 2.37 \times 10^3)$	1.34×10^1 $(1.31 \times 10^{-4}, 1.22 \times 10^4)$	per mL	0.365
μ_2	Death rate of effector CTLs	8.11×10^1 $(5.32 \times 10^1, 9.99 \times 10^1)$	8.41×10^1 $(5.83 \times 10^1, 1.00 \times 10^2)$	per year	0.493
μ_3	Death rate of productively infected CD4 T cells	1.89×10^2 $(4.47 \times 10^1, 3.19 \times 10^2)$	1.49×10^2 $(2.81 \times 10^1, 2.87 \times 10^2)$	per year	0.631
γ	Rate infected CD4 T cells are killed by effector CTLs	9.82 $(3.98 \times 10^{-2}, 5.47 \times 10^1)$	2.24×10^{-1} $(1.71 \times 10^{-2}, 6.26 \times 10^1)$	mL per year	0.738

p	Rate replication competent viral particles were produced by HIV-1 infected CD4 T cells	1.51×10^4 $(1.17 \times 10^3, 1.76 \times 10^5)$	7.04×10^3 $(1.00 \times 10^3, 1.24 \times 10^6)$	per year	0.435
μ_4	Death rate of HIV-1 replication competent viral particles	6.23×10^3 $(1.71 \times 10^3, 9.96 \times 10^3)$	4.61×10^3 $(1.31 \times 10^3, 9.62 \times 10^3)$	per year	0.568
r_2	Growth rate of new CD8 T cells	9.83×10^{-5} $(1.94 \times 10^{-5}, 1.77 \times 10^{-4})$	7.36×10^{-5} $(4.23 \times 10^{-5}, 1.17 \times 10^{-4})$	mL per year	0.593
μ_5	Death rate of total CD8 T cells	6.15×10^1 $(1.50 \times 10^1, 8.18 \times 10^1)$	5.11×10^1 $(2.28 \times 10^1, 7.09 \times 10^1)$	per year	0.659

6.C.3 Natural immune response to HIV-1 in the plasma

The figures from Sections 7.D.6 and 7.D.7 display the mean model predictions and 95% prediction intervals of the progression of untreated HIV-1 in the plasma. Panel (a)-(c) show the fitted data (circle points) and if available unfitted data (star points) for the total CD4 T cells/ml, total CD8 T cells/ml,

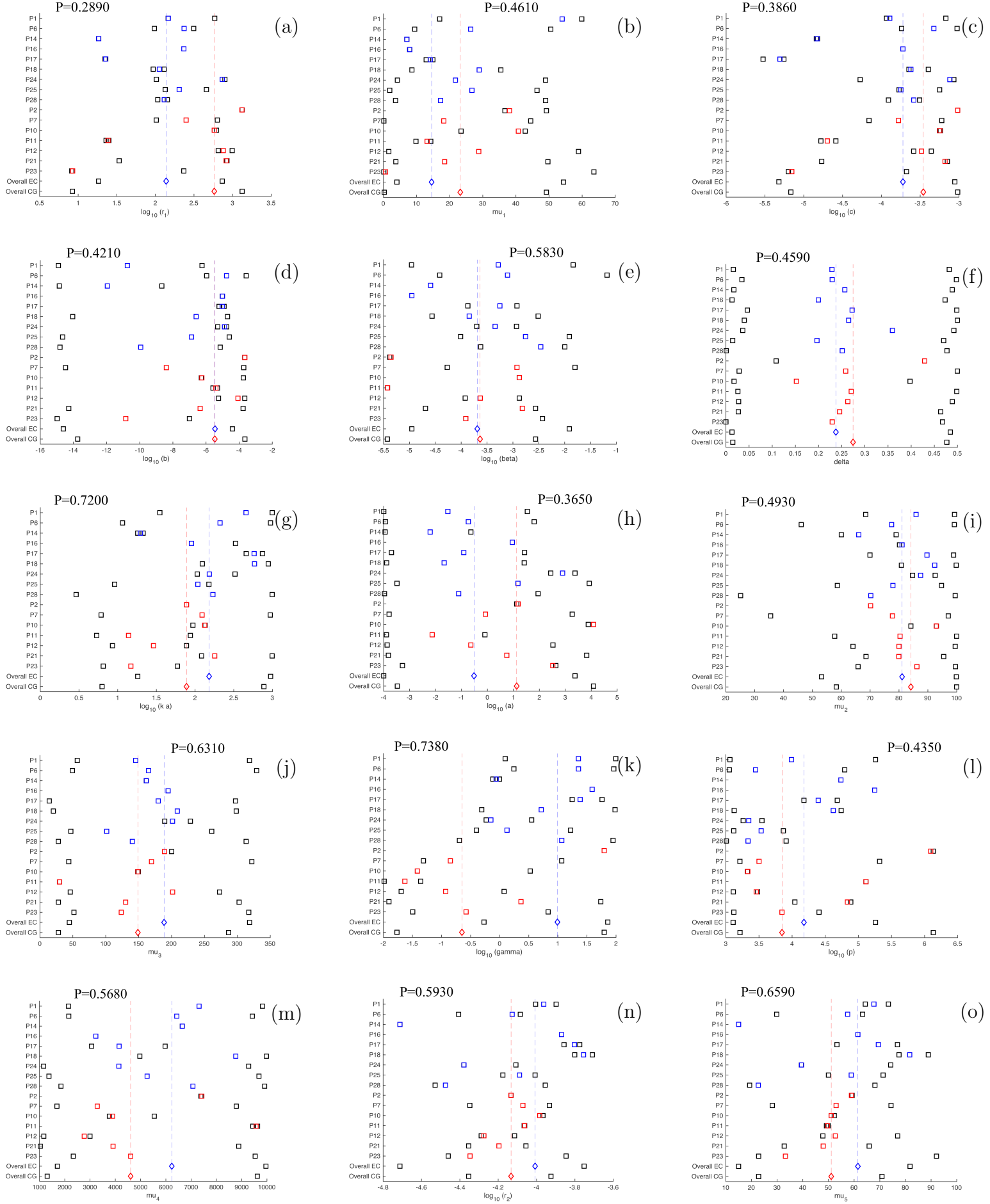

Figure 6.2: Model parameter estimates with the median as the point estimate (blue squares, Elite Controller patients; blue diamond, Elite Controller group pooled; red squares, comparison group patients; red diamond, comparison group pooled), 95% credible intervals (black squares), and P is the probability that the Elite Controller group parameter is greater than the comparison group parameter, $P(\theta_i^{\mathrm{EC}} > \theta_i^{\mathrm{C}})$

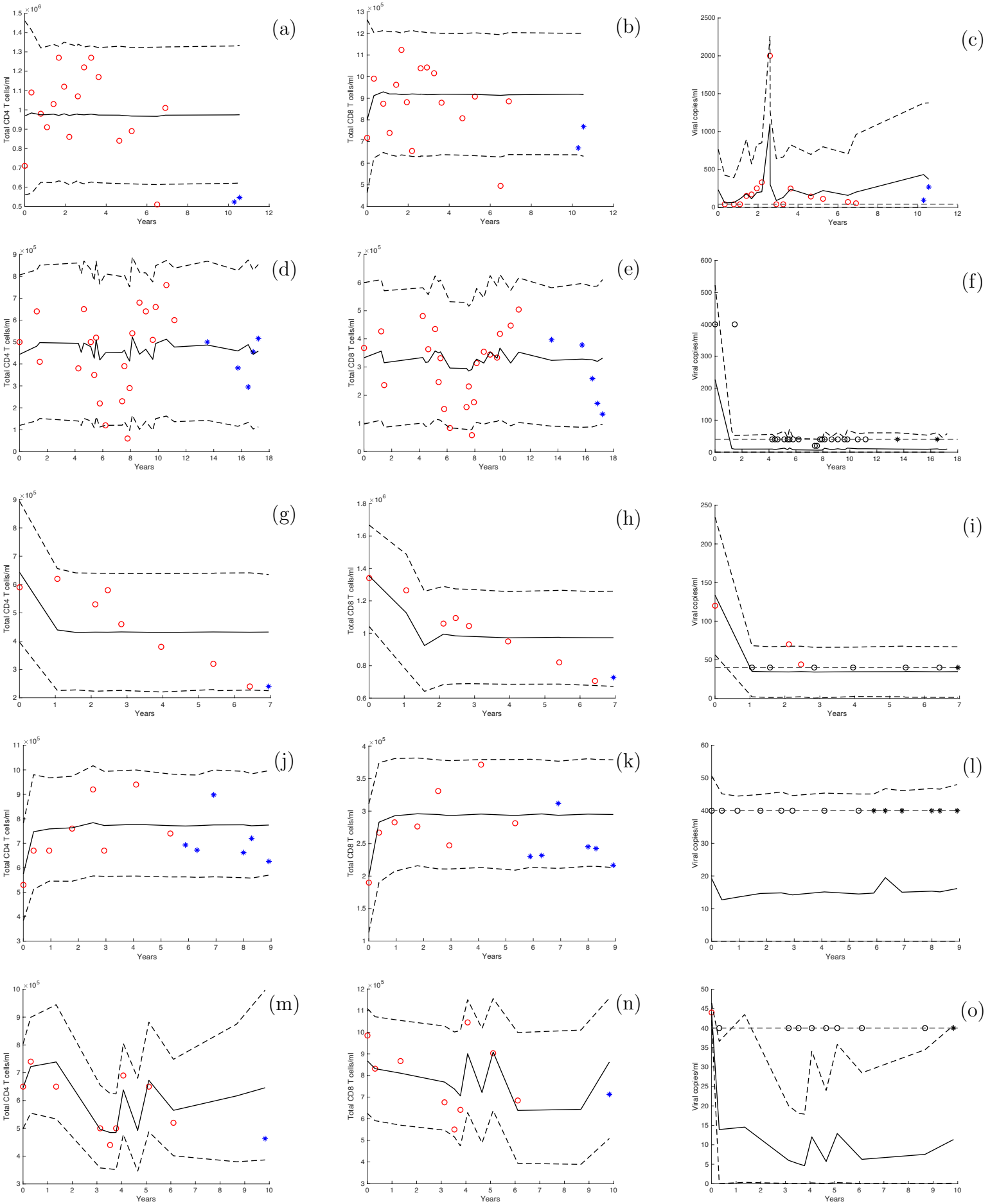

Figure 6.3: Prediction of HIV-1 infection in the plasma for Elite Controllers: row **(a)-(c)** Patient 14; row **(d)-(f)** Patient 16; row **(g)-(i)** Patient 17; row **(j)-(l)** Patient 25; row **(m)-(o)** Patient 28; column **(a)-(m)** total CD4 T cells/ml; column **(b)-(n)** total CD8 T cells/ml; column **(c)-(o)** viral copies/ml. Predictive mean solution (solid black curve), 95% prediction interval (dashed black curves), fitted data (circle points), unfitted data (star points), viral load below detection (black points).

and viral copies/ml, respectively. The CD4 T cell populations are shown in panels (d)-(f). The CD8 T cell populations are shown in panels (g) and (h). The effector response function over time is displayed in panel (i) and the effector response function over the number of effector CTLs is presented in panel (j). Further details about the completion of these predictions are located in Section 7.D.

Figure 6.3 displays the prediction for the HIV-1 Elite Controllers. It is seen in Figure 6.3 that the second data extraction (star points) for the Elite Controllers lie within the 95% prediction intervals, with the exception of the two total CD4 T cells/ml points for Patient 14. In Figure 7.27, the second data extraction (star points) for Patient 7 (which was the only comparison patient that had additional viral load, CD4 absolute, and CD4/CD8 ratio measurements in the second extraction) was also contained within the 95% prediction intervals, except for one total CD8 T cells/ml point.

The estimated values of the parameters, R_1, R_2, and R_3 for each patient are presented in Table 6.4. All patients have an estimated $R_1 > 1$, $R_3 < 0$, and $R_4 < 0$. All patients, except for Patient 6, always have an estimated $R_1 > R_2$. All patients, except for Patient 11, have an estimated $R_2 > 1$. Thus, for the majority of patient models, disease-free equilibriums P_0, P_1, P_2 exist (Theorem 6.1) and are unstable (Theorem 7.1) in $\mathbb{R}^6_+$. Also, for the majority of patient models, the necessary criteria for the existence of productive equilibria of the form P_4 and P_5 is satisfied (Theorem 6.1), though this does not fully guarantee their existence. For Patient 6, there is a slight overlap of R_2 with the lower bound of R_1 such that there is a small possibility that $R_2 > R_1$ instead of $R_1 > R_2$; in this situation, the disease-free equilibriums P_0, P_1 exist, the disease-free equilibrium P_2 may or may not exist, the necessary criteria for

productive equilibria of the form P_4 to exist is satisfied, and the necessary criteria for productive equilibria of the form P_5 to exist may or may not be satisfied (Theorem 6.1), and disease-free equilibriums P_0, P_1 are unstable, with the disease-free equilibrium P_2 being unstable if it exists (Theorem 7.1). For Patient 11, the estimated R_2 value is slightly less than 1, which indicates that the disease-free equilibriums P_0, P_1, P_2 exist, the necessary criteria for productive equilibria of the form P_4 to exist is satisfied, P_5 does not exist (Theorem 6.1), and disease-free equilibriums P_0, P_1 are unstable while the disease-free equilibrium P_2 is locally asymptotically stable (Theorem 7.1). This evidence supports that Patient 11 is on course to achieving productive control of HIV-1 infection in the plasma leading to the disease-free equilibrium, P_2, where there is no productive infection, no HIV-1 specific effector CTLs, and CD4 T cells and CD8 T cells are healthy. (Since latently HIV-1 infected cells are not included in the model, it cannot be suggested that Patient 11 is on course for a complete eradication of HIV-1 in the plasma.) Figure 7.29 displays Patient 11's plausible trajectory to productive control of HIV-1 infection in the plasma.

Table 6.4: Estimated values of the threshold parameters, R_1, R_2, R_3, and R_4 for each patient with the median as the point estimate and 95% credible intervals

Patient number	Elite Controller status	R_1	R_2	R_3	R_4
1	Yes	1.67×10^7 $(1.92 \times 10^1, 3.71 \times 10^{11})$	9.75 $(9.06, 1.01 \times 10^1)$	-1.17×10^1 $(-6.40 \times 10^1, -5.49 \times 10^{-2})$	-1.17×10^1 $(-6.40 \times 10^1, -5.40 \times 10^{-2})$

6	Yes	5.13×10^4 ($3.01 \times 10^1, 6.03 \times 10^{11}$)	3.18×10^1 ($3.02 \times 10^1, 3.30 \times 10^1$)	-1.22 ($-1.47 \times 10^1, -2.09 \times 10^{-2}$)	-1.22 ($-1.47 \times 10^1, -1.57 \times 10^{-2}$)
14	Yes	1.21×10^2 ($2.44 \times 10^1, 3.34 \times 10^2$)	2.23 (2.22, 2.39)	-7.06×10^{-1} ($-3.54, -5.85 \times 10^{-1}$)	-7.06×10^{-1} ($-3.54, -5.85 \times 10^{-1}$)
16	Yes	9.13×10^2 ($6.71, 1.49 \times 10^{10}$)	1.39 (1.30, 1.66)	-5.18 ($-4.09 \times 10^1, -1.61 \times 10^{-1}$)	-5.18 ($-4.09 \times 10^1, -1.61 \times 10^{-1}$)
17	Yes	1.76×10^1 ($1.11 \times 10^1, 2.05 \times 10^1$)	7.58 (6.27, 8.36)	-2.42×10^1 ($-5.75 \times 10^1, -1.76 \times 10^1$)	-2.42×10^1 ($-5.75 \times 10^1, -1.76 \times 10^1$)
18	Yes	7.23×10^1 ($7.22 \times 10^1, 7.39 \times 10^1$)	1.44 (1.44, 1.44)	-3.89×10^1 ($-3.89 \times 10^1, -3.89 \times 10^1$)	-3.89×10^1 ($-3.89 \times 10^1, -3.89 \times 10^1$)
24	Yes	1.32×10^7 ($6.63 \times 10^2, 5.52 \times 10^9$)	1.00 (1.00, 1.00)	-8.69×10^{-1} ($-9.91 \times 10^{-1}, -7.64 \times 10^{-1}$)	-8.69×10^{-1} ($-9.91 \times 10^{-1}, -7.64 \times 10^{-1}$)
25	Yes	9.84×10^1 ($1.02 \times 10^1, 1.31 \times 10^3$)	8.01 (7.63, 8.64)	-2.26×10^1 ($-6.37 \times 10^1, -3.55 \times 10^{-1}$)	-2.26×10^1 ($-6.37 \times 10^1, -3.53 \times 10^{-1}$)
28	Yes	5.19×10^7 ($1.97 \times 10^1, 3.14 \times 10^11$)	4.61 (3.99, 5.06)	-2.25×10^1 ($-8.89 \times 10^1, -1.14 \times 10^{-2}$)	-2.25×10^1 ($-8.89 \times 10^1, -1.08 \times 10^{-2}$)
2	No	5.02×10^6 ($5.89, 3.27 \times 10^10$)	3.32 (2.78, 3.34)	-2.64×10^{-1} ($-3.47, -1.26 \times 10^{-2}$)	-2.64×10^{-1} ($-3.47, -1.20 \times 10^{-2}$)

7	No	1.71×10^5 ($3.99 \times 10^2, 1.69 \times 10^1 3$)	8.20×10^1 ($7.88 \times 10^1, 8.36 \times 10^1$)	-2.36 ($-5.46 \times 10^1, -1.12 \times 10^{-2}$)	-2.35 ($-5.46 \times 10^1, -5.70 \times 10^{-3}$)
10	No	1.61×10^1 ($7.31, 2.35 \times 10^2$)	1.82 (1.67, 1.97)	-1.18×10^{-1} ($-1.18, -1.70 \times 10^{-2}$)	-1.18×10^{-1} ($-1.17, -1.67 \times 10^{-2}$)
11	No	4.87 (3.58, 7.56)	9.88×10^{-1} ($9.83 \times 10^{-1}, 9.94 \times 10^{-1}$)	-2.38×10^{-2} ($-4.40 \times 10^{-2}, -1.03 \times 10^{-2}$)	-2.37×10^{-2} ($-4.40 \times 10^{-2}, -1.03 \times 10^{-2}$)
12	No	4.51×10^3 ($1.54 \times 10^1, 4.86 \times 10^3$)	2.31 (2.28, 2.31)	-3.83×10^{-2} ($-3.35, -3.81 \times 10^{-2}$)	-3.77×10^{-2} ($-3.35, -3.77 \times 10^{-2}$)
21	No	5.01×10^5 ($2.11 \times 10^1, 7.12 \times 10^{11}$)	7.05 (6.26, 7.95)	-1.41×10^{-1} ($-1.16 \times 10^1, -4.17 \times 10^{-2}$)	-1.39×10^{-1} ($-1.16 \times 10^1, -4.07 \times 10^{-2}$)
23	No	2.24×10^1 ($2.24 \times 10^1, 2.30 \times 10^1$)	3.09 (3.09, 3.10)	-6.26×10^1 ($-6.26 \times 10^1, -6.26 \times 10^1$)	-6.26×10^1 ($-6.26 \times 10^1, -6.26 \times 10^1$)

The figures from Sections 7.F.1 and 7.F.2 display the global sensitivity analysis completed for each patient model in order to determine the most important model parameters explaining the total CD4 T cell, total CD8 T cell, and viral load behavior. Panel (a)-(c) show the mean total-order sensitivity index for each parameter along with +/- 2 standard deviations for the total CD4 T cell, total CD8 T cell, and viral load. The symbol $*$ indicates parameters with significant total-order sensitivity index values. The total-order

sensitivity index is the total contribution, main effect and any interactions, of a parameter to the sensitivity outcome of interest. Further information about the completion of the global sensitivity analysis can be found in Section 7.E.

The most important model parameters explaining the total CD4 T cell behavior for the Elite Controller group were the growth rate of new CD8 T cells (r_2) and the death rate of total CD8 T cells (μ_5) with certain Elite Controller patients having importance for the growth rate of new CD4 T cells (r_1) and the death rate of total CD4 T cells (μ_1). This indicates that the observed total CD4 T cell behavior for the Elite Controller group is greatly affected by the population of CD8 T cells that are non HIV-1 specific. Similarly, the most important model parameters explaining the total CD4 T cell behavior for the comparison group were the death rate of total CD8 T cells (μ_5) and the growth rate of new CD8 T cells (r_2). Additionally, the transmission rate of HIV-1 to CD4 T cells (β) and rate HIV-1 infected CD4 T cells are killed by effector CTLs (γ) were also important in explaining the total CD4 T cell behavior for certain comparison group patients, which indicates that HIV-1 infection effects the observed total CD4 T cell behavior for certain comparison group patients.

The most important model parameters explaining the total CD8 T cell behavior for the Elite Controller group were the kill rate of CD4 T cells by effector CD8 CTLs due to other infections (c), the growth rate of new CD4 T cells (r_1), and the death rate of total CD4 T cells (μ_1), and certain Elite Controller patients also had the kill rate of CD4 T cells by effector CD4 CTLs due to other infections (b) and the death rate of total CD8 T cells (μ_5) as important. This implies that the observed total CD8 T cell behavior for the Elite Controller group is greatly affected by the population of CD4 T cells

not infected with HIV-1 and the natural killing of other infections that are not HIV-1 by effector CTLs. Similarly, the most important model parameters explaining the total CD8 T cell behavior for the comparison group were the kill rate of CD4 T cells by effector CD8 CTLs due to other infections (c) and the growth rate of new CD4 T cells (r_1), and certain comparison group patients also have the kill rate of CD4 T cells by effector CD4 CTLs due to other infections (b) and the death rate of total CD4 T cells (μ_1) as important. In contrast, the transmission rate of HIV-1 to CD4 T cells (β), rate HIV-1 infected CD4 T cells are killed by effector CTLs (γ), and death rate of HIV-1 replication competent viral particles (μ_4) were also important in explaining the total CD4 T cell behavior for certain comparison group patients, which indicates that HIV-1 infection also effects the observed total CD8 T cell behavior for certain comparison group patients.

The most important model parameters explaining the viral load behavior for the Elite Controller group were the transmission rate of HIV-1 to CD4 T cells (β), rate HIV-1 infected CD4 T cells are killed by effector CTLs (γ), rate replication competent viral particles were produced by HIV-1 infected CD4 T cells (p), death rate of HIV-1 replication competent viral particles (μ_4), and maximum proliferation rate of the HIV-1 specific effector CTL response ka. In a similar way, the most important model parameters explaining the viral load behavior for the comparison group were the death rate of HIV-1 replication competent viral particles (μ_4), transmission rate of HIV-1 to CD4 T cells (β), and rate HIV-1 infected CD4 T cells are killed by effector CTLs (γ), and certain comparison group patients also had the rate replication competent viral particles were produced by HIV-1 infected CD4 T cells (p) and the maximum proliferation rate of the HIV-1 specific effector CTL response

(ka) as important.

6.D Discussion

This mathematical model reproduces and predicts HIV-1 plasma infection with natural immune responses. This is the first mathematical modeling study to precisely estimate the differences between a group of HIV-1 Elite Controllers and a comparison group of HIV-1 patients using empiric data and it is also the first HIV-1 mathematical model to consider both effector CD4 CTLs' and effector CD8 CTLs' impact on HIV-1 disease and other diseases present in each patient. The response function used for the HIV-1 specific effector CTLs has a biological interpretation based on the phases of antiviral CTL response and it was found that this response function was important for explaining the observed viral load behavior for the HIV-1 patients in this study. The Elite Controller immune response estimates given in this study quantifies a biologically realistic optimal immune response goal for HIV-1 therapeutic initiatives. These biologically realistic estimates can be compared to what current HIV-1 therapies are providing and elucidate gaps where potential improvements can be made to bring HIV-1 patients closer to an Elite Controller type outcome.

The Elite Controller group was found to have a stronger antiviral immune response than the comparison group. Specifically, the pooled estimate of the parameter values for the Elite Controller group indicated that the HIV-1 specific effector CTL response was more effective (the slope of the response function was larger and had a higher stable level) than the comparison group. Also, the pooled estimate of the parameter values for the Elite Controller group revealed that the death rate of productively HIV-1 infected CD4 T cells

was faster (possibly due to a more effective programmed cell death of HIV-1 infected CD4 T cells [121]) and the rate HIV-1 infected CD4 T cells are killed by effector CTLs is greater than the comparison group. The sensitivity analysis further implied the strong natural control of HIV-1 infection of the Elite Controller group by indicating that the observed total CD4 T cell and total CD8 T cell behavior was mainly being explained by immune responses due to other infections and hardly influenced by HIV-1 infection.

In contrast, the comparison group was found to have more chronic immune activation but a less effective immune response. More precisely, the pooled estimate of the parameter values for the comparison group showed that the growth rate of new CD4 T cells and the death rate of the general population of CD8 T cells was more rapid than the Elite Controller group, but the HIV-1 specific effector CTL response, the rate HIV-1 infected CD4 T cells are killed by effector CTLs, and the death rate of productively HIV-1 infected CD4 T cells were all slower than the Elite Controller group. The sensitivity analysis provided further evidence that the immune response of the comparison group was functioning in a less effective manner since the observed total CD4 T cell and total CD8 T cell behavior was being notably influenced by HIV-1 infection.

It was found that the Elite Controller group was significantly older (53.56 ± 10.04 yr) than the comparison group (41.28 ± 8.64 yr). Since the definition of being an Elite Controller from the 2014 literature review study [42] requires a sufficient time period of observation (HIV-1 positive for ≥ 6 months, HIV-1 positive for ≥ 1 year, or HIV-1 positive for ≥ 10 years) and viral suppression, it is possible that the definition of being an Elite Controller causes the Elite Controller group to be significantly older than the comparison group in this study.

It was determined that the comparison group had a significantly lower CD4/CD8 ratio (0.788 ± 0.319) than the Elite Controller group (1.28 ± 0.691) and the mean CD4/CD8 ratio for the comparison group was below the healthy value of 1.0. Additionally, it was found that the comparison group had a significantly higher CD8 absolute count ($1.05 \times 10^6 \pm 5.06 \times 10^5$ cells/mL) than the Elite Controller group ($6.42 \times 10^5 \pm 3.10 \times 10^5$ cells/mL) and the mean CD8 absolute count for the comparison group was outside the healthy range of 1.5×10^5 to 1×10^6 cells/ml. These results further highlight that the comparison group had more chronic immune activation but a less effective immune response than the Elite Controller group.

The Elite Controller group and the comparison group in this study also shared a number of parameter similarities and these parameters were the following: the death rate of total CD4 T cells, kill rate of CD4 T cells by effector CD8 CTLs due to other infections, kill rate of CD4 T cells by effector CD4 CTLs due to other infections, transmission rate of HIV-1 to CD4 T cells, portion of generated HIV-1 specific effector CTLs that are HIV-1 specific effector CD4 CTLs, death rate of effector CTLs, rate replication competent viral particles were produced by HIV-1 infected CD4 T cells, death rate of HIV-1 replication competent viral particles, and growth rate of new CD8 T cells. It is plausible that this implies that the patients comprising the comparison group are in some sense special as well. Even though the comparison group patients did not qualify as Elite Controllers based on the definitions from the 2014 literature review study [42], the comparison group patients all had an adequately long ART-naïve time period indicating their immune responses' limited ability to control HIV-1 without cART. Indeed comparison group Patient 11 certainly displays early signs of being an Elite Controller, with a maintenance of total

CD4 and CD8 T cells and strong reduction of viral load; however, there were not, as of yet, enough laboratory tests for Patient 11 which showed the viral load below the threshold required for an Elite Controller designation.

This study focused on the ART-naïve time period for the Elite Controller and comparison group patients from the Northern Alberta HIV Program. It would be useful to incorporate cART into system (6.1) and fit the HIV-1 plasma infection model during ART-naïve and cART time periods for each patient and note the difference cART has on the antiviral immune response of the patients.

Since plasma viral DNA measurements were not available for the HIV-1 patients in this study, it was not feasible to reasonably estimate the number of CD4 T cells latently infected with HIV-1 for these patients. If plasma viral DNA measurements were available for HIV-1 Elite Controller patients from other clinics, it would be beneficial to include a latent compartment into system (6.1) and estimate the number of CD4 T cells latently infected with HIV-1 for these other patients.

Macrophages were not included in system (6.1) because this would have increased the complexity and uncertainty in the mathematical model. Given that macrophages have a significant role in the formation of viral reservoirs, if plasma viral DNA measurements were available, the inclusion of macrophage compartments into system (6.1) would be enlightening to further assess the size of the latent HIV-1 reservoir.

Approximately 1 % of HIV-1 patients are considered Elite Controllers [42]. Consequently, there is a small amount of data available for modeling Elite Controllers. Furthermore, in order to assess the natural course of HIV-1 infection in the plasma, it is important to have Elite Controller data during an

ART-naïve time period, which is even rarer data to find. This is the reason for the limited number of HIV-1 patients in this study. Fitting system (6.1) with the possible incorporation of cART, latently HIV-1 infected cells, and/or macrophages to a larger group of HIV-1 Elite Controllers and HIV-1 comparison patients from several clinics would be an insightful next step to further confirm the important components of the Elite Controller immune response and provide additional biologically realistic immune response estimates to help with HIV-1 therapeutic objectives.

Chapter 7

Supplementary material for Chapter 6

7.A Local stability of disease-free equilibria

The Jacobian matrix of system (6.1) is

$$J = \begin{bmatrix} r_1 - \mu_1 - cz - 2bx - \beta v & 0 & 0 & -\beta x & -cx & 0 \\ 0 & \delta y \frac{\partial g}{\partial x_E} - \mu_2 - \beta v & \delta g(x_E + z_E) & -\beta x_E & 0 & \delta y \frac{\partial g}{\partial z_E} \\ \beta v & \beta v - \gamma y & -\mu_3 - \gamma(x_E + z_E) & \beta(x + x_E) & 0 & -\gamma y \\ 0 & 0 & p & -\mu_4 & 0 & 0 \\ r_2 z & 0 & 0 & 0 & r_2 x - \mu_5 & 0 \\ 0 & (1-\delta) y \frac{\partial g}{\partial x_E} & (1-\delta) g(x_E + z_E) & 0 & 0 & (1-\delta) y \frac{\partial g}{\partial z_E} - \mu_2 \end{bmatrix},$$

where

$$g(x_E + z_E) = \begin{cases} k(x_E + z_E), & x_E + z_E \leq a \\ ka, & x_E + z_E > a \end{cases},$$

$$\frac{\partial g}{\partial x_E} = \frac{\partial g}{\partial z_E} = \begin{cases} k, & x_E + z_E \leq a \\ 0, & x_E + z_E > a \end{cases}.$$

Theorem 7.1: *1. If $R_1 < 0$, then the disease-free equilibrium P_0 is locally asymptotically stable. If $R_1 > 0$, then P_0 is unstable.*

2. If $0 < R_1 < 1$, then the disease-free equilibrium P_1 is locally asymptotically stable. If $R_1 > 1$, then P_1 is unstable.

3. If $R_2 < 1$ and $R_1 > R_2$, then the disease-free equilibrium P_2 is locally asymptotically stable. If $R_2 > 1$ and $R_1 > R_2$, then P_2 is unstable.

Proof. The Jacobian matrix evaluated at P_0 is

$$J(P_0) = \begin{bmatrix} r_1 - \mu_1 & 0 & 0 & 0 & 0 & 0 \\ 0 & -\mu_2 & 0 & 0 & 0 & 0 \\ 0 & 0 & -\mu_3 & 0 & 0 & 0 \\ 0 & 0 & p & -\mu_4 & 0 & 0 \\ 0 & 0 & 0 & 0 & -\mu_5 & 0 \\ 0 & 0 & 0 & 0 & 0 & -\mu_2 \end{bmatrix}.$$

Since $J(P_0)$ is lower triangular, the eigenvalues of the matrix $J(P_0)$ lie on the main diagonal. If $R_1 < 0$, then all of the eigenvalues are negative and the disease-free equilibrium P_0 is locally asymptotically stable. If $R_1 > 0$, then the first eigenvalue $\mu_1 = r_1 - \mu_1 > 0$ and P_0 is unstable.

The Jacobian matrix evaluated at P_1 is

$$J(P_1) = \begin{bmatrix} \mu_1 - r_1 & 0 & 0 & -\frac{\beta}{b}(r_1 - \mu_1) & -\frac{c}{b}(r_1 - \mu_1) & 0 \\ 0 & -\mu_2 & 0 & 0 & 0 & 0 \\ 0 & 0 & -\mu_3 & \frac{\beta}{b}(r_1 - \mu_1) & 0 & 0 \\ 0 & 0 & p & -\mu_4 & 0 & 0 \\ 0 & 0 & 0 & 0 & -\mu_5 & 0 \\ 0 & 0 & 0 & 0 & 0 & -\mu_2 \end{bmatrix}.$$

Then

$$\det(J(P_1) - \lambda I) = (\lambda - (\mu_1 - r_1))(\mu_2 + \lambda)^2(\mu_5 + \lambda)\left(\lambda^2 + (\mu_4 + \mu_3)\lambda + \mu_3\mu_4 - \frac{p\beta}{b}(r_1 - \mu_1)\right) = 0. \tag{7.1}$$

Solving (7.1), we receive the following eigenvalues:

$\lambda_1 = \mu_1 - r_1$,

$\lambda_{2,3} = -\mu_2 < 0$,

$\lambda_4 = -\mu_5 < 0$, and

$\lambda_{5,6} = \frac{-(\mu_4+\mu_3) \pm (\mu_4+\mu_3)\sqrt{1 - \frac{4\mu_3\mu_4}{(\mu_4+\mu_3)^2}(1 - R_1)}}{2}$.

If $0 < R_1 < 1$, then the real part of every eigenvalue is negative and the disease-free equilibrium P_1 is locally asymptotically stable. If $R_1 > 1$, then the eigenvalue $\lambda_5 > 0$ and P_1 is unstable.

The Jacobian matrix evaluated at P_2 is

$$J(P_2) = \begin{bmatrix} -\frac{b\mu_5}{r_2} & 0 & 0 & -\beta\frac{\mu_5}{r_2} & -c\frac{\mu_5}{r_2} & 0 \\ 0 & -\mu_2 & 0 & 0 & 0 & 0 \\ 0 & 0 & -\mu_3 & \beta\frac{\mu_5}{r_2} & 0 & 0 \\ 0 & 0 & p & -\mu_4 & 0 & 0 \\ \frac{r_2}{c}\left(r_1 - \mu_1 - \frac{b\mu_5}{r_2}\right) & 0 & 0 & 0 & 0 & 0 \\ 0 & 0 & 0 & 0 & 0 & -\mu_2 \end{bmatrix}.$$

Then

$$\det(J(P_2)-\lambda I) = (\mu_2+\lambda)^2(\lambda^2+\frac{b\mu_5}{r_2}\lambda+\mu_5(r_1-\mu_1-\frac{b\mu_5}{r_2}))(\lambda^2+(\mu_4+\mu_3)\lambda+\mu_3\mu_4-\frac{\beta\mu_5 p}{r_2}) = 0. \tag{7.2}$$

Solving (7.2), we receive the following eigenvalues:

$\lambda_{1,2} = -\mu_2 < 0,$
$\lambda_{3,4} = \frac{-\frac{b\mu_5}{r_2} \pm \frac{b\mu_5}{r_2}\sqrt{1-4\frac{r_2^2}{b\mu_5\widetilde{R}}(R_1-R_2)}}{2}$, and
$\lambda_{5,6} = \frac{-(\mu_4+\mu_3)\pm(\mu_4+\mu_3)\sqrt{1-\frac{4\mu_3\mu_4}{(\mu_4+\mu_3)^2}(1-R_2)}}{2}.$

If $R_2 < 1$ and $R_1 > R_2$, then the real part of every eigenvalue is negative and the disease-free equilibrium P_2 is locally asymptotically stable. If $R_2 > 1$ and $R_1 > R_2$, then the eigenvalue $\lambda_5 > 0$ and P_2 is unstable.

□

7.B Data

The data for the NAP HIV-1 patient viral copies, total CD4 T cells, and total CD8 T cells are located in Table 7.1. The University of Alberta ethics protocol

number for the data was Pro0094810.

Table 7.1: NAP HIV-1 patient viral copies, total CD4 T cells, and total CD8 T cells at different times.

Patient	Elite Controller status	Second extraction	Years	Viral copies per ml*	Viral copies below detection	Total CD4 T cells per ml*	Total CD8 T cells per ml*
1	1	0	2.74E-3	5.70E1	0	7.00E5	4.46E5
1	1	0	3.42E-1	4.00E1	1	5.90E5	3.86E5
1	1	0	8.41E-1	4.00E1	1	6.00E5	3.87E5
1	1	0	1.16	4.00E1	1	7.00E5	5.43E5
1	1	0	1.48	4.00E1	1	6.90E5	4.63E5
1	1	0	1.75	4.40E1	0	6.90E5	4.39E5
1	1	0	2.32	4.00E1	1	5.50E5	3.42E5
6	1	0	2.74E-3	5.20E2	0	6.00E5	NA
6	1	0	4.08E-1	5.00E2	0	7.70E5	NA
6	1	0	1.07	5.00E1	0	6.00E5	NA
6	1	0	1.38	5.00E1	0	4.30E5	NA
6	1	0	3.00	5.00E1	0	6.10E5	NA
6	1	0	4.41	NA	0	8.10E5	NA
6	1	0	4.70	5.00E1	0	5.70E5	4.79E5
6	1	0	5.29	NA	0	7.10E5	5.59E5
6	1	0	6.24	4.00E2	0	8.40E5	6.22E5
6	1	0	1.05E1	1.70E2	0	6.40E5	6.40E5
6	1	0	1.12E1	1.20E2	0	8.60E5	8.35E5
6	1	0	1.60E1	2.40E2	0	8.60E5	9.45E5

6	1	0	1.68E1	8.74E2	0	7.00E5	4.86E5
6	1	0	1.70E1	2.94E3	0	8.50E5	1.09E6
6	1	0	1.82E1	5.70E2	0	6.90E5	1.01E6
14	1	0	2.74E-3	NA	0	7.10E5	7.17E5
14	1	0	3.32E-1	4.00E1	0	1.09E6	9.91E5
14	1	0	7.89E-1	4.00E1	0	9.80E5	8.75E5
14	1	0	1.10	4.00E1	0	9.10E5	7.40E5
14	1	0	1.42	1.50E2	0	1.03E6	9.63E5
14	1	0	1.67	1.70E2	0	1.27E6	1.12E6
14	1	0	1.94	2.50E2	0	1.12E6	8.82E5
14	1	0	2.19	3.30E2	0	8.60E5	6.56E5
14	1	0	2.60	2.00E3	0	NA	NA
14	1	0	2.61	NA	0	1.07E6	1.04E6
14	1	0	2.92	4.00E1	0	1.22E6	1.04E6
14	1	0	3.26	4.00E1	0	1.27E6	1.02E6
14	1	0	3.63	2.48E2	0	1.17E6	8.80E5
14	1	0	4.64	1.42E2	0	8.40E5	8.08E5
14	1	0	5.25	1.12E2	0	8.90E5	9.08E5
14	1	0	6.50	7.10E1	0	5.10E5	4.95E5
14	1	0	6.90	5.30E1	0	1.01E6	8.86E5
14	1	1	1.03E1	9.30E1	0	5.23E5	6.71E5
14	1	1	1.05E1	2.68E2	0	5.46E5	7.69E5
16	1	0	2.74E-3	4.00E2	1	5.00E5	3.68E5
16	1	0	1.24	NA	0	6.40E5	4.27E5
16	1	0	1.46	4.00E2	1	4.10E5	2.36E5
16	1	0	4.24	4.00E1	1	3.80E5	4.81E5

16	1	0	4.45	4.00E1	1	NA	NA
16	1	0	4.64	4.00E1	1	6.50E5	3.63E5
16	1	0	5.13	4.00E1	1	5.00E5	4.35E5
16	1	0	5.39	4.00E1	1	3.50E5	2.46E5
16	1	0	5.52	4.00E1	1	5.20E5	3.31E5
16	1	0	5.79	4.00E1	1	2.20E5	1.51E5
16	1	0	6.20	4.00E1	1	1.20E5	8.33E4
16	1	0	7.40	2.00E1	1	2.30E5	1.58E5
16	1	0	7.56	2.00E1	1	3.90E5	2.31E5
16	1	0	7.79	4.00E1	1	6.00E4	5.77E4
16	1	0	7.93	4.00E1	1	2.90E5	1.75E5
16	1	0	8.13	4.00E1	1	5.40E5	3.14E5
16	1	0	8.65	4.00E1	1	6.80E5	3.54E5
16	1	0	9.10	4.00E1	1	6.40E5	3.44E5
16	1	0	9.60	4.00E1	1	5.10E5	3.33E5
16	1	0	9.81	4.00E1	1	6.60E5	4.18E5
16	1	0	1.06E1	4.00E1	1	7.60E5	4.47E5
16	1	0	1.12E1	4.00E1	1	6.00E5	5.04E5
16	1	1	1.35E1	4.00E1	1	5.00E5	3.97E5
16	1	1	1.57E1	NA	0	3.82E5	3.78E5
16	1	1	1.65E1	4.00E1	1	2.95E5	2.59E5
16	1	1	1.68E1	NA	0	4.55E5	1.70E5
16	1	1	1.72E1	NA	0	5.16E5	1.32E5
17	1	0	2.74E-3	1.20E2	0	5.90E5	1.34E6
17	1	0	1.06	4.00E1	1	6.20E5	1.27E6
17	1	0	1.58	4.00E1	1	NA	NA

17	1	0	2.12	7.00E1	0	5.30E5	1.06E6
17	1	0	2.46	4.40E1	0	5.80E5	1.09E6
17	1	0	2.84	4.00E1	1	4.60E5	1.05E6
17	1	0	3.95	4.00E1	1	3.80E5	9.50E5
17	1	0	5.41	NA	0	3.20E5	8.21E5
17	1	0	5.46	4.00E1	1	NA	NA
17	1	0	6.42	4.00E1	1	2.40E5	7.06E5
17	1	1	6.95	4.00E1	1	2.40E5	7.27E5
18	1	0	2.74E-3	7.60E2	0	4.30E5	6.94E5
18	1	0	1.06	1.79E2	0	5.20E5	8.81E5
18	1	0	1.48	4.56E2	0	5.30E5	9.64E5
18	1	0	2.06	4.00E1	1	5.40E5	1.04E6
18	1	0	2.59	4.00E1	1	4.20E5	9.77E5
18	1	0	3.55	4.00E1	1	4.40E5	1.10E6
18	1	0	5.34	4.60E1	0	4.10E5	1.46E6
24	1	0	2.74E-3	5.00E1	1	1.18E6	9.83E5
24	1	0	2.74E-1	2.10E2	0	7.60E5	6.44E5
24	1	0	5.48E-1	4.00E2	1	8.10E5	9.20E5
24	1	0	7.53E-1	1.20E2	0	7.80E5	7.03E5
24	1	0	9.51E-1	1.20E2	0	9.70E5	1.08E6
24	1	0	1.12	4.00E2	0	NA	NA
24	1	0	1.21	NA	0	5.60E5	6.15E5
24	1	0	1.42	5.80E1	0	6.40E5	5.77E5
24	1	0	1.62	2.40E2	0	NA	NA
24	1	0	1.73	NA	0	8.70E5	8.29E5
24	1	0	1.90	1.50E2	0	1.07E6	1.14E6

24	1	0	1.98	4.00E1	1	8.80E5	8.46E5
24	1	0	2.25	2.10E2	0	6.60E5	6.29E5
24	1	0	2.52	4.00E1	1	8.50E5	8.33E5
24	1	0	2.77	6.30E1	0	8.70E5	7.98E5
24	1	0	3.15	4.00E1	1	7.30E5	7.85E5
24	1	0	3.40	1.90E2	0	7.90E5	7.45E5
24	1	0	3.61	1.90E2	0	8.30E5	7.35E5
24	1	0	3.98	4.00E1	1	6.00E5	5.71E5
24	1	0	4.21	4.00E1	1	8.30E5	7.35E5
24	1	0	5.09	4.00E1	1	4.40E5	3.93E5
24	1	0	5.81	2.00E1	1	8.80E5	7.59E5
24	1	0	6.28	4.00E1	1	4.90E5	6.20E5
24	1	0	6.66	4.00E1	1	7.40E5	5.83E5
24	1	0	6.70	4.00	1	NA	NA
24	1	0	7.06	4.00E1	1	9.10E5	1.08E6
24	1	0	7.41	6.30E1	0	8.30E5	7.61E5
24	1	0	7.76	1.14E2	0	8.00E5	7.08E5
24	1	0	8.43	1.93E2	0	7.50E5	8.52E5
24	1	0	8.79	4.00E1	1	7.80E5	9.75E5
24	1	0	9.37	9.00E1	0	7.20E5	6.73E5
24	1	0	9.83	1.82E3	0	NA	NA
25	1	0	2.74E-3	4.00E1	1	5.30E5	1.90E5
25	1	0	3.73E-1	4.00E1	1	6.70E5	2.67E5
25	1	0	9.40E-1	4.00E1	1	6.70E5	2.83E5
25	1	0	1.77	4.00E1	1	7.60E5	2.76E5
25	1	0	2.53	4.00E1	1	9.20E5	3.31E5

25	1	0	2.94	4.00E1	1	6.70E5	2.47E5
25	1	0	4.10	4.00E1	1	9.40E5	3.72E5
25	1	0	5.34	4.00E1	1	7.40E5	2.81E5
25	1	1	5.89	4.00E1	1	6.93E5	2.30E5
25	1	1	6.31	4.00E1	1	6.72E5	2.32E5
25	1	1	6.91	4.00E1	1	8.98E5	3.12E5
25	1	1	8.00	4.00E1	1	6.62E5	2.45E5
25	1	1	8.29	4.00E1	1	7.20E5	2.42E5
25	1	1	8.92	4.00E1	1	6.26E5	2.17E5
28	1	0	2.74E-3	4.40E1	0	6.50E5	9.85E5
28	1	0	3.12E-1	4.00E1	1	7.40E5	8.31E5
28	1	0	1.35	NA	0	6.50E5	8.67E5
28	1	0	3.13	4.00E1	1	5.00E5	6.76E5
28	1	0	3.53	4.00E1	1	4.40E5	5.50E5
28	1	0	3.78	NA	0	5.00E5	6.41E5
28	1	0	4.07	4.00E1	1	6.90E5	1.05E6
28	1	0	4.65	4.00E1	1	NA	NA
28	1	0	5.11	4.00E1	1	6.50E5	9.03E5
28	1	0	6.11	4.00E1	1	5.20E5	6.84E5
28	1	0	8.67	4.00E1	1	NA	NA
28	1	1	9.83	4.00E1	1	4.63E5	7.12E5
2	0	0	2.74E-3	5.80E2	0	5.70E5	1.19E6
2	0	0	3.40E-1	5.10E2	0	5.00E5	9.62E5
2	0	0	6.30E-1	1.60E3	0	7.80E5	1.15E6
2	0	0	9.34E-1	9.30E2	0	NA	NA
2	0	0	1.16	1.40E3	0	6.70E5	1.12E6

2	0	0	1.40	2.00E3	0	5.70E5	1.02E6
2	0	0	1.69	2.80E3	0	6.70E5	1.14E6
2	0	0	1.96	9.70E2	0	7.20E5	1.26E6
2	0	0	2.32	1.88E3	0	6.80E5	1.00E6
2	0	0	2.66	7.70E3	0	6.60E5	1.02E6
2	0	0	3.14	9.51E3	0	6.30E5	1.34E6
7	0	0	2.74E-3	NA	0	8.40E5	NA
7	0	0	1.89E-1	2.28E3	0	NA	NA
7	0	0	3.70E-1	3.20E3	0	6.70E5	9.18E5
7	0	0	6.52E-1	6.80E3	0	7.70E5	1.08E6
7	0	0	9.07E-1	6.90E3	0	8.20E5	1.01E6
7	0	0	1.32	8.40E3	0	7.10E5	1.16E6
7	0	0	1.60	3.10E4	0	7.10E5	9.34E5
7	0	0	1.78	3.50E3	0	6.70E5	1.14E6
7	0	0	2.05	2.90E3	0	8.00E5	1.14E6
7	0	0	2.30	3.70E3	0	6.80E5	1.05E6
7	0	0	2.59	5.70E3	0	8.30E5	1.32E6
7	0	0	2.92	1.20E4	0	5.70E5	8.77E5
7	0	0	3.20	4.50E3	0	7.70E5	1.18E6
7	0	0	3.53	3.10E3	0	7.10E5	1.34E6
7	0	0	3.91	5.70E3	0	6.00E5	9.38E5
7	0	0	4.24	2.10E3	0	7.90E5	1.30E6
7	0	0	4.53	7.20E3	0	5.90E5	9.52E5
7	0	0	4.85	1.40E4	0	8.20E5	1.17E6
7	0	0	5.16	1.10E4	0	6.10E5	1.07E6
7	0	0	5.60	6.20E3	0	8.50E5	1.60E6

7	0	0	6.04	5.40E3	0	7.70E5	1.18E6
7	0	0	6.43	4.90E3	0	6.90E5	1.21E6
7	0	0	6.93	9.12E3	0	8.00E5	1.27E6
7	0	0	7.40	7.69E3	0	8.80E5	1.49E6
7	0	0	7.90	2.60E3	0	7.30E5	1.33E6
7	0	0	8.48	2.05E3	0	7.30E5	1.28E6
7	0	0	9.04	5.93E3	0	7.00E5	1.15E6
7	0	0	9.65	3.07E3	0	8.60E5	1.37E6
7	0	0	1.03E1	9.06E2	0	7.60E5	1.27E6
7	0	0	1.07E1	1.07E3	0	8.00E5	1.54E6
7	0	1	1.16E1	1.40E3	0	8.80E5	1.49E6
7	0	1	1.24E1	4.63E3	0	8.33E5	1.46E6
7	0	1	1.29E1	2.57E3	0	6.29E5	1.14E6
7	0	1	1.38E1	1.82E3	0	7.52E5	1.63E6
7	0	1	1.44E1	6.05E2	0	6.40E5	1.19E6
7	0	1	1.49E1	2.95E3	0	7.05E5	1.41E6
7	0	1	1.53E1	1.13E3	0	7.01E5	1.35E6
10	0	0	2.74E-3	7.50E2	0	7.50E5	1.21E6
10	0	0	1.95E-1	1.70E3	0	8.60E5	1.46E6
10	0	0	4.05E-1	6.60E2	0	9.20E5	1.59E6
10	0	0	7.07E-1	2.60E3	0	8.00E5	1.51E6
10	0	0	9.97E-1	1.10E3	0	1.29E6	2.53E6
10	0	0	1.44	3.00E3	0	1.23E6	2.86E6
10	0	0	1.78	2.20E3	0	1.51E6	2.90E6
10	0	0	2.45	NA	0	1.06E6	2.12E6
10	0	0	3.70	2.80E3	0	1.03E6	2.51E6

10	0	0	4.87	3.40E2	0	8.70E5	1.93E6
10	0	0	6.21	2.70E2	0	7.90E5	1.80E6
10	0	0	7.54	6.35E2	0	8.10E5	1.88E6
10	0	0	8.00	1.82E3	0	1.05E6	2.19E6
10	0	0	8.36	2.60E3	0	5.70E5	1.36E6
10	0	0	9.45	NA	0	7.82E5	1.40E6
10	0	0	9.53	3.00E2	0	7.06E5	6.79E5
11	0	0	2.74E-3	3.70E3	0	6.40E5	6.27E5
11	0	0	2.52E-1	NA	0	5.50E5	4.82E5
11	0	0	5.40E-1	3.50E3	0	5.60E5	4.87E5
11	0	0	8.05E-1	2.60E3	0	4.50E5	4.41E5
11	0	0	1.13	6.90E2	0	5.60E5	4.79E5
11	0	0	1.38	8.80E2	0	4.10E5	3.18E5
11	0	0	1.62	2.10E3	0	5.80E5	4.79E5
11	0	0	2.09	4.00E2	0	8.70E5	5.96E5
11	0	0	2.57	1.60E3	0	6.70E5	5.73E5
11	0	0	2.81	6.60E2	0	5.50E5	4.30E5
11	0	0	3.11	5.70E2	0	7.10E5	5.73E5
11	0	0	3.49	4.50E2	0	7.20E5	5.33E5
11	0	0	3.84	4.70E2	0	5.30E5	4.27E5
11	0	0	4.10	1.30E2	0	5.50E5	4.66E5
11	0	0	4.37	3.30E2	0	7.70E5	5.35E5
11	0	0	4.69	1.10E2	0	7.40E5	6.32E5
11	0	0	5.00	1.30E2	0	5.60E5	4.55E5
11	0	0	5.58	4.80E1	0	5.00E5	4.39E5
11	0	0	5.98	1.20E2	0	7.00E5	3.93E5

11	0	0	6.25	1.50E2	0	5.90E5	4.01E5
11	0	0	6.56	1.70E2	0	4.90E5	3.16E5
11	0	0	6.87	4.90E1	0	6.20E5	4.43E5
11	0	0	7.13	2.20E2	0	5.00E5	3.14E5
11	0	0	7.49	2.40E2	0	6.80E5	4.63E5
11	0	0	7.84	1.20E2	0	5.20E5	3.47E5
11	0	0	8.16	1.60E2	0	4.70E5	3.13E5
11	0	0	8.66	5.20E1	0	4.40E5	2.99E5
11	0	0	9.04	8.30E1	0	5.90E5	4.18E5
11	0	0	9.38	1.25E2	0	6.50E5	4.45E5
11	0	0	9.68	3.83E2	0	5.20E5	4.37E5
11	0	0	1.02E1	4.00E1	1	5.46E5	3.79E5
12	0	0	2.74E-3	8.20E3	0	6.64E5	NA
12	0	0	3.62E-1	3.60E3	0	5.20E5	NA
12	0	0	7.62E-1	3.70E3	0	3.50E5	6.25E5
12	0	0	9.32E-1	2.40E4	0	5.40E5	1.86E6
12	0	0	1.07	5.10E3	0	5.00E5	1.06E6
12	0	0	1.32	1.70E3	0	NA	NA
12	0	0	1.74	4.50E3	0	5.90E5	1.31E6
12	0	0	2.28	3.70E3	0	6.00E5	1.18E6
12	0	0	2.78	8.20E2	0	7.40E5	1.28E6
12	0	0	3.96	1.60E3	0	8.20E5	1.22E6
12	0	0	4.45	5.10E2	0	6.90E5	9.32E5
12	0	0	5.68	5.16E2	0	4.10E5	4.71E5
12	0	0	6.69	1.46E3	0	5.10E5	5.86E5
12	0	0	6.95	8.37E2	0	3.40E5	3.95E5

12	0	0	7.95	3.45E3	0	4.90E5	6.81E5
12	0	0	8.20	4.34E2	0	3.40E5	4.47E5
12	0	0	8.57	1.25E2	0	3.50E5	4.17E5
12	0	0	8.85	1.39E3	0	5.30E5	5.89E5
12	0	0	9.47	6.31E2	0	2.90E5	4.03E5
21	0	0	2.74E-3	5.10E3	0	6.60E5	9.43E5
21	0	0	4.99E-1	8.30E3	0	4.70E5	7.12E5
21	0	0	1.00	7.80E3	0	6.20E5	1.03E6
21	0	0	1.73	1.14E4	0	NA	NA
21	0	0	2.01	7.30E3	0	5.30E5	1.00E6
21	0	0	2.55	9.92E3	0	7.90E5	1.23E6
23	0	0	2.74E-3	7.80E2	0	NA	NA
23	0	0	5.84E-1	7.80E2	0	7.60E5	8.17E5
23	0	0	8.85E-1	7.70E2	0	7.90E5	1.41E6
23	0	0	1.25	6.80E2	0	9.50E5	1.64E6
23	0	0	1.57	5.40E2	0	9.70E5	1.67E6
23	0	0	2.02	4.00E2	0	9.50E5	1.56E6
23	0	0	2.38	3.00E2	0	9.90E5	1.65E6
23	0	0	2.75	6.40E2	0	6.40E5	1.19E6
23	0	0	3.07	2.10E2	0	6.50E5	1.25E6
23	0	0	3.47	2.20E2	0	5.90E5	1.07E6
23	0	0	3.76	4.50E2	0	9.20E5	1.53E6
23	0	0	4.13	6.60E2	0	8.40E5	1.18E6
23	0	0	4.42	1.60E2	0	8.60E5	1.46E6
23	0	0	4.87	9.20E2	0	9.10E5	1.25E6
23	0	0	5.35	1.60E3	0	8.50E5	1.12E6

23	0	0	5.91	1.40E3	0	8.50E5	1.01E6
23	0	0	6.47	NA	0	6.20E5	7.47E5
23	0	0	6.87	1.90E3	0	9.90E5	1.10E6
23	0	0	7.08	NA	0	8.40E5	1.02E6
23	0	0	7.37	2.80E3	0	9.40E5	1.15E6
23	0	0	7.89	2.20E3	0	8.20E5	1.09E6
23	0	0	8.40	NA	0	8.30E5	1.09E6
23	0	0	9.02	3.00E3	0	8.30E5	9.88E5
23	0	0	9.38	3.00E3	0	8.40E5	9.44E5
23	0	0	9.94	2.00E3	0	7.80E5	1.01E6
23	0	0	1.04E1	9.80E3	0	7.40E5	1.00E6
23	0	0	1.09E1	3.80E3	0	6.70E5	8.59E5
23	0	0	1.14E1	2.70E3	0	8.30E5	1.17E6
23	0	0	1.19E1	1.60E3	0	7.70E5	7.94E5
23	0	0	1.25E1	1.61E3	0	7.00E5	8.86E5
23	0	0	1.30E1	1.68E3	0	9.00E5	1.20E6
23	0	0	1.35E1	1.38E3	0	6.60E5	6.41E5
23	0	0	1.38E1	5.04E2	0	6.70E5	8.82E5
23	0	0	1.43E1	1.11E3	0	NA	NA

* If the variable was not measured at a particular time point, then not applicable (NA) is written in the cell.

7.C Prior distributions for Bayesian inference

For parameters that take positive values and that have an uncertainty that spans several orders of magnitude, it is useful to use the loguniform distribution

as the prior distribution [68]. The loguniform distribution views the logarithm range as uniform. Using the loguniform distribution as a prior distribution for a parameter can help Bayesian inference to more easily explore a parameter's uncertainty. It is usual to view the orders of magnitude in terms of base 10. The loguniform distribution is used for certain parameters in this study and it is done by using the following method: the logarithm base 10 of these parameters is fit, consequently the prior of the logarithm base 10 of these parameters is still uniform, and then the logarithm base 10 of these parameters are exponentiated by 10 to transform these parameters back to their original scale inside the likelihood function [68].

Uniform or loguniform prior distributions were specified for the parameters in model (6.1) since there is a general range for these parameters given in the literature. The uniform and loguniform prior distributions used for the model parameters were the same for all of the patients and these are displayed in Table 7.2. The uniform prior distributions for the model initial conditions varied for each patient. The tables displaying the initial condition prior distributions for the HIV-1 Elite Controller patients are located in Section 7.C.1 and the tables displaying the initial condition prior distributions for the HIV-1 patient comparison group are located in Section 7.C.2.

The estimated lifespan of CD4 T cells and CD8 T cells vary across studies [122, 123, 124, 125, 126]. In humans, the estimates are that memory CD4 T cells and CD8 T cells live 0.449 (range, 0.194 - 1.37) and 0.430 (range, 0.310 - 0.633) years, respectively [122]. In humans, effector memory CD4 T cells are found to be able to live for more than 17 years [125]. A mathematical modeling study determined that healthy patients had an average CD4 T cell lifespan of 0.0623 years and an average CD8 T cell lifespan of 0.0685 years

[126]. Another study fit a mathematical model to ten HIV-1 patients and the death rate of activated CD4 T cells was estimated to be in the range from 1.6 to 7.3 per year [127]. An animal model, estimating the lifespan of memory T cells in different locations in the body, found that the average lifespan of memory CD4 T cells in the blood was 0.120 years and the average lifespan of memory CD8 T cells in the blood was 0.0877 years [124]. The range of the lifespan of the total CD4 T cells, total CD8 T cells, and effector CTLs in this study were each given a range from 0.01 to 17 years. Consequently, the uniform prior distributions for the death rate of total CD4 T cells (μ_1), death rate of total CD8 T cells (μ_5), and death rate of effector CTLs (μ_2) in this study were each $U(0.0588, 100)$. In the HIV-1 Elite Controller transplant patient study, the death rate of productively infected CD4 T cells was estimated to be 328.5 per year and the death rate of HIV-1 replication competent viral particles was estimated to be 8395 per year [56]. In the study that fit a mathematical model to ten HIV-1 patients, the death rate of productively infected CD4 T cells was estimated to be in the range from 47.45 to 292 per year [127]. From these estimates, uniform prior distributions for the death rate of productively infected CD4 T cells (μ_3) and the death rate of HIV-1 replication competent viral particles (μ_4) were chosen to be $U(4, 330)$ and $U(1 \times 10^3, 1 \times 10^4)$.

In the HIV-1 Elite Controller transplant patient study, the estimated transmission rate of HIV-1 to CD4 T cells was 6.059×10^{-6} mL per year [56]. In the study that fit a mathematical model to ten HIV-1 patients, the transmission rate of HIV-1 to CD4 T cells was estimated to be in the range from 6.9×10^{-5} to 1.8×10^{-3} mL per year [127]. An earlier mathematical modeling study estimated the transmission rate of HIV-1 to CD4 T cells as 8.8×10^{-6} mL per year [128] and later reports have used the estimate of 3.65×10^{-5}

mL per year [129, 130]. Given these estimates, the loguniform prior distribution chosen for the transmission rate of HIV-1 to CD4 T cells (β) was $\log_{10}(\beta) \sim U(\log_{10}(1 \times 10^{-8}), \log_{10}(1 \times 10^{-1}))$.

The estimated rate replication competent viral particles were produced by HIV-1 infected CD4 T cells was 7.3×10^6 per year in the HIV-1 Elite Controller transplant patient study [56] and had the range from 3.6×10^4 to 2.6×10^6 per year in the ten HIV-1 patient mathematical modeling study [127]. From these estimates, the loguniform prior distribution chosen for the rate replication competent viral particles were produced by HIV-1 infected CD4 T cells (p) was $\log_{10}(p) \sim U(\log_{10}(1 \times 10^3), \log_{10}(1 \times 10^7))$.

Also, in the HIV-1 Elite Controller transplant patient study, the estimated growth rate of new CD4 T cells was 292 per year and the estimated rate infected CD4 T cells are killed by effector CTLs was 0.365 mL per year [56]. From these estimates, the loguniform prior distribution chosen for the growth rate of new CD4 T cells (r_1) was $\log_{10}(r_1) \sim U(\log_{10}(1 \times 10^{-5}), \log_{10}(5 \times 10^3))$ and the loguniform prior distribution chosen for the rate infected CD4 T cells are killed by effector CTLs (γ) was $\log_{10}(\gamma) \sim U(\log_{10}(0.01), \log_{10}(100))$.

The majority of HIV-1 specific effector CTLs generated by the immune system are HIV-1 specific effector CD8 CTLs [41]. Consequently, the uniform prior distribution chosen for the portion of generated HIV-1 specific effector CTLs that are HIV-1 specific effector CD4 CTLs (δ) was $U(0, 0.5)$.

The kill rate of CD4 T cells by effector CD8 CTLs due to other infections that are not HIV-1 (c), the kill rate of CD4 T cells by effector CD4 CTLs due to other infections that are not HIV-1 (b), the growth rate of new CD8 T cells (r_2), the maximum proliferation rate of the HIV-1 specific effector CTL response (ka), and the number of HIV-1 specific effector CTLs at which the

proliferation switches to a maximum rate (a) were not previously estimated and a broad range was chosen for these parameters. The loguniform prior distribution chosen for the kill rate of CD4 T cells by effector CD8 CTLs due to other infections that are not HIV-1 (c) was $\log_{10}(c) \sim U(\log_{10}(1 \times 10^{-8}), \log_{10}(1 \times 10^{-3}))$, the loguniform prior distribution chosen for the kill rate of CD4 T cells by effector CD4 CTLs due to other infections that are not HIV-1 (b) was $\log_{10}(b) \sim U(\log_{10}(1 \times 10^{-15}), \log_{10}(1 \times 10^{-3}))$, the loguniform prior distribution chosen for the growth rate of new CD8 T cells (r_2) was $\log_{10}(r_2) \sim U(\log_{10}(1 \times 10^{-15}), \log_{10}(1 \times 10^{-3}))$, the loguniform prior distribution chosen for the maximum proliferation rate of the HIV-1 specific effector CTL response (ka) was $\log_{10}(ka) \sim U(\log_{10}(1 \times 10^{-5}), \log_{10}(1 \times 10^{3}))$, and the loguniform prior distribution chosen for the number of HIV-1 specific effector CTLs at which the proliferation switches to a maximum rate (a) was $\log_{10}(a) \sim U(\log_{10}(1 \times 10^{-4}), \log_{10}(2 \times 10^{4}))$.

The range of each patient CD4 absolute cells/mL data is used to inform the uniform prior distribution of the initial number of CD4 T cells susceptible to HIV-1 (x_0). The range of each patient CD8 absolute cells/mL data is used to inform the uniform prior distribution of the initial number of CD8 T cells that are non HIV-1 specific (z_0). The range of each patient viral load copies/mL data is used to help inform the uniform prior distribution of the initial number of HIV-1 replication competent viral particles (v_0). It is expected that the initial viral load for each patient is also closely related to the initial number of CD4 T cells productively infected with HIV-1, the initial number of HIV-1 specific effector CD4 CTLs, and the initial number of HIV-1 specific effector CD4 CTLs. As a result, the upper bound of the uniform prior distribution range chosen for v_0 was also used for the uniform prior distribution

of the initial number of CD4 T cells productively infected with HIV-1 (y_0), the initial number of HIV-1 specific effector CD4 CTLs (x_{E0}), and the initial number of HIV-1 specific effector CD8 CTLs (z_{E0}).

Table 7.2: Uniform and loguniform prior distributions for model parameters

Symbol	Parameter	Prior distribution	Unit	Reference(s)
$\log_{10}(r_1)$	Growth rate of new CD4 T cells	$U(\log_{10}(1\times10^{-5}), \log_{10}(5\times10^{3}))$	per year	[56]
μ_1	Death rate of total CD4 T cells	$U(0.0588, 100)$	per year	[122, 123, 124, 125, 126]
$\log_{10}(c)$	Kill rate of CD4 T cells by effector CD8 CTLs due to other infections	$U(\log_{10}(1\times10^{-8}), \log_{10}(1\times10^{-3}))$	mL per year	-
$\log_{10}(b)$	Kill rate of CD4 T cells by effector CD4 CTLs due to other infections	$U(\log_{10}(1\times10^{-15}), \log_{10}(1\times10^{-3}))$	mL per year	-
$\log_{10}(\beta)$	Transmission rate of HIV-1 to CD4 T cells	$U(\log_{10}(1\times10^{-8}), \log_{10}(1\times10^{-1}))$	mL per year	[56]
δ	Portion of generated HIV-1 specific effector CTLs that are HIV-1 specific effector CD4 CTLs	$U(0, 0.5)$	-	-
$\log_{10}(ka)$	Maximum proliferation rate of the HIV-1 specific effector CTL response	$U(\log_{10}(1\times10^{-5}), \log_{10}(1\times10^{3}))$	per year	-

$\log_{10}(a)$	Number of HIV-1 specific effector CTLs at which the proliferation switches to a maximum rate	$U(\log_{10}(1 \times 10^{-4}), \log_{10}(2 \times 10^{4}))$	per mL	-
μ_2	Death rate of effector CTLs	$U(0.0588, 100)$	per year	[122, 123, 124, 125, 126]
μ_3	Death rate of productively infected CD4 T cells	$U(4, 330)$	per year	[56]
$\log_{10}(\gamma)$	Rate infected CD4 T cells are killed by effector CTLs	$U(\log_{10}(0.01), \log_{10}(100))$	mL per year	[56]
$\log_{10}(p)$	Rate replication competent viral particles were produced by HIV-1 infected CD4 T cells	$U(\log_{10}(1 \times 10^{3}), \log_{10}(1 \times 10^{7}))$	per year	[56]
μ_4	Death rate of HIV-1 replication competent viral particles	$U(1 \times 10^{3}, 1 \times 10^{4})$	per year	[56]
$\log_{10}(r_2)$	Growth rate of new CD8 T cells	$U(\log_{10}(1 \times 10^{-15}), \log_{10}(1 \times 10^{-3}))$	mL per year	-
μ_5	Death rate of total CD8 T cells	$U(0.0588, 100)$	per year	[122, 123, 124, 125, 126]

7.C.1 Prior distributions for HIV-1 Elite Controller patient initial conditions

Table 7.3: Uniform prior distributions for Patient 1 initial conditions

Symbol	Parameter	Prior distribution	Unit
x_0	Initial number of CD4 T cells susceptible to HIV-1	$U(5.50 \times 10^5, 8 \times 10^5)$	per mL
x_{E0}	Initial number of HIV-1 specific effector CD4 CTLs	$U(0, 1 \times 10^3)$	per mL
y_0	Initial number of CD4 T cells productively infected with HIV-1	$U(0, 1 \times 10^2)$	per mL
v_0	initial number of HIV-1 replication competent viral particles	$U(4 \times 10^1, 1 \times 10^2)$	per mL
z_0	Initial number of CD8 T cells that are non HIV-1 specific	$U(3 \times 10^5, 8 \times 10^5)$	per mL
z_{E0}	Initial number of HIV-1 specific effector CD8 CTLs	$U(0, 1 \times 10^3)$	per mL

Table 7.4: Uniform prior distributions for Patient 6 initial conditions

Symbol	Parameter	Prior distribution	Unit
x_0	Initial number of CD4 T cells susceptible to HIV-1	$U(4.50 \times 10^5, 8 \times 10^5)$	per mL
x_{E0}	Initial number of HIV-1 specific effector CD4 CTLs	$U(0, 1 \times 10^3)$	per mL

y_0	Initial number of CD4 T cells productively infected with HIV-1	$U(0, 1 \times 10^3)$	per mL
v_0	initial number of HIV-1 replication competent viral particles	$U(5 \times 10^1, 1 \times 10^3)$	per mL
z_0	Initial number of CD8 T cells that are non HIV-1 specific	$U(4.5 \times 10^5, 8 \times 10^5)$	per mL
z_{E0}	Initial number of HIV-1 specific effector CD8 CTLs	$U(0, 1 \times 10^3)$	per mL

Table 7.5: Uniform prior distributions for Patient 14 initial conditions

Symbol	Parameter	Prior distribution	Unit
x_0	Initial number of CD4 T cells susceptible to HIV-1	$U(7 \times 10^5, 1.30 \times 10^6)$	per mL
x_{E0}	Initial number of HIV-1 specific effector CD4 CTLs	$U(0, 4 \times 10^2)$	per mL
y_0	Initial number of CD4 T cells productively infected with HIV-1	$U(0, 4 \times 10^2)$	per mL
v_0	initial number of HIV-1 replication competent viral particles	$U(1, 4 \times 10^2)$	per mL
z_0	Initial number of CD8 T cells that are non HIV-1 specific	$U(6.5 \times 10^5, 1.2 \times 10^6)$	per mL

z_{E0}	Initial number of HIV-1 specific effector CD8 CTLs	$U(0, 4 \times 10^2)$	per mL

Table 7.6: Uniform prior distributions for Patient 16 initial conditions

Symbol	Parameter	Prior distribution	Unit
x_0	Initial number of CD4 T cells susceptible to HIV-1	$U(3.5 \times 10^5, 6.4 \times 10^5)$	per mL
x_{E0}	Initial number of HIV-1 specific effector CD4 CTLs	$U(0, 5 \times 10^2)$	per mL
y_0	Initial number of CD4 T cells productively infected with HIV-1	$U(0, 5 \times 10^2)$	per mL
v_0	initial number of HIV-1 replication competent viral particles	$U(1, 5 \times 10^2)$	per mL
z_0	Initial number of CD8 T cells that are non HIV-1 specific	$U(2.35 \times 10^5, 4.9 \times 10^5)$	per mL
z_{E0}	Initial number of HIV-1 specific effector CD8 CTLs	$U(0, 5 \times 10^2)$	per mL

Table 7.7: Uniform prior distributions for Patient 17 initial conditions

Symbol	Parameter	Prior distribution	Unit

x_0	Initial number of CD4 T cells susceptible to HIV-1	$U(5.9 \times 10^5, 7 \times 10^5)$	per mL
x_{E0}	Initial number of HIV-1 specific effector CD4 CTLs	$U(0, 2 \times 10^2)$	per mL
y_0	Initial number of CD4 T cells productively infected with HIV-1	$U(0, 2 \times 10^2)$	per mL
v_0	initial number of HIV-1 replication competent viral particles	$U(1, 2 \times 10^2)$	per mL
z_0	Initial number of CD8 T cells that are non HIV-1 specific	$U(1.3 \times 10^6, 1.4 \times 10^6)$	per mL
z_{E0}	Initial number of HIV-1 specific effector CD8 CTLs	$U(0, 2 \times 10^2)$	per mL

Table 7.8: Uniform prior distributions for Patient 18 initial conditions

Symbol	Parameter	Prior distribution	Unit
x_0	Initial number of CD4 T cells susceptible to HIV-1	$U(4.1 \times 10^5, 5.5 \times 10^5)$	per mL
x_{E0}	Initial number of HIV-1 specific effector CD4 CTLs	$U(0, 8.5 \times 10^2)$	per mL
y_0	Initial number of CD4 T cells productively infected with HIV-1	$U(0, 8.5 \times 10^2)$	per mL

v_0	initial number of HIV-1 replication competent viral particles	$U(1, 8.5 \times 10^2)$	per mL
z_0	Initial number of CD8 T cells that are non HIV-1 specific	$U(6.5 \times 10^5, 7.5 \times 10^5)$	per mL
z_{E0}	Initial number of HIV-1 specific effector CD8 CTLs	$U(0, 8.5 \times 10^2)$	per mL

Table 7.9: Uniform prior distributions for Patient 24 initial conditions

Symbol	Parameter	Prior distribution	Unit
x_0	Initial number of CD4 T cells susceptible to HIV-1	$U(5.5 \times 10^5, 1.2 \times 10^6)$	per mL
x_{E0}	Initial number of HIV-1 specific effector CD4 CTLs	$U(0, 4 \times 10^2)$	per mL
y_0	Initial number of CD4 T cells productively infected with HIV-1	$U(0, 4 \times 10^2)$	per mL
v_0	initial number of HIV-1 replication competent viral particles	$U(1, 4 \times 10^2)$	per mL
z_0	Initial number of CD8 T cells that are non HIV-1 specific	$U(5.6 \times 10^5, 1.1 \times 10^6)$	per mL
z_{E0}	Initial number of HIV-1 specific effector CD8 CTLs	$U(0, 4 \times 10^2)$	per mL

Table 7.10: Uniform prior distributions for Patient 25 initial conditions

Symbol	Parameter	Prior distribution	Unit
x_0	Initial number of CD4 T cells susceptible to HIV-1	$U(5 \times 10^5, 6.8 \times 10^6)$	per mL
x_{E0}	Initial number of HIV-1 specific effector CD4 CTLs	$U(0, 3.9 \times 10^1)$	per mL
y_0	Initial number of CD4 T cells productively infected with HIV-1	$U(0, 3.9 \times 10^1)$	per mL
v_0	initial number of HIV-1 replication competent viral particles	$U(1, 3.9 \times 10^1)$	per mL
z_0	Initial number of CD8 T cells that are non HIV-1 specific	$U(1 \times 10^5, 3 \times 10^5)$	per mL
z_{E0}	Initial number of HIV-1 specific effector CD8 CTLs	$U(0, 3.9 \times 10^1)$	per mL

Table 7.11: Uniform prior distributions for Patient 28 initial conditions

Symbol	Parameter	Prior distribution	Unit
x_0	Initial number of CD4 T cells susceptible to HIV-1	$U(6 \times 10^5, 8 \times 10^5)$	per mL
x_{E0}	Initial number of HIV-1 specific effector CD4 CTLs	$U(0, 5 \times 10^1)$	per mL

y_0	Initial number of CD4 T cells productively infected with HIV-1	$U(0, 5 \times 10^1)$	per mL
v_0	initial number of HIV-1 replication competent viral particles	$U(1, 5 \times 10^1)$	per mL
z_0	Initial number of CD8 T cells that are non HIV-1 specific	$U(7 \times 10^5, 1.1 \times 10^6)$	per mL
z_{E0}	Initial number of HIV-1 specific effector CD8 CTLs	$U(0, 5 \times 10^1)$	per mL

7.C.2 Prior distributions for HIV-1 patient comparison group initial conditions

Table 7.12: Uniform prior distributions for Patient 2 initial conditions

Symbol	Parameter	Prior distribution	Unit
x_0	Initial number of CD4 T cells susceptible to HIV-1	$U(4.5 \times 10^5, 8 \times 10^5)$	per mL
x_{E0}	Initial number of HIV-1 specific effector CD4 CTLs	$U(0, 1.5 \times 10^3)$	per mL
y_0	Initial number of CD4 T cells productively infected with HIV-1	$U(0, 1.5 \times 10^3)$	per mL

v_0	initial number of HIV-1 replication competent viral particles	$U(1 \times 10^2, 1.5 \times 10^3)$	per mL
z_0	Initial number of CD8 T cells that are non HIV-1 specific	$U(8 \times 10^5, 1.25 \times 10^6)$	per mL
z_{E0}	Initial number of HIV-1 specific effector CD8 CTLs	$U(0, 1.5 \times 10^3)$	per mL

Table 7.13: Uniform prior distributions for Patient 7 initial conditions

Symbol	Parameter	Prior distribution	Unit
x_0	Initial number of CD4 T cells susceptible to HIV-1	$U(6 \times 10^5, 1 \times 10^6)$	per mL
x_{E0}	Initial number of HIV-1 specific effector CD4 CTLs	$U(0, 3 \times 10^3)$	per mL
y_0	Initial number of CD4 T cells productively infected with HIV-1	$U(0, 3 \times 10^3)$	per mL
v_0	initial number of HIV-1 replication competent viral particles	$U(1 \times 10^3, 3 \times 10^3)$	per mL
z_0	Initial number of CD8 T cells that are non HIV-1 specific	$U(8 \times 10^5, 1.1 \times 10^6)$	per mL
z_{E0}	Initial number of HIV-1 specific effector CD8 CTLs	$U(0, 3 \times 10^3)$	per mL

Table 7.14: Uniform prior distributions for Patient 10 initial conditions

Symbol	Parameter	Prior distribution	Unit
x_0	Initial number of CD4 T cells susceptible to HIV-1	$U(5.5 \times 10^5, 1 \times 10^6)$	per mL
x_{E0}	Initial number of HIV-1 specific effector CD4 CTLs	$U(0, 2 \times 10^3)$	per mL
y_0	Initial number of CD4 T cells productively infected with HIV-1	$U(0, 2 \times 10^3)$	per mL
v_0	initial number of HIV-1 replication competent viral particles	$U(1 \times 10^2, 2 \times 10^3)$	per mL
z_0	Initial number of CD8 T cells that are non HIV-1 specific	$U(1.1 \times 10^6, 1.4 \times 10^6)$	per mL
z_{E0}	Initial number of HIV-1 specific effector CD8 CTLs	$U(0, 2 \times 10^3)$	per mL

Table 7.15: Uniform prior distributions for Patient 11 initial conditions

Symbol	Parameter	Prior distribution	Unit
x_0	Initial number of CD4 T cells susceptible to HIV-1	$U(4.5 \times 10^5, 8 \times 10^5)$	per mL
x_{E0}	Initial number of HIV-1 specific effector CD4 CTLs	$U(0, 4.5 \times 10^3)$	per mL

y_0	Initial number of CD4 T cells productively infected with HIV-1	$U(0, 4.5 \times 10^3)$	per mL
v_0	initial number of HIV-1 replication competent viral particles	$U(3 \times 10^3, 4.5 \times 10^3)$	per mL
z_0	Initial number of CD8 T cells that are non HIV-1 specific	$U(4.5 \times 10^5, 8 \times 10^5)$	per mL
z_{E0}	Initial number of HIV-1 specific effector CD8 CTLs	$U(0, 4.5 \times 10^3)$	per mL

Table 7.16: Uniform prior distributions for Patient 12 initial conditions

Symbol	Parameter	Prior distribution	Unit
x_0	Initial number of CD4 T cells susceptible to HIV-1	$U(4 \times 10^5, 9 \times 10^5)$	per mL
x_{E0}	Initial number of HIV-1 specific effector CD4 CTLs	$U(0, 1 \times 10^4)$	per mL
y_0	Initial number of CD4 T cells productively infected with HIV-1	$U(0, 1 \times 10^4)$	per mL
v_0	initial number of HIV-1 replication competent viral particles	$U(1 \times 10^3, 1 \times 10^4)$	per mL
z_0	Initial number of CD8 T cells that are non HIV-1 specific	$U(4 \times 10^5, 2 \times 10^6)$	per mL

z_{E0}	Initial number of HIV-1 specific effector CD8 CTLs	$U(0, 4.5 \times 10^3)$	per mL

Table 7.17: Uniform prior distributions for Patient 21 initial conditions

Symbol	Parameter	Prior distribution	Unit
x_0	Initial number of CD4 T cells susceptible to HIV-1	$U(4 \times 10^5, 7.5 \times 10^5)$	per mL
x_{E0}	Initial number of HIV-1 specific effector CD4 CTLs	$U(0, 1 \times 10^4)$	per mL
y_0	Initial number of CD4 T cells productively infected with HIV-1	$U(0, 1 \times 10^4)$	per mL
v_0	initial number of HIV-1 replication competent viral particles	$U(1, 1 \times 10^4)$	per mL
z_0	Initial number of CD8 T cells that are non HIV-1 specific	$U(7 \times 10^5, 1.1 \times 10^6)$	per mL
z_{E0}	Initial number of HIV-1 specific effector CD8 CTLs	$U(0, 1 \times 10^4)$	per mL

Table 7.18: Uniform prior distributions for Patient 23 initial conditions

Symbol	Parameter	Prior distribution	Unit

x_0	Initial number of CD4 T cells susceptible to HIV-1	$U(5.9 \times 10^5, 9.9 \times 10^5)$	per mL
x_{E0}	Initial number of HIV-1 specific effector CD4 CTLs	$U(0, 1.5 \times 10^3)$	per mL
y_0	Initial number of CD4 T cells productively infected with HIV-1	$U(0, 1.5 \times 10^3)$	per mL
v_0	initial number of HIV-1 replication competent viral particles	$U(1 \times 10^2, 1.5 \times 10^3)$	per mL
z_0	Initial number of CD8 T cells that are non HIV-1 specific	$U(7 \times 10^5, 1.6 \times 10^6)$	per mL
z_{E0}	Initial number of HIV-1 specific effector CD8 CTLs	$U(0, 1.5 \times 10^3)$	per mL

7.D Model fitting and prediction using Bayesian inference

For each HIV-1 patient, the parameters in system (6.1) were fit simultaneously to that patient's viral load, CD4 absolute, and CD8 absolute data. The estimated parameter values for system (6.1) for each patient are located in Sections 7.D.4 and 7.D.5 with the point estimate in the tables being the maximum posterior. The fit of system (6.1) to the data for each patient are visualized in Sections 7.D.6 and 7.D.7. The method of Bayesian inference was used for

fitting system (6.1) simultaneously to three datasets for each patient and this method is described below.

Let $D_j = \{d_1^j, \ldots, d_{n_j}^j\}$ and $T_j = \{t_1^j, \ldots, t_{n_j}^j\}$ denote the patient data and times, where index $j = 1$ indicates the patient's viral load data, index $j = 2$ indicates the patient's CD4 absolute data, and index $j = 3$ indicates the patient's CD8 absolute data. Let $D = \{D_1, D_2, D_3\}$ and $T = \{T_1, T_2, T_3\}$.

System (6.1) was solved numerically by using the MATLAB function *ode15s* with the option setting *odeset('Vectorized', 'on')* to speed up the numerical solver and an additional ODE solving event that would stop the *ode15s* numerical solver if it was taking longer than 10 seconds to solve system (6.1) [115]. Parameter vector guesses that caused the *ode15s* numerical solver to take longer than 10 seconds to solve system (6.1) were considered to be poor parameter vector guesses and assigned a log likelihood value of -Inf in MATLAB.

The parameter vector to be estimated in system (6.1) is

$$\boldsymbol{\nu} = \langle \log_{10}(r_1), \mu_1, \log_{10}(c), \log_{10}(b), \log_{10}(\beta), \delta, \log_{10}(ka), \log_{10}(a), \mu_2, \mu_3, \log_{10}(\gamma), \log_{10}(p), \mu_4, \log_{10}(r_2), \mu_5, x_0, x_{E0}, y_0, v_0, z_0, z_{E0} \rangle.$$

Let the model solution vector over time for HIV-1 replication competent viral particles per ml, CD4 T cells susceptible to HIV-1 per ml, and CD8 T cells that are non HIV-1 specific per ml, be given by $v(\boldsymbol{\nu}, t)$, $x(\boldsymbol{\nu}, t)$, and $z(\boldsymbol{\nu}, t)$ respectively. The dataset D_1 will be described by the model solution vector over time $v(\boldsymbol{\nu}, t)$, the dataset D_2 will be described by the model solution vector over time $x(\boldsymbol{\nu}, t)$, and dataset D_3 will be described by the model solution vector over time $z(\boldsymbol{\nu}, t)$.

Since the HIV-1 patient data as visualized in Sections 7.D.6 and 7.D.7 display a variety of patterns and scatter around the trends, a Gaussian distribution with non-constant variance over time is chosen to describe each of the datasets D_1, D_2, and D_3 for every patient. As this HIV-1 patient data can still be considered count data, which is most likely overdispersed (variance of the data is larger than the mean of the data), the non-constant variance over time in the Gaussian distribution is described by a constant multiplied by the mean, $\frac{1}{\tau_i^j} = v^j \mu_i^j$.

Hence, for each HIV-1 patient, with $j = 1, 2, 3$ datasets, the probability of observing d_i^j is given by the Gaussian distribution with non-constant variance over time, $\frac{1}{\tau_i^j} = v^j \mu_i^j$:

$$f(d_i^j) = \sqrt{\frac{\tau_i^j}{2\pi}} \exp(-\frac{1}{2}\tau_i^j (d_i^j - \mu_i^j)^2) = \sqrt{\frac{1}{2\pi v^j \mu_i^j}} \exp(-\frac{1}{2v^j \mu_i^j}(d_i^j - \mu_i^j)^2) \quad (7.3)$$

with the mean $\mu_i^j > 0$, the variance $\frac{1}{\tau_i^j} = v^j \mu_i^j > 0$, and $v^j \geq 1$ is a constant. In this distribution, both the mean μ_i^j and the variance $\frac{1}{\tau_i^j} = v^j \mu_i^j$ change depending on the time t_i^j. The constant $v^j \geq 1$ is specific to the j^{th} data set D_j and determines the most likely shape of the Gaussian distribution with non-constant variance over time given the data D_j. Here $\mu_i^1 = v(\boldsymbol{\nu}, t_i^1)$, $\mu_i^2 = x(\boldsymbol{\nu}, t_i^2)$, and $\mu_i^3 = z(\boldsymbol{\nu}, t_i^3)$.

For each dataset D_j, the following loguniform prior distribution was chosen for v^j:

$$\log_{10}(v^j) \sim U(\log_{10}(1), \log_{10}(\zeta)),$$

where $\zeta = \frac{\frac{1}{n_j}\sum_{i=1}^{n_j}(d_i^j - \bar{D}_j)^2}{\bar{D}_j}$, and $\bar{D}_j$ is the mean of the dataset D_j. The numerator here is the estimated variance that would result from using the mean $\bar{D}_j$ as the model to describe the dataset D_j. The denominator is the mean $\bar{D}_j$. The value of ζ represents the largest anticipated amount of overdispersion needed to describe the dataset D_j.

Let $\boldsymbol{\phi} = \langle \log_{10}(v^1), \log_{10}(v^2), \log_{10}(v^3) \rangle$. Given the extra parameters in vector $\boldsymbol{\phi}$, we want to estimate the vector $\boldsymbol{\theta} = \langle \boldsymbol{\nu}, \boldsymbol{\phi} \rangle$.

The probability model for data sets $D = \{D_1, D_2, D_3\}$ is

$$P(D|\boldsymbol{\theta}) = \prod_{j=1,2,3} \prod_{i=1}^{n_j} f(d_i^j). \tag{7.4}$$

The likelihood function for $\boldsymbol{\theta}$ is given by

$$L(\boldsymbol{\theta}) = CP(D|\boldsymbol{\theta}), \tag{7.5}$$

where C is any positive constant not depending on $\boldsymbol{\theta}$ used to simplify the likelihood function. For more information about Bayesian inference for dynamical systems and combining probability models, please see Chapter 2.

If any of the ode compartment solutions from the numerical solver contained negative values, the parameter vector guesses that caused the ode compartment solution(s) to contain negative values were penalized in the likelihood function in the following way: for each ode compartment solution that went below zero, the log likelihood was subtracted by $\frac{-1\times 10^6}{6}$.

When the viral load data that was used for the fitting was below detection, parameter vector guesses that caused the v model solution to be above the limit of detection of the viral load data were penalized in the likelihood function

in the following way: at each time point that the v model solution was above the limit of detection of the viral load data, the log likelihood was subtracted by $\frac{-1\times10^6}{n_1}$. Also, to ensure a realistic fit of the viral load data, if a parameter vector guess caused the v model solution to go above two times the maximum of the viral load data, the log likelihood was subtracted by -1×10^6.

In humans, the lifespan of memory CD4 T cells, 0.449 (range, 0.194 - 1.37) years, is generally longer than for the lifespan of memory CD8 T cells, 0.430 (range, 0.310 - 0.633) years [122]. Also, activated effector T cells are short-lived cells in comparison to memory T cells [131]. Productively HIV-1 infected CD4 T cells and viral particles die rapidly in comparison to non HIV-1 infected CD4 T cells [56]. It is assumed based off of the literature that $\mu_1 < \mu_5 < \mu_2$ and that $\mu_1 < \mu_3 < \mu_4$. If a parameter vector guess caused these death rate inequalities to not be true, then the log likelihood was subtracted by -1×10^6.

The prior distribution for $\boldsymbol{\theta}$ is equal to the product of the uniform distributions specified for the parameters in $\boldsymbol{\theta}$.

The fitting for each patient was completed using the Diffusive Nested Sampling (DNS) program "MatlabDiffNestAlg" discussed in Section 3.C [9].

The MATLAB implementation of the DNS algorithm, "MatlabDiffNestAlg", was used with the following settings: five particles; the number of samples needed above the current likelihood cut off to create another level was 1000 with at least 1500 samples per level overall; the diffusivity term $\lambda = 90$; the number of samples used during the second phase of the sampler was 1×10^5; the tolerance used to stop level creation was generally set to 1×10^{-2} (patients 1, 2, 7, 10, 11, 12 only needed a tolerance of 10^{-1}, and patient 24 needed a lower tolerance of 10^{-3}); $C = 100$, which is the number providing the amount of confidence in the theoretical expectation $X_{j+1} = \exp(-1)X_j$; every iteration

sample was saved; $\beta = 100$, which is the parameter that controls the strength of the effect to correct the mass X values in the second phase of the DNS algorithm; and the proposal distribution that utilized the standard Cauchy distribution discussed in Section 3.B.2 was used for the parameter proposals.

Figure 3.4 displays the posterior weights over the $\log(X)$ values. There is a clear peak of the posterior weights and the samples to the left of the peak have small posterior weights in comparison to the peak weight values, and this indicates that the algorithm converged to the posterior distribution.

For parameters that used an assumed loguniform prior distribution, the resulting samples from the DNS algorithm for these parameters can be exponentiated by 10 to transform these parameter samples back to their original scale.

The Bayesian p-value, p_B, for each patient are located in Table 7.19. The Bayesian p-values indicate that there is no evidence against the null hypothesis that the model predictions fit the data at the α level of 0.05.

Table 7.19: Bayesian p-value, p_B, for each mathematical model fit to the NAP HIV-1 patient data

Patient number	p_B
1	0.4115
6	0.3248
14	0.2864
16	0.2534
17	0.2645
18	0.3698
24	0.0900

25	0.3436
28	0.4685
2	0.2785
7	0.2327
10	0.2124
11	0.3242
12	0.4190
21	0.2605
23	0.3718

The 95% prediction intervals for each HIV-1 patient, with $j = 1, 2, 3$ datasets, are determined by the posterior predictive distribution as described in Section 2.K.

7.D.1 HIV-1 Elite Controller patients DNS convergence plots

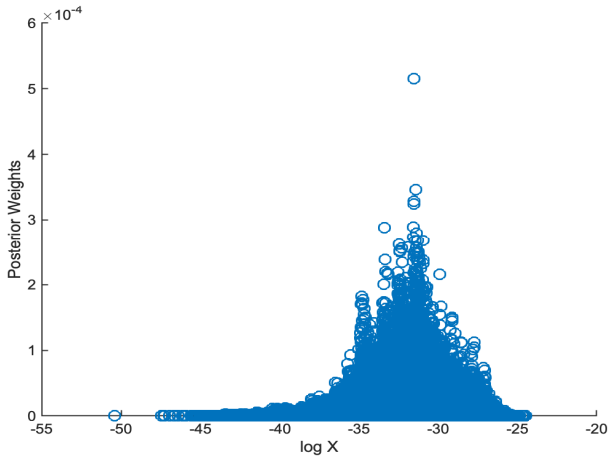

Figure 7.1: Posterior weights over the $\log(X)$ values for Patient 1 fitting

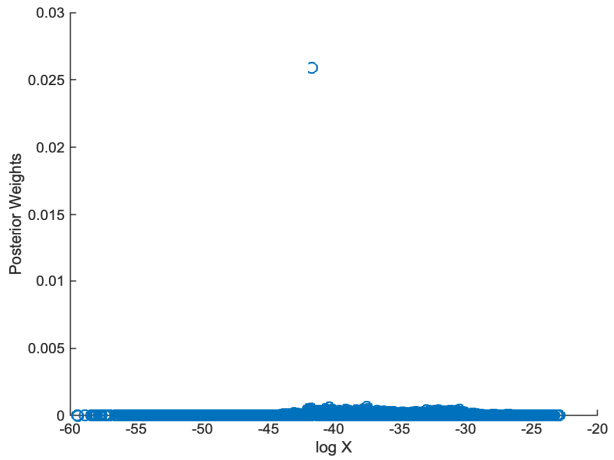

Figure 7.2: Posterior weights over the $\log(X)$ values for Patient 6 fitting

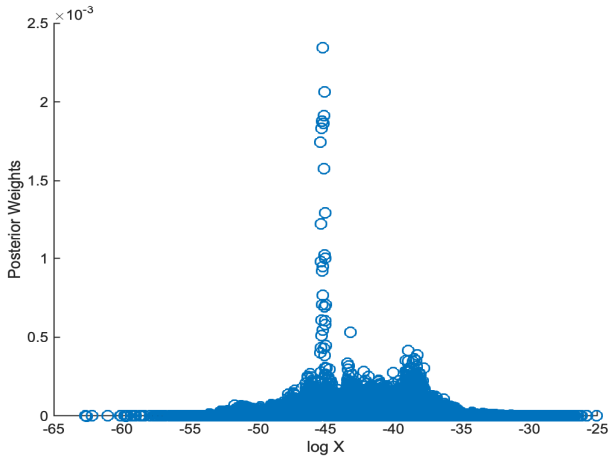

Figure 7.3: Posterior weights over the $\log(X)$ values for Patient 14 fitting

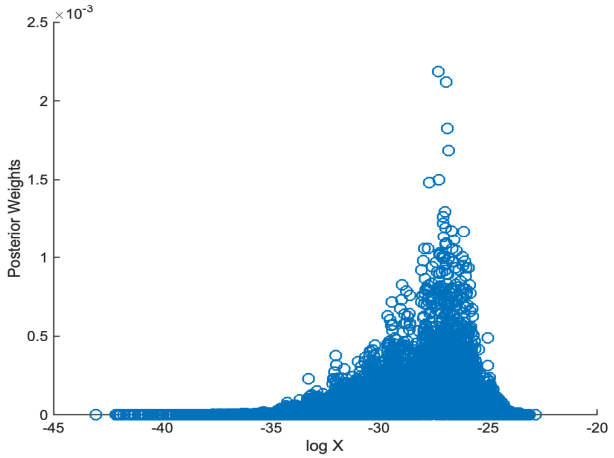

Figure 7.4: Posterior weights over the $\log(X)$ values for Patient 16 fitting

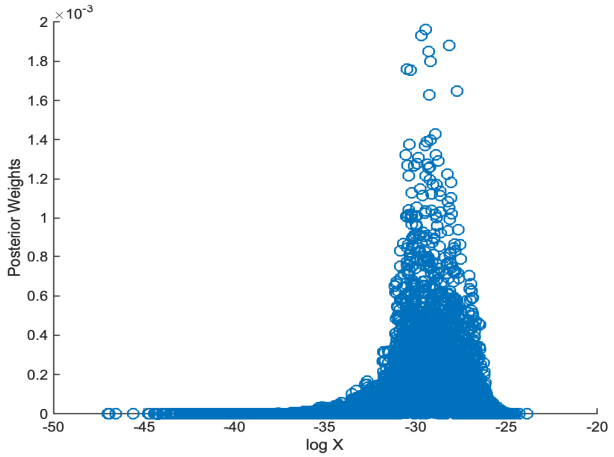

Figure 7.5: Posterior weights over the $\log(X)$ values for Patient 17 fitting

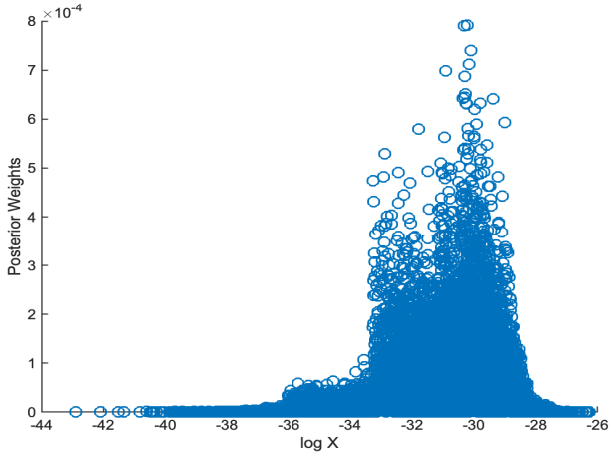

Figure 7.6: Posterior weights over the $\log(X)$ values for Patient 18 fitting

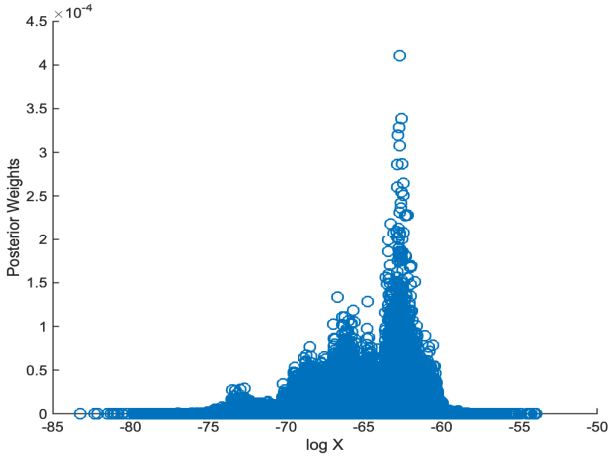

Figure 7.7: Posterior weights over the $\log(X)$ values for Patient 24 fitting

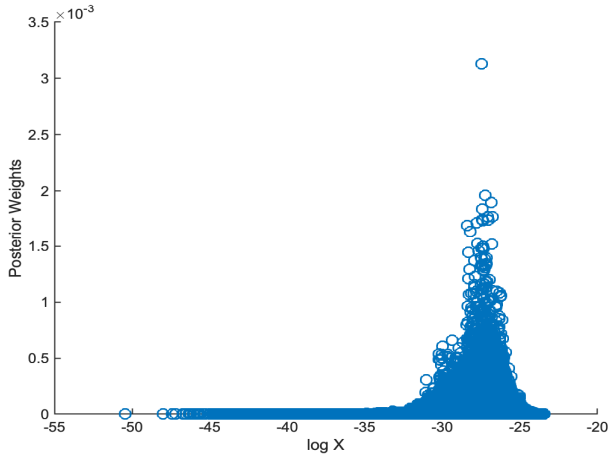

Figure 7.8: Posterior weights over the $\log(X)$ values for Patient 25 fitting

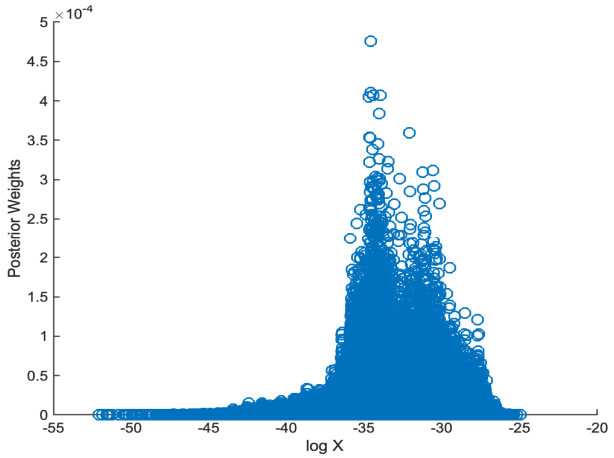

Figure 7.9: Posterior weights over the $\log(X)$ values for Patient 28 fitting

7.D.2 HIV-1 patient comparison group DNS convergence plots

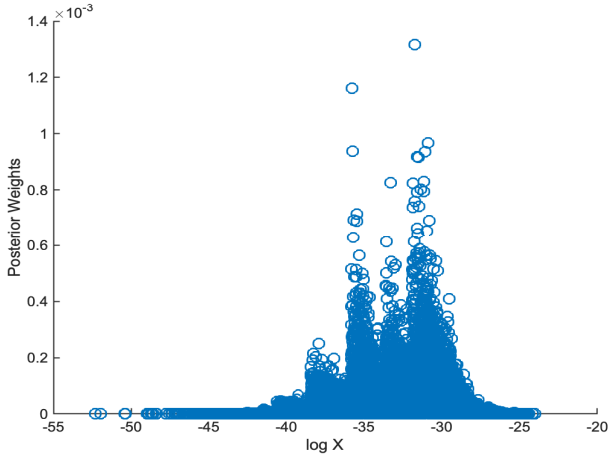

Figure 7.10: Posterior weights over the $\log(X)$ values for Patient 2 fitting

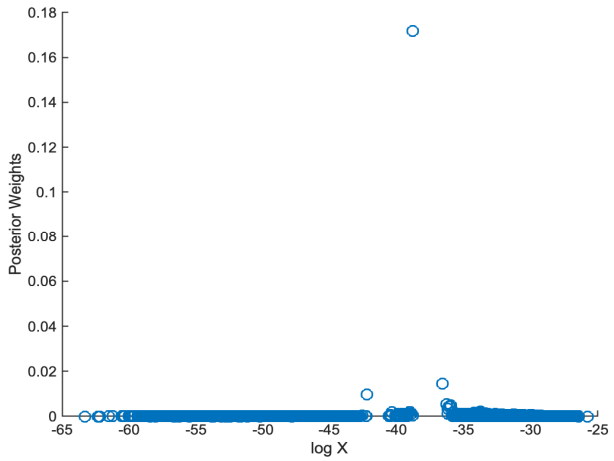

Figure 7.11: Posterior weights over the $\log(X)$ values for Patient 7 fitting

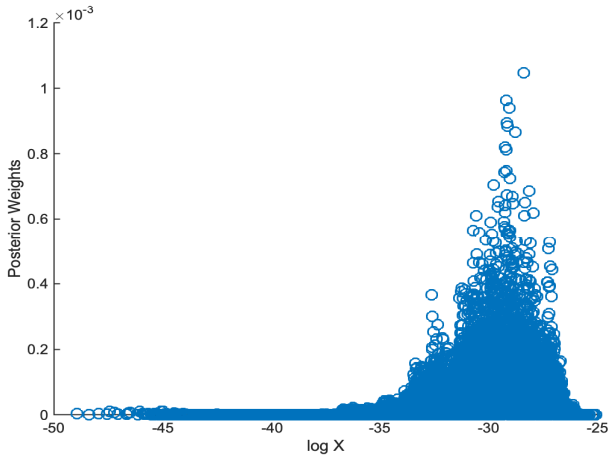

Figure 7.12: Posterior weights over the $\log(X)$ values for Patient 10 fitting

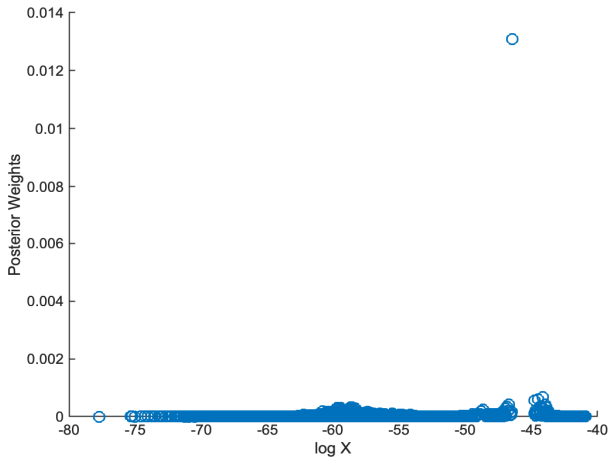

Figure 7.13: Posterior weights over the $\log(X)$ values for Patient 11 fitting

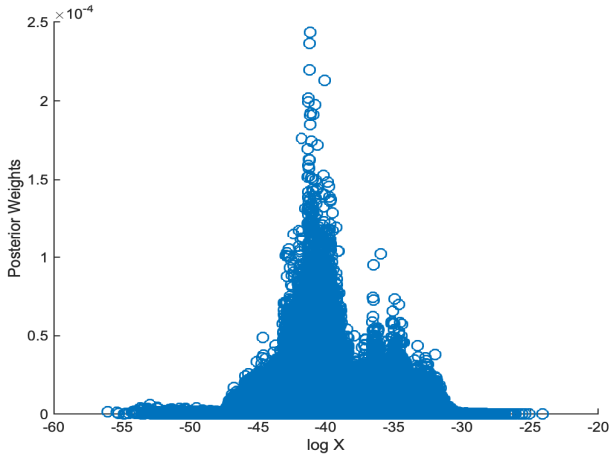

Figure 7.14: Posterior weights over the $\log(X)$ values for Patient 12 fitting

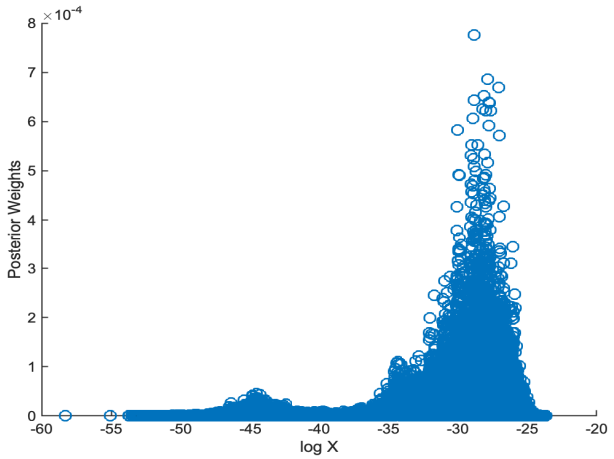

Figure 7.15: Posterior weights over the $\log(X)$ values for Patient 21 fitting

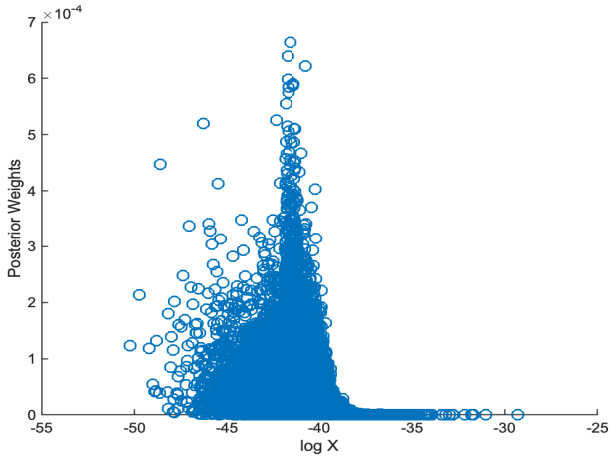

Figure 7.16: Posterior weights over the $\log(X)$ values for Patient 23 fitting

7.D.3 Pooled estimates

The pooled estimate of the parameter values for system (6.1) for the HIV-1 Elite Controller group and HIV-1 comparison group was found by taking 1×10^4 random samples from each patient's posterior distribution. The posterior random samples were combined for all of the HIV-1 Elite Controller patients and the posterior random samples were combined for all of the HIV-1 comparison group patients. The median of the combined posterior distribution for each of the groups was used as the point estimate and the 95% credible intervals for each of the combined posterior distributions was also determined.

The probability that an Elite Controller group parameter is greater than a comparison group parameter, $P\left(\theta_i^{\mathrm{EC}} > \theta_i^{\mathrm{C}}\right)$, was found by taking 1×10^3 random samples from each parameter's combined marginal posterior distribution. The probability was estimated by finding the proportion of times that θ_i^{EC} exceeded θ_i^{C} in each of the group's combined marginal posterior distributions.

7.D.4 HIV-1 Elite Controller patients fitted parameters

Table 7.20: Fitted parameter estimates in $\boldsymbol{\theta}$ with the maximum posterior as the point estimate and 95% credible intervals for Patient 1

Symbol	Parameter	Estimate (95% credible interval)	Unit
r_1	Growth rate of new CD4 T cells	1.07×10^2 $(1.07 \times 10^2, 1.43 \times 10^2)$	per year
μ_1	Death rate of total CD4 T cells	4.63×10^1 $(3.67, 4.90 \times 10^1)$	per year

c	Kill rate of CD4 T cells by effector CD8 CTLs due to other infections	1.32×10^{-4} $(1.23 \times 10^{-4}, 3.11 \times 10^{-4})$	mL per year
b	Kill rate of CD4 T cells by effector CD4 CTLs due to other infections	1.13×10^{-9} $(1.13 \times 10^{-15}, 6.23 \times 10^{-6})$	mL per year
β	Transmission rate of HIV-1 to CD4 T cells	9.76×10^{-3} $(3.19 \times 10^{-5}, 9.81 \times 10^{-3})$	mL per year
δ	Portion of generated HIV-1 specific effector CTLs that are HIV-1 specific effector CD4 CTLs	2.04×10^{-1} $(7.55 \times 10^{-4}, 4.77 \times 10^{-1})$	-
ka	Maximum proliferation rate of the HIV-1 specific effector CTL response	9.41×10^{2} $(1.66, 7.86 \times 10^{2})$	per year
a	Number of HIV-1 specific effector CTLs at which the proliferation switches to a maximum rate	4.71×10^{1} $(1.03 \times 10^{-4}, 8.82 \times 10^{1})$	per mL
μ_2	Death rate of effector CTLs	8.48×10^{1} $(2.51 \times 10^{1}, 9.95 \times 10^{1})$	per year
μ_3	Death rate of productively infected CD4 T cells	1.60×10^{2} $(2.78 \times 10^{1}, 3.13 \times 10^{2})$	per year
γ	Rate infected CD4 T cells are killed by effector CTLs	9.60 $(5.59 \times 10^{-2}, 6.40 \times 10^{1})$	mL per year

p	Rate replication competent viral particles were produced by HIV-1 infected CD4 T cells	6.75×10^3 $(1.02 \times 10^3, 8.13 \times 10^3)$	per year
μ_4	Death rate of HIV-1 replication competent viral particles	9.04×10^3 $(1.85 \times 10^3, 9.91 \times 10^3)$	per year
r_2	Growth rate of new CD8 T cells	1.07×10^{-4} $(2.96 \times 10^{-5}, 1.11 \times 10^{-4})$	mL per year
μ_5	Death rate of total CD8 T cells	6.71×10^1 $(1.93 \times 10^1, 6.81 \times 10^1)$	per year
x_0	Initial number of CD4 T cells susceptible to HIV-1	6.61×10^5 $(6.25 \times 10^5, 7.43 \times 10^5)$	per mL
x_{E0}	Initial number of HIV-1 specific effector CD4 CTLs	4.29×10^1 $(3.77 \times 10^1, 9.76 \times 10^2)$	per mL
y_0	Initial number of CD4 T cells productively infected with HIV-1	3.93×10^1 $(8.28 \times 10^{-1}, 9.58 \times 10^1)$	per mL
v_0	initial number of HIV-1 replication competent viral particles	5.39×10^1 $(4.05 \times 10^1, 9.01 \times 10^1)$	per mL
z_0	Initial number of CD8 T cells that are non HIV-1 specific	5.06×10^5 $(4.03 \times 10^5, 5.54 \times 10^5)$	per mL
z_{E0}	Initial number of HIV-1 specific effector CD8 CTLs	3.47×10^2 $(3.39, 9.32 \times 10^2)$	per mL

v^1	parameter determining most likely shape of Gaussian distribution with non-constant variance given viral load data	$1.81\ (1.00, 1.15 \times 10^3)$	per mL
v^2	parameter determining most likely shape of Gaussian distribution with non-constant variance given total CD4 T cell data	5.25×10^2 $(4.81 \times 10^2, 4.88 \times 10^3)$	per mL
v^3	parameter determining most likely shape of Gaussian distribution with non-constant variance given total CD8 T cell data	8.25×10^3 $(3.16 \times 10^3, 8.58 \times 10^3)$	per mL

Table 7.21: Fitted parameter estimates in $\boldsymbol{\theta}$ with the maximum posterior as the point estimate and 95% credible intervals for Patient 6

Symbol	Parameter	Estimate (95% credible interval)	Unit
r_1	Growth rate of new CD4 T cells	2.04×10^2 $(1.34 \times 10^2, 4.59 \times 10^2)$	per year
μ_1	Death rate of total CD4 T cells	$4.63 \times 10^1\ (3.68, 4.71 \times 10^1)$	per year
c	Kill rate of CD4 T cells by effector CD8 CTLs due to other infections	1.79×10^{-4} $(1.70 \times 10^{-4}, 5.63 \times 10^{-4})$	mL per year

b	Kill rate of CD4 T cells by effector CD4 CTLs due to other infections	4.28×10^{-7} $(1.30 \times 10^{-15}, 1.01 \times 10^{-5})$	mL per year
β	Transmission rate of HIV-1 to CD4 T cells	1.23×10^{-2} $(9.90 \times 10^{-5}, 1.23 \times 10^{-2})$	mL per year
δ	Portion of generated HIV-1 specific effector CTLs that are HIV-1 specific effector CD4 CTLs	2.20×10^{-1} $(1.46 \times 10^{-2}, 4.75 \times 10^{-1})$	-
ka	Maximum proliferation rate of the HIV-1 specific effector CTL response	1.51×10^{2} $(9.13, 1.51 \times 10^{2})$	per year
a	Number of HIV-1 specific effector CTLs at which the proliferation switches to a maximum rate	8.40×10^{3} $(3.71 \times 10^{-4}, 8.40 \times 10^{3})$	per mL
μ_2	Death rate of effector CTLs	6.21×10^{1} $(5.86 \times 10^{1}, 9.47 \times 10^{1})$	per year
μ_3	Death rate of productively infected CD4 T cells	9.15×10^{1} $(4.70 \times 10^{1}, 2.61 \times 10^{2})$	per year
γ	Rate infected CD4 T cells are killed by effector CTLs	3.61 $(2.19 \times 10^{-2}, 1.47 \times 10^{1})$	mL per year
p	Rate replication competent viral particles were produced by HIV-1 infected CD4 T cells	1.38×10^{3} $(1.35 \times 10^{3}, 7.38 \times 10^{3})$	per year

μ_4	Death rate of HIV-1 replication competent viral particles	9.68×10^3 $(1.37 \times 10^3, 9.68 \times 10^3)$	per year
r_2	Growth rate of new CD8 T cells	6.68×10^{-5} $(6.67 \times 10^{-5}, 9.83 \times 10^{-5})$	mL per year
μ_5	Death rate of total CD8 T cells	5.04×10^1 $(4.96 \times 10^1, 7.13 \times 10^1)$	per year
x_0	Initial number of CD4 T cells susceptible to HIV-1	6.58×10^5 $(5.30 \times 10^5, 7.28 \times 10^5)$	per mL
x_{E0}	Initial number of HIV-1 specific effector CD4 CTLs	4.87×10^2 $(1.15 \times 10^2, 1.00 \times 10^3)$	per mL
y_0	Initial number of CD4 T cells productively infected with HIV-1	1.68×10^2 $(5.63 \times 10^1, 9.32 \times 10^2)$	per mL
v_0	initial number of HIV-1 replication competent viral particles	4.91×10^2 $(1.02 \times 10^2, 8.34 \times 10^2)$	per mL
z_0	Initial number of CD8 T cells that are non HIV-1 specific	7.49×10^5 $(5.61 \times 10^5, 7.95 \times 10^5)$	per mL
z_{E0}	Initial number of HIV-1 specific effector CD8 CTLs	1.22×10^2 $(5.83 \times 10^1, 9.80 \times 10^2)$	per mL
v^1	parameter determining most likely shape of Gaussian distribution with non-constant variance given viral load data	1.57×10^2 $(2.08 \times 10^2, 9.39 \times 10^2)$	per mL

v^2	parameter determining most likely shape of Gaussian distribution with non-constant variance given total CD4 T cell data	1.54×10^4 $(1.15 \times 10^4, 2.18 \times 10^4)$	per mL
v^3	parameter determining most likely shape of Gaussian distribution with non-constant variance given total CD8 T cell data	3.94×10^4 $(2.04 \times 10^4, 3.93 \times 10^4)$	per mL

Table 7.22: Fitted parameter estimates in $\boldsymbol{\theta}$ with the maximum posterior as the point estimate and 95% credible intervals for Patient 14

Symbol	Parameter	Estimate (95% credible interval)	Unit
r_1	Growth rate of new CD4 T cells	1.03×10^2 $(1.03 \times 10^2, 7.95 \times 10^2)$	per year
μ_1	Death rate of total CD4 T cells	4.90×10^1 $(4.22, 4.90 \times 10^1)$	per year
c	Kill rate of CD4 T cells by effector CD8 CTLs due to other infections	5.39×10^{-5} $(5.32 \times 10^{-5}, 8.62 \times 10^{-4})$	mL per year
b	Kill rate of CD4 T cells by effector CD4 CTLs due to other infections	5.08×10^{-6} $(5.08 \times 10^{-6}, 1.75 \times 10^{-5})$	mL per year

β	Transmission rate of HIV-1 to CD4 T cells	1.18×10^{-3} $(2.00 \times 10^{-4}, 1.17 \times 10^{-3})$	mL per year
δ	Portion of generated HIV-1 specific effector CTLs that are HIV-1 specific effector CD4 CTLs	4.60×10^{-1} $(3.35 \times 10^{-2}, 4.92 \times 10^{-1})$	-
ka	Maximum proliferation rate of the HIV-1 specific effector CTL response	1.41×10^{2} $(1.07 \times 10^{2}, 3.29 \times 10^{2})$	per year
a	Number of HIV-1 specific effector CTLs at which the proliferation switches to a maximum rate	2.13×10^{3} $(2.75 \times 10^{2}, 2.37 \times 10^{3})$	per mL
μ_2	Death rate of effector CTLs	9.00×10^{1} $(8.47 \times 10^{1}, 9.25 \times 10^{1})$	per year
μ_3	Death rate of productively infected CD4 T cells	2.16×10^{2} $(1.90 \times 10^{2}, 2.29 \times 10^{2})$	per year
γ	Rate infected CD4 T cells are killed by effector CTLs	1.09 $(5.86 \times 10^{-1}, 3.54)$	mL per year
p	Rate replication competent viral particles were produced by HIV-1 infected CD4 T cells	3.51×10^{3} $(1.83 \times 10^{3}, 3.51 \times 10^{3})$	per year
μ_4	Death rate of HIV-1 replication competent viral particles	9.27×10^{3} $(1.16 \times 10^{3}, 9.28 \times 10^{3})$	per year
r_2	Growth rate of new CD8 T cells	7.30×10^{-5} $(4.18 \times 10^{-5}, 7.81 \times 10^{-5})$	mL per year

μ_5	Death rate of total CD8 T cells	7.43×10^1 $(3.94 \times 10^1, 7.42 \times 10^1)$	per year
x_0	Initial number of CD4 T cells susceptible to HIV-1	1.18×10^6 $(7.64 \times 10^5, 1.18 \times 10^6)$	per mL
x_{E0}	Initial number of HIV-1 specific effector CD4 CTLs	3.51×10^2 $(6.75 \times 10^1, 3.72 \times 10^2)$	per mL
y_0	Initial number of CD4 T cells productively infected with HIV-1	1.71×10^2 $(1.76 \times 10^1, 2.98 \times 10^2)$	per mL
v_0	initial number of HIV-1 replication competent viral particles	1.31×10^2 $(7.73, 3.80 \times 10^2)$	per mL
z_0	Initial number of CD8 T cells that are non HIV-1 specific	7.09×10^5 $(6.69 \times 10^5, 1.08 \times 10^6)$	per mL
z_{E0}	Initial number of HIV-1 specific effector CD8 CTLs	3.23×10^1 $(1.10 \times 10^1, 2.93 \times 10^2)$	per mL
v^1	parameter determining most likely shape of Gaussian distribution with non-constant variance given viral load data	4.56×10^1 $(3.87 \times 10^1, 6.58 \times 10^2)$	per mL
v^2	parameter determining most likely shape of Gaussian distribution with non-constant variance given total CD4 T cell data	3.56×10^4 $(2.22 \times 10^4, 3.78 \times 10^4)$	per mL

v^3	parameter determining most likely shape of Gaussian distribution with non-constant variance given total CD8 T cell data	2.67×10^4 $(1.74 \times 10^4, 2.65 \times 10^4)$	per mL

Table 7.23: Fitted parameter estimates in $\boldsymbol{\theta}$ with the maximum posterior as the point estimate and 95% credible intervals for Patient 16

Symbol	Parameter	Estimate (95% credible interval)	Unit
r_1	Growth rate of new CD4 T cells	1.13×10^2 $(9.18 \times 10^1, 1.30 \times 10^2)$	per year
μ_1	Death rate of total CD4 T cells	3.52×10^1 $(8.61, 3.54 \times 10^1)$	per year
c	Kill rate of CD4 T cells by effector CD8 CTLs due to other infections	2.58×10^{-4} $(2.26 \times 10^{-4}, 4.03 \times 10^{-4})$	mL per year
b	Kill rate of CD4 T cells by effector CD4 CTLs due to other infections	9.32×10^{-8} $(1.49 \times 10^{-15}, 1.85 \times 10^{-5})$	mL per year
β	Transmission rate of HIV-1 to CD4 T cells	8.04×10^{-5} $(2.74 \times 10^{-5}, 3.07 \times 10^{-3})$	mL per year
δ	Portion of generated HIV-1 specific effector CTLs that are HIV-1 specific effector CD4 CTLs	3.78×10^{-1} $(2.46 \times 10^{-2}, 4.84 \times 10^{-1})$	-

ka	Maximum proliferation rate of the HIV-1 specific effector CTL response	6.79×10^2 $(1.24 \times 10^2, 8.84 \times 10^2)$	per year
a	Number of HIV-1 specific effector CTLs at which the proliferation switches to a maximum rate	1.59×10^{-4} $(1.07 \times 10^{-4}, 2.62 \times 10^1)$	per mL
μ_2	Death rate of effector CTLs	8.74×10^1 $(8.08 \times 10^1, 9.98 \times 10^1)$	per year
μ_3	Death rate of productively infected CD4 T cells	4.40×10^1 $(2.04 \times 10^1, 2.98 \times 10^2)$	per year
γ	Rate infected CD4 T cells are killed by effector CTLs	8.72×10^1 $(1.61 \times 10^{-1}, 4.09 \times 10^1)$	mL per year
p	Rate replication competent viral particles were produced by HIV-1 infected CD4 T cells	3.23×10^4 $(1.33 \times 10^3, 5.50 \times 10^4)$	per year
μ_4	Death rate of HIV-1 replication competent viral particles	9.52×10^3 $(5.28 \times 10^3, 9.98 \times 10^3)$	per year
r_2	Growth rate of new CD8 T cells	1.74×10^{-4} $(1.58 \times 10^{-4}, 1.95 \times 10^{-4})$	mL per year
μ_5	Death rate of total CD8 T cells	8.23×10^1 $(7.80 \times 10^1, 8.89 \times 10^1)$	per year
x_0	Initial number of CD4 T cells susceptible to HIV-1	4.05×10^5 $(3.55 \times 10^5, 5.72 \times 10^5)$	per mL
x_{E0}	Initial number of HIV-1 specific effector CD4 CTLs	7.18×10^1 $(2.62 \times 10^1, 4.84 \times 10^2)$	per mL

y_0	Initial number of CD4 T cells productively infected with HIV-1	2.03×10^2 $(1.78 \times 10^1, 4.84 \times 10^2)$	per mL
v_0	initial number of HIV-1 replication competent viral particles	1.48×10^2 $(2.42 \times 10^1, 3.75 \times 10^2)$	per mL
z_0	Initial number of CD8 T cells that are non HIV-1 specific	3.04×10^5 $(2.40 \times 10^5, 4.27 \times 10^5)$	per mL
z_{E0}	Initial number of HIV-1 specific effector CD8 CTLs	3.19×10^2 $(1.49 \times 10^1, 4.81 \times 10^2)$	per mL
v^1	parameter determining most likely shape of Gaussian distribution with non-constant variance given viral load data	6.33 $(1.01, 1.21 \times 10^2)$	per mL
v^2	parameter determining most likely shape of Gaussian distribution with non-constant variance given total CD4 T cell data	7.01×10^4 $(4.35 \times 10^4, 7.36 \times 10^4)$	per mL
v^3	parameter determining most likely shape of Gaussian distribution with non-constant variance given total CD8 T cell data	3.94×10^4 $(2.65 \times 10^4, 4.94 \times 10^4)$	per mL

Table 7.24: Fitted parameter estimates in $\boldsymbol{\theta}$ with the maximum posterior as the point estimate and 95% credible intervals for Patient 17

Symbol	Parameter	Estimate (95% credible interval)	Unit
r_1	Growth rate of new CD4 T cells	2.24×10^1 $(2.23 \times 10^1, 2.28 \times 10^1)$	per year
μ_1	Death rate of total CD4 T cells	1.49×10^1 $(1.29 \times 10^1, 1.49 \times 10^1)$	per year
c	Kill rate of CD4 T cells by effector CD8 CTLs due to other infections	5.42×10^{-6} $(2.99 \times 10^{-6}, 5.55 \times 10^{-6})$	mL per year
b	Kill rate of CD4 T cells by effector CD4 CTLs due to other infections	5.63×10^{-6} $(6.58 \times 10^{-6}, 1.22 \times 10^{-5})$	mL per year
β	Transmission rate of HIV-1 to CD4 T cells	4.12×10^{-4} $(1.35 \times 10^{-4}, 1.20 \times 10^{-3})$	mL per year
δ	Portion of generated HIV-1 specific effector CTLs that are HIV-1 specific effector CD4 CTLs	2.79×10^{-1} $(4.63 \times 10^{-2}, 4.98 \times 10^{-1})$	-
ka	Maximum proliferation rate of the HIV-1 specific effector CTL response	7.42×10^2 $(4.58 \times 10^2, 7.42 \times 10^2)$	per year
a	Number of HIV-1 specific effector CTLs at which the proliferation switches to a maximum rate	3.40×10^1 $(1.10 \times 10^{-4}, 2.14 \times 10^1)$	per mL

μ_2	Death rate of effector CTLs	9.43×10^1 $(7.03 \times 10^1, 9.93 \times 10^1)$	per year
μ_3	Death rate of productively infected CD4 T cells	3.07×10^2 $(1.42 \times 10^1, 2.97 \times 10^2)$	per year
γ	Rate infected CD4 T cells are killed by effector CTLs	9.09×10^1 $(1.76 \times 10^1, 5.75 \times 10^1)$	mL per year
p	Rate replication competent viral particles were produced by HIV-1 infected CD4 T cells	2.49×10^4 $(1.51 \times 10^4, 4.80 \times 10^4)$	per year
μ_4	Death rate of HIV-1 replication competent viral particles	2.82×10^3 $(3.11 \times 10^3, 5.97 \times 10^3)$	per year
r_2	Growth rate of new CD8 T cells	1.65×10^{-4} $(1.39 \times 10^{-4}, 1.68 \times 10^{-4})$	mL per year
μ_5	Death rate of total CD8 T cells	6.83×10^1 $(5.33 \times 10^1, 7.69 \times 10^1)$	per year
x_0	Initial number of CD4 T cells susceptible to HIV-1	6.14×10^5 $(5.96 \times 10^5, 6.99 \times 10^5)$	per mL
x_{E0}	Initial number of HIV-1 specific effector CD4 CTLs	2.92×10^1 $(4.10, 1.73 \times 10^2)$	per mL
y_0	Initial number of CD4 T cells productively infected with HIV-1	1.76×10^2 $(6.34, 1.92 \times 10^2)$	per mL
v_0	initial number of HIV-1 replication competent viral particles	1.27×10^2 $(8.93 \times 10^1, 1.90 \times 10^2)$	per mL

z_0	Initial number of CD8 T cells that are non HIV-1 specific	1.34×10^6 $(1.30 \times 10^6, 1.40 \times 10^6)$	per mL
z_{E0}	Initial number of HIV-1 specific effector CD8 CTLs	5.59×10^1 $(9.98, 1.93 \times 10^2)$	per mL
v^1	parameter determining most likely shape of Gaussian distribution with non-constant variance given viral load data	6.94 $(4.20, 1.11 \times 10^1)$	per mL
v^2	parameter determining most likely shape of Gaussian distribution with non-constant variance given total CD4 T cell data	2.55×10^4 $(1.55 \times 10^4, 2.85 \times 10^4)$	per mL
v^3	parameter determining most likely shape of Gaussian distribution with non-constant variance given total CD8 T cell data	1.20×10^4 $(6.81 \times 10^3, 2.80 \times 10^4)$	per mL

Table 7.25: Fitted parameter estimates in $\boldsymbol{\theta}$ with the maximum posterior as the point estimate and 95% credible intervals for Patient 18

Symbol	Parameter	Estimate (95% credible interval)	Unit
r_1	Growth rate of new CD4 T cells	2.34×10^2 $(2.34 \times 10^2, 2.34 \times 10^2)$	per year

μ_1	Death rate of total CD4 T cells	$7.97\ (7.92, 7.98)$	per year
c	Kill rate of CD4 T cells by effector CD8 CTLs due to other infections	1.89×10^{-4} $(1.89 \times 10^{-4}, 1.89 \times 10^{-4})$	mL per year
b	Kill rate of CD4 T cells by effector CD4 CTLs due to other infections	9.85×10^{-6} $(9.63 \times 10^{-6}, 9.85 \times 10^{-6})$	mL per year
β	Transmission rate of HIV-1 to CD4 T cells	1.11×10^{-5} $(1.11 \times 10^{-5}, 1.11 \times 10^{-5})$	mL per year
δ	Portion of generated HIV-1 specific effector CTLs that are HIV-1 specific effector CD4 CTLs	4.11×10^{-1} $(1.32 \times 10^{-2}, 4.73 \times 10^{-1})$	-
ka	Maximum proliferation rate of the HIV-1 specific effector CTL response	8.98×10^{1} $(8.98 \times 10^{1}, 3.33 \times 10^{2})$	per year
a	Number of HIV-1 specific effector CTLs at which the proliferation switches to a maximum rate	$9.11\ (9.10, 9.13)$	per mL
μ_2	Death rate of effector CTLs	8.11×10^{1} $(8.02 \times 10^{1}, 8.11 \times 10^{1})$	per year
μ_3	Death rate of productively infected CD4 T cells	1.95×10^{2} $(1.95 \times 10^{2}, 1.95 \times 10^{2})$	per year
γ	Rate infected CD4 T cells are killed by effector CTLs	3.89×10^{1} $(3.89 \times 10^{1}, 3.89 \times 10^{1})$	mL per year

p	Rate replication competent viral particles were produced by HIV-1 infected CD4 T cells	1.76×10^5 $(1.76 \times 10^5, 1.76 \times 10^5)$	per year
μ_4	Death rate of HIV-1 replication competent viral particles	3.23×10^3 $(3.23 \times 10^3, 3.23 \times 10^3)$	per year
r_2	Growth rate of new CD8 T cells	1.35×10^{-4} $(1.35 \times 10^{-4}, 1.35 \times 10^{-4})$	mL per year
μ_5	Death rate of total CD8 T cells	6.15×10^1 $(6.15 \times 10^1, 6.15 \times 10^1)$	per year
x_0	Initial number of CD4 T cells susceptible to HIV-1	4.79×10^5 $(4.51 \times 10^5, 5.07 \times 10^5)$	per mL
x_{E0}	Initial number of HIV-1 specific effector CD4 CTLs	7.19×10^2 $(1.29 \times 10^2, 7.19 \times 10^2)$	per mL
y_0	Initial number of CD4 T cells productively infected with HIV-1	2.51×10^2 $(2.35 \times 10^2, 3.40 \times 10^2)$	per mL
v_0	initial number of HIV-1 replication competent viral particles	5.65×10^2 $(4.94 \times 10^2, 5.66 \times 10^2)$	per mL
z_0	Initial number of CD8 T cells that are non HIV-1 specific	6.75×10^5 $(6.51 \times 10^5, 6.85 \times 10^5)$	per mL
z_{E0}	Initial number of HIV-1 specific effector CD8 CTLs	6.16×10^2 $(6.16 \times 10^2, 8.31 \times 10^2)$	per mL

v^1	parameter determining most likely shape of Gaussian distribution with non-constant variance given viral load data	2.30×10^1 $(6.15, 2.00 \times 10^2)$	per mL
v^2	parameter determining most likely shape of Gaussian distribution with non-constant variance given total CD4 T cell data	5.88×10^3 $(3.01 \times 10^3, 5.93 \times 10^3)$	per mL
v^3	parameter determining most likely shape of Gaussian distribution with non-constant variance given total CD8 T cell data	3.64×10^4 $(1.87 \times 10^4, 4.69 \times 10^4)$	per mL

Table 7.26: Fitted parameter estimates in $\boldsymbol{\theta}$ with the maximum posterior as the point estimate and 95% credible intervals for Patient 24

Symbol	Parameter	Estimate (95% credible interval)	Unit
r_1	Growth rate of new CD4 T cells	1.85×10^1 $(1.84 \times 10^1, 1.85 \times 10^1)$	per year
μ_1	Death rate of total CD4 T cells	7.09 $(7.06, 7.11)$	per year
c	Kill rate of CD4 T cells by effector CD8 CTLs due to other infections	1.46×10^{-5} $(1.45 \times 10^{-5}, 1.50 \times 10^{-5})$	mL per year

b	Kill rate of CD4 T cells by effector CD4 CTLs due to other infections	2.56×10^{-11} $(1.03E-15 \times 10^{-15}, 1.82 \times 10^{-9})$	mL per year
β	Transmission rate of HIV-1 to CD4 T cells	2.57×10^{-5} $(2.57 \times 10^{-5}, 2.57 \times 10^{-5})$	mL per year
δ	Portion of generated HIV-1 specific effector CTLs that are HIV-1 specific effector CD4 CTLs	4.70×10^{-2} $(1.32 \times 10^{-2}, 4.86 \times 10^{-1})$	-
ka	Maximum proliferation rate of the HIV-1 specific effector CTL response	1.95×10^{1} $(1.82 \times 10^{1}, 2.13 \times 10^{1})$	per year
a	Number of HIV-1 specific effector CTLs at which the proliferation switches to a maximum rate	8.92×10^{-4} $(1.02 \times 10^{-4}, 2.28 \times 10^{-1})$	per mL
μ_2	Death rate of effector CTLs	6.38×10^{1} $(6.00 \times 10^{1}, 7.90 \times 10^{1})$	per year
μ_3	Death rate of productively infected CD4 T cells	1.62×10^{2} $(1.62 \times 10^{2}, 1.62 \times 10^{2})$	per year
γ	Rate infected CD4 T cells are killed by effector CTLs	8.80×10^{-1} $(7.64 \times 10^{-1}, 9.91 \times 10^{-1})$	mL per year
p	Rate replication competent viral particles were produced by HIV-1 infected CD4 T cells	5.45×10^{4} $(5.45 \times 10^{4}, 5.45 \times 10^{4})$	per year

μ_4	Death rate of HIV-1 replication competent viral particles	6.65×10^3 $(6.65 \times 10^3, 6.65 \times 10^3)$	per year
r_2	Growth rate of new CD8 T cells	1.94×10^{-5} $(1.94 \times 10^{-5}, 1.94 \times 10^{-5})$	mL per year
μ_5	Death rate of total CD8 T cells	1.50×10^1 $(1.50 \times 10^1, 1.50 \times 10^1)$	per year
x_0	Initial number of CD4 T cells susceptible to HIV-1	8.18×10^5 $(8.17 \times 10^5, 8.31 \times 10^5)$	per mL
x_{E0}	Initial number of HIV-1 specific effector CD4 CTLs	8.23×10^1 $(7.01 \times 10^{-1}, 3.15 \times 10^2)$	per mL
y_0	Initial number of CD4 T cells productively infected with HIV-1	3.23×10^2 $(6.13 \times 10^1, 4.00 \times 10^2)$	per mL
v_0	initial number of HIV-1 replication competent viral particles	1.52×10^1 $(1.04, 4.66 \times 10^1)$	per mL
z_0	Initial number of CD8 T cells that are non HIV-1 specific	6.95×10^5 $(6.79 \times 10^5, 6.98 \times 10^5)$	per mL
z_{E0}	Initial number of HIV-1 specific effector CD8 CTLs	1.92×10^1 $(1.58 \times 10^{-1}, 3.36 \times 10^2)$	per mL
v^1	parameter determining most likely shape of Gaussian distribution with non-constant variance given viral load data	5.71×10^2 $(5.45 \times 10^2, 5.71 \times 10^2)$	per mL

v^2	parameter determining most likely shape of Gaussian distribution with non-constant variance given total CD4 T cell data	2.57×10^4 $(1.92 \times 10^4, 2.66 \times 10^4)$	per mL
v^3	parameter determining most likely shape of Gaussian distribution with non-constant variance given total CD8 T cell data	3.29×10^4 $(2.69 \times 10^4, 3.31 \times 10^4)$	per mL

Table 7.27: Fitted parameter estimates in $\boldsymbol{\theta}$ with the maximum posterior as the point estimate and 95% credible intervals for Patient 25

Symbol	Parameter	Estimate (95% credible interval)	Unit
r_1	Growth rate of new CD4 T cells	1.81×10^2 $(9.71 \times 10^1, 3.14 \times 10^2)$	per year
μ_1	Death rate of total CD4 T cells	4.43×10^1 $(9.45, 5.05 \times 10^1)$	per year
c	Kill rate of CD4 T cells by effector CD8 CTLs due to other infections	4.62×10^{-4} $(1.75 \times 10^{-4}, 9.31 \times 10^{-4})$	mL per year
b	Kill rate of CD4 T cells by effector CD4 CTLs due to other infections	1.29×10^{-6} $(1.09 \times 10^{-6}, 2.66 \times 10^{-4})$	mL per year

β	Transmission rate of HIV-1 to CD4 T cells	6.27×10^{-3} $(3.34 \times 10^{-6}, 3.30 \times 10^{-2})$	mL per year
δ	Portion of generated HIV-1 specific effector CTLs that are HIV-1 specific effector CD4 CTLs	2.88×10^{-1} $(3.69 \times 10^{-2}, 4.98 \times 10^{-1})$	-
ka	Maximum proliferation rate of the HIV-1 specific effector CTL response	5.06×10^{1} $(7.68, 9.20 \times 10^{2})$	per year
a	Number of HIV-1 specific effector CTLs at which the proliferation switches to a maximum rate	3.10 $(1.17 \times 10^{-4}, 6.31 \times 10^{1})$	per mL
μ_2	Death rate of effector CTLs	9.74×10^{1} $(4.75 \times 10^{1}, 9.95 \times 10^{1})$	per year
μ_3	Death rate of productively infected CD4 T cells	6.87×10^{1} $(4.94 \times 10^{1}, 3.29 \times 10^{2})$	per year
γ	Rate infected CD4 T cells are killed by effector CTLs	5.28×10^{1} $(3.56 \times 10^{-1}, 6.37 \times 10^{1})$	mL per year
p	Rate replication competent viral particles were produced by HIV-1 infected CD4 T cells	1.15×10^{3} $(1.02 \times 10^{3}, 5.75 \times 10^{4})$	per year
μ_4	Death rate of HIV-1 replication competent viral particles	9.13×10^{3} $(2.16 \times 10^{3}, 9.42 \times 10^{3})$	per year
r_2	Growth rate of new CD8 T cells	7.17×10^{-5} $(3.92 \times 10^{-5}, 8.23 \times 10^{-5})$	mL per year

μ_5	Death rate of total CD8 T cells	5.76×10^1 $(2.98 \times 10^1, 6.33 \times 10^1)$	per year
x_0	Initial number of CD4 T cells susceptible to HIV-1	5.29×10^5 $(5.11 \times 10^5, 6.63 \times 10^5)$	per mL
x_{E0}	Initial number of HIV-1 specific effector CD4 CTLs	2.71 $(2.70, 3.89 \times 10^1)$	per mL
y_0	Initial number of CD4 T cells productively infected with HIV-1	6.61 $(9.99 \times 10^{-1}, 3.63 \times 10^1)$	per mL
v_0	initial number of HIV-1 replication competent viral particles	3.69×10^1 $(1.01, 3.71 \times 10^1)$	per mL
z_0	Initial number of CD8 T cells that are non HIV-1 specific	2.75×10^5 $(1.48 \times 10^5, 2.89 \times 10^5)$	per mL
z_{E0}	Initial number of HIV-1 specific effector CD8 CTLs	2.33×10^1 $(1.20, 3.76 \times 10^1)$	per mL
v^1	parameter determining most likely shape of Gaussian distribution with non-constant variance given viral load data	3.15 $(1.08, 9.14)$	per mL
v^2	parameter determining most likely shape of Gaussian distribution with non-constant variance given total CD4 T cell data	3.79×10^2 $(3.55 \times 10^3, 2.08 \times 10^4)$	per mL

v^3	parameter determining most likely shape of Gaussian distribution with non-constant variance given total CD8 T cell data	8.57×10^3 $(3.05 \times 10^3, 8.07 \times 10^3)$	per mL

Table 7.28: Fitted parameter estimates in $\boldsymbol{\theta}$ with the maximum posterior as the point estimate and 95% credible intervals for Patient 28

Symbol	Parameter	Estimate (95% credible interval)	Unit
r_1	Growth rate of new CD4 T cells	1.47×10^2 $(1.46 \times 10^2, 5.87 \times 10^2)$	per year
μ_1	Death rate of total CD4 T cells	5.42×10^1 $(6.16, 5.46 \times 10^1)$	per year
c	Kill rate of CD4 T cells by effector CD8 CTLs due to other infections	1.20×10^{-4} $(1.14 \times 10^{-4}, 6.69 \times 10^{-4})$	mL per year
b	Kill rate of CD4 T cells by effector CD4 CTLs due to other infections	2.57×10^{-8} $(1.01 \times 10^{-15}, 5.31 \times 10^{-7})$	mL per year
β	Transmission rate of HIV-1 to CD4 T cells	1.85×10^{-2} $(1.10 \times 10^{-5}, 1.46 \times 10^{-2})$	mL per year
δ	Portion of generated HIV-1 specific effector CTLs that are HIV-1 specific effector CD4 CTLs	1.35×10^{-1} $(2.53 \times 10^{-2}, 4.93 \times 10^{-1})$	-

ka	Maximum proliferation rate of the HIV-1 specific effector CTL response	7.37×10^2 $(7.93, 9.44 \times 10^2)$	per year
a	Number of HIV-1 specific effector CTLs at which the proliferation switches to a maximum rate	7.49×10^{-4} $(1.01 \times 10^{-4}, 3.93 \times 10^1)$	per mL
μ_2	Death rate of effector CTLs	9.84×10^1 $(6.83 \times 10^1, 9.92 \times 10^1)$	per year
μ_3	Death rate of productively infected CD4 T cells	2.26×10^2 $(5.87 \times 10^1, 3.18 \times 10^2)$	per year
γ	Rate infected CD4 T cells are killed by effector CTLs	2.50×10^1 $(1.18 \times 10^{-2}, 8.89 \times 10^1)$	mL per year
p	Rate replication competent viral particles were produced by HIV-1 infected CD4 T cells	1.11×10^3 $(1.09 \times 10^3, 1.80 \times 10^5)$	per year
μ_4	Death rate of HIV-1 replication competent viral particles	6.93×10^3 $(2.15 \times 10^3, 9.82 \times 10^3)$	per year
r_2	Growth rate of new CD8 T cells	1.08×10^{-4} $(9.89 \times 10^{-5}, 1.26 \times 10^{-4})$	mL per year
μ_5	Death rate of total CD8 T cells	6.73×10^1 $(6.44 \times 10^1, 7.34 \times 10^1)$	per year
x_0	Initial number of CD4 T cells susceptible to HIV-1	6.08×10^5 $(6.00 \times 10^5, 7.30 \times 10^5)$	per mL
x_{E0}	Initial number of HIV-1 specific effector CD4 CTLs	4.09×10^1 $(3.83 \times 10^{-1}, 4.66 \times 10^1)$	per mL

y_0	Initial number of CD4 T cells productively infected with HIV-1	3.63×10^1 $(1.63 \times 10^{-1}, 4.71 \times 10^1)$	per mL
v_0	initial number of HIV-1 replication competent viral particles	4.40×10^1 $(4.27 \times 10^1, 4.60 \times 10^1)$	per mL
z_0	Initial number of CD8 T cells that are non HIV-1 specific	8.98×10^5 $(7.76 \times 10^5, 9.26 \times 10^5)$	per mL
z_{E0}	Initial number of HIV-1 specific effector CD8 CTLs	3.92×10^1 $(6.63 \times 10^{-1}, 4.74 \times 10^1)$	per mL
v^1	parameter determining most likely shape of Gaussian distribution with non-constant variance given viral load data	1.09×10^{-4} $(1.03 \times 10^{-4}, 2.74 \times 10^{-2})$	per mL
v^2	parameter determining most likely shape of Gaussian distribution with non-constant variance given total CD4 T cell data	3.64×10^3 $(2.06 \times 10^3, 1.23 \times 10^4)$	per mL
v^3	parameter determining most likely shape of Gaussian distribution with non-constant variance given total CD8 T cell data	1.27×10^4 $(5.98 \times 10^3, 2.57 \times 10^4)$	per mL

7.D.5 HIV-1 patient comparison group fitted parameters

Table 7.29: Fitted parameter estimates in $\boldsymbol{\theta}$ with the maximum posterior as the point estimate and 95% credible intervals for Patient 2

Symbol	Parameter	Estimate (95% credible interval)	Unit
r_1	Growth rate of new CD4 T cells	2.33×10^2 $(8.26, 2.33 \times 10^2)$	per year
μ_1	Death rate of total CD4 T cells	1.34 $(2.37 \times 10^{-1}, 6.37 \times 10^1)$	per year
c	Kill rate of CD4 T cells by effector CD8 CTLs due to other infections	1.96×10^{-4} $(2.45 \times 10^{-6}, 1.96 \times 10^{-4})$	mL per year
b	Kill rate of CD4 T cells by effector CD4 CTLs due to other infections	6.85×10^{-15} $(1.01 \times 10^{-15}, 1.01 \times 10^{-7})$	mL per year
β	Transmission rate of HIV-1 to CD4 T cells	1.09×10^{-3} $(1.23 \times 10^{-4}, 3.73 \times 10^{-3})$	mL per year
δ	Portion of generated HIV-1 specific effector CTLs that are HIV-1 specific effector CD4 CTLs	6.25×10^{-2} $(5.43 \times 10^{-6}, 4.68 \times 10^{-1})$	-
ka	Maximum proliferation rate of the HIV-1 specific effector CTL response	4.41×10^1 $(4.23, 5.03 \times 10^1)$	per year

a	Number of HIV-1 specific effector CTLs at which the proliferation switches to a maximum rate	5.03×10^2 $(3.87 \times 10^{-4}, 3.41 \times 10^2)$	per mL
μ_2	Death rate of effector CTLs	9.71×10^1 $(6.58 \times 10^1, 9.96 \times 10^1)$	per year
μ_3	Death rate of productively infected CD4 T cells	1.35×10^2 $(5.17 \times 10^1, 3.17 \times 10^2)$	per year
γ	Rate infected CD4 T cells are killed by effector CTLs	3.35 $(1.26 \times 10^{-2}, 3.47)$	mL per year
p	Rate replication competent viral particles were produced by HIV-1 infected CD4 T cells	5.93×10^3 $(1.00 \times 10^3, 2.52 \times 10^4)$	per year
μ_4	Death rate of HIV-1 replication competent viral particles	2.34×10^3 $(2.34 \times 10^3, 9.55 \times 10^3)$	per year
r_2	Growth rate of new CD8 T cells	3.58×10^{-5} $(3.46 \times 10^{-5}, 1.43 \times 10^{-4})$	mL per year
μ_5	Death rate of total CD8 T cells	2.31×10^1 $(2.28 \times 10^1, 9.21 \times 10^1)$	per year
x_0	Initial number of CD4 T cells susceptible to HIV-1	5.66×10^5 $(5.30 \times 10^5, 7.11 \times 10^5)$	per mL
x_{E0}	Initial number of HIV-1 specific effector CD4 CTLs	1.18×10^3 $(2.56 \times 10^{-1}, 1.34 \times 10^3)$	per mL
y_0	Initial number of CD4 T cells productively infected with HIV-1	6.45×10^1 $(3.96 \times 10^1, 1.39 \times 10^3)$	per mL

v_0	initial number of HIV-1 replication competent viral particles	6.07×10^2 $(1.93 \times 10^2, 1.47 \times 10^3)$	per mL
z_0	Initial number of CD8 T cells that are non HIV-1 specific	1.05×10^6 $(9.37 \times 10^5, 1.24 \times 10^6)$	per mL
z_{E0}	Initial number of HIV-1 specific effector CD8 CTLs	1.18×10^3 $(2.15 \times 10^1, 1.45 \times 10^3)$	per mL
v^1	parameter determining most likely shape of Gaussian distribution with non-constant variance given viral load data	2.76×10^3 $(4.42 \times 10^2, 3.06 \times 10^3)$	per mL
v^2	parameter determining most likely shape of Gaussian distribution with non-constant variance given total CD4 T cell data	4.90×10^2 $(1.62 \times 10^3, 8.35 \times 10^3)$	per mL
v^3	parameter determining most likely shape of Gaussian distribution with non-constant variance given total CD8 T cell data	8.98×10^3 $(6.22 \times 10^3, 1.20 \times 10^4)$	per mL

Table 7.30: Fitted parameter estimates in $\boldsymbol{\theta}$ with the maximum posterior as the point estimate and 95% credible intervals for Patient 7

Symbol	Parameter	Estimate (95% credible interval)	Unit
r_1	Growth rate of new CD4 T cells	6.76×10^2 $(3.46 \times 10^1, 8.46 \times 10^2)$	per year
μ_1	Death rate of total CD4 T cells	6.55×10^1 $(3.76, 4.97 \times 10^1)$	per year
c	Kill rate of CD4 T cells by effector CD8 CTLs due to other infections	4.75×10^{-4} $(1.70 \times 10^{-5}, 7.08 \times 10^{-4})$	mL per year
b	Kill rate of CD4 T cells by effector CD4 CTLs due to other infections	8.24×10^{-5} $(5.22 \times 10^{-15}, 1.73 \times 10^{-4})$	mL per year
β	Transmission rate of HIV-1 to CD4 T cells	4.78×10^{-5} $(2.04 \times 10^{-5}, 2.74 \times 10^{-3})$	mL per year
δ	Portion of generated HIV-1 specific effector CTLs that are HIV-1 specific effector CD4 CTLs	9.14×10^{-2} $(2.65 \times 10^{-2}, 4.65 \times 10^{-1})$	-
ka	Maximum proliferation rate of the HIV-1 specific effector CTL response	7.83×10^2 $(1.21 \times 10^2, 9.95 \times 10^2)$	per year
a	Number of HIV-1 specific effector CTLs at which the proliferation switches to a maximum rate	8.57×10^3 $(1.52 \times 10^{-4}, 6.68 \times 10^3)$	per mL
μ_2	Death rate of effector CTLs	7.98×10^1 $(6.63 \times 10^1, 9.55 \times 10^1)$	per year

μ_3	Death rate of productively infected CD4 T cells	2.36×10^2 $(2.80 \times 10^1, 3.03 \times 10^2)$	per year
γ	Rate infected CD4 T cells are killed by effector CTLs	8.51×10^{-2} $(1.25 \times 10^{-2}, 5.46 \times 10^1)$	mL per year
p	Rate replication competent viral particles were produced by HIV-1 infected CD4 T cells	1.05×10^4 $(1.10 \times 10^4, 7.69 \times 10^4)$	per year
μ_4	Death rate of HIV-1 replication competent viral particles	1.30×10^3 $(1.29 \times 10^3, 9.15 \times 10^3)$	per year
r_2	Growth rate of new CD8 T cells	8.89×10^{-5} $(4.42 \times 10^{-5}, 8.80 \times 10^{-5})$	mL per year
μ_5	Death rate of total CD8 T cells	6.59×10^1 $(3.28 \times 10^1, 6.59 \times 10^1)$	per year
x_0	Initial number of CD4 T cells susceptible to HIV-1	8.27×10^5 $(7.32 \times 10^5, 9.73 \times 10^5)$	per mL
x_{E0}	Initial number of HIV-1 specific effector CD4 CTLs	1.41×10^3 $(8.33 \times 10^1, 2.44 \times 10^3)$	per mL
y_0	Initial number of CD4 T cells productively infected with HIV-1	1.41×10^3 $(2.15 \times 10^2, 2.98 \times 10^3)$	per mL
v_0	initial number of HIV-1 replication competent viral particles	1.30×10^3 $(1.01 \times 10^3, 2.89 \times 10^3)$	per mL
z_0	Initial number of CD8 T cells that are non HIV-1 specific	9.09×10^5 $(8.30 \times 10^5, 1.08 \times 10^6)$	per mL

z_{E0}	Initial number of HIV-1 specific effector CD8 CTLs	3.05×10^2 $(1.37 \times 10^2, 2.72 \times 10^3)$	per mL
v^1	parameter determining most likely shape of Gaussian distribution with non-constant variance given viral load data	1.84×10^3 $(2.57 \times 10^3, 4.63 \times 10^3)$	per mL
v^2	parameter determining most likely shape of Gaussian distribution with non-constant variance given total CD4 T cell data	9.02×10^3 $(5.41 \times 10^3, 8.61 \times 10^3)$	per mL
v^3	parameter determining most likely shape of Gaussian distribution with non-constant variance given total CD8 T cell data	2.50×10^4 $(1.87 \times 10^4, 2.66 \times 10^4)$	per mL

Table 7.31: Fitted parameter estimates in $\boldsymbol{\theta}$ with the maximum posterior as the point estimate and 95% credible intervals for Patient 10

Symbol	Parameter	Estimate (95% credible interval)	Unit
r_1	Growth rate of new CD4 T cells	9.25×10^2 $(6.53 \times 10^2, 9.89 \times 10^2)$	per year
μ_1	Death rate of total CD4 T cells	2.70×10^1 $(1.40, 5.88 \times 10^1)$	per year

c	Kill rate of CD4 T cells by effector CD8 CTLs due to other infections	4.18×10^{-4} $(2.61 \times 10^{-4}, 4.40 \times 10^{-4})$	mL per year
b	Kill rate of CD4 T cells by effector CD4 CTLs due to other infections	6.43×10^{-5} $(4.04 \times 10^{-12}, 2.05 \times 10^{-4})$	mL per year
β	Transmission rate of HIV-1 to CD4 T cells	2.34×10^{-4} $(1.17 \times 10^{-4}, 1.33 \times 10^{-3})$	mL per year
δ	Portion of generated HIV-1 specific effector CTLs that are HIV-1 specific effector CD4 CTLs	2.14×10^{-1} $(3.44 \times 10^{-2}, 4.94 \times 10^{-1})$	-
ka	Maximum proliferation rate of the HIV-1 specific effector CTL response	1.05×10^{2} $(8.24, 7.75 \times 10^{1})$	per year
a	Number of HIV-1 specific effector CTLs at which the proliferation switches to a maximum rate	2.24×10^{3} $(1.17 \times 10^{-4}, 3.18 \times 10^{2})$	per mL
μ_2	Death rate of effector CTLs	7.83×10^{1} $(6.41 \times 10^{1}, 9.95 \times 10^{1})$	per year
μ_3	Death rate of productively infected CD4 T cells	2.09×10^{2} $(4.61 \times 10^{1}, 2.73 \times 10^{2})$	per year
γ	Rate infected CD4 T cells are killed by effector CTLs	1.74×10^{-2} $(1.71 \times 10^{-2}, 1.18)$	mL per year

p	Rate replication competent viral particles were produced by HIV-1 infected CD4 T cells	2.99×10^3 $(1.29 \times 10^3, 3.01 \times 10^3)$	per year
μ_4	Death rate of HIV-1 replication competent viral particles	3.13×10^3 $(1.17 \times 10^3, 3.00 \times 10^3)$	per year
r_2	Growth rate of new CD8 T cells	5.31×10^{-5} $(5.14 \times 10^{-5}, 7.68 \times 10^{-5})$	mL per year
μ_5	Death rate of total CD8 T cells	5.15×10^1 $(4.78 \times 10^1, 7.70 \times 10^1)$	per year
x_0	Initial number of CD4 T cells susceptible to HIV-1	8.06×10^5 $(5.71 \times 10^5, 9.78 \times 10^5)$	per mL
x_{E0}	Initial number of HIV-1 specific effector CD4 CTLs	1.36×10^2 $(1.16 \times 10^2, 1.96 \times 10^3)$	per mL
y_0	Initial number of CD4 T cells productively infected with HIV-1	8.02×10^1 $(6.92 \times 10^1, 1.91 \times 10^3)$	per mL
v_0	initial number of HIV-1 replication competent viral particles	5.97×10^2 $(1.64 \times 10^2, 1.81 \times 10^3)$	per mL
z_0	Initial number of CD8 T cells that are non HIV-1 specific	1.35×10^6 $(1.11 \times 10^6, 1.39 \times 10^6)$	per mL
z_{E0}	Initial number of HIV-1 specific effector CD8 CTLs	2.98×10^2 $(4.09 \times 10^1, 1.90 \times 10^3)$	per mL

v^1	parameter determining most likely shape of Gaussian distribution with non-constant variance given viral load data	1.97×10^2 $(3.37 \times 10^2, 5.51 \times 10^2)$	per mL
v^2	parameter determining most likely shape of Gaussian distribution with non-constant variance given total CD4 T cell data	5.08×10^4 $(3.44 \times 10^4, 5.88 \times 10^4)$	per mL
v^3	parameter determining most likely shape of Gaussian distribution with non-constant variance given total CD8 T cell data	1.21×10^5 $(8.40 \times 10^4, 1.90 \times 10^5)$	per mL

Table 7.32: Fitted parameter estimates in $\boldsymbol{\theta}$ with the maximum posterior as the point estimate and 95% credible intervals for Patient 11

Symbol	Parameter	Estimate (95% credible interval)	Unit
r_1	Growth rate of new CD4 T cells	2.35×10^1 $(2.30 \times 10^1, 2.50 \times 10^1)$	per year
μ_1	Death rate of total CD4 T cells	1.38×10^1 $(9.84, 1.43 \times 10^1)$	per year
c	Kill rate of CD4 T cells by effector CD8 CTLs due to other infections	1.78×10^{-5} $(1.66 \times 10^{-5}, 2.59 \times 10^{-5})$	mL per year

b	Kill rate of CD4 T cells by effector CD4 CTLs due to other infections	2.84×10^{-6} $(2.64 \times 10^{-6}, 4.91 \times 10^{-6})$	mL per year
β	Transmission rate of HIV-1 to CD4 T cells	3.77×10^{-6} $(3.75 \times 10^{-6}, 3.78 \times 10^{-6})$	mL per year
δ	Portion of generated HIV-1 specific effector CTLs that are HIV-1 specific effector CD4 CTLs	4.70×10^{-1} $(2.56 \times 10^{-2}, 4.98 \times 10^{-1})$	-
ka	Maximum proliferation rate of the HIV-1 specific effector CTL response	1.46×10^{1} $(3.59, 7.13 \times 10^{1})$	per year
a	Number of HIV-1 specific effector CTLs at which the proliferation switches to a maximum rate	4.07×10^{-3} $(1.00 \times 10^{-4}, 7.14 \times 10^{-1})$	per mL
μ_2	Death rate of effector CTLs	7.92×10^{1} $(5.78 \times 10^{1}, 1.00 \times 10^{2})$	per year
μ_3	Death rate of productively infected CD4 T cells	2.97×10^{1} $(2.97 \times 10^{1}, 2.99 \times 10^{1})$	per year
γ	Rate infected CD4 T cells are killed by effector CTLs	2.54×10^{-2} $(1.03 \times 10^{-2}, 4.40 \times 10^{-2})$	mL per year
p	Rate replication competent viral particles were produced by HIV-1 infected CD4 T cells	1.30×10^{5} $(1.30 \times 10^{5}, 1.31 \times 10^{5})$	per year

μ_4	Death rate of HIV-1 replication competent viral particles	9.61×10^3 $(9.45 \times 10^3, 9.63 \times 10^3)$	per year
r_2	Growth rate of new CD8 T cells	8.65×10^{-5} $(8.62 \times 10^{-5}, 8.67 \times 10^{-5})$	mL per year
μ_5	Death rate of total CD8 T cells	4.98×10^1 $(4.92 \times 10^1, 4.99 \times 10^1)$	per year
x_0	Initial number of CD4 T cells susceptible to HIV-1	5.84×10^5 $(5.06 \times 10^5, 6.65 \times 10^5)$	per mL
x_{E0}	Initial number of HIV-1 specific effector CD4 CTLs	8.65×10^2 $(1.44 \times 10^1, 3.96 \times 10^3)$	per mL
y_0	Initial number of CD4 T cells productively infected with HIV-1	2.73×10^3 $(9.65 \times 10^2, 4.50 \times 10^3)$	per mL
v_0	initial number of HIV-1 replication competent viral particles	3.79×10^3 $(3.01 \times 10^3, 4.38 \times 10^3)$	per mL
z_0	Initial number of CD8 T cells that are non HIV-1 specific	5.28×10^5 $(4.66 \times 10^5, 7.11 \times 10^5)$	per mL
z_{E0}	Initial number of HIV-1 specific effector CD8 CTLs	2.76×10^2 $(7.10 \times 10^1, 4.07 \times 10^3)$	per mL
v^1	parameter determining most likely shape of Gaussian distribution with non-constant variance given viral load data	2.23×10^2 $(1.25 \times 10^2, 7.30 \times 10^2)$	per mL

v^2	parameter determining most likely shape of Gaussian distribution with non-constant variance given total CD4 T cell data	1.76×10^4 $(1.25 \times 10^4, 1.85 \times 10^4)$	per mL
v^3	parameter determining most likely shape of Gaussian distribution with non-constant variance given total CD8 T cell data	1.57×10^4 $(1.05 \times 10^4, 1.81 \times 10^4)$	per mL

Table 7.33: Fitted parameter estimates in $\boldsymbol{\theta}$ with the maximum posterior as the point estimate and 95% credible intervals for Patient 12

Symbol	Parameter	Estimate (95% credible interval)	Unit
r_1	Growth rate of new CD4 T cells	5.80×10^2 $(5.79 \times 10^2, 6.18 \times 10^2)$	per year
μ_1	Death rate of total CD4 T cells	4.03×10^1 $(2.34 \times 10^1, 4.28 \times 10^1)$	per year
c	Kill rate of CD4 T cells by effector CD8 CTLs due to other infections	5.66×10^{-4} $(5.60 \times 10^{-4}, 5.74 \times 10^{-4})$	mL per year
b	Kill rate of CD4 T cells by effector CD4 CTLs due to other infections	5.49×10^{-7} $(1.10 \times 10^{-10}, 1.79 \times 10^{-4})$	mL per year

β	Transmission rate of HIV-1 to CD4 T cells	1.33×10^{-3} $(1.33 \times 10^{-3}, 1.33 \times 10^{-3})$	mL per year
δ	Portion of generated HIV-1 specific effector CTLs that are HIV-1 specific effector CD4 CTLs	6.32×10^{-2} $(1.74 \times 10^{-2}, 3.98 \times 10^{-1})$	-
ka	Maximum proliferation rate of the HIV-1 specific effector CTL response	1.33×10^{2} $(9.38 \times 10^{1}, 1.34 \times 10^{2})$	per year
a	Number of HIV-1 specific effector CTLs at which the proliferation switches to a maximum rate	1.22×10^{4} $(7.68 \times 10^{3}, 1.22 \times 10^{4})$	per mL
μ_2	Death rate of effector CTLs	9.30×10^{1} $(8.41 \times 10^{1}, 9.30 \times 10^{1})$	per year
μ_3	Death rate of productively infected CD4 T cells	1.49×10^{2} $(1.49 \times 10^{2}, 1.50 \times 10^{2})$	per year
γ	Rate infected CD4 T cells are killed by effector CTLs	3.84×10^{-2} $(3.84 \times 10^{-2}, 3.35)$	mL per year
p	Rate replication competent viral particles were produced by HIV-1 infected CD4 T cells	2.15×10^{3} $(2.12 \times 10^{3}, 2.15 \times 10^{3})$	per year
μ_4	Death rate of HIV-1 replication competent viral particles	3.89×10^{3} $(3.77 \times 10^{3}, 5.54 \times 10^{3})$	per year
r_2	Growth rate of new CD8 T cells	1.04×10^{-4} $(1.04 \times 10^{-4}, 1.08 \times 10^{-4})$	mL per year

μ_5	Death rate of total CD8 T cells	5.11×10^1 $(5.11 \times 10^1, 5.24 \times 10^1)$	per year
x_0	Initial number of CD4 T cells susceptible to HIV-1	7.99×10^5 $(6.57 \times 10^5, 8.98 \times 10^5)$	per mL
x_{E0}	Initial number of HIV-1 specific effector CD4 CTLs	8.49×10^3 $(8.46 \times 10^3, 8.68 \times 10^3)$	per mL
y_0	Initial number of CD4 T cells productively infected with HIV-1	2.04×10^3 $(2.03 \times 10^3, 7.41 \times 10^3)$	per mL
v_0	initial number of HIV-1 replication competent viral particles	5.98×10^3 $(4.82 \times 10^3, 6.99 \times 10^3)$	per mL
z_0	Initial number of CD8 T cells that are non HIV-1 specific	1.37×10^6 $(1.22 \times 10^6, 1.52 \times 10^6)$	per mL
z_{E0}	Initial number of HIV-1 specific effector CD8 CTLs	3.42×10^3 $(1.97 \times 10^3, 3.44 \times 10^3)$	per mL
v^1	parameter determining most likely shape of Gaussian distribution with non-constant variance given viral load data	1.63×10^3 $(1.12 \times 10^3, 4.78 \times 10^3)$	per mL
v^2	parameter determining most likely shape of Gaussian distribution with non-constant variance given total CD4 T cell data	2.32×10^4 $(1.57 \times 10^4, 3.88 \times 10^4)$	per mL

v^3	parameter determining most likely shape of Gaussian distribution with non-constant variance given total CD8 T cell data	1.54×10^5 $(9.47 \times 10^4, 1.77 \times 10^5)$	per mL

Table 7.34: Fitted parameter estimates in $\boldsymbol{\theta}$ with the maximum posterior as the point estimate and 95% credible intervals for Patient 21

Symbol	Parameter	Estimate (95% credible interval)	Unit
r_1	Growth rate of new CD4 T cells	1.05×10^2 $(1.03 \times 10^2, 6.35 \times 10^2)$	per year
μ_1	Death rate of total CD4 T cells	3.12×10^1 $(1.46 \times 10^{-1}, 4.45 \times 10^1)$	per year
c	Kill rate of CD4 T cells by effector CD8 CTLs due to other infections	7.38×10^{-5} $(6.93 \times 10^{-5}, 5.99 \times 10^{-4})$	mL per year
b	Kill rate of CD4 T cells by effector CD4 CTLs due to other infections	2.38×10^{-8} $(1.37 \times 10^{-15}, 1.54 \times 10^{-4})$	mL per year
β	Transmission rate of HIV-1 to CD4 T cells	4.73×10^{-5} $(4.95 \times 10^{-5}, 1.57 \times 10^{-2})$	mL per year

δ	Portion of generated HIV-1 specific effector CTLs that are HIV-1 specific effector CD4 CTLs	1.86×10^{-1} $(2.85 \times 10^{-2}, 5.00 \times 10^{-1})$	-
ka	Maximum proliferation rate of the HIV-1 specific effector CTL response	6.72×10^{2} $(8.14 \times 10^{-1}, 9.43 \times 10^{2})$	per year
a	Number of HIV-1 specific effector CTLs at which the proliferation switches to a maximum rate	8.18×10^{2} $(1.12 \times 10^{-4}, 1.46 \times 10^{3})$	per mL
μ_2	Death rate of effector CTLs	5.54×10^{1} $(3.97 \times 10^{1}, 9.94 \times 10^{1})$	per year
μ_3	Death rate of productively infected CD4 T cells	1.87×10^{2} $(4.38 \times 10^{1}, 3.22 \times 10^{2})$	per year
γ	Rate infected CD4 T cells are killed by effector CTLs	7.28×10^{-2} $(4.26 \times 10^{-2}, 1.16 \times 10^{1})$	mL per year
p	Rate replication competent viral particles were produced by HIV-1 infected CD4 T cells	1.50×10^{5} $(1.39 \times 10^{3}, 1.88 \times 10^{5})$	per year
μ_4	Death rate of HIV-1 replication competent viral particles	8.02×10^{3} $(1.69 \times 10^{3}, 8.76 \times 10^{3})$	per year
r_2	Growth rate of new CD8 T cells	8.55×10^{-5} $(4.49 \times 10^{-5}, 1.17 \times 10^{-4})$	mL per year
μ_5	Death rate of total CD8 T cells	5.31×10^{1} $(2.81 \times 10^{1}, 7.45 \times 10^{1})$	per year

x_0	Initial number of CD4 T cells susceptible to HIV-1	6.69×10^5 $(5.32 \times 10^5, 7.47 \times 10^5)$	per mL
x_{E0}	Initial number of HIV-1 specific effector CD4 CTLs	3.89×10^3 $(7.79 \times 10^2, 9.93 \times 10^3)$	per mL
y_0	Initial number of CD4 T cells productively infected with HIV-1	5.13×10^3 $(1.28 \times 10^2, 9.51 \times 10^3)$	per mL
v_0	initial number of HIV-1 replication competent viral particles	5.20×10^3 $(3.32 \times 10^3, 6.98 \times 10^3)$	per mL
z_0	Initial number of CD8 T cells that are non HIV-1 specific	7.56×10^5 $(7.40 \times 10^5, 1.10 \times 10^6)$	per mL
z_{E0}	Initial number of HIV-1 specific effector CD8 CTLs	8.65×10^3 $(2.02 \times 10^2, 9.60 \times 10^3)$	per mL
v^1	parameter determining most likely shape of Gaussian distribution with non-constant variance given viral load data	4.98 $(2.91 \times 10^1, 4.54 \times 10^2)$	per mL
v^2	parameter determining most likely shape of Gaussian distribution with non-constant variance given total CD4 T cell data	8.73×10^3 $(6.64 \times 10^3, 1.65 \times 10^4)$	per mL

v^3	parameter determining most likely shape of Gaussian distribution with non-constant variance given total CD8 T cell data	1.70×10^4 $(1.03 \times 10^4, 2.38 \times 10^4)$	per mL

Table 7.35: Fitted parameter estimates in $\boldsymbol{\theta}$ with the maximum posterior as the point estimate and 95% credible intervals for Patient 23

Symbol	Parameter	Estimate (95% credible interval)	Unit
r_1	Growth rate of new CD4 T cells	1.33×10^3 $(1.32 \times 10^3, 1.33 \times 10^3)$	per year
μ_1	Death rate of total CD4 T cells	4.92×10^1 $(3.67 \times 10^1, 4.92 \times 10^1)$	per year
c	Kill rate of CD4 T cells by effector CD8 CTLs due to other infections	9.61×10^{-4} $(9.61 \times 10^{-4}, 9.61 \times 10^{-4})$	mL per year
b	Kill rate of CD4 T cells by effector CD4 CTLs due to other infections	2.17×10^{-4} $(2.17 \times 10^{-4}, 2.22 \times 10^{-4})$	mL per year
β	Transmission rate of HIV-1 to CD4 T cells	4.16×10^{-6} $(4.16 \times 10^{-6}, 4.41 \times 10^{-6})$	mL per year

δ	Portion of generated HIV-1 specific effector CTLs that are HIV-1 specific effector CD4 CTLs	3.90×10^{-1} $(1.08 \times 10^{-1}, 4.67 \times 10^{-1})$	-
ka	Maximum proliferation rate of the HIV-1 specific effector CTL response	7.76×10^{1} $(7.75 \times 10^{1}, 7.76 \times 10^{1})$	per year
a	Number of HIV-1 specific effector CTLs at which the proliferation switches to a maximum rate	1.34×10^{1} $(1.34 \times 10^{1}, 1.52 \times 10^{1})$	per mL
μ_2	Death rate of effector CTLs	7.02×10^{1} $(7.02 \times 10^{1}, 7.02 \times 10^{1})$	per year
μ_3	Death rate of productively infected CD4 T cells	2.00×10^{2} $(1.89 \times 10^{2}, 2.00 \times 10^{2})$	per year
γ	Rate infected CD4 T cells are killed by effector CTLs	6.26×10^{1} $(6.26 \times 10^{1}, 6.26 \times 10^{1})$	mL per year
p	Rate replication competent viral particles were produced by HIV-1 infected CD4 T cells	1.35×10^{6} $(1.24 \times 10^{6}, 1.35 \times 10^{6})$	per year
μ_4	Death rate of HIV-1 replication competent viral particles	7.39×10^{3} $(7.39 \times 10^{3}, 7.42 \times 10^{3})$	per year
r_2	Growth rate of new CD8 T cells	7.36×10^{-5} $(7.35 \times 10^{-5}, 7.36 \times 10^{-5})$	mL per year
μ_5	Death rate of total CD8 T cells	5.92×10^{1} $(5.90 \times 10^{1}, 5.92 \times 10^{1})$	per year

x_0	Initial number of CD4 T cells susceptible to HIV-1	9.67×10^5 $(9.67 \times 10^5, 9.78 \times 10^5)$	per mL
x_{E0}	Initial number of HIV-1 specific effector CD4 CTLs	1.41×10^3 $(6.39 \times 10^2, 1.41 \times 10^3)$	per mL
y_0	Initial number of CD4 T cells productively infected with HIV-1	1.19×10^3 $(7.17 \times 10^2, 1.19 \times 10^3)$	per mL
v_0	initial number of HIV-1 replication competent viral particles	2.67×10^2 $(2.67 \times 10^2, 6.96 \times 10^2)$	per mL
z_0	Initial number of CD8 T cells that are non HIV-1 specific	1.41×10^6 $(1.19 \times 10^6, 1.41 \times 10^6)$	per mL
z_{E0}	Initial number of HIV-1 specific effector CD8 CTLs	5.20×10^2 $(5.20 \times 10^2, 5.80 \times 10^2)$	per mL
v^1	parameter determining most likely shape of Gaussian distribution with non-constant variance given viral load data	7.37×10^2 $(4.79 \times 10^2, 1.05 \times 10^3)$	per mL
v^2	parameter determining most likely shape of Gaussian distribution with non-constant variance given total CD4 T cell data	1.46×10^4 $(1.06 \times 10^4, 1.48 \times 10^4)$	per mL

v^3	parameter determining most likely shape of Gaussian distribution with non-constant variance given total CD8 T cell data	5.29×10^4 $(4.24 \times 10^4, 5.93 \times 10^4)$	per mL

7.D.6 HIV-1 Elite Controller patients mathematical model plots

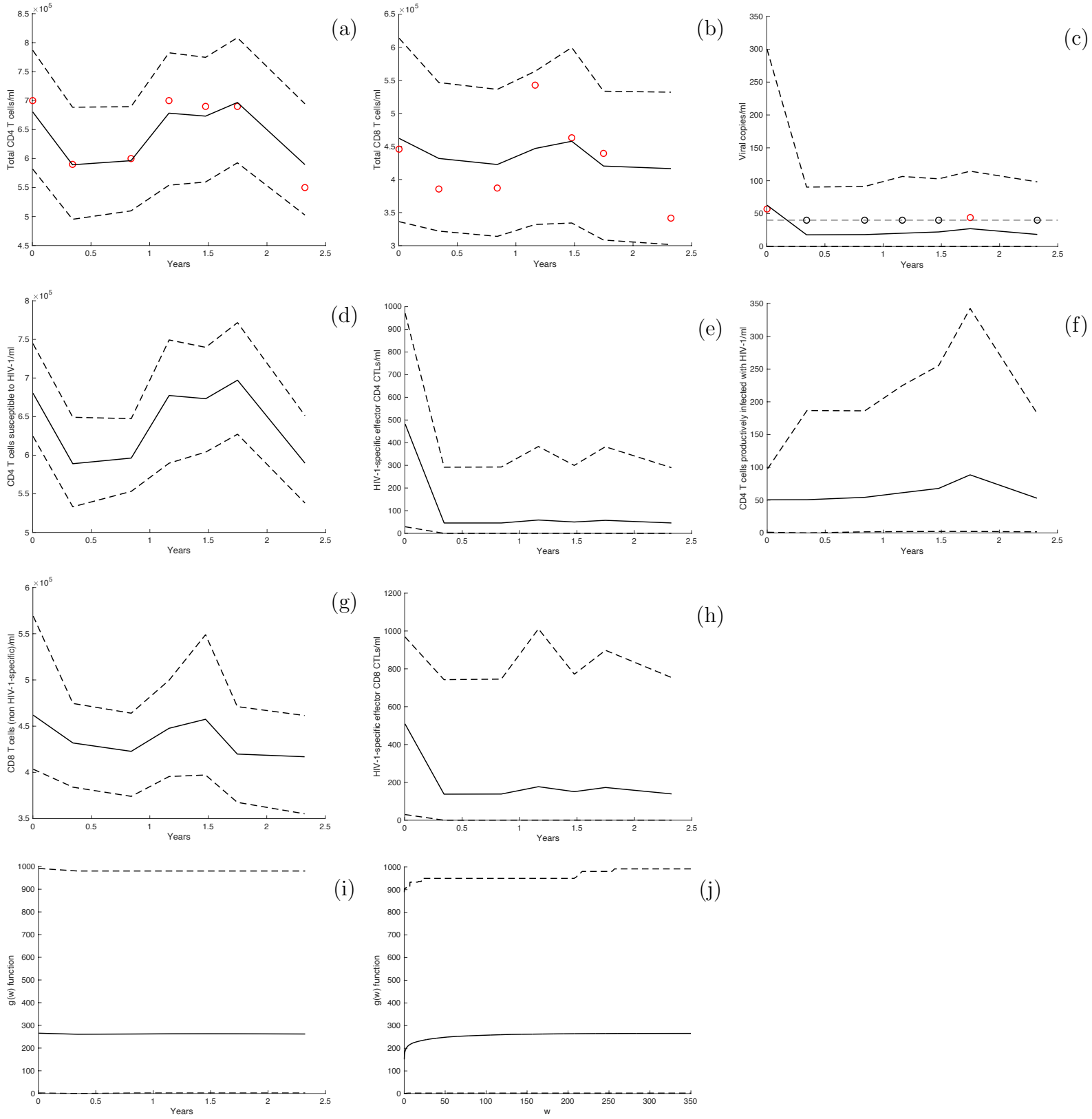

Figure 7.17: Modeling HIV-1 infection in the plasma for Patient 1: **(a)** total CD4 T cells/ml, **(b)** total CD8 T cells/ml, **(c)** viral copies/ml; **(d)** CD4 T cells susceptible to HIV-1/ml, **(e)** HIV-1-specific effector CD4 CTLs/ml, **(f)** CD4 T cells productively infected with HIV-1/ml; **(g)** CD8 T cells (non HIV-1-specific)/ml, and **(h)** HIV-1-specific effector CD8 CTLs/ml; **(i)** effector response function over time, and **(j)** effector response function over the number of effector CTLs. The predictive mean solution is given by the solid black curve, the 95% prediction interval is given by the dashed black curves, and the circle points denote the fitted data. (Note: the black points on the viral copies figure denote that the viral load was below detection and the value of each black point was the limit of detection at that time)

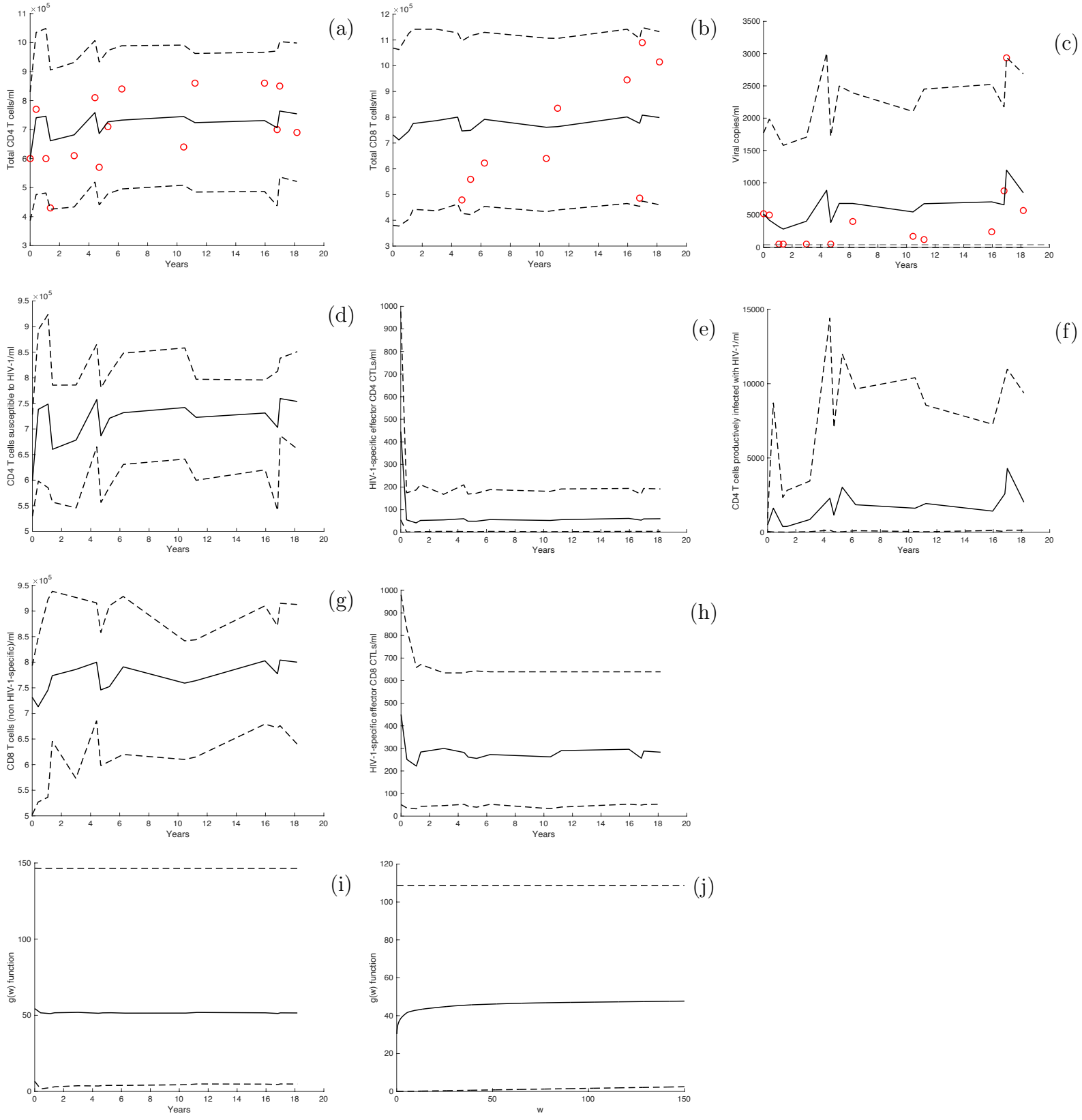

Figure 7.18: Modeling HIV-1 infection in the plasma for Patient 6: **(a)** total CD4 T cells/ml, **(b)** total CD8 T cells/ml, **(c)** viral copies/ml; **(d)** CD4 T cells susceptible to HIV-1/ml, **(e)** HIV-1-specific effector CD4 CTLs/ml, **(f)** CD4 T cells productively infected with HIV-1/ml; **(g)** CD8 T cells (non HIV-1-specific)/ml, and **(h)** HIV-1-specific effector CD8 CTLs/ml; **(i)** effector response function over time, and **(j)** effector response function over the number of effector CTLs. The predictive mean solution is given by the solid black curve, the 95% prediction interval is given by the dashed black curves, and the circle points denote the fitted data.

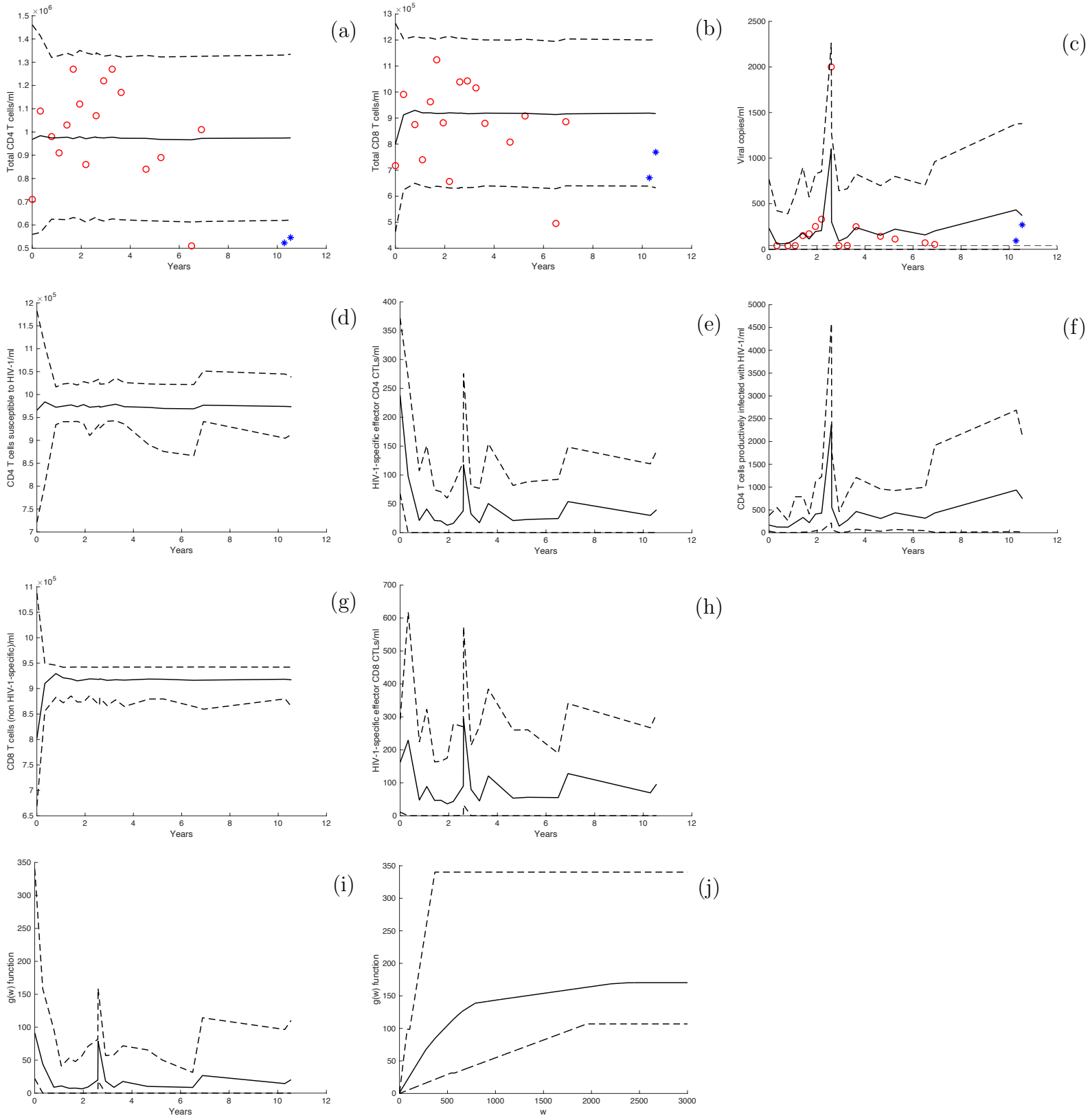

Figure 7.19: Modeling HIV-1 infection in the plasma for Patient 14: **(a)** total CD4 T cells/ml, **(b)** total CD8 T cells/ml, **(c)** viral copies/ml; **(d)** CD4 T cells susceptible to HIV-1/ml, **(e)** HIV-1-specific effector CD4 CTLs/ml, **(f)** CD4 T cells productively infected with HIV-1/ml; **(g)** CD8 T cells (non HIV-1-specific)/ml, and **(h)** HIV-1-specific effector CD8 CTLs/ml; **(i)** effector response function over time, and **(j)** effector response function over the number of effector CTLs. The predictive mean solution is given by the solid black curve, the 95% prediction interval is given by the dashed black curves, the circle points denote the fitted data, and the star points display the unfitted data.

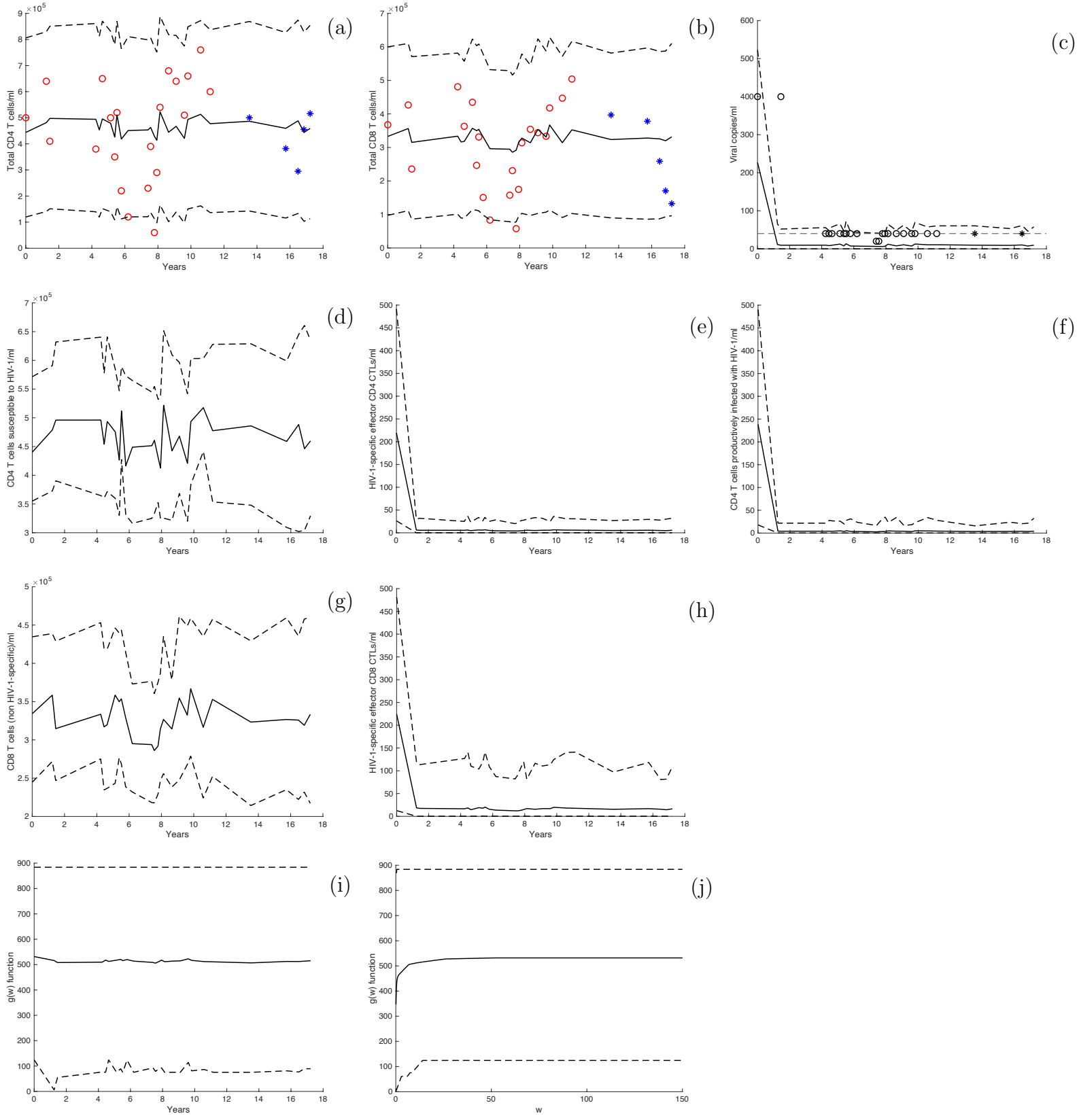

Figure 7.20: Modeling HIV-1 infection in the plasma for Patient 16: **(a)** total CD4 T cells/ml, **(b)** total CD8 T cells/ml, **(c)** viral copies/ml; **(d)** CD4 T cells susceptible to HIV-1/ml, **(e)** HIV-1-specific effector CD4 CTLs/ml, **(f)** CD4 T cells productively infected with HIV-1/ml; **(g)** CD8 T cells (non HIV-1-specific)/ml, and **(h)** HIV-1-specific effector CD8 CTLs/ml; **(i)** effector response function over time, and **(j)** effector response function over the number of effector CTLs. The predictive mean solution is given by the solid black curve, the 95% prediction interval is given by the dashed black curves, the circle points denote the fitted data, and the star points display the unfitted data. (Note: the black points on the viral copies figure denote that the viral load was below detection and the value of each black point was the limit of detection at that time)

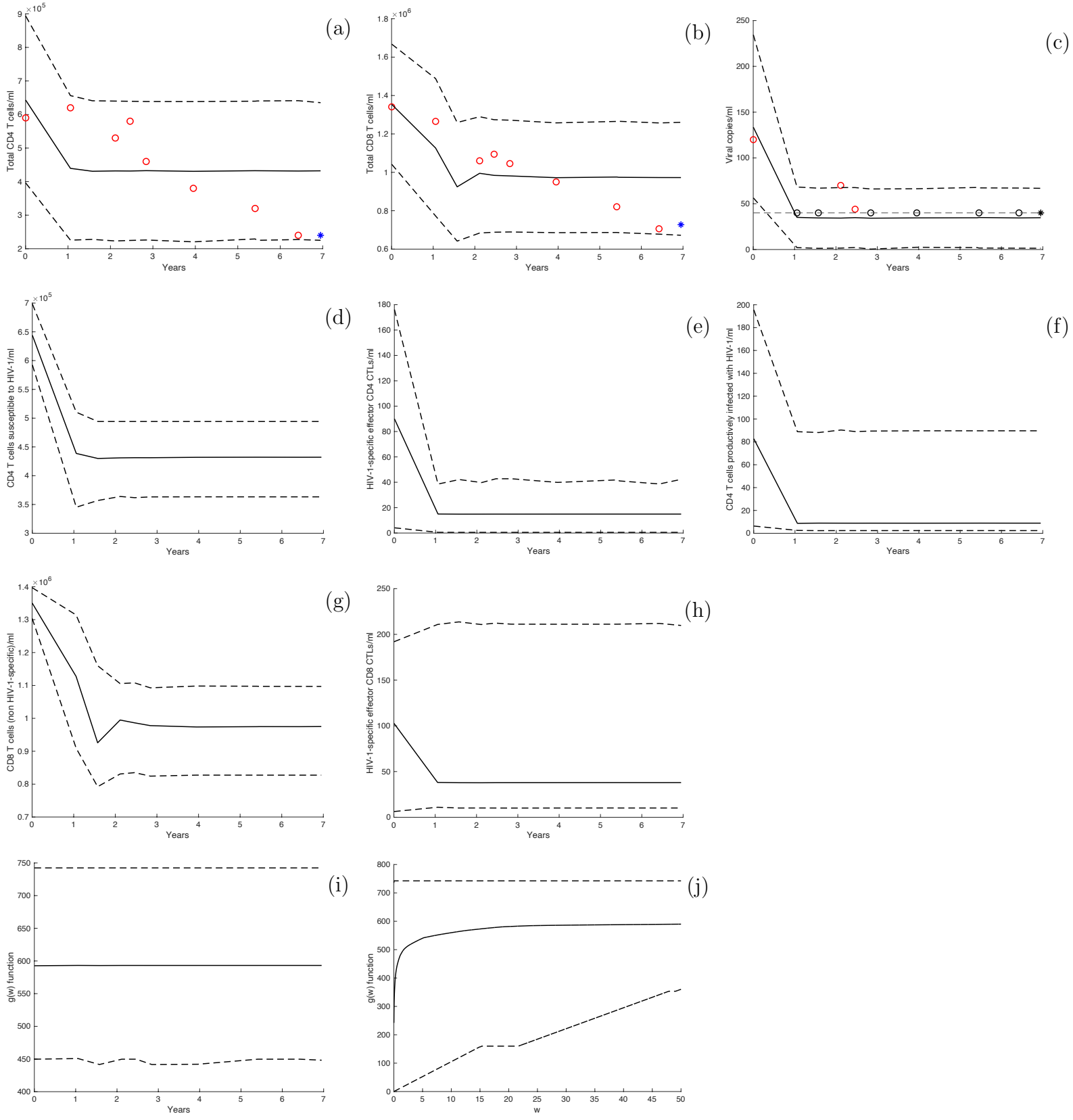

Figure 7.21: Modeling HIV-1 infection in the plasma for Patient 17: **(a)** total CD4 T cells/ml, **(b)** total CD8 T cells/ml, **(c)** viral copies/ml; **(d)** CD4 T cells susceptible to HIV-1/ml, **(e)** HIV-1-specific effector CD4 CTLs/ml, **(f)** CD4 T cells productively infected with HIV-1/ml; **(g)** CD8 T cells (non HIV-1-specific)/ml, and **(h)** HIV-1-specific effector CD8 CTLs/ml; **(i)** effector response function over time, and **(j)** effector response function over the number of effector CTLs. The predictive mean solution is given by the solid black curve, the 95% prediction interval is given by the dashed black curves, the circle points denote the fitted data, and the star point displays the unfitted data. (Note: the black points on the viral copies figure denote that the viral load was below detection and the value of each black point was the limit of detection at that time)

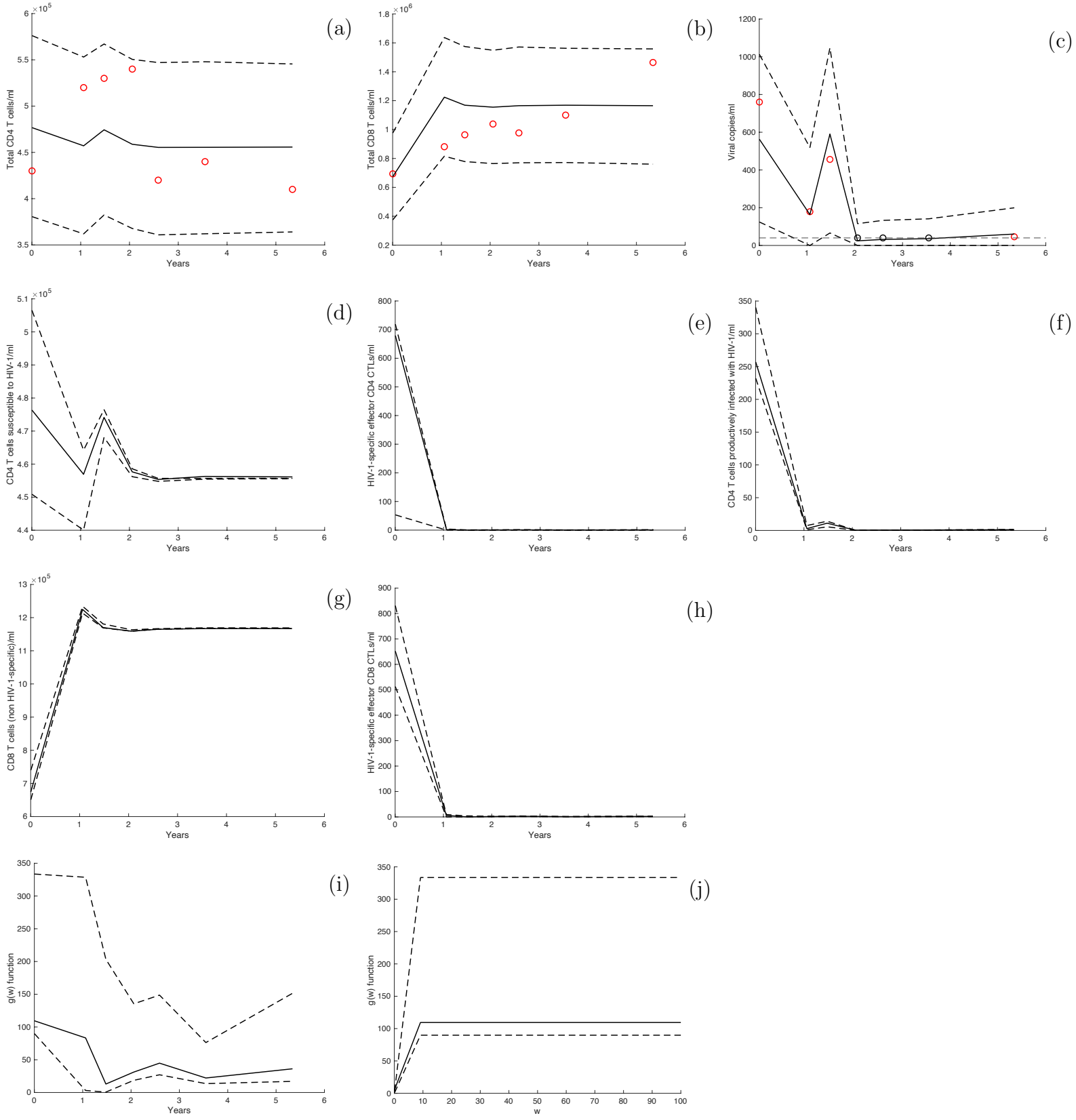

Figure 7.22: Modeling HIV-1 infection in the plasma for Patient 18: **(a)** total CD4 T cells/ml, **(b)** total CD8 T cells/ml, **(c)** viral copies/ml; **(d)** CD4 T cells susceptible to HIV-1/ml, **(e)** HIV-1-specific effector CD4 CTLs/ml, **(f)** CD4 T cells productively infected with HIV-1/ml; **(g)** CD8 T cells (non HIV-1-specific)/ml, and **(h)** HIV-1-specific effector CD8 CTLs/ml; **(i)** effector response function over time, and **(j)** effector response function over the number of effector CTLs. The predictive mean solution is given by the solid black curve, the 95% prediction interval is given by the dashed black curves, and the circle points denote the fitted data. (Note: the black points on the viral copies figure denote that the viral load was below detection and the value of each black point was the limit of detection at that time)

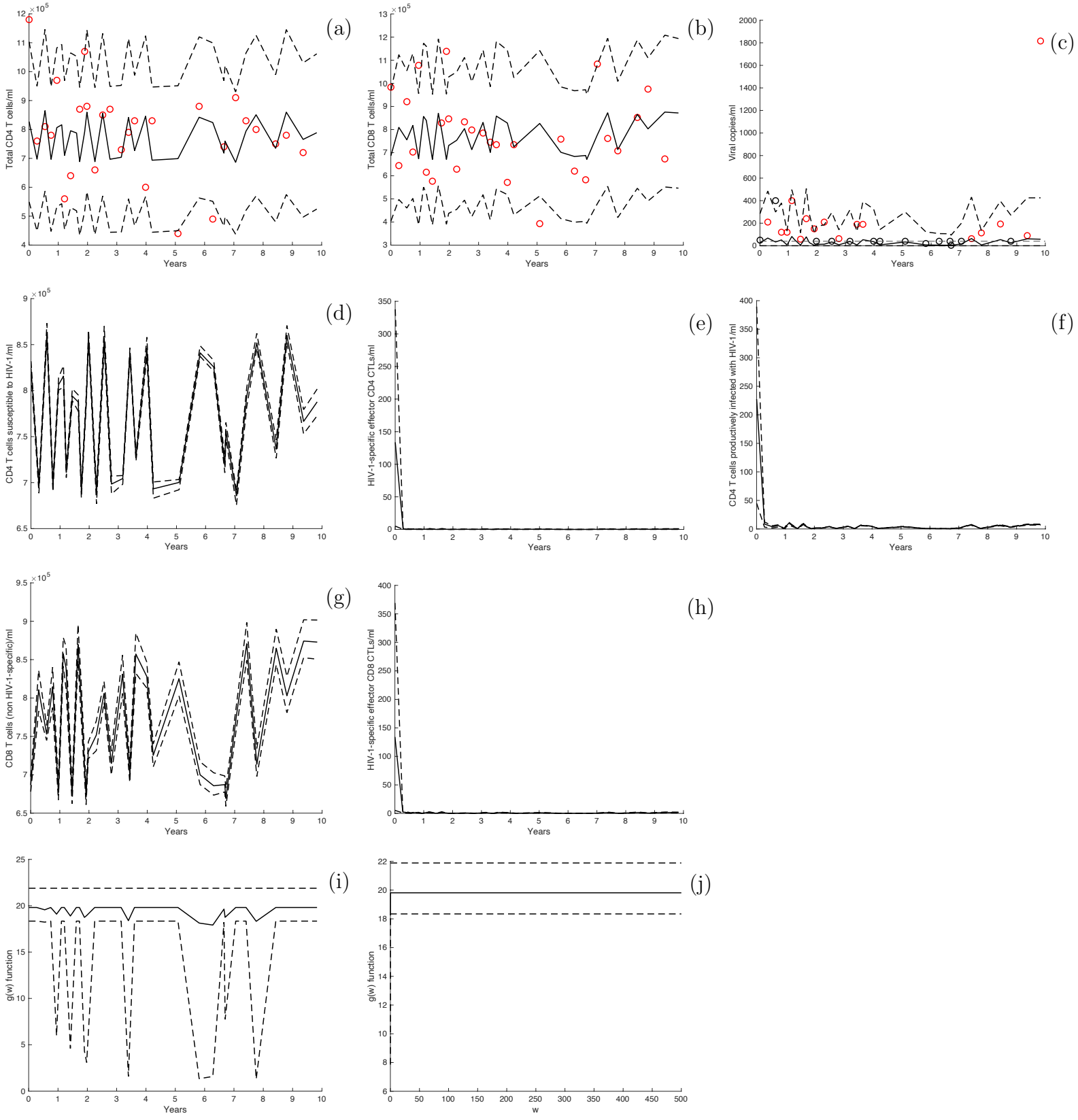

Figure 7.23: Modeling HIV-1 infection in the plasma for Patient 24: **(a)** total CD4 T cells/ml, **(b)** total CD8 T cells/ml, **(c)** viral copies/ml; **(d)** CD4 T cells susceptible to HIV-1/ml, **(e)** HIV-1-specific effector CD4 CTLs/ml, **(f)** CD4 T cells productively infected with HIV-1/ml; **(g)** CD8 T cells (non HIV-1-specific)/ml, and **(h)** HIV-1-specific effector CD8 CTLs/ml; **(i)** effector response function over time, and **(j)** effector response function over the number of effector CTLs. The predictive mean solution is given by the solid black curve, the 95% prediction interval is given by the dashed black curves, and the circle points denote the fitted data. (Note: the black points on the viral copies figure denote that the viral load was below detection and the value of each black point was the limit of detection at that time)

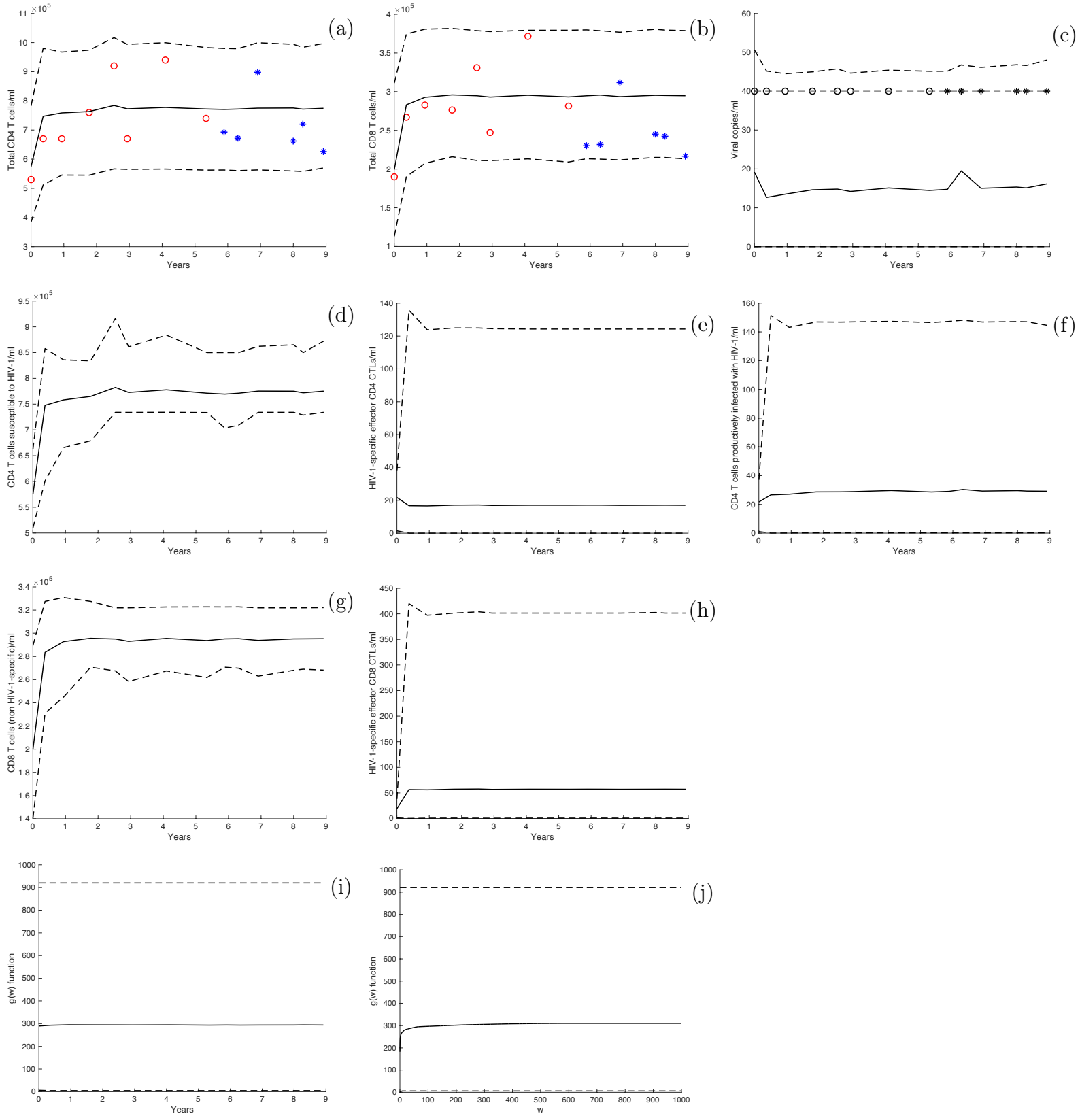

Figure 7.24: Modeling HIV-1 infection in the plasma for Patient 25: **(a)** total CD4 T cells/ml, **(b)** total CD8 T cells/ml, **(c)** viral copies/ml; **(d)** CD4 T cells susceptible to HIV-1/ml, **(e)** HIV-1-specific effector CD4 CTLs/ml, **(f)** CD4 T cells productively infected with HIV-1/ml; **(g)** CD8 T cells (non HIV-1-specific)/ml, and **(h)** HIV-1-specific effector CD8 CTLs/ml; **(i)** effector response function over time, and **(j)** effector response function over the number of effector CTLs. The predictive mean solution is given by the solid black curve, the 95% prediction interval is given by the dashed black curves, the circle points denote the fitted data, and the star points display the unfitted data. (Note: the black points on the viral copies figure denote that the viral load was below detection and the value of each black point was the limit of detection at that time)

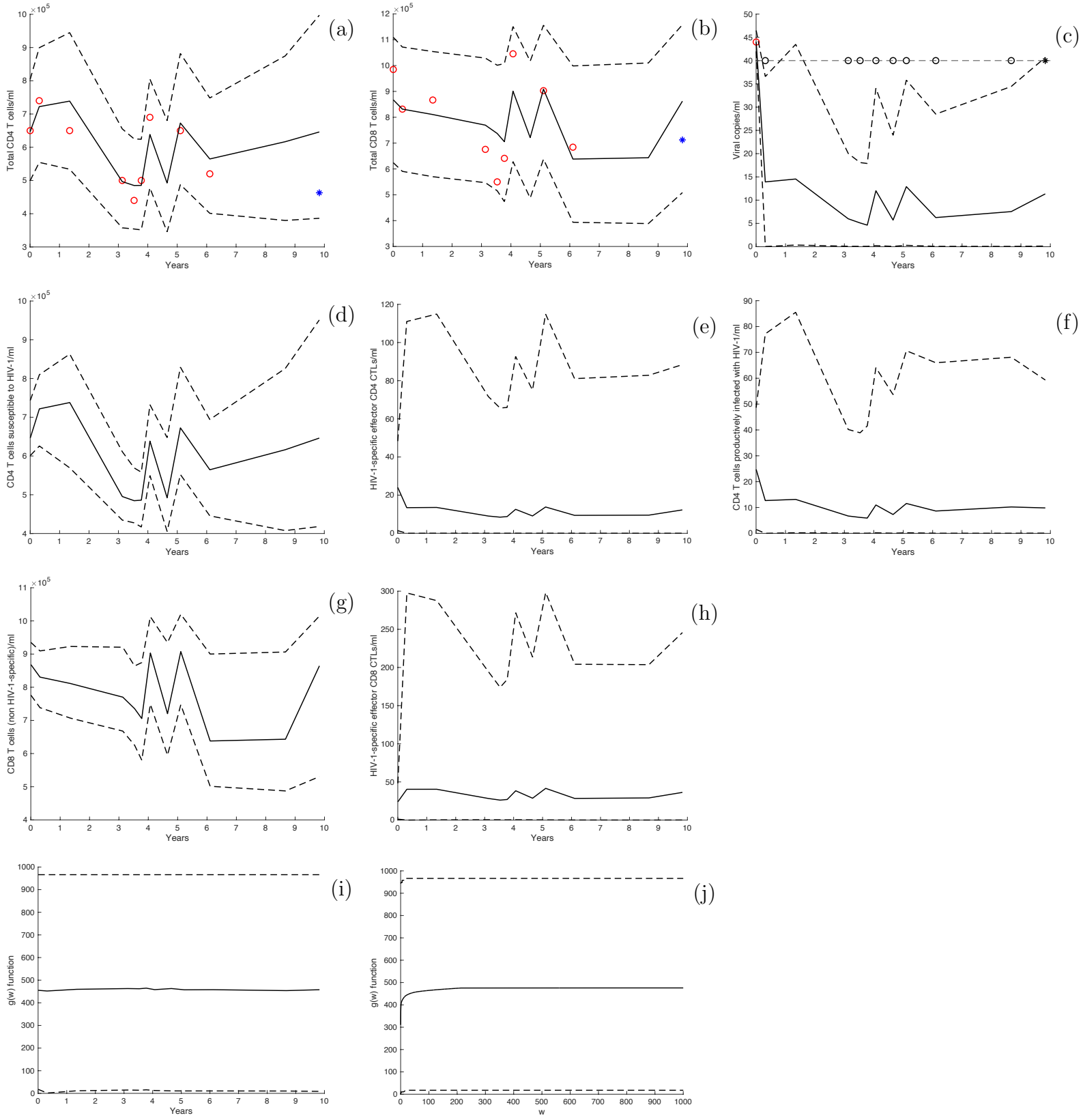

Figure 7.25: Modeling HIV-1 infection in the plasma for Patient 28: **(a)** total CD4 T cells/ml, **(b)** total CD8 T cells/ml, **(c)** viral copies/ml; **(d)** CD4 T cells susceptible to HIV-1/ml, **(e)** HIV-1-specific effector CD4 CTLs/ml, **(f)** CD4 T cells productively infected with HIV-1/ml; **(g)** CD8 T cells (non HIV-1-specific)/ml, and **(h)** HIV-1-specific effector CD8 CTLs/ml; **(i)** effector response function over time, and **(j)** effector response function over the number of effector CTLs. The predictive mean solution is given by the solid black curve, the 95% prediction interval is given by the dashed black curves, the circle points denote the fitted data, and the star point displays the unfitted data. (Note: the black points on the viral copies figure denote that the viral load was below detection and the value of each black point was the limit of detection at that time)

7.D.7 HIV-1 patient comparison group mathematical model plots

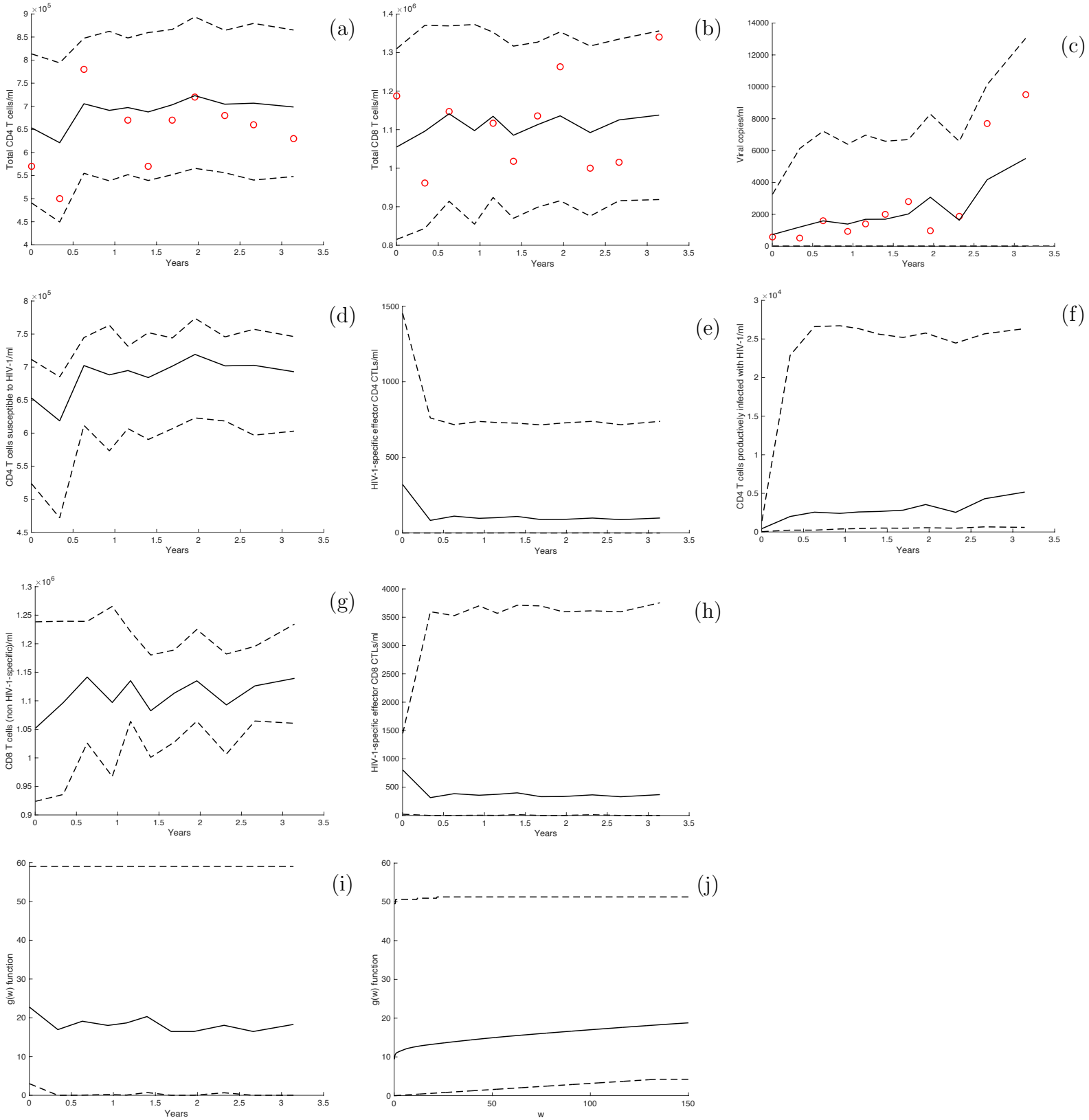

Figure 7.26: Modeling HIV-1 infection in the plasma for Patient 2: **(a)** total CD4 T cells/ml, **(b)** total CD8 T cells/ml, **(c)** viral copies/ml; **(d)** CD4 T cells susceptible to HIV-1/ml, **(e)** HIV-1-specific effector CD4 CTLs/ml, **(f)** CD4 T cells productively infected with HIV-1/ml; **(g)** CD8 T cells (non HIV-1-specific)/ml, and **(h)** HIV-1-specific effector CD8 CTLs/ml; **(i)** effector response function over time, and **(j)** effector response function over the number of effector CTLs. The predictive mean solution is given by the solid black curve, the 95% prediction interval is given by the dashed black curves, and the circle points denote the fitted data.

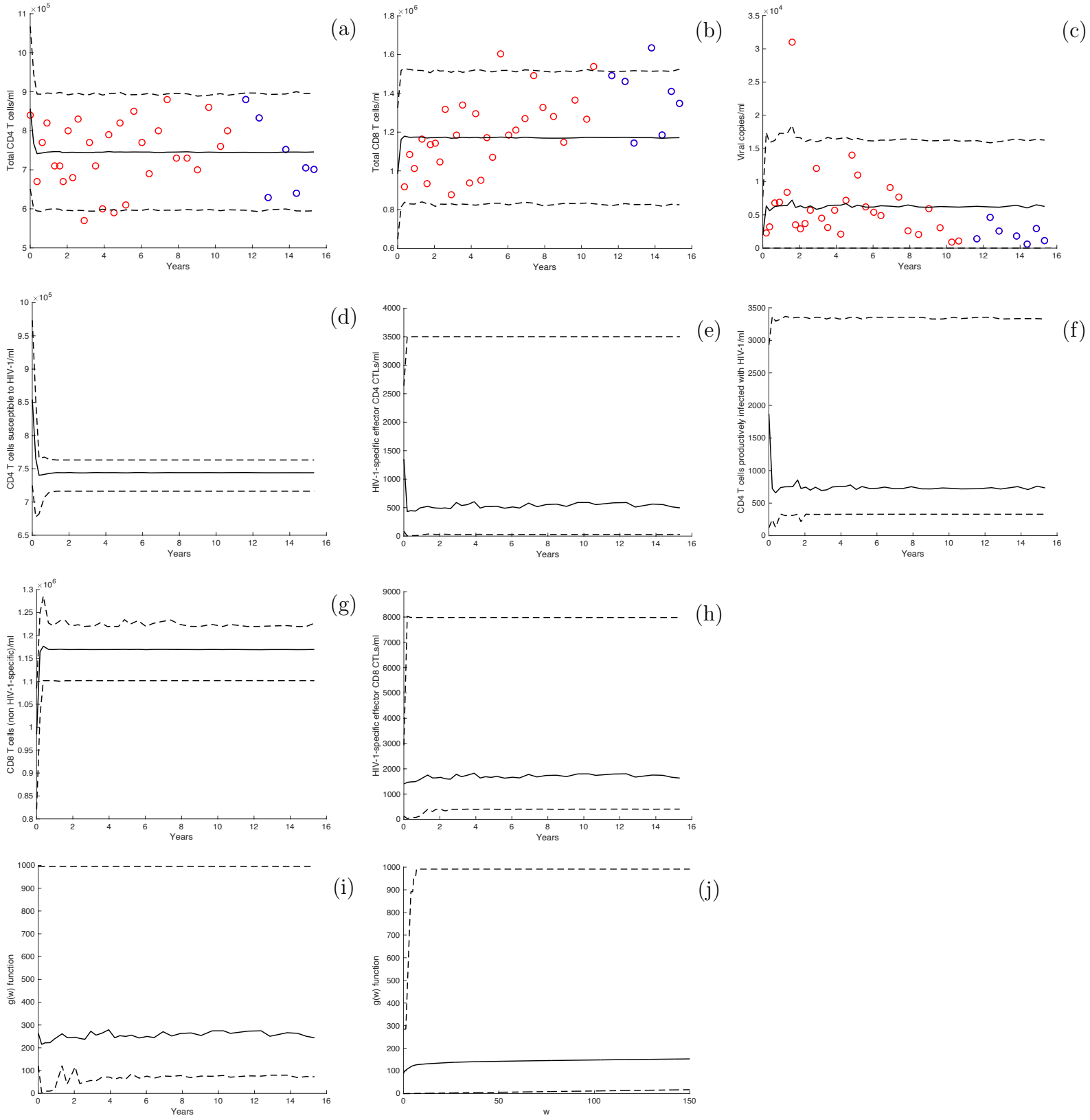

Figure 7.27: Modeling HIV-1 infection in the plasma for Patient 7: **(a)** total CD4 T cells/ml, **(b)** total CD8 T cells/ml, **(c)** viral copies/ml; **(d)** CD4 T cells susceptible to HIV-1/ml, **(e)** HIV-1-specific effector CD4 CTLs/ml, **(f)** CD4 T cells productively infected with HIV-1/ml; **(g)** CD8 T cells (non HIV-1-specific)/ml, and **(h)** HIV-1-specific effector CD8 CTLs/ml; **(i)** effector response function over time, and **(j)** effector response function over the number of effector CTLs. The predictive mean solution is given by the solid black curve, the 95% prediction interval is given by the dashed black curves, the circle points denote the fitted data, and the star points display the unfitted data.

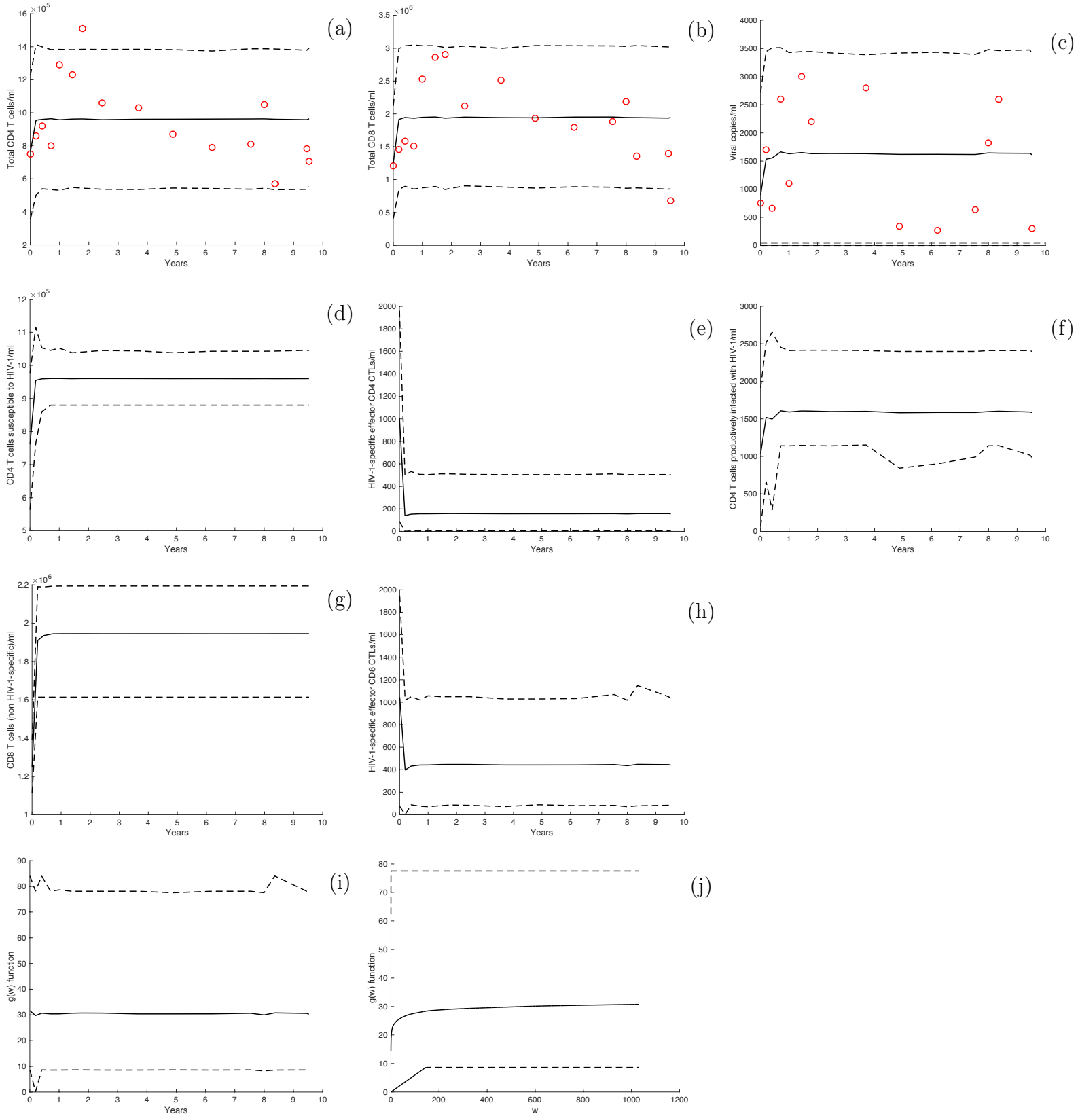

Figure 7.28: Modeling HIV-1 infection in the plasma for Patient 10: **(a)** total CD4 T cells/ml, **(b)** total CD8 T cells/ml, **(c)** viral copies/ml; **(d)** CD4 T cells susceptible to HIV-1/ml, **(e)** HIV-1-specific effector CD4 CTLs/ml, **(f)** CD4 T cells productively infected with HIV-1/ml; **(g)** CD8 T cells (non HIV-1-specific)/ml, and **(h)** HIV-1-specific effector CD8 CTLs/ml; **(i)** effector response function over time, and **(j)** effector response function over the number of effector CTLs. The predictive mean solution is given by the solid black curve, the 95% prediction interval is given by the dashed black curves, and the circle points denote the fitted data.

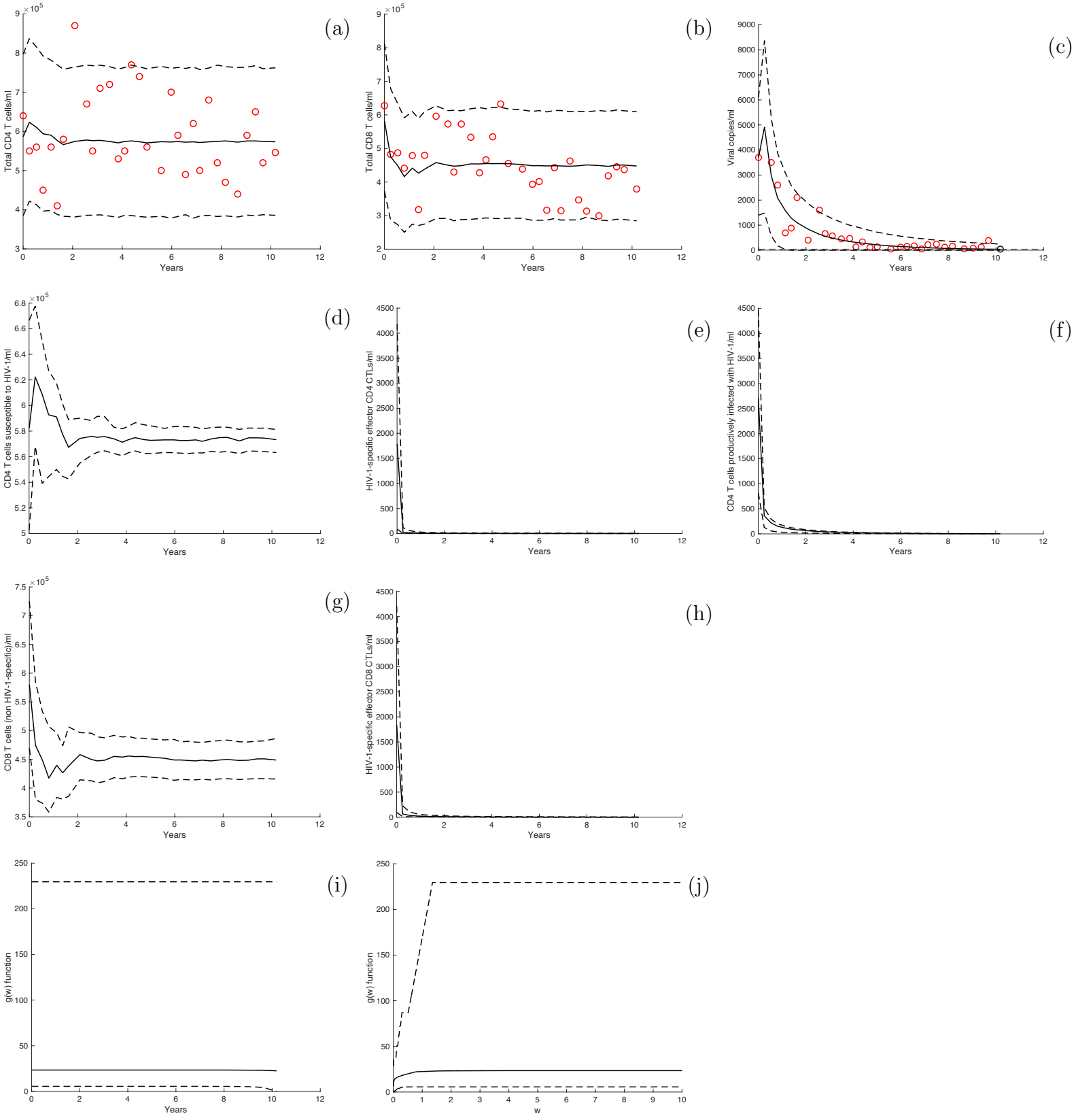

Figure 7.29: Modeling HIV-1 infection in the plasma for Patient 11: **(a)** total CD4 T cells/ml, **(b)** total CD8 T cells/ml, **(c)** viral copies/ml; **(d)** CD4 T cells susceptible to HIV-1/ml, **(e)** HIV-1-specific effector CD4 CTLs/ml, **(f)** CD4 T cells productively infected with HIV-1/ml; **(g)** CD8 T cells (non HIV-1-specific)/ml, and **(h)** HIV-1-specific effector CD8 CTLs/ml; **(i)** effector response function over time, and **(j)** effector response function over the number of effector CTLs. The predictive mean solution is given by the solid black curve, the 95% prediction interval is given by the dashed black curves, and the circle points denote the fitted data. (Note: the black points on the viral copies figure denote that the viral load was below detection and the value of each black point was the limit of detection at that time)

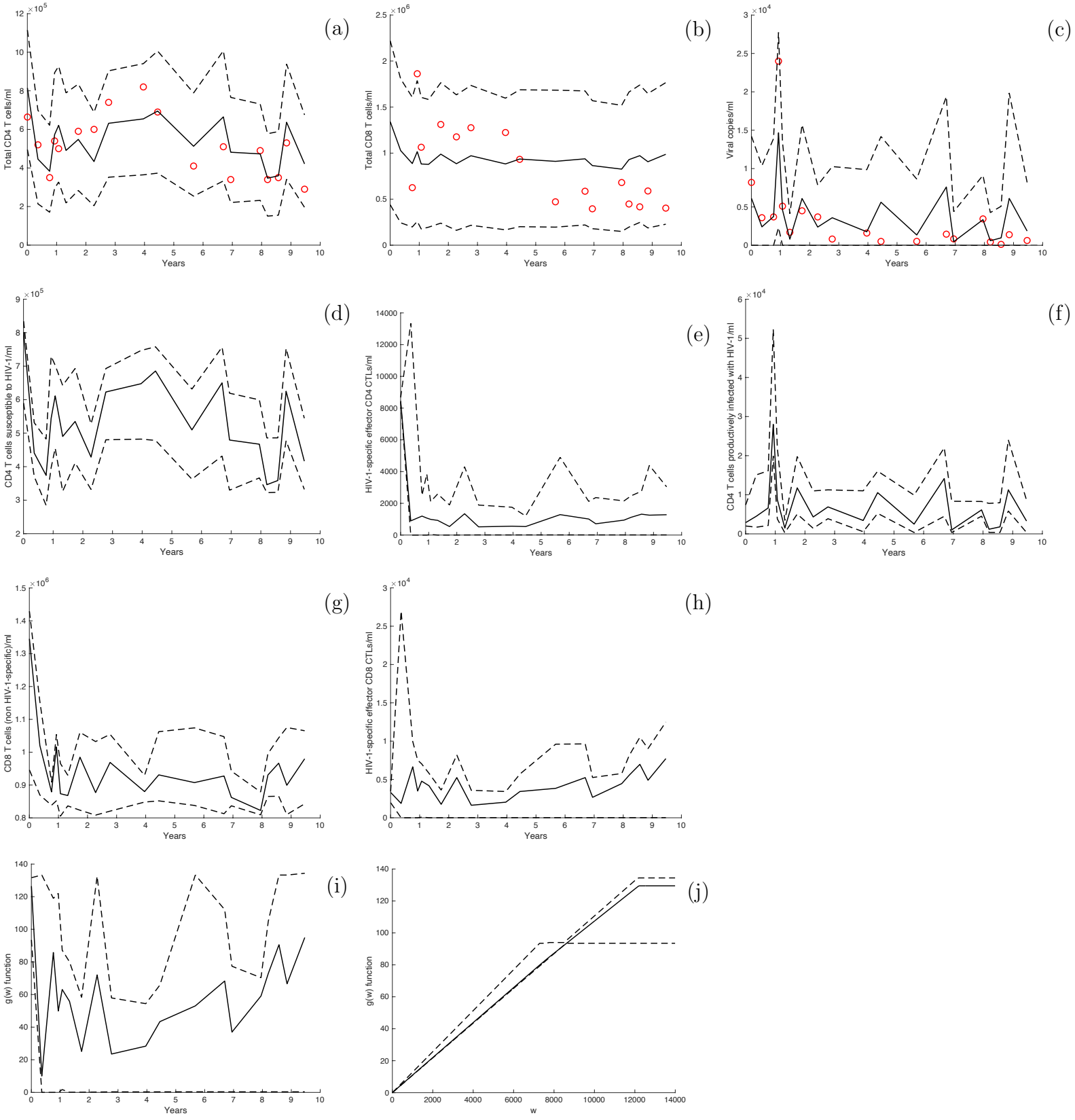

Figure 7.30: Modeling HIV-1 infection in the plasma for Patient 12: **(a)** total CD4 T cells/ml, **(b)** total CD8 T cells/ml, **(c)** viral copies/ml; **(d)** CD4 T cells susceptible to HIV-1/ml, **(e)** HIV-1-specific effector CD4 CTLs/ml, **(f)** CD4 T cells productively infected with HIV-1/ml; **(g)** CD8 T cells (non HIV-1-specific)/ml, and **(h)** HIV-1-specific effector CD8 CTLs/ml; **(i)** effector response function over time, and **(j)** effector response function over the number of effector CTLs. The predictive mean solution is given by the solid black curve, the 95% prediction interval is given by the dashed black curves, and the circle points denote the fitted data.

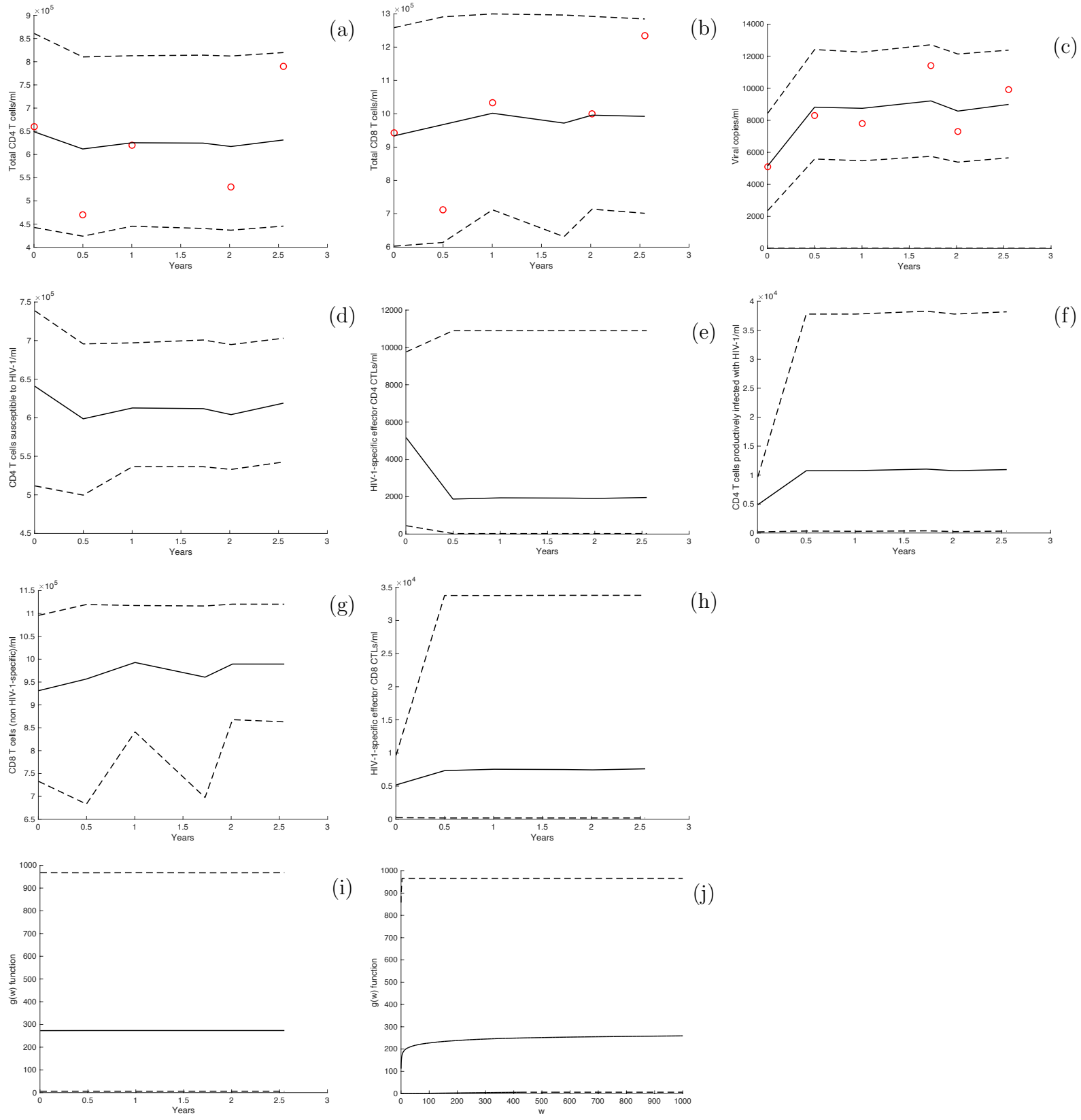

Figure 7.31: Modeling HIV-1 infection in the plasma for Patient 21: **(a)** total CD4 T cells/ml, **(b)** total CD8 T cells/ml, **(c)** viral copies/ml; **(d)** CD4 T cells susceptible to HIV-1/ml, **(e)** HIV-1-specific effector CD4 CTLs/ml, **(f)** CD4 T cells productively infected with HIV-1/ml; **(g)** CD8 T cells (non HIV-1-specific)/ml, and **(h)** HIV-1-specific effector CD8 CTLs/ml; **(i)** effector response function over time, and **(j)** effector response function over the number of effector CTLs. The predictive mean solution is given by the solid black curve, the 95% prediction interval is given by the dashed black curves, and the circle points denote the fitted data.

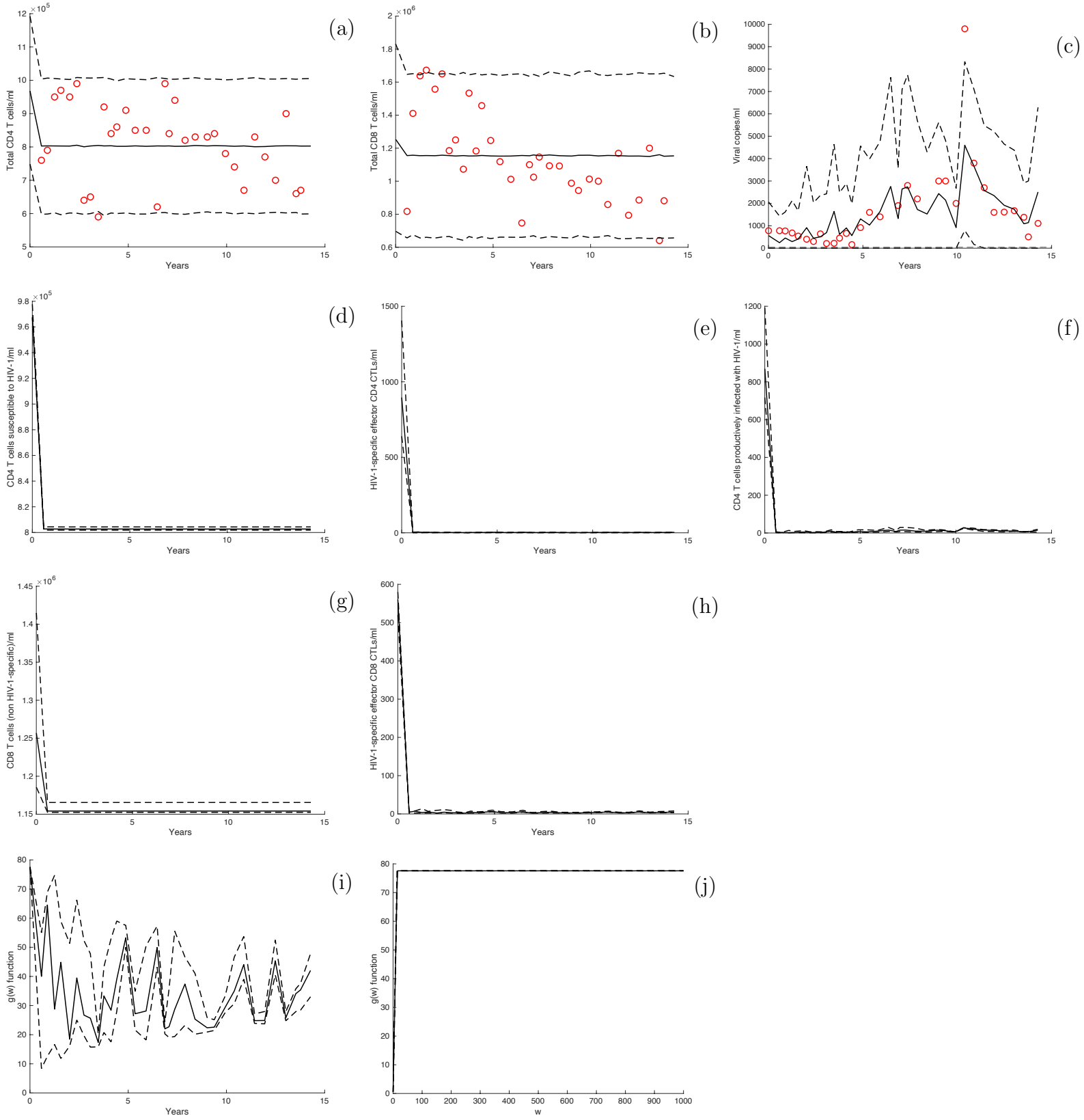

Figure 7.32: Modeling HIV-1 infection in the plasma for Patient 23: **(a)** total CD4 T cells/ml, **(b)** total CD8 T cells/ml, **(c)** viral copies/ml; **(d)** CD4 T cells susceptible to HIV-1/ml, **(e)** HIV-1-specific effector CD4 CTLs/ml, **(f)** CD4 T cells productively infected with HIV-1/ml; **(g)** CD8 T cells (non HIV-1-specific)/ml, and **(h)** HIV-1-specific effector CD8 CTLs/ml; **(i)** effector response function over time, and **(j)** effector response function over the number of effector CTLs. The predictive mean solution is given by the solid black curve, the 95% prediction interval is given by the dashed black curves, and the circle points denote the fitted data.

7.E Extended Fourier amplitude sensitivity test

The extended Fourier amplitude sensitivity test (eFAST) was used to determine the most important parameters in system (6.1) that explained the total CD4 T cells/ml, total CD8 T cells/ml, and viral copies/ml for each HIV-1 patient. The sensitivity analysis results for each patient are displayed in Sections 7.F.1 and 7.F.2.

eFAST is a variance-based global sensitivity analysis method. Global sensitivity analysis quantifies the importance of model parameters and the interactions of model parameters with respect to a specific model outcome [132]. Variance-based methods quantify the fraction of a model outcome's variance that can be explained by the variation of the model parameters [133, 134]. In eFAST, the model outcome variance is partitioned by varying different parameters at different frequencies, and then Fourier analysis is used to measure the strength of each parameter's frequency in the model outcome's variance [134]. Therefore, how strongly a parameter's frequency propagates through to the model outcome of interest is a measure that indicates the sensitivity of the model outcome of interest to the parameter [134]. In the eFAST method, the total-order sensitivity index was used to rank the importance of the model parameters to the outcome of interest; the total-order sensitivity index is a necessary and sufficient index to use for assessing the sensitivity of non-linear models [133]. The sum of the total-order sensitivity indexes is equal to 1 if the model is linear and greater than 1 if the model is non-linear [133]. The eFAST method is a recommended global sensitivity analysis method to use when non-monotonicities are present in the model outcomes, and global sensitivity methods such as partial rank correlation coefficient (PRCC) are less accurate when

non-monotonicities are present in the model outcomes [133, 134].

Since the total CD4 T cells/ml ($x(t) + x_E(t) + y(t)$), total CD8 T cells/ml ($z(t) + z_E(t)$), and viral copies/ml ($v(t)$) from the model output varies over time, a single measure given by the integration of total CD4 T cells/ml, total CD8 T cells/ml, and viral copies/ml over the time period was used as the model outcome of interest for the eFAST global sensitivity analysis method.

The sensitivity of the total CD4 T cells/ml, total CD8 T cells/ml, and viral copies/ml for each patient was assessed for the following parameters in system (6.1): $r_1, \mu_1, c, b, \beta, \delta, ka, a, \mu_2, \mu_3, \gamma, p, \mu_4, r_2, \mu_5$. A dummy parameter that does not affect the model was included in the sensitivity analysis in order to more accurately discern the important parameters [133, 134]. For the sensitivity analysis, the initial conditions in system (6.1) for each patient were fixed at their estimated maximum posterior values contained in Sections 7.D.4 and 7.D.5.

A relevant hyperrectangle for the parameters was chosen for each patient to run this global sensitivity analysis. The range of a $(1 - \alpha)100\%$ credible interval for each parameter from the Bayesian inference fitting for each patient was used to inform the end points of each side of the hyperrectangle. A hyperrectangle which has the same side values as a $(1-\alpha)100\%$ credible interval for each parameter will, in general, cover more high dimensional space than the posterior density bounded by the $(1 - \alpha)100\%$ credible interval values. As a result, the hyperrectangle will, in general, include parameter regions that correspond to very low posterior density values and these parameter regions can cause the numerical solving of system (6.1) to fail. In order to lessen the possibility of the numerical solver failing in the sensitivity analysis method, a 90% credible interval was used for each parameter from the Bayesian inference

fitting to inform the end points of each side of the hyperrectangle. For the following patients it was necessary to narrow the end points of each side of the hyperrectangle further in order to complete the sensitivity analysis: Patient 2, a 60% credible interval was used; Patient 6, a 80% credible interval was used; Patient 7, a 60% credible interval was used; Patient 14, a 65% credible interval was used; Patient 21, a 35% credible interval was used; and Patient 28, a 75% credible interval was used. The dummy parameter was always given the range from 1 to 10.

The eFAST method used in this study runs in the following way [134, 133, 135]:

- a sinusoidal function of a certain frequency is used for each parameter, which is called a search curve
    - N_s denotes the total number of samples on each search curve
- since the sinusoidal function is a symmetric function, the sinusoidal function will at some point repeat the same samples, and hence a resampling technique using a phase-shift is employed to be more efficient with model evaluations
    - N_r denotes the number of times search curve resampling is completed for each parameter
- Fourier analysis is done independently over each of the search curves for each parameter obtaining N_r number of total-order sensitivity index samples for each parameter

- a multiple comparison test is used to test if the total-order sensitivity index samples for each model parameter are statistically greater than the total-order sensitivity index samples of the dummy parameter
    - one-way ANOVA is used first to test if the means of the total-order sensitivity index for each parameter are statistically not all the same
    - if the one-way ANOVA test concludes that the means are statistically not all the same, then a one-sided Dunnett's test was used with the control as the total-order sensitivity index from the dummy parameter and alternative hypothesis that the mean total-order sensitivity index for the compared model parameter is statistically greater than the mean total-order sensitivity index from the dummy parameter

The eFAST method sampling was completed using an eFAST MATLAB implementation code [136]. Once the eFAST method sampling was performed for each patient the multiple comparison test was run on MATLAB using the functions "anova1" and "multcompare". A previous sensitivity analysis study determined that $N_r = 40$ was an appropriate value to find the important parameters in a eFAST method sampling [133] and the value of $N_r = 40$ was used in this study. Furthermore, the previous sensitivity analysis study advised using the following settings for eFast [133]: $M = 4$, which is the maximum number of terms in the truncated Fourier series; $\omega_{\max} = 8$, which is the largest frequency that gets assigned to a parameter currently being examined for sensitivity to the outcome of interest; a well-balanced sampling scheme satisfies the equation $\omega_{\max} = \frac{N_s - N_R - 1}{2M}$ and this equation implies, given the other values, that $N_s = 105$. These recommendations were used in the

eFAST method sampling for this study.

7.F Sensitivity analysis plots for each patient

7.F.1 HIV-1 Elite Controller patients sensitivity analysis plots

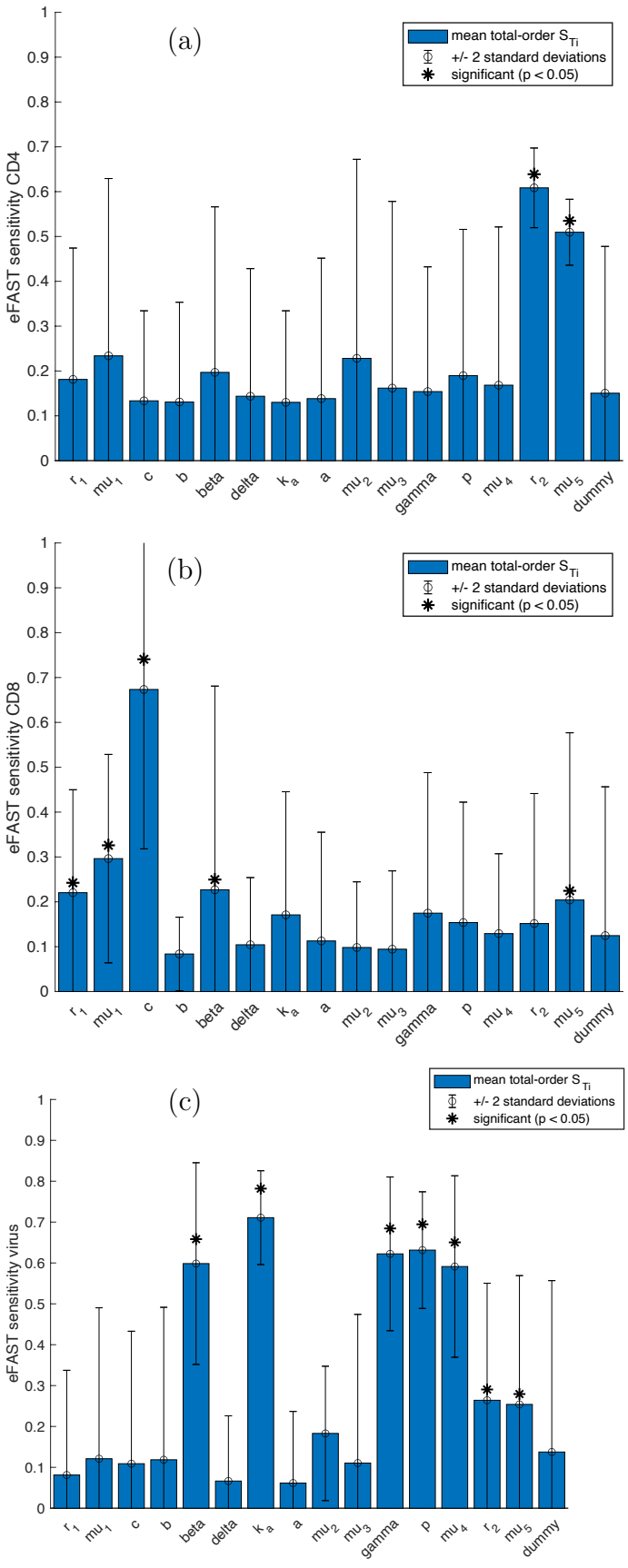

Figure 7.33: eFAST sensitivity analysis for the **(a)** total CD4 T cells, **(b)** total CD8 T cells and **(c)** viral load for Patient 1. The blue bar denotes the mean total-order S_{T_i} and the error bar displays +/- 2 standard deviations for each parameter. The symbol $*$ indicates parameters with total-order values significantly different ($p < 0.05$) than the dummy parameter.

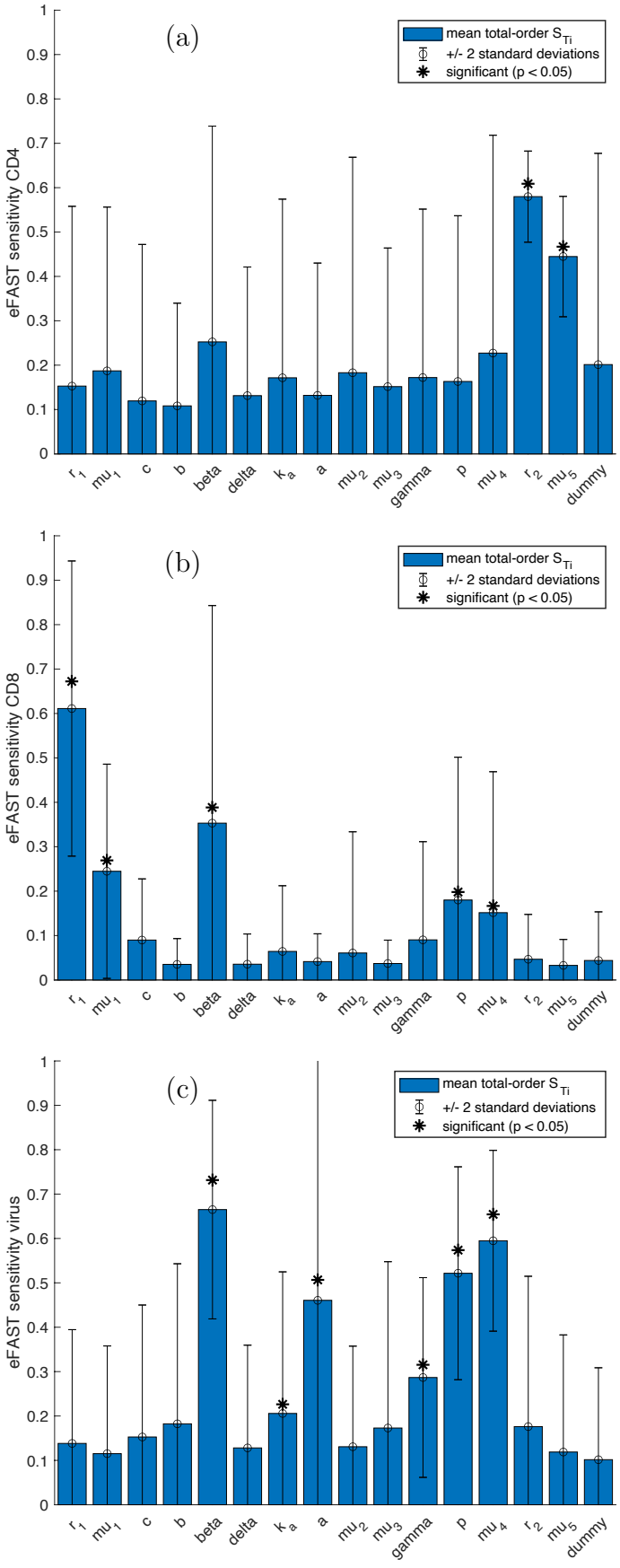

Figure 7.34: eFAST sensitivity analysis for the **(a)** total CD4 T cells, **(b)** total CD8 T cells and **(c)** viral load for Patient 6. The blue bar denotes the mean total-order S_{T_i} and the error bar displays +/- 2 standard deviations for each parameter. The symbol $*$ indicates parameters with total-order values significantly different ($p < 0.05$) than the dummy parameter.

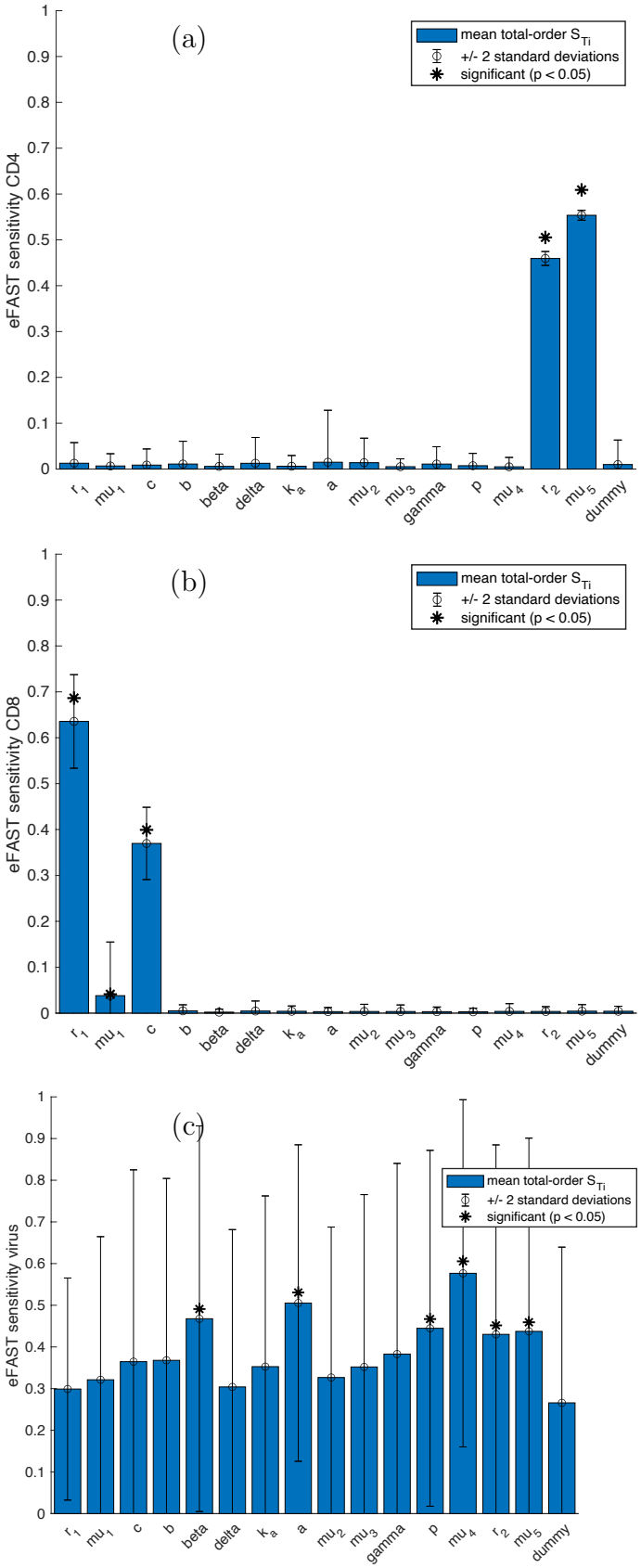

Figure 7.35: eFAST sensitivity analysis for the **(a)** total CD4 T cells, **(b)** total CD8 T cells and **(c)** viral load for Patient 14. The blue bar denotes the mean total-order S_{T_i} and the error bar displays +/- 2 standard deviations for each parameter. The symbol $*$ indicates parameters with total-order values significantly different ($p < 0.05$) than the dummy parameter.

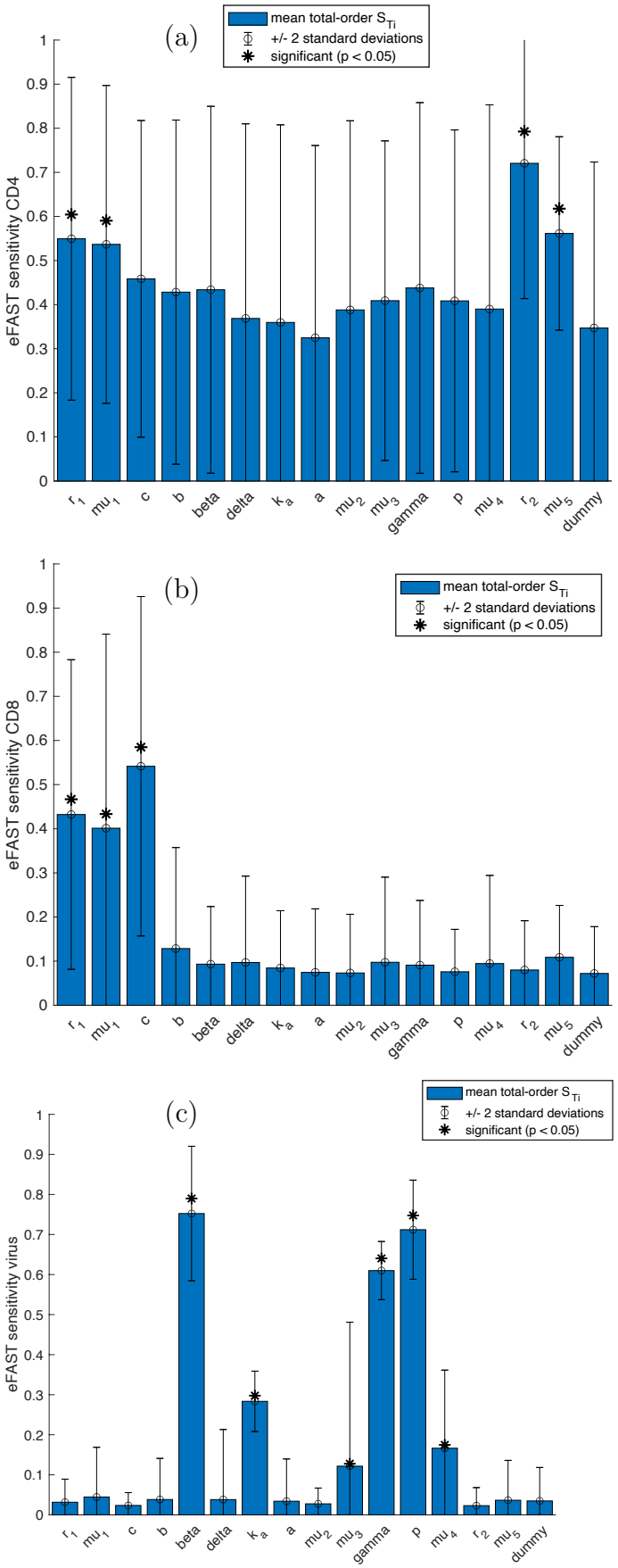

Figure 7.36: eFAST sensitivity analysis for the **(a)** total CD4 T cells, **(b)** total CD8 T cells and **(c)** viral load for Patient 16. The blue bar denotes the mean total-order S_{T_i} and the error bar displays +/- 2 standard deviations for each parameter. The symbol $*$ indicates parameters with total-order values significantly different ($p < 0.05$) than the dummy parameter.

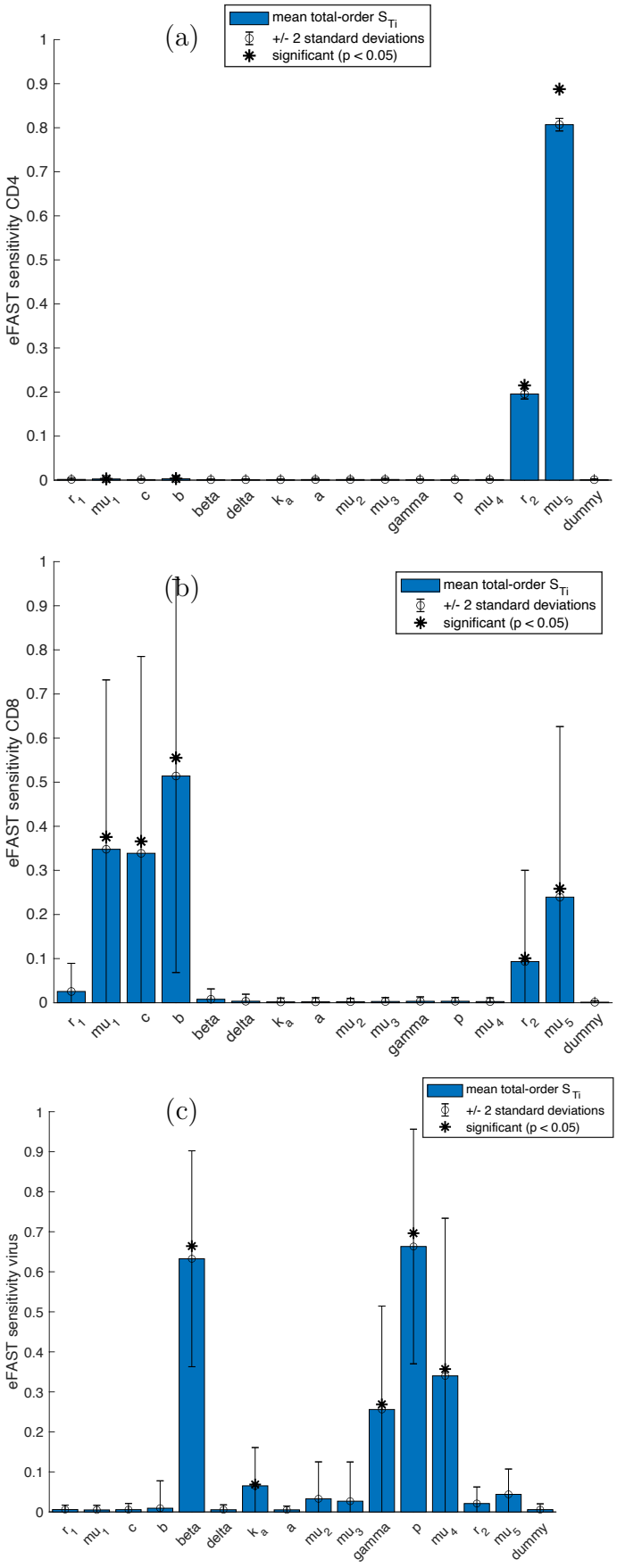

Figure 7.37: eFAST sensitivity analysis for the **(a)** total CD4 T cells, **(b)** total CD8 T cells and **(c)** viral load for Patient 17. The blue bar denotes the mean total-order S_{T_i} and the error bar displays +/- 2 standard deviations for each parameter. The symbol $*$ indicates parameters with total-order values significantly different ($p < 0.05$) than the dummy parameter.

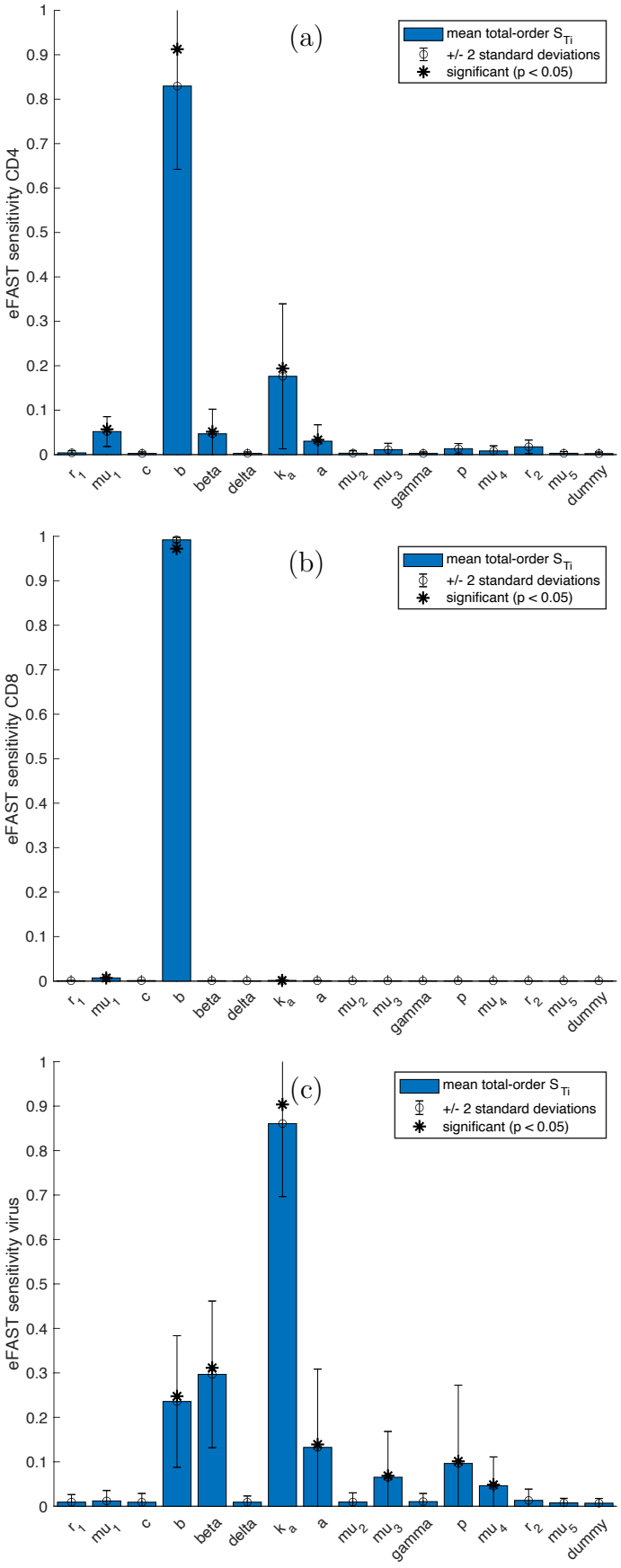

Figure 7.38: eFAST sensitivity analysis for the **(a)** total CD4 T cells, **(b)** total CD8 T cells and **(c)** viral load for Patient 18. The blue bar denotes the mean total-order S_{T_i} and the error bar displays +/- 2 standard deviations for each parameter. The symbol $*$ indicates parameters with total-order values significantly different ($p < 0.05$) than the dummy parameter.

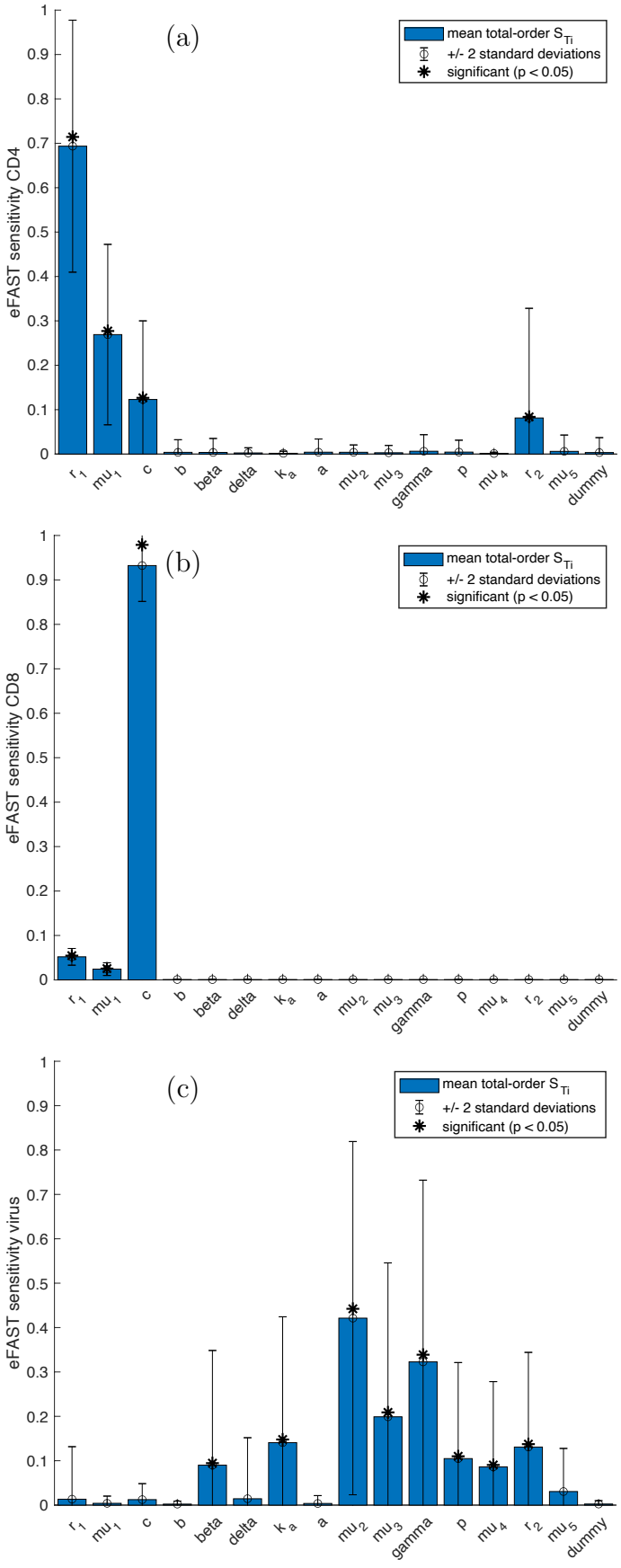

Figure 7.39: eFAST sensitivity analysis for the **(a)** total CD4 T cells, **(b)** total CD8 T cells and **(c)** viral load for Patient 24. The blue bar denotes the mean total-order S_{T_i} and the error bar displays +/- 2 standard deviations for each parameter. The symbol $*$ indicates parameters with total-order values significantly different ($p < 0.05$) than the dummy parameter.

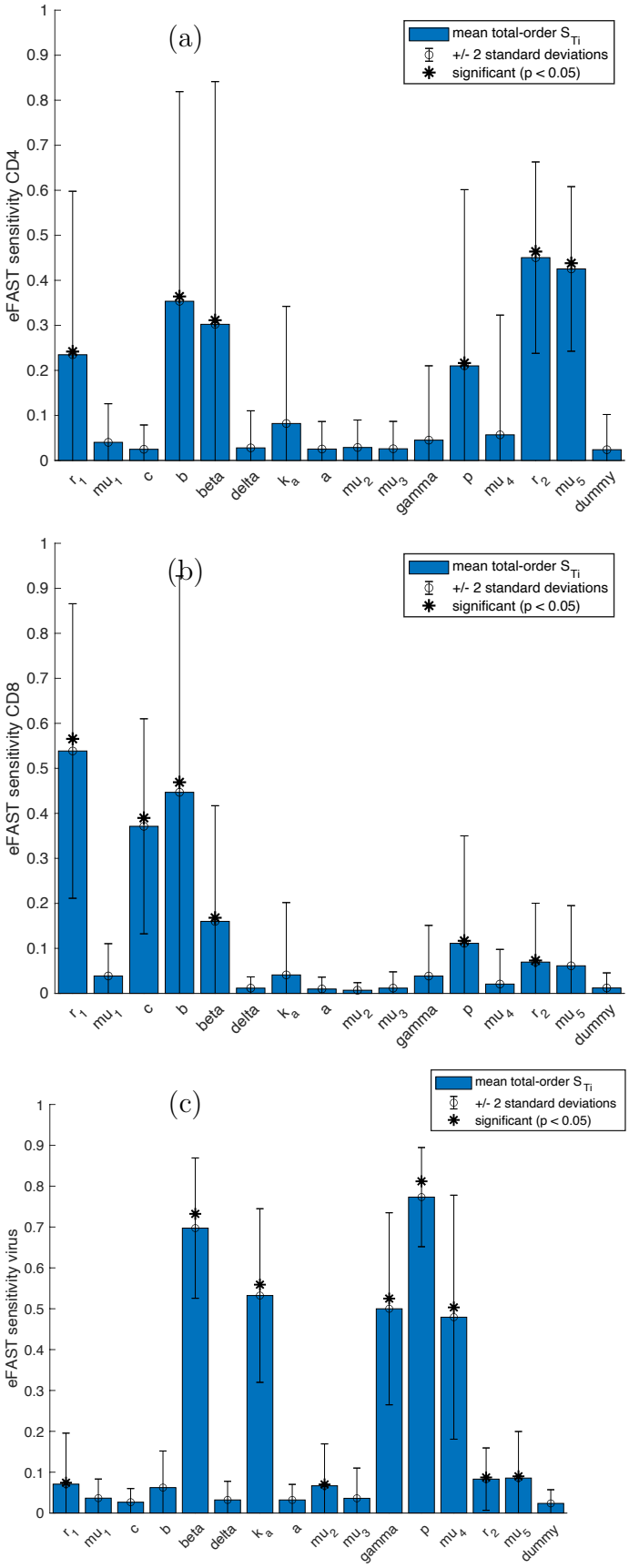

Figure 7.40: eFAST sensitivity analysis for the **(a)** total CD4 T cells, **(b)** total CD8 T cells and **(c)** viral load for Patient 25. The blue bar denotes the mean total-order S_{T_i} and the error bar displays +/- 2 standard deviations for each parameter. The symbol $*$ indicates parameters with total-order values significantly different ($p < 0.05$) than the dummy parameter.

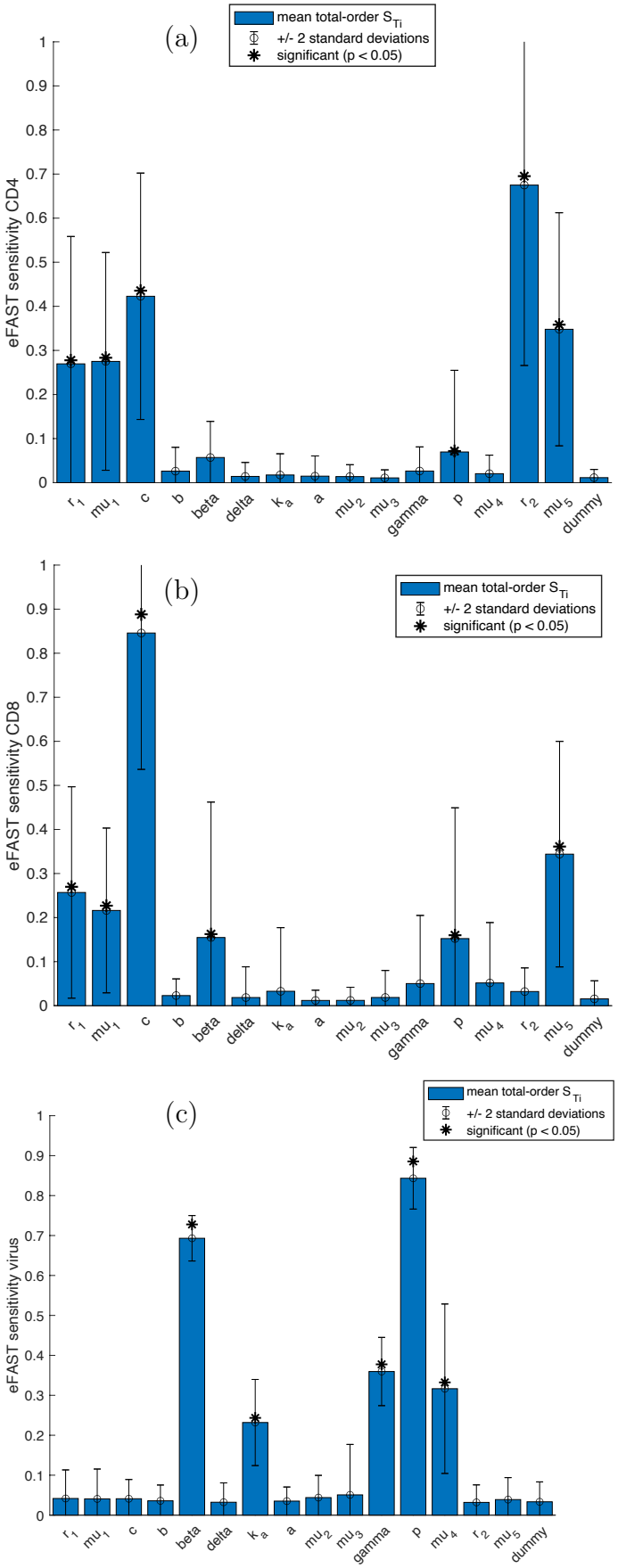

Figure 7.41: eFAST sensitivity analysis for the **(a)** total CD4 T cells, **(b)** total CD8 T cells and **(c)** viral load for Patient 28. The blue bar denotes the mean total-order S_{T_i} and the error bar displays +/- 2 standard deviations for each parameter. The symbol $*$ indicates parameters with total-order values significantly different ($p < 0.05$) than the dummy parameter.

7.F.2 HIV-1 patient comparison group sensitivity analysis plots

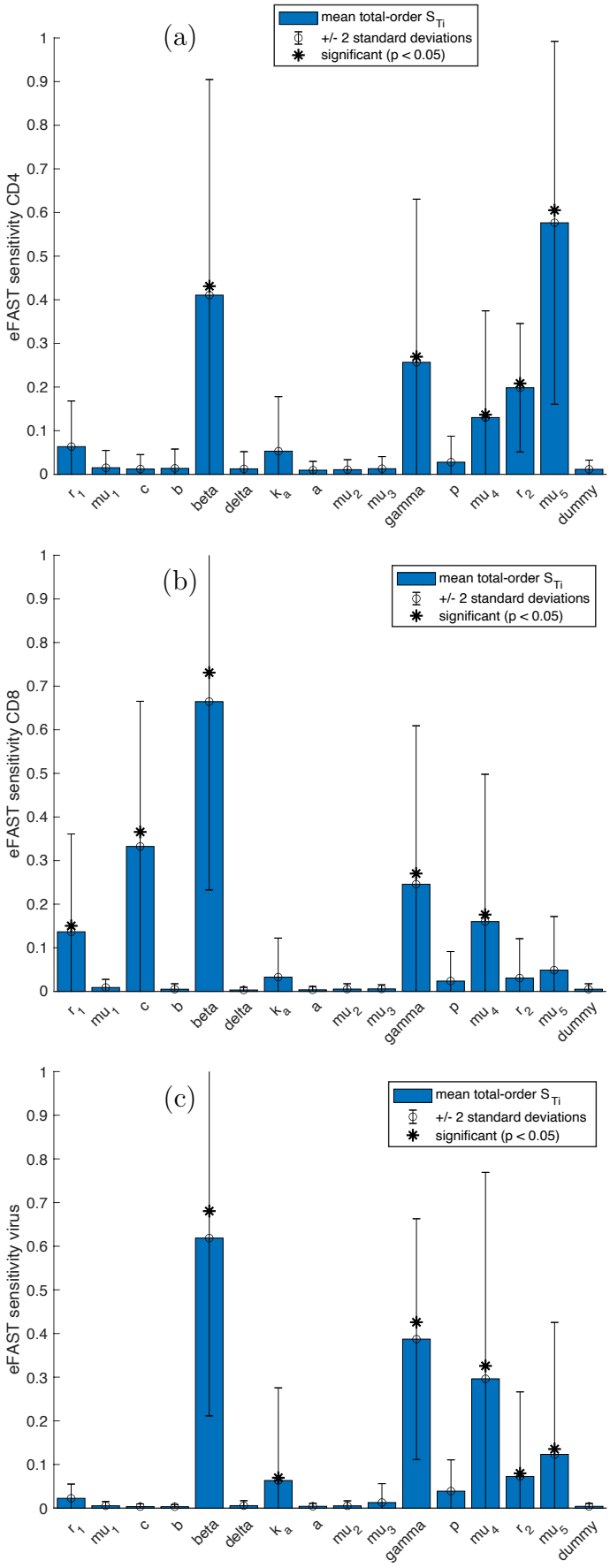

Figure 7.42: eFAST sensitivity analysis for the **(a)** total CD4 T cells, **(b)** total CD8 T cells and **(c)** viral load for Patient 2. The blue bar denotes the mean total-order S_{T_i} and the error bar displays +/- 2 standard deviations for each parameter. The symbol $*$ indicates parameters with total-order values significantly different ($p < 0.05$) than the dummy parameter.

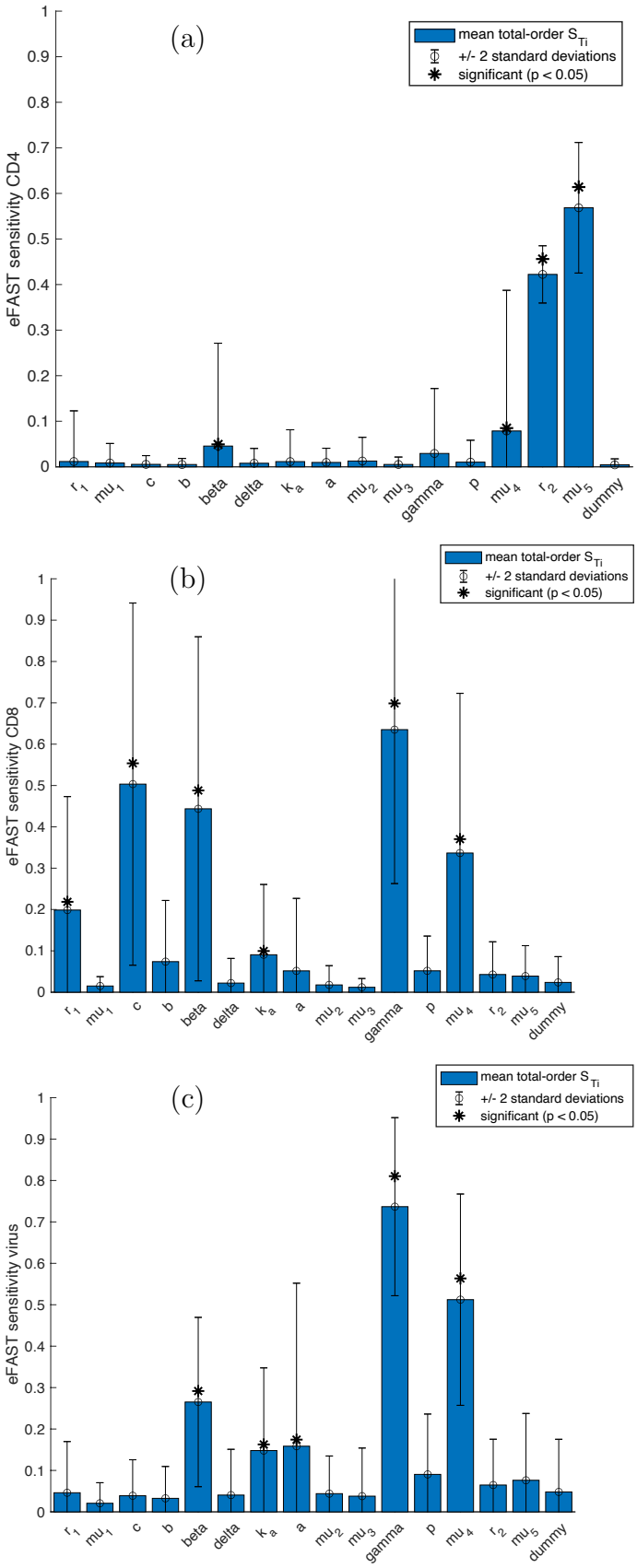

Figure 7.43: eFAST sensitivity analysis for the **(a)** total CD4 T cells, **(b)** total CD8 T cells and **(c)** viral load for Patient 7. The blue bar denotes the mean total-order S_{T_i} and the error bar displays +/- 2 standard deviations for each parameter. The symbol $*$ indicates parameters with total-order values significantly different ($p < 0.05$) than the dummy parameter.

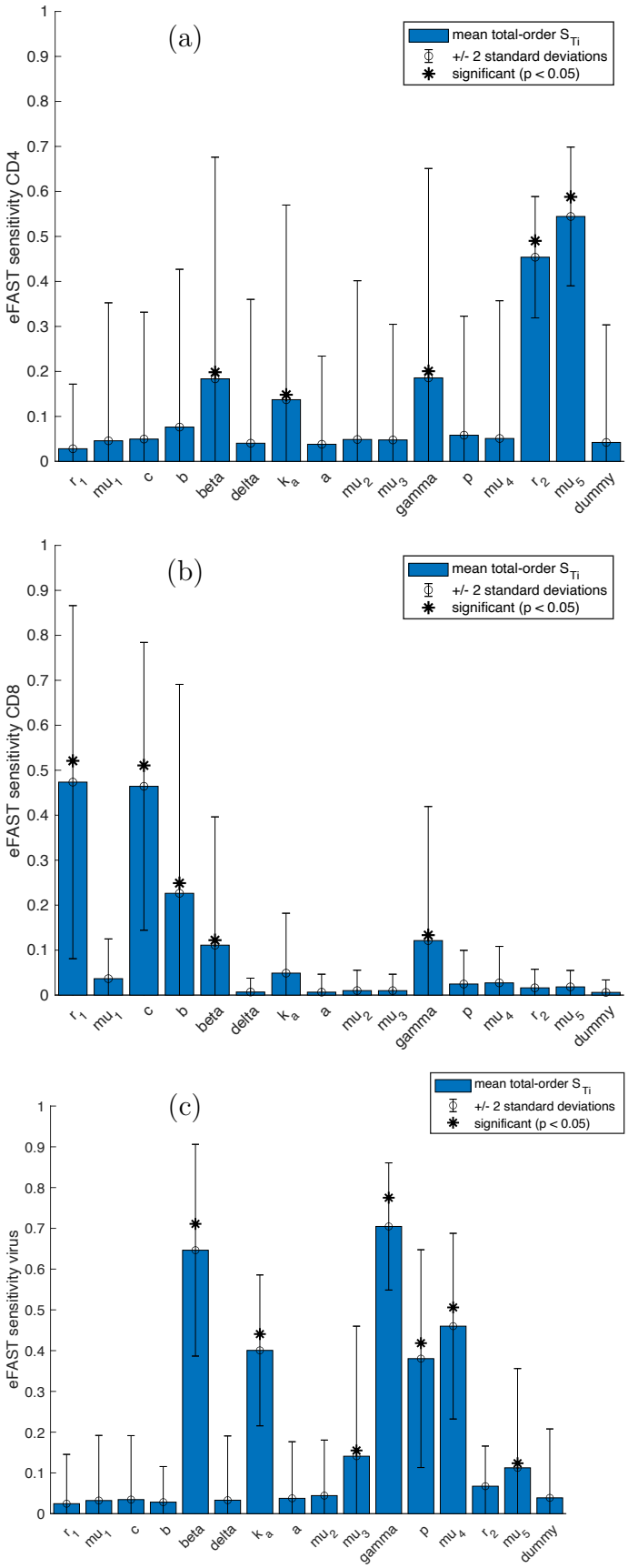

Figure 7.44: eFAST sensitivity analysis for the **(a)** total CD4 T cells, **(b)** total CD8 T cells and **(c)** viral load for Patient 10. The blue bar denotes the mean total-order S_{T_i} and the error bar displays +/- 2 standard deviations for each parameter. The symbol $*$ indicates parameters with total-order values significantly different ($p < 0.05$) than the dummy parameter.

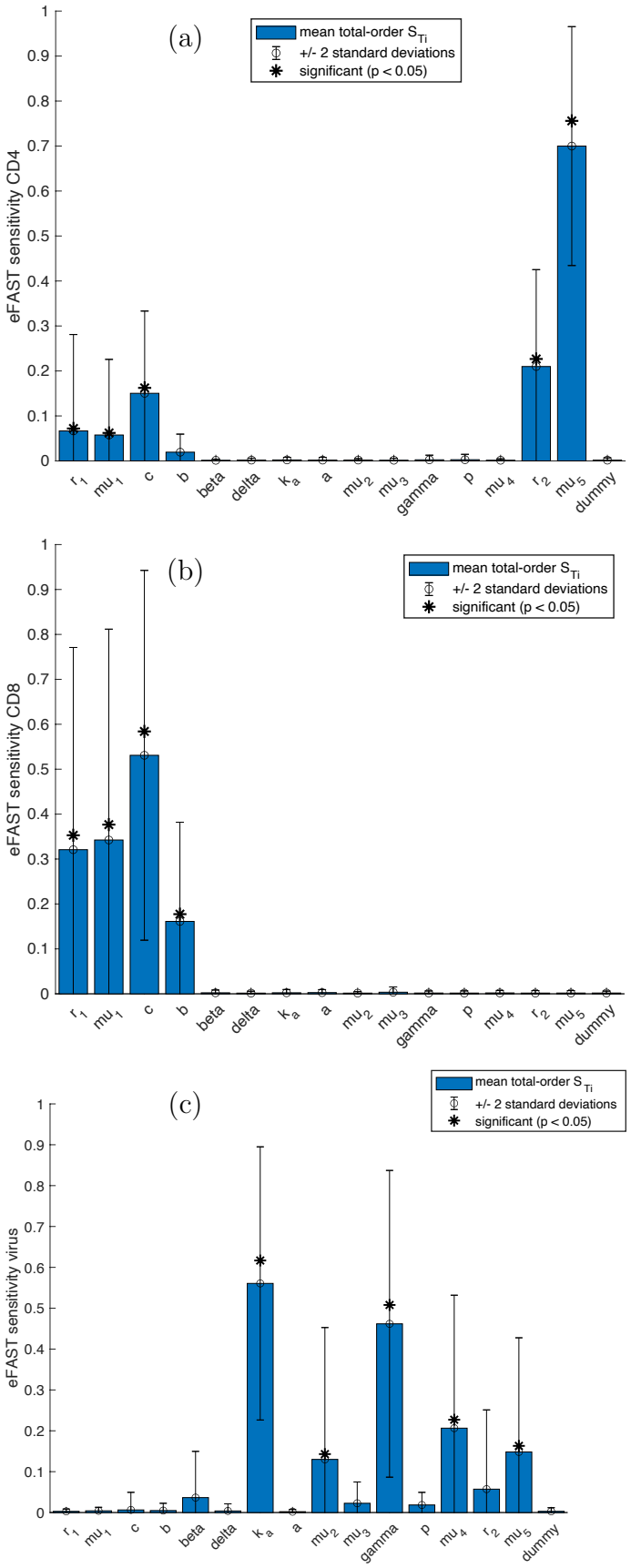

Figure 7.45: eFAST sensitivity analysis for the **(a)** total CD4 T cells, **(b)** total CD8 T cells and **(c)** viral load for Patient 11. The blue bar denotes the mean total-order S_{T_i} and the error bar displays +/- 2 standard deviations for each parameter. The symbol $*$ indicates parameters with total-order values significantly different ($p < 0.05$) than the dummy parameter.

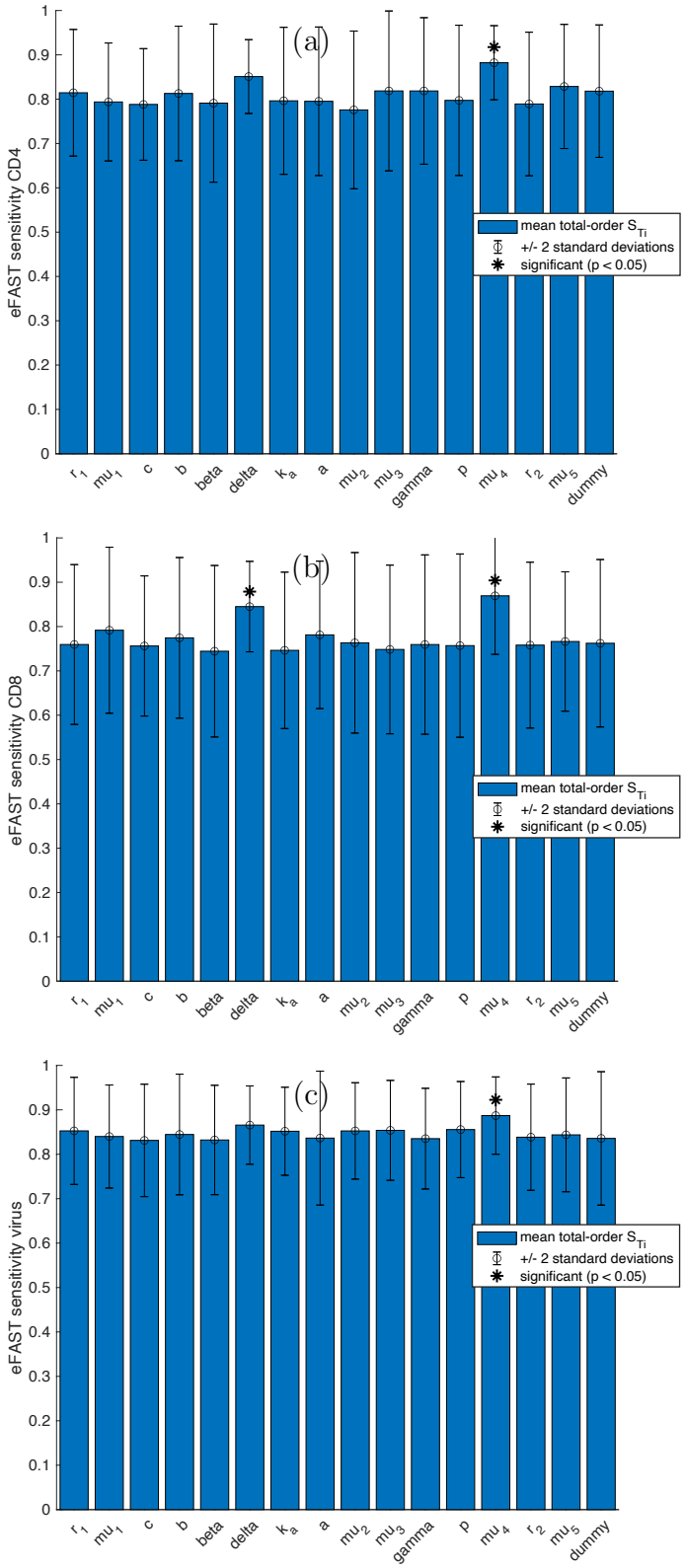

Figure 7.46: eFAST sensitivity analysis for the **(a)** total CD4 T cells, **(b)** total CD8 T cells and **(c)** viral load for Patient 12. The blue bar denotes the mean total-order S_{T_i} and the error bar displays +/- 2 standard deviations for each parameter. The symbol $*$ indicates parameters with total-order values significantly different ($p < 0.05$) than the dummy parameter.

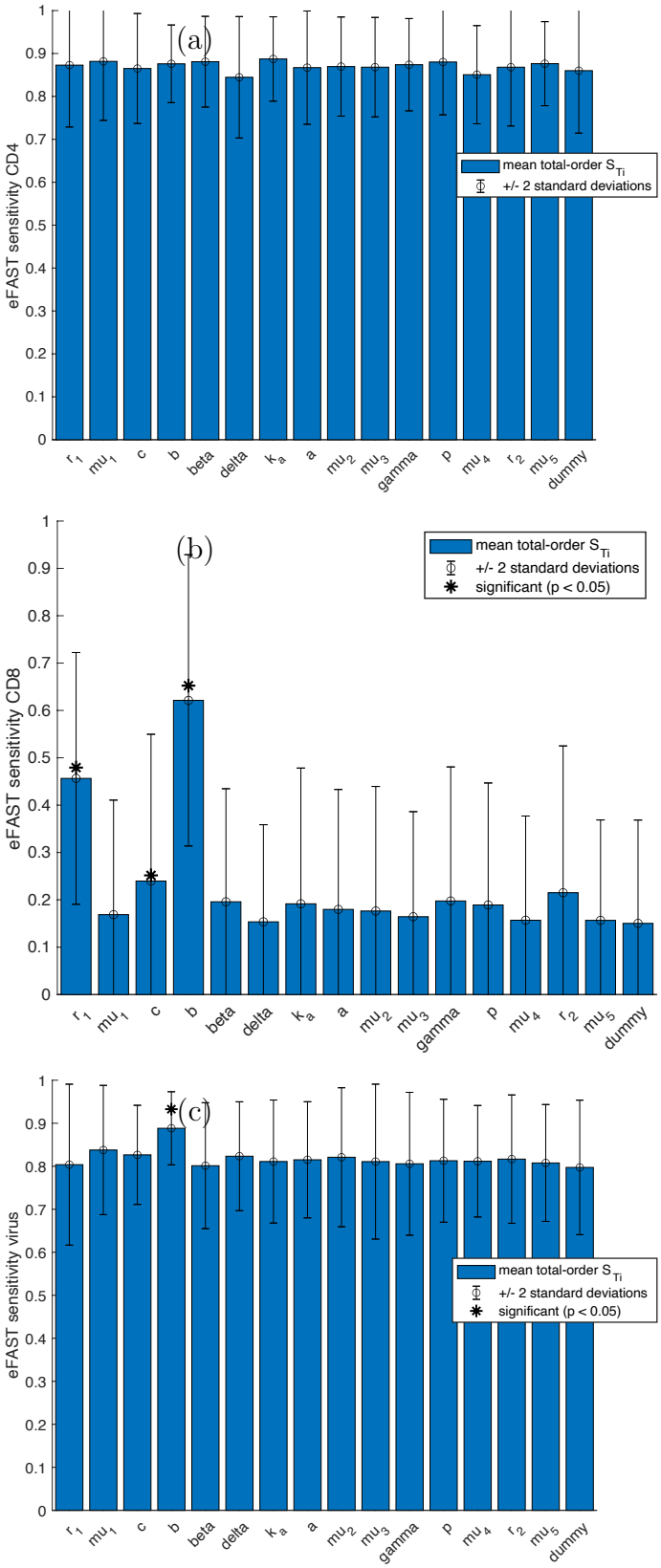

Figure 7.47: eFAST sensitivity analysis for the **(a)** total CD4 T cells, **(b)** total CD8 T cells and **(c)** viral load for Patient 21. The blue bar denotes the mean total-order S_{T_i} and the error bar displays +/- 2 standard deviations for each parameter. The symbol $*$ indicates parameters with total-order values significantly different ($p < 0.05$) than the dummy parameter.

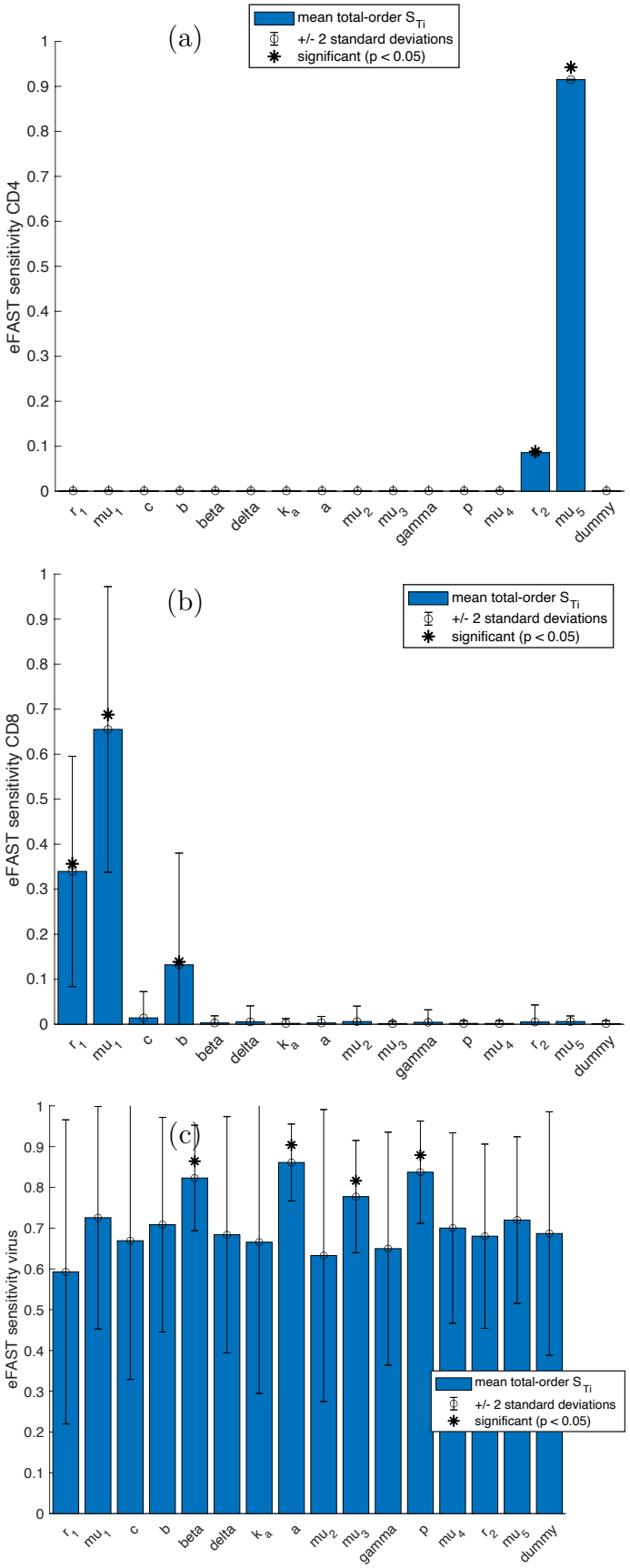

Figure 7.48: eFAST sensitivity analysis for the **(a)** total CD4 T cells, **(b)** total CD8 T cells and **(c)** viral load for Patient 23. The blue bar denotes the mean total-order S_{T_i} and the error bar displays +/- 2 standard deviations for each parameter. The symbol $*$ indicates parameters with total-order values significantly different ($p < 0.05$) than the dummy parameter.

Chapter 8

Conclusion

This thesis has presented a detailed methodology for completing dynamical system parameter estimation using Bayesian inference and this methodology was used to investigate critical HIV-1 therapeutic initiatives: "Shock and Kill" strategy in the brain and the natural control of the virus in the plasma. Both the HIV-1 brain macrophage infection model (4.1) and the HIV-1 plasma infection model (6.1) recapitulated the observed infection process in the brain and plasma, respectively.

The HIV-1 brain macrophage infection model was the first mathematical model to qualitatively analyze the dynamics of latently and productively infected cells in the brain during HIV-1 and SIV infection and quantify the size of the latent reservoir in the brain for SIV animal studies. Moreover, after this latent reservoir was estimated, the effect of LRA in the brain was evaluated and the mathematical model indicated that there exists a biologically realistic parameter regime where the "Shock and Kill" therapy strategy is safe and effective in the brain.

A full mathematical analysis of the "Shock and Kill" model given by equa-

tions (4.5) is warranted to further investigate solutions that lead to a safe and effective "Shock and Kill" strategy in the brain. Indeed, developing mathematical models that incorporate a more realistic additional kill term in equations (4.5) to kill reactivated infected brain macrophages by host immune responses is needed to test different treatment strategies. Potential strategies could be to bolster the CD8+ T cell response in the brain to kill reactivated infected brain macrophages or to strengthen the innate mechanisms in the brain that lead to programmed cell death in reactivated infected brain macrophages. Using HIV-1 post-mortem patient data and other SIV animal models such as ones that use Indian rhesus macaques that have a longer duration of infection would assist in further validating the qualitative behaviors of the mathematical models for HIV-1 brain infection.

The HIV-1 plasma infection model was the first HIV-1 mathematical model to consider both effector CD4 CTLs' and effector CD8 CTLs' impact on HIV-1 disease and other diseases present in each patient, and this was the first mathematical modeling study to directly estimate the differences between a group of HIV-1 Elite Controllers with a comparison group of HIV-1 patients using empiric data. The Elite Controller group was found to have a stronger antiviral immune response than the comparison group. In contrast, the comparison group was found to have more chronic immune activation but a less effective immune response. The Elite Controller immune response estimates provided in this study quantifies a biologically realistic optimal immune response goal for HIV-1 therapeutic initiatives.

It would be useful to incorporate cART into the HIV-1 plasma infection model and fit the HIV-1 plasma infection model during ART-naïve and cART time periods for each patient and note the difference cART has on the an-

tiviral immune response of the patients. If plasma viral DNA measurements were available for HIV-1 Elite Controller patients from other clinics, it would be beneficial to include a latent compartment into system (6.1) and estimate the number of CD4 T cells latently infected with HIV-1 for these other patients. Given that macrophages have a significant role in the formation of viral reservoirs, if plasma viral DNA measurements were available, the inclusion of macrophage compartments into system (6.1) would be enlightening to further assess the size of the latent HIV-1 reservoir. Fitting system (6.1) with the possible modifications mentioned to a larger group of HIV-1 Elite Controllers and HIV-1 comparison patients from several clinics would be an insightful next step to further confirm the important components of the Elite Controller immune response and provide additional biologically realistic immune response estimates to help with HIV-1 therapeutic objectives.

Bibliography

[1] W. C. Roda, M. Y. Li, M. S. Akinwumi, E. L. Asahchop, B. B. Gelman, K. W. Witwer, and C. Power, "Modeling brain lentiviral infections during antiretroviral therapy in aids," *J Neurovirol*, vol. 23, no. 4, pp. 577–586, 2017.

[2] W. C. Roda, "Bayesian inference for dynamical systems," *Infect Dis Model*, vol. 5, pp. 221–232, 2020 (Reproduced with permission from KeAi Communications Co., Ltd).

[3] W. C. Roda, M. B. Varughese, D. Han, and M. Y. Li, "Why is it difficult to accurately predict the covid-19 epidemic?," *Infect Dis Model*, vol. 5, pp. 271–281, 2020 (Reproduced with permission from KeAi Communications Co., Ltd).

[4] W. C. Roda, S. Liu, C. Power, and M. Y. Li, "Modeling the effects of latency reversing drugs during hiv-1 and siv brain infection with implications for the "shock and kill" strategy," *Bull Math Biol*, vol. 83, no. 4, p. 39, 2021 (Reproduced with permission from Springer Nature).

[5] E. F. Balcom, W. C. Roda, E. A. Cohen, M. Y. Li, and C. Power, "Hiv-1 persistence in the central nervous system: viral and host determinants during antiretroviral therapy," *Curr Opin Virol*, vol. 38, pp. 54–62, 2019.

[6] M. Alluqmani, W. Roda, M. Qqrmli, G. Blevins, F. Giuliani, and C. Power, "Differential disease phenotypes and progression in relapsing-remitting multiple sclerosis: comparative analyses of single canadian and saudi arabian clinics," *BMC Neurol*, vol. 21, no. 295, 2021.

[7] N. Mohammadzadeh, W. Roda, W. G. Branton, J. Clain, H. Rabezanahary, O. Zghidi-Abouzid, and B. B. Gelman, "Lentiviral infections persist in brain despite effective antiretroviral therapy and neuroimmune activation," *mBio*, vol. 12, no. 6, p. e0278421, 2021.

[8] A. S. Ciupeanu, M. Varughese, W. C. Roda, D. Han, Q. Cheng, and M. Y. Li, "Mathematical modeling of the dynamics of covid-19 variants

of concern: asymptotic and finite-time perspectives," *Infect Dis Model*, vol. 7, no. 4, pp. 581–596, 2022.

[9] W. C. Roda and D. Han, *MatlabDiffNestAlg: V1.4 (1.4)*. Zenodo, 2023.

[10] W. C. Roda, "Modeling brain lentiviral infections during antiretroviral therapy in aids," Master's thesis, University of Alberta, 2016.

[11] B. J. Brewer, L. B. Partay, and G. Csanyi, "Diffusive nested sampling," *Stat Comput*, vol. 21, no. 4, pp. 649–656, 2011.

[12] B. J. Brewer and D. Foreman-Mackey, "Diffusive nested sampling in c++ and python," *J Stat*, vol. 86, no. 7, pp. 1–33, 2016.

[13] UNAIDS, "Global hiv and aids statistics." https://www.unaids.org/en/resources/fact-sheet, June 20 2023.

[14] C. W. Dieffenbach and A. S. Fauci, "Thirty years of hiv and aids: Future challenges and opportunities," *Ann Intern Med*, vol. 154, no. 11, pp. 766–771, 2011.

[15] A. S. Fauci and H. C. Lane, "Four decades of hiv/aids - much accomplished, much to do," *N Engl J Med*, vol. 383, no. 1, pp. 1–4, 2020.

[16] S. G. Deeks, J. Overbaugh, A. Phillips, and S. Buchbinder, "Hiv infection," *Nat Rev Dis Primers*, vol. 1, pp. 1–22, 2015.

[17] G. van Marle, D. L. Church, F. van der Meer, and M. J. Gill, "Combating the hiv reservoirs," *Biotechnol Genet Eng Rev*, vol. 34, no. 1, pp. 76–89, 2018.

[18] H. Loucif, S. Gouard, X. Dagenais-Lussier, A. Murira, and J. V. G. S. Stager, C. Tremblay, "Deciphering natural control of hiv-1: A valuable strategy to achieve antiretroviral therapy termination," *Cytokine Growth Factor Rev*, vol. 40, pp. 90–98, 2018.

[19] E. Eisele and R. F. Siliciano, "Redefining the viral reservoirs that prevent hiv-1 eradication," *Immunity*, vol. 37, no. 3, pp. 377–88, 2012.

[20] A. Battistini and M. Sgarbanti, "Hiv-1 latency: an update of molecular mechanisms and therapeutic strategies," *Viruses*, vol. 6, no. 4, pp. 1715–1758, 2014.

[21] Y. Kim, J. L. Anderson, and S. R. Lewin, "Getting the "kill" into "shock and kill": Strategies to eliminate latent hiv," *Cell Host Microbe*, vol. 23, no. 1, pp. 14–26, 2018.

[22] A. Hargrave, A. S. Mustafa, A. Hanif, J. H. Tunio, and S. N. M. Hanif, "Current status of hiv-1 vaccines," *Vaccines (Basel)*, vol. 9, no. 9, p. 1026, 2021.

[23] E. J. Singer and N. M. Nemanim, "The persistence of hiv-associated neurocognitive disorder (hand) in the era of combined antiretroviral therapy (cart)," in *Global Virology II - HIV and NeuroAIDS* (P. Shapshak, A. Levine, B. Foley, C. Somboonwit, E. Singer, F. Chiappelli, and J. T. Sinnott, eds.), pp. 375–403, Springer Science+Business Media, LLC, 2017.

[24] L. Annamalai, V. Bhaskar, D. R. Pauley, H. Knight, K. Williams, M. Lentz, E. Ratai, S. V. Westmoreland, R. G. González, and S. P. O'Neil, "Impact of short-term combined antiretroviral therapy on brain virus burden in simian immunodeficiency virus-infected and cd8+ lymphocyte-depleted rhesus macaques," *Am J Pathol*, vol. 177, no. 2, pp. 777–791, 2010.

[25] M. K. Patrick, J. B. Johnston, and C. Power, "Lentiviral neuropathogenesis: comparative neuroinvasion, neurotropism, neurovirulence, and host neurosusceptibility," *J Virol*, vol. 76, no. 16, pp. 7923–7931, 2002.

[26] F. González-Scarano and J. Martin-Garcia, "The neuropathogenesis of aids," *Nat Rev Immunol*, vol. 5, pp. 69–81, 2005.

[27] J. H. Campbell, E. M. Ratai, P. Autissier, D. J. Nolan, S. Tse, A. D. Miller, R. G. González, M. Salemi, T. H. Burdo, and K. C. Williams, "Anti-α4 antibody treatment blocks virus traffic to the brain and gut early, and stabilizes cns injury late in infection," *PLoS Pathog*, vol. 10, no. 12, pp. 1–15, 2014.

[28] L. Gerngross and T. Fischer, "Evidence for cfms signaling in hiv production by brain macrophages and microglia," *J Neurovirol*, vol. 21, no. 3, pp. 249–56, 2015.

[29] P. Vivithanaporn, G. Heo, J. Gamble, H. B. Krentz, A. Hoke, M. J. Gill, and C. Power, "Neurologic disease burden in treated hiv/aids predicts survival," *Neurology*, vol. 75, pp. 1150–1158, 2010.

[30] B. B. Gelman, J. G. Lisinicchia, S. Morgello, E. Masliah, D. Commins, C. L. Achim, H. S. Fox, D. L. Kolson, I. Grant, E. Singer, C. T. Yiannoutsos, S. Sherman, G. Gensler, D. J. Moore, T. Chen, and V. M. Soukup, "Neurovirological correlation with hiv-associated neurocognitive disorders and encephalitis in a haart-era cohort," *J Acquir Immune Defic Syndr*, vol. 62, no. 5, pp. 487–495, 2013.

[31] M. C. Zink, A. K. Brice, K. M. Kelly, S. E. Queen, L. Gama, M. Li, R. J. Adams, C. Bartizal, J. Varrone, S. A. Rabi, D. R. Graham, P. M. Tarwater, J. L. Mankowski, and J. E. Clements, "Simian immunodeficiency virus-infected macaques treated with highly active antiretroviral therapy have reduced central nervous system viral replication and inflammation but persistence of viral dna," *J Infect Dis*, vol. 202, no. 1, pp. 161–170, 2010.

[32] L. Gama, C. M. Abreu, E. N. Shirk, S. L. Price, M. Li, G. M. Laird, K. A. Pate, S. W. Wietgrefe, S. L. O'Connor, L. Pianowski, A. T. Haase, C. V. Lint, R. F. Siliciano, and J. E. Clements, "Reactivation of simian immunodeficiency virus reservoirs in the brain of virally suppressed macaques," *AIDS*, vol. 31, no. 1, pp. 5–14, 2017.

[33] C. Cassioli and C. T. Baldari, "The expanding arsenal of cytotoxic t cells," *Front. Immunol.*, vol. 13, no. 883010, 2022.

[34] S. L. Swain, K. K. McKinstry, and T. M. Strutt, "Expanding roles for cd4+ t cells in immunity to viruses," *Nat Rev Immunol*, vol. 12, no. 2, pp. 136–148, 2012.

[35] E. Muraro, A. Merlo, D. Martorelli, M. Cangemi, S. D. Santa, R. Dolcetti, and A. Rosato, "Fighting viral infections and virus-driven tumors with cytotoxic cd4+ t cells," *Front. Immunol.*, vol. 8, no. 197, 2017.

[36] G. B. Pier, J. B. Lyczak, and L. M. Wetzler, eds., *Immunology, Infection and Immunity*. ASM Press, 2004.

[37] C. Hoeks, G. Duran, N. Hellings, and B. Broux, "When helpers go above and beyond: development and characterization of cytotoxic cd4+ t cells," *Front. Immunol.*, vol. 13, no. 951900, 2022.

[38] A. Takeuchi and T. Saito, "Cd4 ctl, a cytotoxic subset of cd4+ t cells, their differentiation and function," *Front. Immunol.*, vol. 8, no. 194, p. eCollection2017, 2017.

[39] W. Cui and S. M. Kaech, "Generation of effector cd8+ t cells and their conversion to memory t cells," *Immunol Rev*, no. 236, pp. 151–166, 2010.

[40] S. Johnson, M. Eller, J. E. Teigler, S. M. Maloveste, B. T. Schultz, D. Z. Soghoian, R. Lu, A. F. Oster, A.-L. Chenine, G. Alter, U. Dittmer, M. Marovich, M. L. Robb, N. L. Michael, D. Bolton, and H. Streeck, "Cooperativity of hiv-specific cytolytic cd4 t cells and cd8 t cells in control of hiv viremia," *J Virol*, vol. 89, no. 15, pp. 7494–7505, 2015.

[41] C. Phetsouphanh, D. Aldridge, E. Marchi, C. M. L. Munier, J. Meyerowitz, L. Murray, C. V. Vuuren, D. Goedhals, S. Fidler, A. Kelleher, P. Klenerman, and J. Frater, "Maintenance of functional cd57+ cytolytic cd4+ t cells in hiv+ elite controllers," *Front. Immunol.*, vol. 10, no. 1844, 2019.

[42] A. D. Olson, L. Meyer, M. Prins, R. Thiebaut, D. Gurdasani, M. Guiguet, M. L. Chaix, P. Amornkul, A. Babiker, M. S. Sandhu, and K. Porter, "An evaluation of hiv elite controller definitions within a large seroconverter cohort collaboration," *PLoS One*, vol. 9, no. 1, p. e86719, 2014.

[43] K. A. Freedberg, C. Possas, S. Deeks, A. L. Ross, K. L. Rosettie, M. D. Mascio, C. Collins, R. P. Walensky, and Y. Yazdanpanah, "The hiv cure research agenda: The role of mathematical modelling and cost-effectiveness analysis," *J Virus Erad*, vol. 1, no. 4, pp. 245–249, 2015.

[44] Q. Li, F. Lu, and K. Wang, "Modeling of hiv-1 infection: Insights to the role of monocytes/macrophages, latently infected t4 cells, haart regimes," *PLoS One*, 2012.

[45] M. Joly and J. M. Pinto, "An in-depth analysis of the hiv-1/aids dynamics by comprehensive mathematical modeling," *Math Comput Model*, 2011.

[46] Y. Huang, C. Zhang, J. Wu, and J. Lou, "Modelling the hiv persistence through the network of lymphocyte recirculation in vivo," *Infect Dis Model*, vol. 2, no. 1, pp. 90–99, 2017.

[47] K. A. Lindl, D. R. Marks, and D. L. Kolson, "Hiv-associated neurocognitive disorder: pathogenesis and therapeutic opportunities," *J Neuroimmune Pharmacol*, vol. 5, pp. 294–309, 2010.

[48] M. A. Nowak and R. M. May, *Virus dynamics. Mathematical principles of immunology and virology.* Oxford: Oxford University Press, 2000.

[49] D. E. Kirschner and A. S. Perelson, "A model for the immune system response to hiv: Azt treatment studies," in *Mathematical population dynamics: analysis of heterogeneity, vol. 1, theory of epidemics* (O. Arino, D. E. Axelrod, M. Kimmel, and M. Langlais, eds.), pp. 295–310, Winnipeg: Wuerz Publishing Ltd, 1995.

[50] J. G. Walsh, S. N. Reinke, M. K. Mamik, B. A. McKenzie, F. Maingat, W. G. Branton, D. I. Broadhurst, and C. Power, "Rapid inflammasome activation in microglia contributes to brain disease in hiv/aids," *Retrovirology*, vol. 11, no. 35, 2014.

[51] C. T. Barker and N. K. Vaidya, "Modeling hiv-1 infection in the brain," *PLoS Comput Biol*, vol. 16, no. 11, p. e1008305, 2020.

[52] D. Wodarz and M. A. Nowak, "Specific therapy regimes could lead to long-term immunological control of hiv," *Proc Natl Acad Sci U S A*, vol. 96, no. 25, pp. 14464–9, 1999.

[53] D. Wodarz, "Helper-dependent vs. helper-independent ctl responses in hiv infection: implications for drug therapy and resistance," *J Theor Biol*, vol. 213, no. 3, pp. 447–459, 2001.

[54] H. Chang and A. Astolfi, "Activation of immune response in disease dynamics via controlled drug scheduling," *IEEE Transactions on Automation Science and Engineering*, vol. 6, no. 2, pp. 248–255, 2009.

[55] W. Kim, H. B. Chung, and C. C. Chung, "Constant drug dose in human immuno-deficiency virus-infected patients to induce long-term non-progressor status: bifurcation and controllability approach," *IET Syst Biol*, vol. 7, no. 3, pp. 79–88, 2013.

[56] N. M. Smith, P. Mlcochova, S. A. Watters, M. M. Aasa-Chapman, N. Rabin, S. Moore, S. G. Edwards, J. A. Garson, P. R. Grant, R. B. Ferns, A. Kashuba, N. P. Mayor, J. Schellekens, S. G. Marsh, A. J. McMichael, A. S. Perelson, D. Pillay, N. Goonetilleke, and R. K. Gupta, "Proof-of-principle for immune control of global hiv-1 reactivation in vivo," *Clin Infect Dis*, vol. 61, no. 1, pp. 120–8, 2015.

[57] O. Ghasemi, M. L. Lindsey, T. Yang, N. Nguyen, Y. Huang, and Y.-F. Jin, "Bayesian parameter estimation for nonlinear modelling of biological pathways," *BMC Syst Biol*, vol. 5, no. Suppl 3, p. S9, 2011.

[58] C. F. Higham and D. Husmeier, "A bayesian approach for parameter estimation in the extended clock gene circuit of arabidopsis thaliana," *BMC Bioinformatics*, vol. 14, no. Suppl 10, p. S3, 2013.

[59] V. Periwal, C. C. Chow, R. N. Bergman, M. Ricks, G. L. Vega, and A. E. Sumner, "Evaluation of quantitative models of the effect of insulin on lipolysis and glucose disposal," *Am J Physiol Regul Integr Comp Physiol*, vol. 295, pp. R1089–R1096, 2008.

[60] J. Vanlier, C. A. Tiemann, P. A. J. Hilbers, and N. A. W. van Riel, "A bayesian approach to targeted experiment design," *Bioinformatics*, vol. 28, no. 8, pp. 1136–1142, 2012.

[61] Y. Z. Ma and A. Berndsen, "How to combine correlated data sets - a bayesian hyperparameter matrix method," *Astronomy and Computing*, vol. 5, pp. 45–56, 2014.

[62] L. J. Bain and M. Engelhardt, *Introduction to Probability and Mathematical Statistics*. Duxbury Thomas Learning, 1992.

[63] D. C. Montgomery, E. A. Peck, and G. G. Vining, *Introduction to Linear Regression Analysis*. Hoboken-New Jersey: John Wiley & Sons, Inc., 2006.

[64] B. Bolker, *Ecological Models and Data in R*. Princeton-New Jersey: Princeton University Press, 2007.

[65] A. Linden and S. Mantyniemi, "Using the negative binomial distribution to model overdispersion in ecological count data," *Ecology*, vol. 92, no. 7, pp. 1414–1421, 2011.

[66] J. G. Kalbfleisch, *Statistical Inference*. Springer-Verlag, 1985.

[67] M. Chen, Q. Shao, and J. G. Ibrahim, *Monte Carlo Methods in Bayesian Computation*. New York-New York: Springer-Verlag, 2000.

[68] B. J. Brewer, *Bayesian Astrophysics*, ch. Bayesian inference and computation: a beginner's guide. Cambridge University Press, 2018.

[69] S. M. Lynch, *Introduction to applied Bayesian statistics and estimation for social scientists*. New York: Springer, 2007.

[70] J. Goodman and J. Weare, "Ensemble samplers with affine invariance," *Communications in Applied Mathematics and Computational Science*, vol. 5, no. 1, pp. 65–80, 2010.

[71] C. Weikun, "A parallel implementation of mcmc," pp. 1–8, 2015.

[72] A. Gelman and S. P. Brooks, "General methods for monitoring convergence of iterative simulations," *J Comp Graph Stat*, vol. 7, no. 4, pp. 434–455, 1998.

[73] A. Gelman, X.-L. Meng, and H. S. Stern, "Bayesian tests for goodness of fit using tail area probabilities," Tech. Rep. 372, University of California, October 1992.

[74] A. Gelman, J. B. Carlin, H. S. Stern, and D. B. Dunson, *Bayesian Data Analysis*. Chapman and Hall/CRC, third edition ed., 2013.

[75] J. Skilling, "Nested sampling for general bayesian computation," *Bayesian Anal*, vol. 1, no. 4, pp. 833–859, 2006.

[76] C. M. Pooley and G. Marion, "Bayesian model evidence as a practical alternative to deviance information criterion," *R Soc Open Sci*, vol. 5, no. 3, p. 171519, 2018.

[77] C. P. Robert, N. Chopin, and J. Rousseau, "Harold jeffreys's theory of probability revisited," *Stat Sci*, vol. 24, no. 2, pp. 141–172, 2009.

[78] L. J. Bain and M. Engelhardt, *Introduction to Probability and Mathematical Statistics*. Brooks/Cole, second edition ed., 1987.

[79] B. J. Brewer, "Dnest5." [GitHub Source code], 2020.

[80] S. G. Deeks, S. R. Lewin, and L. G. Bekker, "The end of hiv: Still a very long way to go, but progress continues," *PLoS Med*, vol. 14, no. 11, p. e1002466, 2017.

[81] G. Wandeler, L. F. Johnson, and M. Egger, "Trends in life expectancy of hiv-positive adults on art across the globe: comparisons with general population," *Curr Opin HIV AIDS*, vol. 11, no. 5, pp. 492–500, 2016.

[82] L. J. Henderson, L. B. Reoma, J. A. Kovacs, and A. Nath, "Advances toward curing hiv-1 infection in tissue reservoirs," *J. Virol.*, vol. 94, no. 3, pp. e00375–19, 2020.

[83] C. Wallet, M. D. Rovere, J. V. Assche, F. Daouad, S. D. Wit2, V. Gautier, P. W. G. Mallon, A. Marcello, C. V. Lint, O. Rohr, and C. Schwartz, "Microglial cells: the main hiv-1 reservoir in the brain," *Front. Cell. Infect. Microbiol.*, vol. 9, no. 362, 2019.

[84] Y. Wang, M. Liu, Q. Lu, M. Farrell, J. M. Lappin, J. Shi, L. Lu, and Y. Bao, "Global prevalence and burden of hiv-associated neurocognitive disorder: A meta-analysis," *Neurol.*, vol. 95, no. 19, pp. e2610–e2621, 2020.

[85] D. Graham, L. Gama, S. E. Queen, M. Li, A. K. Brice, K. M. Kelly, J. L. Mankowski, J. E. Clements, and M. C. Zink, "Initiation of haart during acute simian immunodeficiency virus infection rapidly controls virus replication in the cns by enhancing immune activity and preserving protective immune responses," *J Neurovirol*, vol. 17, pp. 120–130, 2011.

[86] J. E. Clements, M. Li, L. Gama, B. Bullock, L. M. Carruth, J. L. Mankowski, and M. C. Zink, "The central nervous system is a viral

reservoir in simian immunodeficiency virus-infected macaques on combined antiretroviral therapy: A model for human immunodeficiency virus patients on highly active antiretroviral therapy," *J Neurovirol*, vol. 11, no. 2, pp. 180–9, 2005.

[87] E. A. Hernandez-Vargas, "Modeling kick-kill strategies toward hiv cure," *Front. Immunol.*, vol. 8, p. 995, 2020.

[88] L. Bracq, M. Xie, S. Benichou, and J. Bouchet, "Mechanisms for cell-to-cell transmission of hiv-1," *Front. Immunol.*, vol. 9, no. 260, 2018.

[89] M. Dupont and Q. J. Sattentau, "Macrophage cell-cell interactions promoting hiv-1 infection," *Viruses*, vol. 12, no. 492, 2020.

[90] N. Cifuentes-Munoza, F. E. Najjarb, and R. E. Dutch, "Viral cell-to-cell spread: conventional and non-conventional ways," *Adv. Virus Res.*, vol. 108, pp. 85–125, 2020.

[91] K. Askew, K. Li, A. Olmos-Alonso, F. Garcia-Moreno, Y. Liang, P. Richardson, T. Tipton, M. A. Chapman, K. Riecken, S. Beccari, A. Sierra, Z. Molnár, M. S. Cragg, O. Garaschuk, V. H. Perry, and D. Gomez-Nicola, "Coupled proliferation and apoptosis maintain the rapid turnover of microglia in the adult brain," *Cell Rep*, vol. 18, no. 2, pp. 391–405, 2017.

[92] V. Lutgen, S. D. Narasipura, H. J. Barbian, M. Richards, J. Wallace, R. Razmpour, T. Buzhdygan, S. H. Ramirez, L. Prevedel, E. A. Eugenin, and L. Al-Harthi, "Hiv infects astrocytes in vivo and egresses from the brain to the periphery," *PLoS Pathog*, vol. 16, no. 6, p. e1008381, 2020.

[93] E. L. Asahchop, O. Meziane, M. K. Mamik, W. F. Chan, W. G. Branton, L. Resch, M. J. Gill, E. Haddad, J. V. Guimond, M. A. Wainberg, G. B. Baker, E. A. Cohen, and C. Power, "Reduced antiretroviral drug efficacy and concentration in hiv-infected microglia contributes to viral persistence in brain," *Retrovirology*, vol. 14, no. 47, 2017.

[94] J. J. Cenker, R. D. Stultz, and D. McDonald, "Brain microglial cells are highly susceptible to hiv-1 infection and spread," *AIDS Res Hum Retrov*, vol. 33, no. 11, pp. 1155–1165, 2017.

[95] V. Gupta and N. M. Dixit, "Trade-off between synergy and efficacy in combinations of hiv-1 latency-reversing agents," *PLoS Comput Biol*, vol. 14, no. 2, p. e1006004, 2018.

[96] C. Gavegnano and R. F. Schinazi, "Antiretroviral therapy in macrophages: implication for hiv eradication," *Antivir Chem Chemother*, vol. 20, no. 2, pp. 63–78, 2009.

[97] O. Diekmann, J. A. P. Heesterbeek, and J. A. J. Metz, "On the definition and the computation of the basic reproduction ratio r0 in models for infectious diseases in heterogeneous populations," *J Math Biol*, vol. 28, pp. 365–382, 1990.

[98] P. van den Driessche and J. Watmough, "Reproduction numbers and sub-threshold endemic equilibria for compartmental models of disease transmission," *Math Biosci*, vol. 180, pp. 29–48, 2002.

[99] C. L. Althaus, B. Joos, A. S. Perelson, and H. F. Günthard, "Quantifying the turnover of transcriptional subclasses of hiv-1-infected cells," *PLoS Comput Biol*, vol. 10, no. 10, p. e1003871, 2014.

[100] J. E. Clements, T. Babas, J. L. Mankowski, K. Suryanarayana, M. P. Jr., P. M. Tarwater, J. D. Lifson, and M. C. Zink, "The central nervous system as a reservoir for simian immunodeficiency virus (siv): steady-state levels of siv dna in brain from acute through asymptomatic infection," *J Infect Dis*, vol. 186, pp. 905–913, 2002.

[101] C. R. Avalos, S. L. Price, E. R. Forsyth, J. N. Pin, E. N. Shirk, B. T. Bullock, S. E. Queen, M. Li, D. Gellerup, S. L. O'Connor, M. C. Zink, J. L. Mankowski, L. Gama, and J. E. Clements, "Quantitation of productively infected monocytes and macrophages of simian immunodeficiency virus-infected macaques," *J Virol*, vol. 90, no. 12, pp. 5643–5656, 2016.

[102] T. Babas, D. Muñoz, J. L. Mankowski, P. M. Tarwater, J. E. Clements, and M. C. Zink, "Role of microglial cells in selective replication of simian immunodeficiency virus genotypes in the brain," *J Virol*, vol. 77, no. 1, pp. 208–216, 2003.

[103] S. A. Barber, L. Gama, J. M. Dudaronek, T. Voelker, P. M. Tarwater, and J. E. Clements, "Mechanism for the establishment of transcriptional hiv latency in the brain in a simian immunodeficiency virus-macaque model," *J Infect Dis*, vol. 193, no. 7, pp. 963–970, 2006.

[104] K. L. Helke, S. E. Queen, P. M. Tarwater, J. Turchan-Cholewo, A. Nath, M. C. Zink, D. N. Irani, and J. L. Mankowski, "14-3-3 protein in csf: an early predictor of siv cns disease," *J Neuropathol Exp Neurol*, vol. 64, no. 3, pp. 202–208, 2005.

[105] K. A. Meulendyke, S. E. Queen, E. L. Engle, E. N. Shirk, J. Liu, J. P. Steiner, A. Nath, P. M. Tarwater, D. R. Graham, J. L. Mankowski, and M. C. Zink, "Combination fluconazole/paroxetine treatment is neuroprotective despite ongoing neuroinflammation and viral replication in an siv model of hiv neurological disease," *J Neurovirol*, vol. 20, no. 6, pp. 591–602, 2014.

[106] K. W. Witwer, L. Gama, M. Li, C. M. Bartizal, S. E. Queen, J. J. Varrone, A. K. Brice, D. R. Graham, P. M. Tarwater, J. L. Mankowski, M. C. Zink, and J. E. Clements, "Coordinated regulation of siv replication and immune responses in the cns," *PLoS One*, vol. 4, no. 12, p. e8129, 2009.

[107] M. C. Zink, K. Suryanarayana, J. L. Mankowski, A. Shen, M. P. Jr., J. P. Spelman, D. L. Carter, R. J. Adams, J. D. Lifson, and J. E. Clements, "High viral load in the cerebrospinal fluid and brain correlates with severity of simian immunodeficiency virus encephalitis," *J Virol*, vol. 73, no. 12, pp. 10480–10488, 1999.

[108] M. C. Zink, J. Uhrlaub, J. DeWitt, T. Voelker, B. Bullock, J. Mankowski, P. Tarwater, J. Clements, and S. Barber, "Neuroprotective and anti–human immunodeficiency virus activity of minocycline," *JAMA*, vol. 293, no. 16, pp. 2003–2011, 2005.

[109] H. R. Thieme, "Asymptotically autonomous differential equations in the plane," *The Rocky Mountain Journal of Mathematics*, vol. 24, no. 1, pp. 351–380, 1994.

[110] C. Castillo-Chavez and H. R. Thieme, "Asymptotically autonomous epidemic models," *Technical report (Cornell University. Mathematical Sciences Institute)*, vol. 94, no. 38, 1994.

[111] R. Suspène and A. Meyerhans, "Quantification of unintegrated hiv-1 dna at the single cell level in vivo," *PLoS One*, vol. 7, no. 5, p. e36246, 2012.

[112] F. A. C. Azevedo, L. R. B. Carvalho, L. T. Grinberg, J. M. Farfel, R. E. L. Ferretti, R. E. P. Leite, and et al, "Equal numbers of neuronal and nonneuronal cells make the human brain an isometrically scaled-up primate brain," *J Comp Neurol*, vol. 513, pp. 532–541, 2009.

[113] S. Herculano-Houzel, "The glia/neuron ratio: how it varies uniformly across brain structures and species and what that means for brain physiology and evolution," *Glia*, vol. 62, pp. 1377–1391, 2014.

[114] P. Hartmann, A. Ramseier, F. Gudat, M. J. Mihatsch, and W. Polasek, "Normal weight of the brain in adults in relation to age, sex, body height and weight," *Pathologe*, vol. 15, no. 3, pp. 165–170, 1994.

[115] T. M. Inc. Matlab version 9.7.0.1261785 Natick, Massachusetts., 2019.

[116] A. Grinsted, "Markov chain monte carlo sampling of posterior distribution." http://www.mathworks.com/matlabcentral/fileexchange/49820-grinsted-gwmcmc, 2015.

[117] A. Gelman and S. P. Brooks, "General methods for monitoring convergence of iterative simulations," *J Comp Graph Stat*, vol. 7, no. 4, pp. 434–455, 1998.

[118] K. K. V. Vijayan, K. P. Karthigeyan, S. P. Tripathi, and L. E. Hanna, "Pathophysiology of cd4+ t-cell depletion in hiv-1 and hiv-2 infections," *Front. Immunol.*, vol. 8, no. 580, 2017.

[119] R. Mascarau, M. Woottum, L. Fromont, R. Gence, V. Cantaloube-Ferrieu, Z. Vahlas, K. Leveque, F. Bertrand, T. Beunon, A. Metais, H. E. Costa, N. Jabrane-Ferrat, Y. Gallois, N. Guibert, J.-L. Davignon, G. Favre, I. Maridonneau-Parini, R. Poincloux, B. Lagane, S. Benichou, B. Raynaud-Messina, and C. Verollet, "Productive hiv-1 infection of tissue macrophages by fusion with infected cd4+ t cells," *J Cell Biol*, vol. 222, no. 5, p. e202205103, 2023.

[120] M. M. Salih, M. Almehmadi, A. Shafie, A. Alsharif, N. Alsiwiehri, A. El-Askary, K. Alzahrani, A. Aljuaid, O. Abdulaziz, A. A. Alrehaili, A. A. Almalki, H. S. Alzahrani, M. Halawi, S. Almalki, E. Alosimi, and A. F. Gharib, "Evaluation of cd4+:cd8+ ratio in patients with cervical cancer and the levels of inflammatory markers," *In Vivo*, vol. 36, no. 5, pp. 2414–2421, 2022.

[121] A. C. Paim, N. W. Cummins, S. Natesampillai, E. Garcia-Rivera, N. Kogan, U. Neogi, A. Sönnerborg, M. Sperk, G. D. Bren, S. Deeks, E. Polley, and A. D. Badley, "Hiv elite control is associated with reduced trailshort expression," *AIDS*, vol. 33, no. 11, pp. 1757–1763, 2019.

[122] L. Westera, J. Drylewicz, I. den Braber, T. Mugwagwa, I. van der Maas, L. Kwast, T. Volman, E. H. R. van de Weg-Schrijver, I. Bartha, G. Spierenburg, K. Gaiser, M. T. Ackermans, B. Asquith, R. J. de Boer, K. Tesselaar, and J. A. M. Borghans, "Closing the gap between t-cell life span estimates from stable isotope-labeling studies in mice and humans," *Blood*, vol. 122, no. 13, pp. 2205–2212, 2013.

[123] N. Vrisekoop, I. den Braber, A. B. de Boer, A. F. C. Ruiter, M. T. Ackermans, S. N. van der Crabben, E. H. R. Schrijver, G. Spierenburg, H. P. Sauerwein, M. D. Hazenberg, R. J. de Boer, F. Miedema, J. A. M. Borghans, and K. Tesselaar, "Sparse production but preferential incorporation of recently produced naive t cells in the human peripheral pool," *Proc Natl Acad Sci U S A*, vol. 105, no. 16, pp. 6115–6120, 2008.

[124] M. Baliu-Pique, M. W. Verheij, J. Drylewicz, L. Ravesloot, R. J. de Boer, A. Koets, K. Tesselaar, and J. A. M. Borghans, "Short lifespans of memory t-cells in bone marrow, blood, and lymph nodes suggest that t-cell memory is maintained by continuous self-renewal of recirculating cells," *Front. Immunol.*, vol. 9, no. 2054, 2018.

[125] H. Imamichi, V. Natarajan, J. W. Adelsberger, C. A. Rehm, R. A. Lempicki, B. Das, A. Hazen, T. Imamichi, and H. C. Lane, "Lifespan of effector memory cd4 t cells determined by replication-incompetent integrated hiv-1 provirus," *AIDS*, vol. 28, no. 8, pp. 1091–1099, 2014.

[126] H. Mohri, A. S. Perelson, K. Tung, R. M. Ribeiro, B. Ramratnam, M. Markowitz, R. Kost, A. Hurley, L. Weinberger, D. Cesar, M. K. Hellerstein, and D. D. Ho, "Increased turnover of t lymphocytes in hiv-1 infection and its reduction by antiretroviral therapy," *J Exp Med*, vol. 194, no. 9, pp. 1277–1287, 2001.

[127] M. A. Stafford, L. Corey, Y. Cao, E. S. Daar, D. D. Ho, and A. S. Perelson, "Modeling plasma virus concentration during primary hiv infection," *J Theor Biol*, vol. 203, no. 3, pp. 285–301, 2000.

[128] A. S. Perelson, D. E. Kirschner, and R. D. Boer, "Dynamics of hiv infection of cd4 t cells," *Math Biosci*, vol. 114, no. 1, pp. 81–125, 1993.

[129] F. H. Omondi, H. Sudderuddin, A. Shahid, N. N. Kinloch, B. R. Jones, R. L. Miller, O. Tsai, D. MacMillan, A. Trocha, M. A. Brockman, C. J. Brumme, J. B. Joy, R. Liang, B. D. Walker, and Z. L. Brumme, "Hiv proviral burden, genetic diversity, and dynamics in viremic controllers who subsequently initiated suppressive antiretroviral therapy," *mBio*, vol. 12, no. 6, p. e0249021, 2021.

[130] M. D. Pankau, D. B. Reeves, E. Harkins, K. Ronen, W. Jaoko, K. Mandaliya, S. M. Graham, R. S. McClelland, F. A. M. IV, J. T. Schiffer, J. Overbaugh, and D. A. Lehman, "Dynamics of hiv dna reservoir seeding in a cohort of superinfected kenyan women," *PLoS Pathog*, vol. 16, no. 2, p. e1008286, 2020.

[131] B. V. Kumar, T. Connors, and D. L. Farber, "Human t cell development, localization, and function throughout life," *Immunity*, vol. 48, no. 2, pp. 202–213, 2018.

[132] X. Zhou, H. Lin, and H. Lin, *Encyclopedia of GIS*, ch. Global sensitivity analysis. Springer New York, NY, 2008.

[133] A. Dela, B. Shtylla, and L. de Pillis, "Multi-method global sensitivity analysis of mathematical models," *J Theor Biol*, vol. 546, no. 111159, 2022.

[134] S. Marino, I. B. Hogue, C. J. Ray, and D. E. Kirschner, "A methodology for performing global uncertainty and sensitivity analysis in systems biology," *J Theor Biol*, vol. 254, no. 1, pp. 178–196, 2008.

[135] A. Saltelli, S. Tarantola, and K. P.-S. Chan, "A quantitative model-independent method for global sensitivity analysis of model output," *Technometrics*, vol. 41, no. 1, pp. 39–56, 1999.

[136] D. Kirschner, "Uncertainty and sensitivity functions and implementation." http://malthus.micro.med.umich.edu/lab/usadata/, 2008.